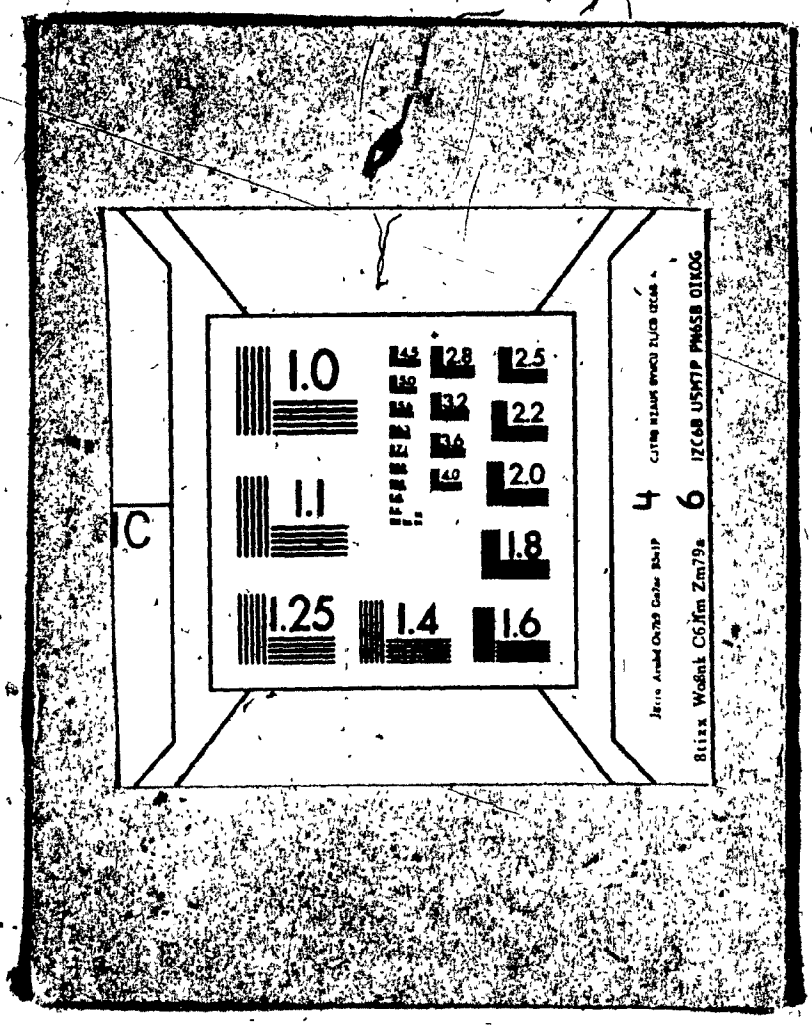
1.0
1.1
1.25
1.4
1.6
2.0
2.2
2.5
2.8
C

ON BANDWIDTH EFFICIENT SPECTRAL SHAPING METHODS

AND

DIGITAL MODULATION TECHNIQUES IN LINEAR AND NONLINEAR CHANNELS

John Chen-yuan Huang

A Thesis

in

The Department

of

Electrical Engineering

Presented in Partial Fulfillment of the Requirements
for the degree of Doctor of Philosophy at
Concordia University
Montréal, Québec, Canada

March, 1979

ABSTRACT

ON BANDWIDTH EFFICIENT SPECTRAL SHAPING METHODS AND DIGITAL MODULATION TECHNIQUES IN LINEAR AND NONLINEAR CHANNELS

John Chen-yuan Huang, Ph. D.
Concordia University, 1979

In this thesis, the performance of various digital modulation schemes in both linear and nonlinear channels is investigated. Specifically, this thesis covers the following three subjects:

(i) Baseband pulse shaping techniques and data pattern dependent jitter.

(ii) Partial Response (PR) signaling schemes and the performance of QPRS (Quadrature Partial Response Signaling) digital radio systems in linear and nonlinear channels.

(iii) Performance of QPSK (Quaternary Phase Shift Keyed), OKQPSK (Offset Keyed QPSK) and MSK (Minimum Shift Keyed) signals through cascaded nonlinear bandlimited satellite channels.

First, an analytical method to predict the data pattern dependent jitter is presented. Results obtained by this method are shown to be in excellent agreement with those obtained by computer simulation and laboratory measurement. This method can thus be used to evaluate system tolerance of a designed filter.

In order to find methods that can generate an ISI (Intersymbol Interference) and jitter free bandlimited Nyquist signal, a double-intervaled raised cosine pulse and its spectral characteristics are studied. Based on this study, a search for new double-intervaled pulses having low spectral sidelobes is conducted. Pulses having desirable spectral characteristics

and their application in communication systems are discussed.

Following this, two methods for the generation of ISI and jitter free Nyquist signals are described. The first one uses the concept of pulse overlapping while the second one incorporates Feher's nonlinear switching concept. These two methods are equivalent as they can generate the same output signals. Measured results obtained on the hardware implementation of the nonlinear switching concept agree favourably with Feher's predictions. The simplicity of its design and its low cost will enable this type of nonlinear switching filter to be used for low bit rate satellite communication systems.

It is found that the concept of pulse overlapping can also be applied to the generation of multi-level PR signals. This approach presents a simplified method to study the characteristics of PR signaling schemes. Such innovation provides an additional insight into the physical interpretation of the PR signaling technique.

Lender's PR system model is studied and extended to other PR systems. The additional signal to noise requirement of this model over the ideal binary system is compared with that of Kretzmer's and Qureshi's models. The merits of each system model in practical applications are also assessed.

A computer simulation is used to study filtering effects and nonlinearity on the performance of QPRS digital radio systems. Results from the filtering optimization show that, if performance degradation less than 2 dB from theoretical prediction is desired, filter passband ripples should be less than

0.01 dB and filter phase distortion should be minimized. Based on the results of the nonlinearity study, it is recommended that the power amplifier used in the QPRS radio system should be placed before the PR filter and it should be operated in the pseudo-linear region.

An analysis is undertaken to study the amplitude fluctuations, both the overall average and at the sampling instants of filtered QPSK, OKQPSK and MSK signals. The result is verified by computer simulation. Two types of spectrum spreading, which occur when a filtered PSK signal is hardlimited, are also experimentally demonstrated.

Computer simulation programs are developed to study the performance of bandlimited QPSK, OKQPSK and MSK signals through cascaded nonlinearities. Results from this study show that in the narrowband channel, QPSK is the optimal modulation technique. On the other hand, OKQPSK performs slightly better than QPSK and MSK in the wideband model.

In summary, this thesis covers an in-depth and timely study on subjects of current interest. The results presented will find immediate application both in digital radio and in satellite communication systems.

RESUME

La performance de plusieurs méthodes de modulations numériques, tant dans le cas de canaux linéaires que nonlinéaires, est étudiée dans cette thèse. En particulier on abordera les 3 sujets suivants:

(i) Les techniques de mise en forme impulsionelles en bande de base et la gigue dépendante de la séquence de données.

(ii) Les méthodes de signalisation par réponse partielle (partial response signaling), et la performance de la signalisation par quadrature de la réponse partielle (Quadrature Partial Response Signaling, QPRS) lorsqu'elle est utilisée pour la radio numérique dans des canaux linéaires et nonlinéaires.

(iii) La performance de signaux QPSK (modulation de phase par quadrature), OKQPSK (QPSK décalé) et de MSK (modulation a décalage minimal) lorsqu'ils sont transmis dans des canaux de satellites nonlinéaires et avec une bande passante limitée.

Une méthode analytique pour prédire la gigue de phase dépendante de la séquence de données sera présentée. Il sera démontré que les résultats obtenus par cette méthode sont en excellent accord avec ceux obtenus par simulation sur ordinateur et par des mesures faites en laboratoire. Cette méthode peut être utilisée pour évaluer la tolérance du système à l'endroit d'un filtre qui a été conçu.

Afin de trouver des méthodes de génération de signaux a bande limitée qui sont exempts, à la fois d'interférence entre les impulsions successives (ISI) et de gigue de phase, une impulsion à accroissement cosinusoidal à double intervalle et son spectre seront étudiés. Cette étude sert de point

de départ à la recherche d'impulsions à double intervalle qui possèdent des lobes secondaires atténués par rapport au lobe principal. Des impulsions ayant ces caractéristiques sont présentées ainsi que leurs applications dans des systèmes de communications.

Deux méthodes pour la génération de signaux de Nyquist exempt d'ISI et de gigue de phase sont décrites. La premièr e utilise le concept de superposition impulsionelle alors que la seconde utilise le concept de commutation nonlinéaire de Feher. Les 2 méthodes sont équivalentes en ce sens qu'elles peuvent générer les mêmes signaux de sortie. Les expériences menées sur l'implantation en matériel du concept de commutation nonlinéaire donnent des résultats expérimentaux se comparant favorablement aux prédictions de Feher. Ce type de filtre à commutation nonlinéaire s'avère fort approprié, tant du point de vue de sa simplicité que de son coût peu élevé, pour les systèmes de communication par satellites ayant un faible taux de transmission de données.

De plus, nous trouvons que le concept de superposition impulsionnelle peut aussi être appliqué à la génération de signalisations à niveaux multiples du type réponse partielle. Cette approche permet d'utiliser une méthode simple pour l'étude des caractéristiques des différentes signalisations PR (réponse partielle). Une telle innovation permet une meilleure compréhension de l'interprétation physique des techniques de réponse partielle (PR).

Le modèle du système PR de Lender est étudié et appliqué à d'autres systèmes PR. Les exigences supplémentaires en rapport signal-bruit par rapport au système binaire sont comparées aux exigences semblables dans les modèles de Kretzmer et Qureshi. Une évaluation

est faite des mérites de chaque système dans des applications pratiques.

L'effet des nonlinéarités et du filtrage sur la performance de systèmes de radio numérique de type QPRS est étudié en utilisant une simulation sur ordinateur. Les résultats de l'optimisation du filtrage montrent que pour obtenir une dégradation de moins 2 dB de la prédiction théorique, les ondulations dans la bande passante du filtre doivent être moindre que .01 dB et que la distortion de phase du filtre doit être minimisée. A partir de ces études de nonlinéarités, il est recommandé que l'amplificateur de puissance utilisé dans un système radio QPRS soit placé avant les filtres PR et qu'il soit exploité dans la région pseudo-linéaire.

Une analyse est faite des fluctuations d'amplitudes, tant moyenne qu'à l'instant d'échantillonage, dans le cas du QPSK, OKQPSK et ASK. Le résultat est vérifié par simulation sur ordinateur. Des résultats expérimentaux portant sur deux types d'élargissement spectral sont présentés; ils se produisent lorsqu'un signal filtré et modulé en phase est passé dans un limiteur dur.

Des simulations sur ordinateur sont utilisées pour étudier la performance de signaux à bande limitée de type QPSK, OKQPSK et ASK lorsqu'ils passent dans plusieurs nonlinéarités. L'étude montre que pour des canaux à bande passante limitée le QPSK est la technique optimale de modulation. D'autre part, pour de grandes largeurs de bande la technique OKQPSK donne une meilleure performance que les autres techniques ayant fait l'objet de l'étude.

En résumé, cette thèse présente une étude exhaustive et pertinente sur des sujets d'intérêts contemporains. Les résultats présentés trouveront des applications tant, dans le domaine de la radio numérique que dans les systèmes de communications par satellite.

ACKNOWLEDGMENTS

I wish to express my sincere gratitude to Dr. Kamilo Feher, my thesis supervisor, who not only has been guiding me technically throughout the course of this study but also sharing with me his valuable personal experience as a working engineer. To Dean Dr. Swamy, Chairman Dr. Antoniou and Graduate Program Director Dr. Ramachandran, I owe my thankfulness for their continuous encouragement.

Special thanks should go to Mr. M. Morris, Manager, Electronic Development Engineering, Spar Aerospace Limited, for his encouraging support throughout this study. I also wish to thank many of my colleagues at Spar, especially Dr. H.K. Au, Mr. R. de Cristofaro and Mr. T. Le-Ngoc for helpful discussions and critical reviewing. Editing assistance from Messrs. M. Wachira, A. Guibord and B. Ghicopoulos, all of the University of Ottawa, are greatly appreciated. I am also indebted to Mr. E. Perera and Mr. M. Gendron, for their assistance on time-sharing editing and hardware implementation, respectively.

Financial assistance from the Concordia University Fellowship Award Committee is greatly appreciated.

I wish to extend my thanks to Miss D. Bentley for English correction and Miss V. Stott for typing the complete manuscript. I shall also remember the valuable personal encouragement from Dr. Feher's parents, Mr. and Mrs. Feher, Sr.

Finally, I wish to dedicate this thesis to my parents and especially to my wife, who has shared with me both the joy and the frustration of my study. Without her continuous encouragement, I would never have had the opportunity to complete this thesis.

TABLE OF CONTENTS

APPENDIX -

LIST OF FIGURES

Chapter 3 ---

LIST OF TABLES

LIST OF ABBREVIATIONS

AM	Amplitude Modulation
AM/AM conversion	AM to AM conversion
AM/PM conversion	AM to PM conversion
BPF	Bandpass Filter
b/s/Hz	Bit per second per Hertz
CGN	Coloured Gaussian Noise
DC	Direct Current
E_w	Eye width or horizontal eye opening
FFSK	Fast Frequency Shift Keyed
FFT	Fast Fourier Transform
FM	Frequency Modulation
f_N	Nyquist frequency
HPA	High Power Amplifier
J_{pp}	Peak to peak jitter
LPF	Low Pass Filter
MSK	Minimum Shift Keyed
MUX	Multiplexer
NRZ	Non-Return-to-Zero
OKQPSK	Offset Keyed QPSK
PAM	Pulse Amplitude Modulation
p(e)	Probability of error
PM	Phase Modulation
PR	Partial Response

QPSK	Quaternary Phase Shift Keyed
QPRS	Quadrature Partial Response System
rms	root mean square
RF	Radio frequency
RxF	Receiver filter
S/N or SNR	Signal to Noise Ratio
TWT	Traveling Wave Tube
TxF	Transmit Filter
WGN	White Gaussian Noise
α	Cosine rolloff factor

CHAPTER 1

Chapter 1

Introduction

In digital communication systems, a rectangular pulse occupying a unit bit duration T is frequently used, both for theoretical consideration and practical implementation. In the Non-Return-to-Zero (NRZ) coding scheme, a 1 symbol is represented by a rectangular pulse of amplitude + A volts for the duration of T second while a 0 symbol is represented by a rectangular pulse of amplitude - A volts having the same duration. A segment of an NRZ coded random data stream is shown in Fig. 1. 1. An NRZ coded data stream has a (sin x/x) shaped power spectrum with relatively slow decaying sidelobes. For conservation of available channel bandwidth, a bandlimiting filter is therefore required. The spectrum of the filtered signal should contain little or no energy outside its allocated channel bandwidth in order not to interfere with signals in the neighboring channels [Feher, 1. 1].

Nyquist's first theorem on data transmission stipulates a brick-wall ideal filter for minimum bandwidth transmission without Intersymbol Interference (ISI). This ideal filter has a unity gain amplitude function up to the Nyquist frequency, which is half of the bit rate frequency of the random data stream. Beyond the Nyquist frequency, this filter has an infinite attenuation slope as shown in Fig. 1. 2. The ideal Nyquist filter also has a linear phase function.

However, the ideal Nyquist filter is not physically realizable because

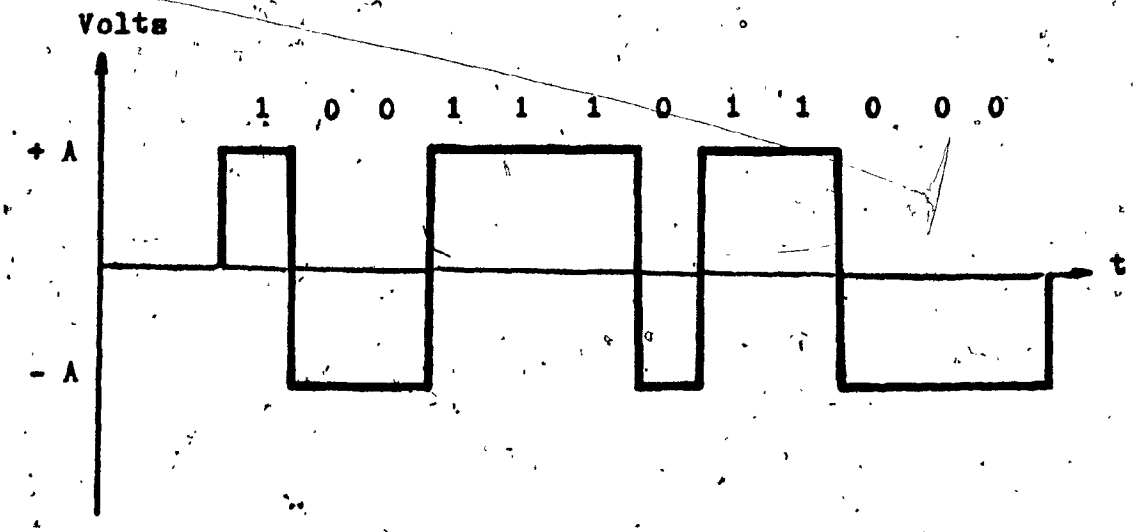

Fig. 1.1 A Segment of NRZ Coded Binary Data Stream

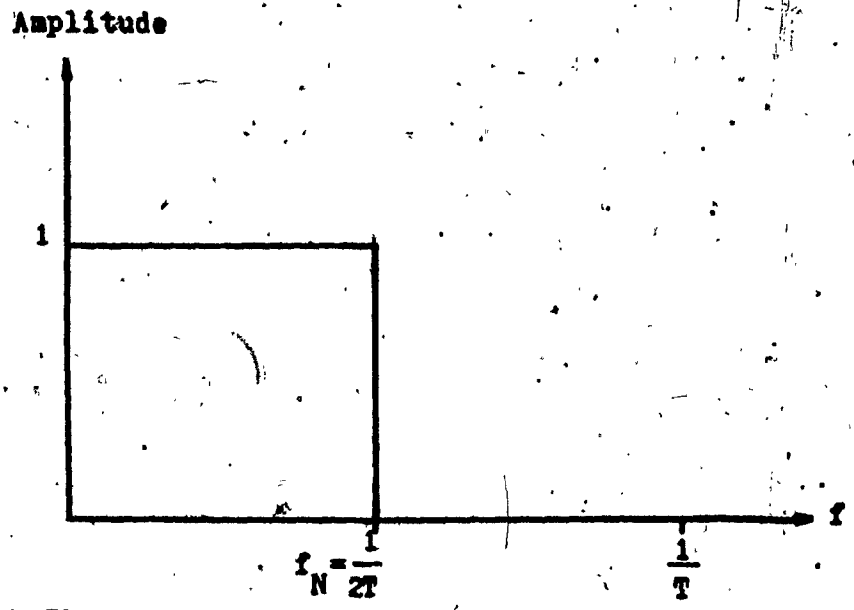

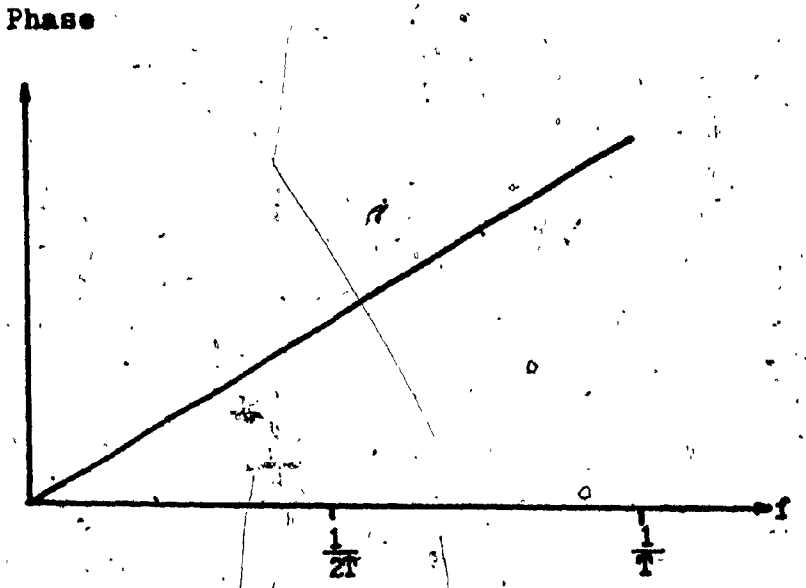

Fig. 1.2 Ideal Brick-wall Nyquist Filter

of the infinite number of sections involved. In Chapter 2, an analytical method which shows theoretically that there is a 100% peak-to-peak jitter in a system using the ideal Nyquist filter will be presented. In other words, the minimum bandwidth system has no timing error tolerance.

This analytical study is motivated by the computer simulation results presented by El-Torky and Feher [1.2], in which they showed that jitter exists in a raised cosine type of Nyquist filter even though there is no ISI at the sampling instants. The raised cosine filters are a general class of Nyquist filters which meet the requirement of Nyquist's second theorem. Raised cosine filters with a rolloff factor α between 0.3 and 1 are practically realizable and frequently find applications in digital communication systems.

The presented analytical method is then further applied to study jitter effects and amplitude fluctuations of a signal passing through a raised cosine filter. Results obtained from this study will be compared with those of Ref. [1.2] and laboratory measurements.

Feher has suggested [Gendron and Feher, 1.3], in the generation of a random data stream, the notion of switching on and off certain portions of an analog waveform. The selection of analog waveform shape depends on the correlation between the neighboring bits of a binary random data stream. In Chapter 2, it will be shown that this nonlinear switching concept can be related to the overlapping pulses, i.e., pulses that occupy a two-bit interval. For this purpose, a study on double-intervaled pulses

and their spectral characteristics will therefore be undertaken.

The considered pulse shaping is a nonlinear spectral shaping scheme. It is well known that a single-intervaled half-cosine pulse has a much faster spectral rolloff than that of a rectangular pulse of the same duration. [Bennett and Davey, 1.4]. Yet its main spectral lobe width is 50% wider. A single-intervaled raised-cosine pulse has an even faster spectral rolloff than that of a half-cosine pulse. Its main spectral lobe width, on the other hand, is 100% wider than that of the rectangular pulse.

It is also known that a double-intervaled overlapping pulse has a fast spectral rolloff but its main spectral lobe width is confined within that of a single-intervaled rectangular pulse [Bennett and Davey, 1.4]. In the literature, the double-intervaled pulses have not received enough attention until recently [Greenstein, 1.5] [Aulin and Sundberg , 1.6]. To be useful for data transmission, these double-intervaled pulses must satisfy certain criteria. These criteria, which will be established in this thesis, are to ensure zero ISI and jitter free data transmission. A search for new double-intervaled pulses which satisfy these criteria will then be conducted. These new double-intervaled pulses generally have lower spectral sidelobes than those of the rectangular pulse. An important feature of these new pulses is that their main spectral lobe width is confined within that of the rectangular pulse.

Afterwards, a pulse overlapping method and Feher's nonlinear switching

method for the generation of ISI and jitter free Nyquist signals will be described. These two methods will be shown to produce the same output signal. Thus these two methods are equivalent.

A hardware implementation of the nonlinear switching filter will be described. Measured results from the designed circuitry, which is a modified version of that given in [1, 3], will then be presented.

Another alternative for bandwidth efficient data transmission using realizable filters is by introducing correlation between neighboring bits of the random data stream [Lender, 1.8] [Kretzmer, 1.9] [Kabal and Pasupathy, 1.10]. The correlative coding scheme, commonly known as partial response (PR), allows transmission at the Nyquist rate of 2 b/s/Hz or even higher with filters whose amplitude transfer functions have a more gentle rolloff.

In Chapter 3, after a brief review of PR signaling schemes, the concept of pulse overlapping introduced earlier in Chapter 2 will be applied to the generation of multi-level PR signals. It will be shown that pulse overlapping is equivalent to introducing correlation between the data bits when multi-level pulse trains are generated. By finding the multi-intervaled overlapping pulses, different types of PR signaling schemes are obtained. Their spectral characteristics are derived. This approach provides additional insight into the physical interpretation of PR signaling techniques.

Afterwards, Lender's system model for the modified duobinary (class 4 PR) will be analyzed and extended to other PR systems. Results for this third model will be compared with the other two systems models proposed by [Kretzmer, 1.9] and [Qureshi et al, 1.11]. The merits of each system model, based on design and application consideration, will also be assessed.

In the literature, the effect of a practical PR filter on the performance of a radio transmission system has not been documented in sufficient detail. Furthermore, the effect of nonlinearity on its performance has not yet been published. To study these effects, a computer simulation program will be developed. As the Quadrature Partial Response System (QPRS) is the most widely used modulation technique using PR signaling scheme, in this thesis, we will concentrate on this type of modulation system.

A simple guideline for evaluating the performance of a digital radio system will be presented. The performance of some digital radio systems, using QPRS, will be compared and summarized in a table for easy reference.

For digital satellite communication systems, conventional Quaernary Phase-Shift Keying (QPSK), Offset Keyed QPSK (OKQPSK) and Minimum Shift Keying (MSK), are the three modulation schemes most widely considered. In the literature, QPSK is frequently used in digital transmission systems. This is because of its bandwidth efficiency, low error rate and simple hardware design [Feher, 1.1].

OKQPSK, also known as Staggered QPSK, was first proposed by [Chang, 1.12] and later on, generalized by [Saltzberg, 1.13]. It can also be considered as a double binary PSK system [Kwan, 1.14]. Due to the delay of half a symbol interval between its in-phase and quadrature phase channels, OKQPSK has less overall amplitude fluctuations. In Ref. [1.15], Rhodes demonstrated by computer simulation that filtered OKQPSK, when hardlimited, suffers less spectrum spreading than that of filtered and limited QPSK.

MSK, as a special case of OKQPSK, was first patented in 1960 by [Doelz and Heald, 1.16]. It can also be viewed as a form of coherent Frequency Shift Keying (FSK) with a frequency deviation ratio of 0.5. In this view, it is also known as Fast FSK as it can transmit faster pulse trains than any other ordinary FSK or binary PSK of equal bandwidth and signal to noise ratio [de Buda, 1.17]. Owing to its constant envelope and continuous phase nature, an MSK signal, when hardlimited, suffers even less degree of spectrum regeneration than that of OKQPSK [Rhodes, 1.15].

Based on the spectrum regeneration phenomenon, it has been predicted that either OKQPSK or MSK is more suitable than QPSK for use in bandlimited nonlinear satellite channels. In satellite communication systems, bandlimiting is required in order to conserve available bandwidth, while the power amplifiers are normally operated near saturation because of the power constraint. In this mode of operation, these power amplifiers exhibit the nonlinear characteristics of AM/AM and AM/PM conversions.

Recently, Murakami et al [1.18] showed in their computer simulation results that in the INTELSAT type of channel (60 Mb/s in a bandwidth of 36 MHz), QPSK performs better than OKQPSK or MSK.* They also showed that QPSK has less phase noise in the recovered carrier than that of OKQPSK and MSK. Huang and Feher [1.19] also demonstrated in their cascaded-nonlinearity studies using computer simulations, that QPSK outperforms OKQPSK and MSK in the two narrowband models. In the wideband model, OKQPSK performs slightly better than QPSK and MSK.

This conclusion is also reached separately by [Harris, 1.20], [Lundquist, 1.21] and [Chakraborty et al, 1.22]. On the contrary, it does not agree with that obtained by [Constellano, 1.23]. It is noted that Constellano considered only one nonlinearity in his simulation study.

To analyze these findings, in Chapter 4 we will first consider the amplitude fluctuations of filtered QPSK, OKQPSK and MSK signals. This analysis includes the overall average amplitude fluctuations as well as

* A $(\cdot)^4$ multiplier for carrier recovery is assumed.

those at the sampling instants. Results will be verified by computer simulations.

Computer simulation methods developed for the evaluation of the performance of bandlimited QPSK, OKQPSK and MSK signals through cascaded nonlinearities, as in a typical satellite channel, will be presented. Results from this simulation study will be compared with those from the references quoted above.

Because of the complexity of modeling the nonlinear characteristics of a power amplifier, the exact cause of the spectrum spreading phenomenon mentioned earlier is still under debate [Robinson et al, 1.24] [Moreno, 1.25]. In Chapter 2, two types of baseband signals are considered, one jitter free and the other with certain amount of jitter. An experiment will be carried out to study the spectrum spreading phenomenon by first modulating these two types of signals separately with a carrier and then hardlimiting the modulated signals respectively. This experiment will demonstrate the effect of data pattern jitter on the modification of the restored spectrum caused by hardlimiting.

In short, this thesis is developed in three separate chapters from baseband pulse shaping and PR coding schemes to the study of the performance of various modulation techniques in both linear and nonlinear communication channels. Both theoretical derivations and computer simulation results are presented and verified by laboratory measurements.

CHAPTER 2

Chapter 2

Techniques to Generate ISI and Jitter Free Bandlimited Nyquist Signals and a Method to Analyze Jitter Effects

2.1 Introduction

The objective of this chapter is two-fold:

1) Analyze the data pattern dependent jitter resulting from the effect of the infinitely long oscillating tails of the Nyquist pulses when they are used as signaling elements in a random data stream.
2) Study techniques that can generate intersymbol interference (ISI) and also jitter free bandlimited Nyquist signals.

The jitter study is approached by first considering the worst combination of the input data patterns and then analyzing the effect of the oscillating tails of the Nyquist pulses on the zero crossings of the eye patterns of the resulting data stream. Using this approach, it is possible to sketch the boundary traces of the eye patterns and to compute the peak-to-peak jitter and the amplitude fluctuations of the random data stream. Results obtained from this jitter study will provide a tool for a communication design engineer to analyze system tolerance due to the imperfections of the filters.

The Nyquist pulses contain the sin x/x factor and have infinitely long oscillating tails [Bennett and Davey, 2.1] [Lucky et al, 2.2]. They

satisfy the Nyquist zero-crossing criterion, i. e., the pulses have their zero-crossings at the sampling instants except at the mid point of the main pulse lobe. Thus, when they are used as signalling elements in a synchronous random data stream, the system will not exhibit any ISI. Nevertheless, because of the effect of the infinitely long oscillating tails of the Nyquist pulses, the resulting signal contains data pattern dependent jitter. Hence the timing jitter studied in this chapter will be called data pattern jitter.

Traces that form the boundary of the eye patterns of the resulting data stream will be identified as arising from certain worst combinations of the input data pattern. The peak-to-peak jitter and the amplitude overshoot that appear in the eye patterns will then be computed and compared with those of the computer simulated and laboratory measured eye diagrams.

In order to introduce techniques that can generate ISI and jitter free bandlimited Nyquist signals, time-limited pulses occupying one or two bit intervals and their spectral properties will be investigated. Afterwards, two techniques that can generate ISI and also jitter free bandlimited Nyquist signals will be presented. The first technique uses the principals of synchronously overlapping double-intervaled pulses while the second technique employs the concept of nonlinear switching.

Time-limited double-intervaled raised-cosine pulses have been well described in the literature [Bennett and Davey, 2.1] [Lucky et al, 2.3].

In this chapter, time-limited, double-intervaled pulses that can be used to generate ISI and jitter free Nyquist signals will be analyzed. New double-intervaled pulses that can be used for this purpose are proposed and their spectral properties studied. The criterion used in the search of these double-intervaled pulses is that the main spectral lobe of the pulse should not be widened while the sidelobes should be lower than those of a single-intervaled rectangular pulse.

Afterwards, it will be shown that by synchronously overlapping the double-intervaled pulses, ISI and jitter free signal transmission can be obtained. Based on this principle of pulse overlapping, a method which can generate bandwidth efficient and jitter free data streams will be presented.

It is found that the resultant data streams which are generated by the pulse-overlapping technique can also be obtained by a nonlinear switching method. Boolean equations for the logic circuitry to connect or disconnect the corresponding pre-chosen segment of an analog waveform will be established. Based on this nonlinear switching concept, circuit implementation of a nonlinear switching filter will be described using both the sine and triangular waves.

For the non-linear switching filter using the sine wave, the resultant output signal has an in-band to out-of-band energy ratio of 20dB at 1.4 f_N and of 26dB at 1.6 f_N where f_N is the Nyquist frequency

corresponding to half the bit rate of the input random data stream. This filtered signal is also ISI and jitter free. It is expected that this filter might find applications in low bit rate satellite communication systems.

2.2 Nyquist Pulses and Timing Jitter

Nyquist's three theorems on data transmission in a bandlimited channel stipulate the conditions for signal transmission without inter-symbol interference (ISI) [Bennet and Davey, 2.1]. Although an ideal brick-wall ($\alpha = 0$) Nyquist channel having minimum bandwidth assumes that there will be no ISI, it has found no practical applications. Not only is the infinite slope cutoff of the Nyquist filter unattainable because of the infinite number of sections which are needed to produce the required delay, but also its $\sin x/x$ type of impulse response is not desirable because of its slow rate of decay. One effect associated with this slow decay is that the resulting system has practically no margin for error in sampling times or other system perturbation.

The requirement of precise timing in the Nyquist minimum bandwidth system can be demonstrated by showing the large ISI that arises due to some slight timing errors [Bennett, 2.3]. In this section, this problem will be approached in a different way, by studying the eye width closure or the peak-to-peak jitter of the eye pattern which exists in the Nyquist minimum bandwidth system. Our approach can be used to plot the eye pattern and compute the eye width and the peak-to-peak jitter that arises from the superposition of the oscillating tails of the Nyquist pulses.

This method can also be used to compute the peak voltage of the bandlimited random signal which occurs between multiples of the bit

interval T. The occurrence of very high voltage peaks is another seriqus problem which also arises in the Nyquist minimum bandwidth system. As there is always a certain amount of nonlinearity exhibited in most of the practical transmission channels, the large fluctuation in the signal can cause severe performance degradation.

2.2.1 Peak-to-Peak Jitter

The impulse response of a raised cosine filter is:

$$s(x) = \frac{\sin(\pi x)}{(\pi x)} \quad \frac{\cos(\alpha \pi x)}{(1-\alpha^2 x^2)} \tag{2.1}$$

where, $x = \frac{t}{T}$ is the normalized time, with T being the bit interval.

and α is the rolloff factor of the raised-cosine filter.

In this section, this impulse response is defined as a Nyquist pulse whose Fourier transform is:

$$S(f) = \begin{cases} 1 & |f| \leq \frac{1}{2T}(1-\alpha) \\ \frac{1}{2}\left\{1-\sin\left[\frac{\pi T}{\alpha}\left(f-\frac{1}{2T}\right)\right]\right\} & \frac{1}{2T}(1-\alpha) \leq |f| \leq \frac{1}{2T}(1+\alpha) \end{cases} \tag{2.2}$$

As in [Bennet and Davey, 2.1], the spectral density of the Nyquist pulse $W_s(f)$ is related to its Fourier transform as follows:

$$W_s(f) = \frac{|S(f)|^2}{T} \tag{2.3}$$

A Nyquist pulse with $\alpha = 0$, 0.5 and 1, and its corresponding spectral density are shown in Figs. 2.1.a and 2.1.b. The Nyquist pulses, as defined in Eq. (2.1), contain the factor $\sin x/x$ which have zero values at $x = \pm n$ where $n = 1, 2, 3, \ldots$. As shown in Fig. 2, 1.b, the Nyquist pulse has a bandlimited spectrum and can also be called a frequency-limited pulse.

Conceptually, one way to generate a random synchronous data stream using Nyquist pulses as signaling elements is shown in Fig. 2.2. The data stream represented by the impulse trains is passed through a raised-cosine filter whose transfer function is given by Eq. (2.2). The output data stream is then formed of synchronously overlapping Nyquist pulses. The zero crossings of the oscillating tails of the Nyquist pulses assure that there will be no ISI at the sampling instants.

The main pulse lobe of the time-domain Nyquist pulse, as shown in Fig. 2.1.a., occupies a two-bit interval. Thus, when it is used as a signaling element in a random data stream which exhibits no ISI, it must overlap synchronously with the previous and future pulses as shown in Figs. 2.3. and 2.4. This means that the main pulse lobe of the Nyquist pulse representing the 1 or 0 symbol must start at the middle of the main pulse lobe of the previous pulse. The Nyquist pulse having a positive main pulse lobe, is used to represent the 1 symbol and the one having a negative main pulse lobe, is used to represent the 0 symbol. By signaling synchronously in this way, zero ISI at sampling instants is then guaranteed.

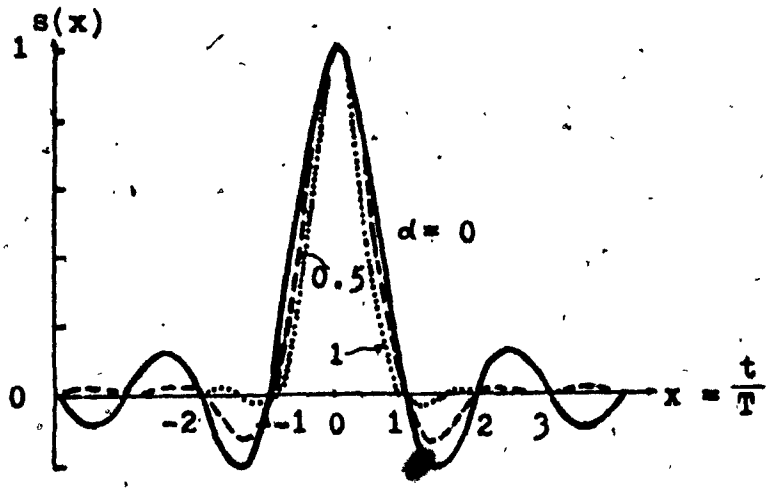

a.

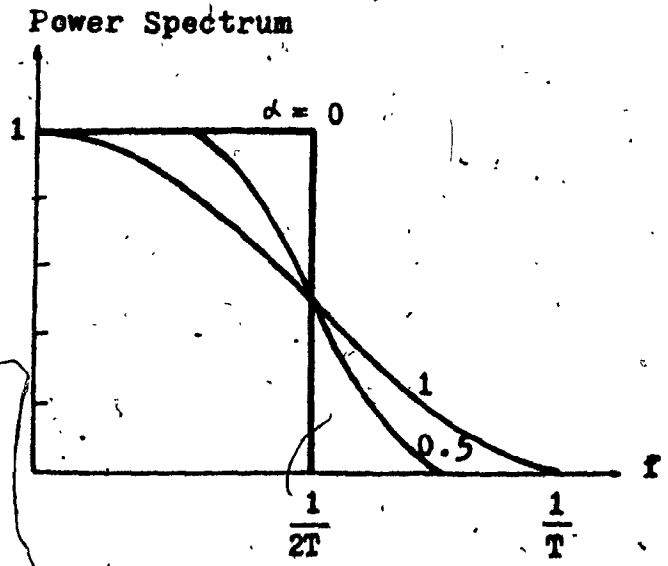

b

Fig. 2.1 a. Nyquist Pulses with $\alpha = 0, 0.5$ and 1

b. Corresponding Power Spectra

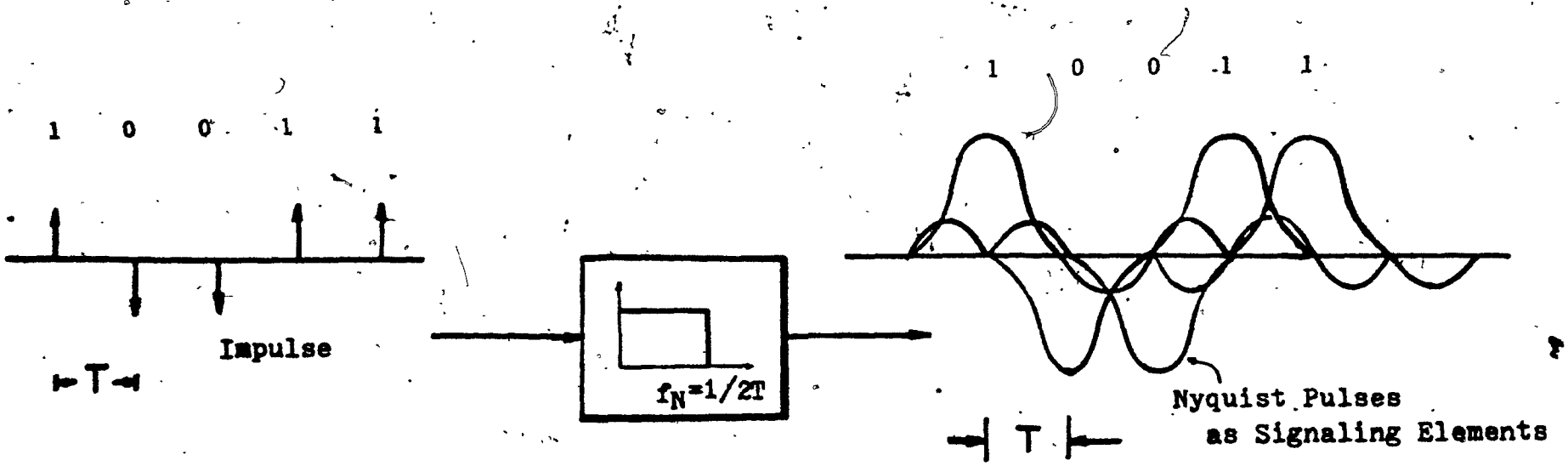

Fig. 2.2 Generation of a Random Data Stream Having Nyquist Pulses as Signaling Elements by Passing Impulse Train Through a Nyquist Filter

If the present bit is a 1 (represented by the solid line s(x) in Fig. 2. 3. a.) and the future bit is a 0 (represented by the dotted line -s(1-x) in the same figure, which is an inverted and shifted Nyquist pulse) then, the resultant signal waveform in the normalized time interval from 0 to 1 would be r(x) = (s(x) - s(1-x)) had there been no effect from the oscillating tails of the past and future pulses. In other words, for this case, it is assumed that the effect of the oscillating tails of the past and future pulses is cancelled, exerting zero effect on the resultant signal r(x), represented by curve R in Fig. 2. 3. a. This situation arises when the consecutive tails have the same values but opposite polarity as shown in the following four data patterns:

	n past bits	present bit	forthcoming bit	n future bits
(A)	....0 0 0 0 0 0	1	0	1 1 1 1 1 1.....
(B)	....1 1 1 1 1 1	1	0	0 0 0 0 0.....
(C)	....1 0 1 0 1 0	1	0	1 0 1 0 1 0.....
(D)	....0 1 0 1 0 1	1	0	0 1 0 1 0 1.....

(2. 4)

As an example, for the data pattern shown in row (A) which is depicted in Fig. 2. 3. a., the first oscillating tails of the pulses s(x+1) and s(x-2) in the normalized time interval from 0 to 1 have the same magnitudes but are of opposite signs. A similiar case exists with the second oscillating tails of the pulses s(x+2) and s(x-3) and so on. This means

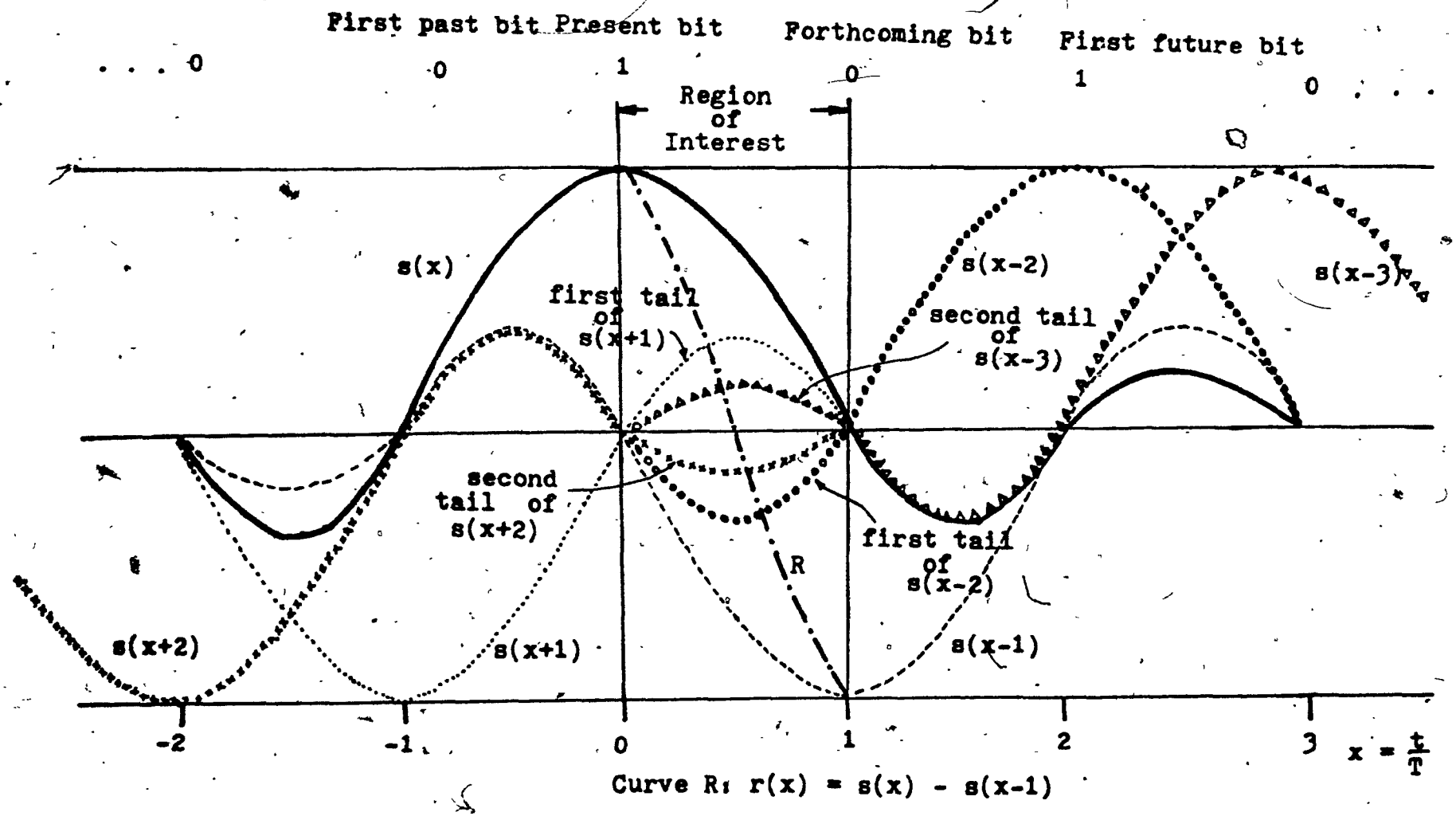

Fig. 2.3.a Example Illustrating the Generation of Curve R from the Data Pattern .... 0 0 1 0 1 1 1 .... Having Nyquist Pulses as Signaling Elements

that the oscillating tails of the past pulses and the future pulses (excluding the forthcoming bit which is assumed to be '0') are subtracting each other. The net effect due to these oscillating tails, in the region of interest for $0 \leq x \leq 1$, is thus null. This is represented by curve R in Fig. 2.3.a. For the data patterns shown in rows (B), (C) or (D), similiar subtracting effect among the oscillating tails of the past and future pulses also yields curve R.

On the other hand, if there is some effect from the oscillating tails of the past and future pulses, the resultant signal waveform in the normalized time interval $0 \leq x \leq 1$ is then shifted either to the left or right of curve R. The maximum amount of shifting to the left or right of curve R can be found by studying the worst data patterns as follows:

The maximum shift to the left (curve A in Fig. 2.3b.)

This situation arises for an input data pattern such as:

$$\underbrace{\ldots.0\,1\,0\,1\,0\,1}_{\text{n past bits}} \quad \underbrace{(1)}_{\text{present bit}} \quad \underbrace{(0)}_{\substack{\text{forth-}\\\text{coming}\\\text{bit}}} \quad \underbrace{1\,0\,1\,0\,1\,0\ldots..}_{\text{n future bits}} \qquad (2.5)$$

In this case, the oscillating tails of the n past bits and of the n future bits all have negative values. The effect of the resulting sum of the oscillating tails of the past and future pulses is such that it subtracts the highest possible amount (worst combination) from curve R in the normalized time interval of $0 \leq x \leq 1$.

The resultant signal shape a(x), as represented by curve A in Fig. 2.3.b, is calculated from the following formula:

$$a(x) = r(x) - \left[\text{the sum of the oscillating tails of the past and future pulses}\right]$$

$$= s(x) - s(1-x) + s(x+1) + s(x-2) - s(x+2) + s(x-3) + s(x+3) + s(x-4) - s(x+4) + s(x-5) + \ldots\ldots \quad \text{for } 0 \leq x \leq 1 \qquad (2.6)$$

Notice that s(x+1) and s(x-2) both have negative values for $0 \leq x \leq 1$ while s(x+2) and s(x-3) are positive. Similarly, s(x+3) and s(x-4) are negative while s(x+4) and s(x-5) are positive. And so on.

In Eq. (2.6), the terms in the first bracket represent the resultant signal waveform (curve R) of the main pulse lobes of the present bit and the forthcoming bit if the effect of the oscillating tails of the past and other future pulses is assumed to be non-existent. The two terms in the second bracket are due to the first oscillating tails of the first past pulse and the second forthcoming pulse if the definition given in Eq. (2.5) is adopted. The two terms in the third bracket are due to the second oscillating tails of the second past pulse and the second future pulse. Extending further, this explanation can be applied to the other terms in the infinite series (2.6). It is seen that in this case all these

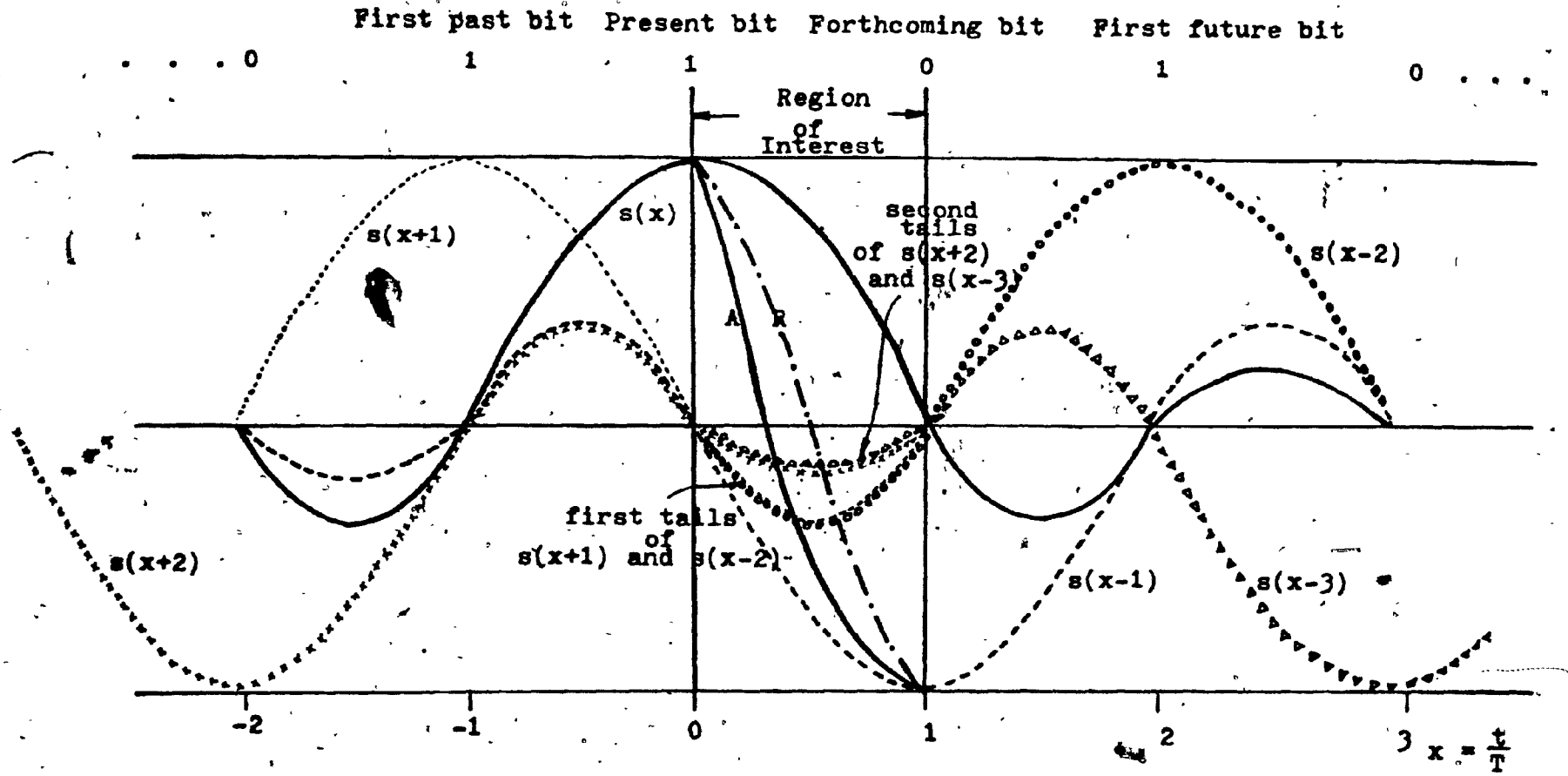

Curve A: $a(x) = s(x) - s(x-1) + s(x+1) + s(x-2) - s(x+2) + s(x-3) + \ldots\ldots\ldots$

Fig. 2.3.b Example Illustrating How Curve R is Shifted to Curve A due to the Effect of the Oscillating Tails of the Past and Future Nyquist Pulses

terms are subtractive from the two terms in the first bracket. Any data pattern other than that of Eq. (2.5) will shift the curve R somewhat less than that of curve A as the resulting effect of the oscillating tails of the past and future pulses becomes less subtractive. For practical purposes, it is only essential to know the maximum shift as this gives the peak-to-peak timing jitter.

The maximum shift to the right (curve B in Fig. 2.3.c)

Contrary to the previous case, if the effect of the oscillating tails of the past and future pulses (excluding again the forthcoming bit) is to add the highest possible amount to curve R, then, curve R will be shifted to the extreme right, resulting in curve B. This arises when we have an input data pattern such as:

$$\underbrace{.....101010}_{\text{n past bits}} \quad \underbrace{(1)}_{\text{present bit}} \quad \underbrace{(0)}_{\text{forth-coming bit}} \quad \underbrace{010101.....}_{\text{n future bits}} \tag{2.7}$$

In this case, the resultant signal wave form b(x) represented by curve B in Fig. 2.3.c can be calculated from the following formula:

$$b(x) = r(x) + \left[\text{the sum of the oscillating tails of the past and future pulses}\right]$$

$$= s(x) - s(x-1) - s(x+1) + s(x-2) + s(x+2) + s(x-3) - s(x+3) + s(x-4) + s(x+4) + s(x-5) - \ldots\ldots \quad \text{for } 0 \leq x \leq 1 \tag{2.8}$$

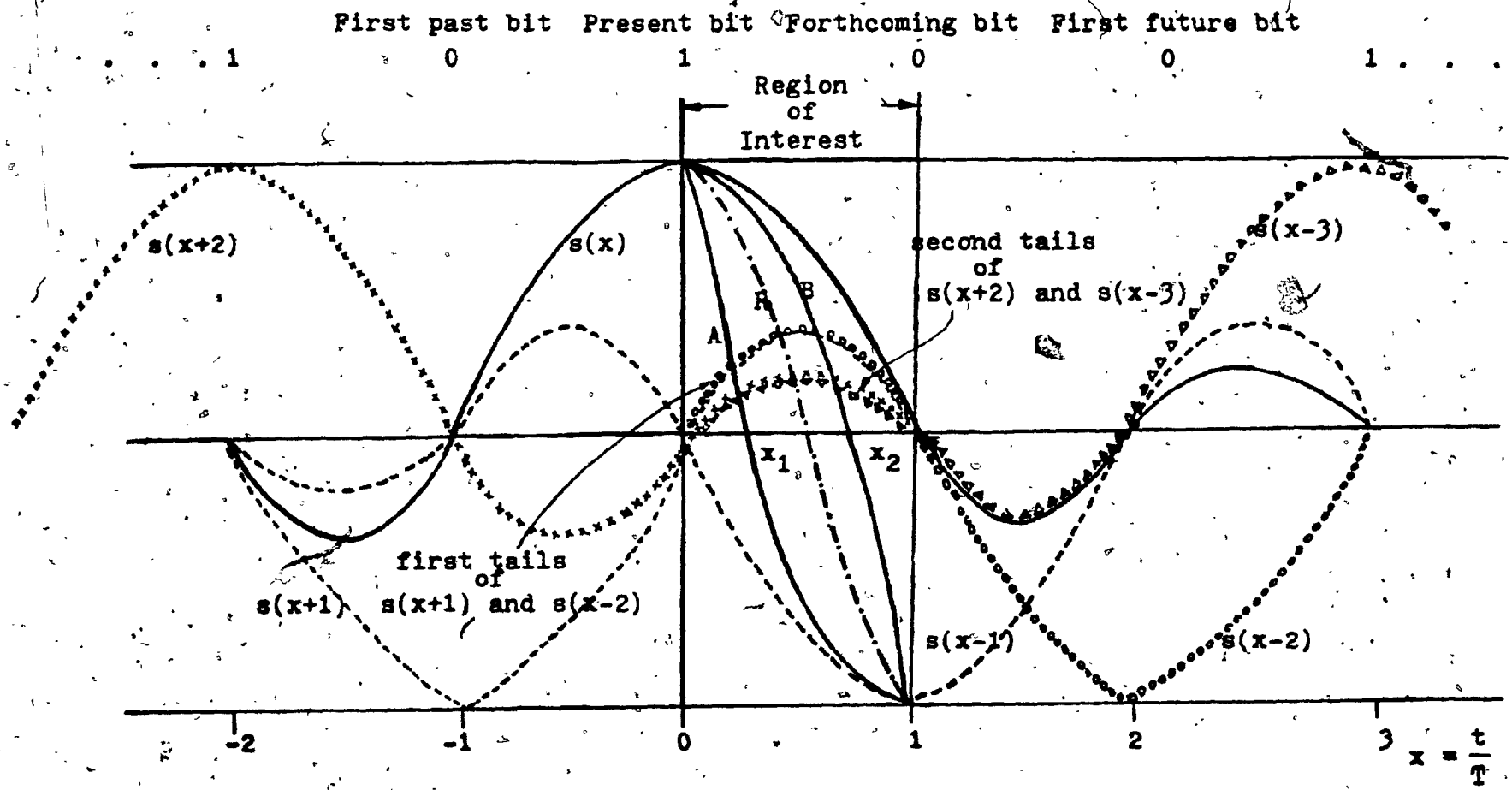

Fig. 2.3.c Example Illustrating How Curve A is Shifted to Curve B due to the Effect of the Oscillating Tails of the Past and Future Nyquist Pulses

From the zero crossings of curves A and B (x_1 and x_2 shown in Fig. 2.3.c respectively) and due to the symmetry of the eye pattern, the peak-to-peak jitter J_{pp} is given by:

$$J_{pp} = \text{peak-to-peak jitter} = (x_2 - x_1) \cdot 100\% \qquad (2.9)$$

where,

x_1 and x_2 are obtained by computing the roots of Eqs. (2.6) and (2.8) or by plotting point by point the functions a(x) and b(x). The peak-to-peak jitter J_{pp} for random data streams using Nyquist pulses with different α's as signaling elements will be computed and compared with the measured results in Section 2.2.3.

Another parameter that is frequently used in describing the characteristics of the eye pattern is the eye width. The eye width, which is also known as the horizontal eye opening, is defined as:

$$E_w = 1 - J_{pp} \qquad (2.10)$$

2.2.2. Amplitude Fluctuations: Overshoot and Undershoot

Following the discussion given in the previous section, it is found that when the Nyquist pulses are used as signaling elements in a random data stream, the peak-to-peak jitter in the zero crossings of the eye pattern of the resulting data stream can be computed by considering the worst input data patterns. In this section, the amplitude fluctuations of the resulting data stream will be studied using a similar approach to that described in the previous section.

In the following analysis, the present bit will again be assumed to be 1 and the forthcoming bit will also be assumed to be 1. The resultant signal waveform in the interval $0 \leq x \leq 1$ would then be $q(x) = s(x) + s(x-1)$ had there been no effect from the oscillating tails of the previous and future pulses. This situation arises if one of the following data pattern occurs:

	n past bits	present bit	forthcoming bit	'n' future bits
(A)	..... 0 1 0 1 0 1	1	1	0 1 0 1 0 1 .....
(B)	..... 1 0 1 0 1 0	1	1	1 0 1 0 1 0 .....
(C)	..... 1 1 1 1 1 1	1	1	0 0 0 0 0 0 .....
(D)	..... 0 0 0 0 0 0	1	1	1 1 1 1 1 1 .....

(2.11)

As an example, in the case of the data patterns shown in row (A), which is depicted in Fig. 2.4.a, the first oscillating tails of the pulses $s(x+1)$ and $s(x-2)$ in the normalized time interval from 0 to 1 have the same magnitude but are of opposite signs. A similar case exists with

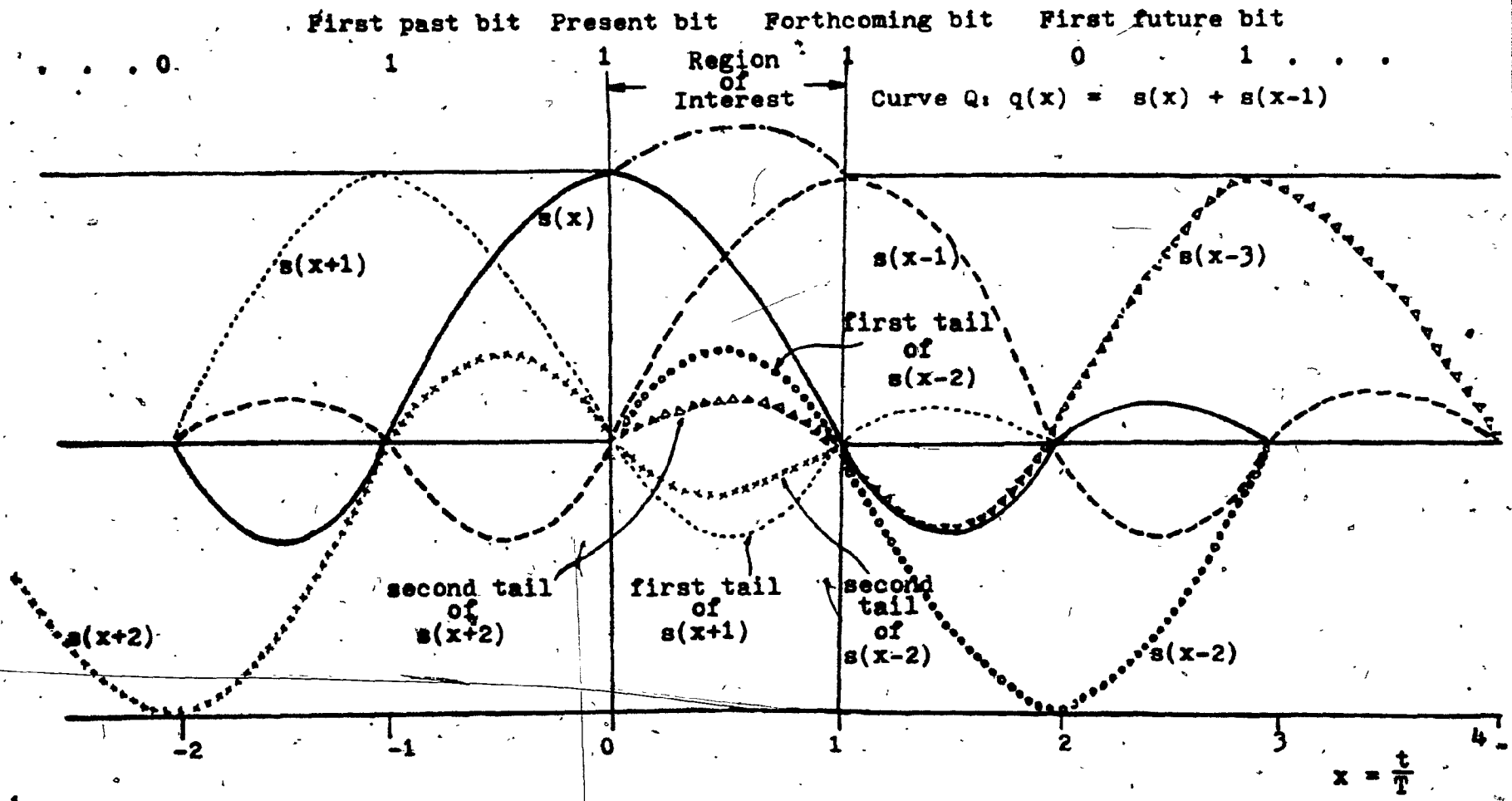

Fig. 2.4.a Example Illustrating the Generation of Curve Q from the Data Pattern ... 0 1 1 1 0 1 .... Having Nyquist Pulses as Signaling Elements

the second oscillating tails of the pulses s(x+2) and s(x-3) and so on. This means that the oscillating tails of the past and future pulses (excluding the forthcoming bit, which is assumed to be 1) are subtracting each other. The net effect due to these oscillating tails in the region of interest for $0 \leq x \leq 1$ is thus null. This situation gives curve Q of Fig. 2.4.a. For the data patterns shown in rows (B), (C) and (D), similar subtracting effects among the oscillating tails of the past and future pulses also yield curve Q.

In a similar manner as the shifting of curve R to its left or right, curve Q is shifted upward or downward if there is some effect from the oscillating tails of the past and future pulses in the normalized time interval $0 \leq x \leq 1$. The maximum amount of shifting upward or downward of curve Q can again be found by studying the worst data patterns.

The maximum amount of shift upward (Overshoot):

This situation arises when the oscillating tails of the past and future pulses add the highest possible amount to curve Q. The input data pattern for such a case is given by:

$$\underbrace{.....010101}_{\text{n past bits}} \quad \underbrace{1}_{\substack{\text{present}\\ \text{bit}}} \quad \underbrace{1}_{\substack{\text{forth-}\\ \text{coming}\\ \text{bit}}} \quad \underbrace{010101.....}_{\text{'n future bits}} \qquad (2.12)$$

As shown in Fig. 2.4.b, the oscillating tails of the past and future pulses are all additive. Therefore the effect of the oscillating

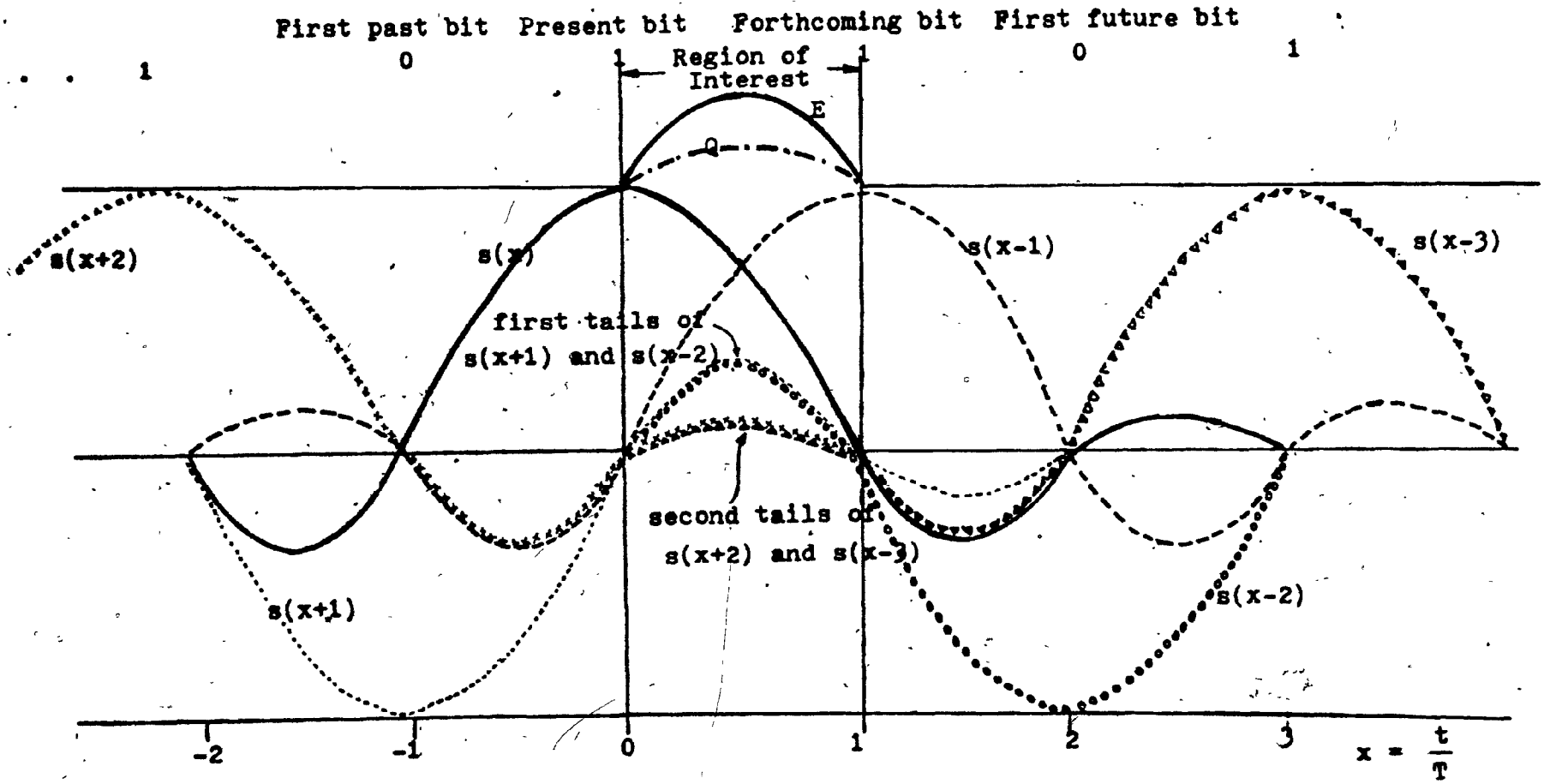

Fig. 2.4.b Example Illustrating How Curve Q is Shifted to Curve E due to the Effect of the Oscillating Tails of the Past and Future Nyquist Pulses

tails of the past and future pulses is such that it shifts curve Q most upward in the normalized time interval $0 \leq x \leq 1$.

The equation $e(x)$ represented by curve E in Fig. 2. 4. b for maximal overshoot is calculated based on the following formula:

$$e(x) = q(x) + \left[\text{the sum of the oscillating tails of the past and future pulses}\right]$$

$$= s(x) + s(x-1) + s(x+1) + s(x-2) - s(x+2) + s(x-3) + s(x+3) + s(x-4) - s(x+4) + s(x-5) + \ldots\ldots \quad \text{for } 0 \leq x \leq 1 \tag{2.13}$$

The peak overshoot voltage, which will be used later on as a measure of amplitude fluctuations of the signal having the Nyquist pulses as signaling elements, is defined as:

$$P_{overshoot} = (\text{Maximum Value of curve E}) - 1 = e\left(\tfrac{1}{2}\right) - 1 \text{ volt} \tag{2.14}$$

The maximum amount of shift downward (undershoot)

This situation is contrary to that described in the overshoot case. In this situation the effect of the oscillating tails of the past and future pulses becomes most subtractive. The maximum shift downward of curve Q occurs if the following data pattern occurs:

$$\underbrace{\ldots\ldots\ 0\ 1\ 0\ 1\ 0\ 1}_{\text{n past bits}} \quad \underset{\text{present bit}}{(1)} \quad \underset{\substack{\text{forth-}\\\text{coming}\\\text{bit}}}{(i)} \quad \underbrace{1\ 0\ 1\ 0\ 1\ 0\ \ldots\ldots}_{\text{n future bits}} \tag{2.15}$$

The resultant signal waveform f(x) represented by curve F, as shown in Fig. 2. 4. c, is calculated from the following formula:

$$\begin{aligned} f(x) &= q(x) - \left[\text{the sum of the oscillating tails of the past and future pulses}\right] \\ &= s(x) + s(x-1) + s(x+1) + s(x-2) \\ &\quad - s(x+2) + s(x-3) \\ &\quad + s(x+3) + s(x-4) \\ &\quad - s(x+4) + s(x-5) \\ &\quad + \ldots\ldots \qquad \text{for } 0 \leq x \leq 1 \end{aligned} \tag{2.16}$$

2. 2. 3. Eye Diagram

In this section, the boundaries of an eye diagram are derived by computing Eqs. (2. 6), (2. 8), (2. 13) and (2. 16). This information enables the system engineer to study the distortion of the signal caused by the imperfections of the designed jitters.

Using the four curves A, B, E and F shown in Figs. 2. 3. b, 2. 3. c, 2. 4. b and 2. 4. c, the eye diagram of the synchronous random data stream which uses the Nyquist pulses as signaling elements, can be constructed as shown in Fig. 2. 5. a. For illustrative purposes, the case for the $\alpha = 0.3$ Nyquist pulse is used.

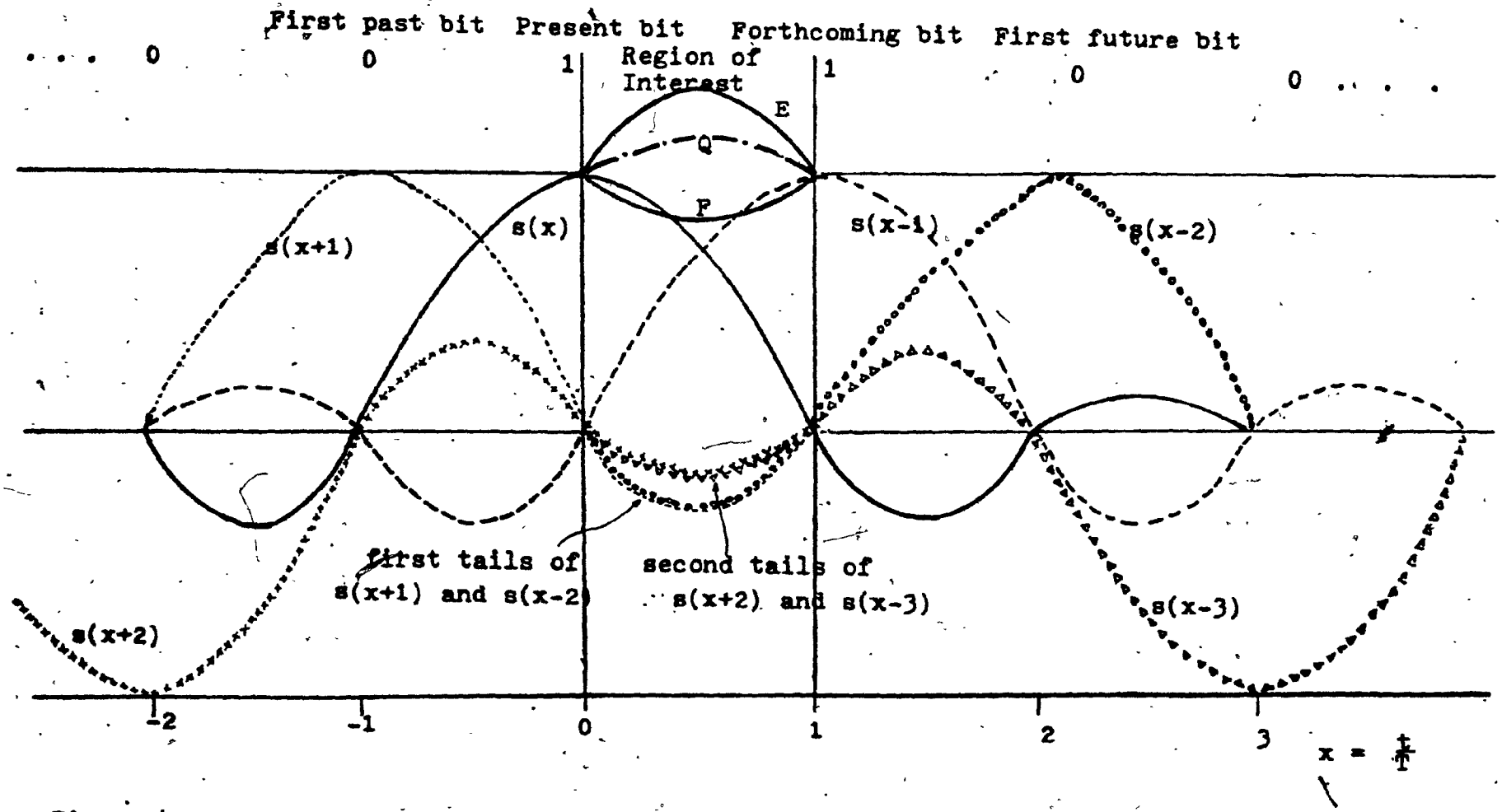

Fig. 2.4.c Example Illustrating How Curve Q is Shifted to Curve F due to the Effect of the Oscillating Tails of the Past and Future Nyquist Pulses

Curves A, B, E and F are used to sketch one fourth of the eye diagram. The curves marked A', B', E', and F' in the normalized time interval $-1 \leq x \leq 0$ are the mirror images of curves A, B, E, and F. The eight curves marked $\bar{A}$, $\bar{B}$, $\bar{E}$, $\bar{F}$, $\bar{A}'$, $\bar{B}'$, $\bar{E}'$, and $\bar{F}'$ are the mirror images of curves A, B, E, F, A', B', E', and F' about the horizontal time axis. In this manner, the boundaries of the complete eye diagram can be constructed by virtue of the symmetry of the eye.

In a similar manner, the boundary of the eye diagram for the case when the $\alpha = 0.4$ Nyquist pulses are used in a synchronous random data stream can be constructed as shown in Fig. 2.5.b.

These eye diagrams show that in the center of the eye there is a 100% opening. This means that there is no ISI if the signal is sampled there. Due to the effect of the oscillating tails of the Nyquist pulses, a 38% peak-to-peak timing jitter occurs in the eye diagram of the data stream formed of the $\alpha = 0.3$ Nyquist pulses and a 26% peak-to-peak jitter occurs in the case of the $\alpha = 0.4$ Nyquist pulse.

The eye diagrams plotted in Fig. 2.5 are constructed based on the assumption that the effect of the oscillating tails comes only from six past pulses and six future pulses, i.e., n=6 in (2.5), (2.9), (2.12) and (2.15). The effect of the oscillating tails of the other past and future pulses is assumed to be nil in the calculation.

In order to analyze the validity of this assumption, the probability

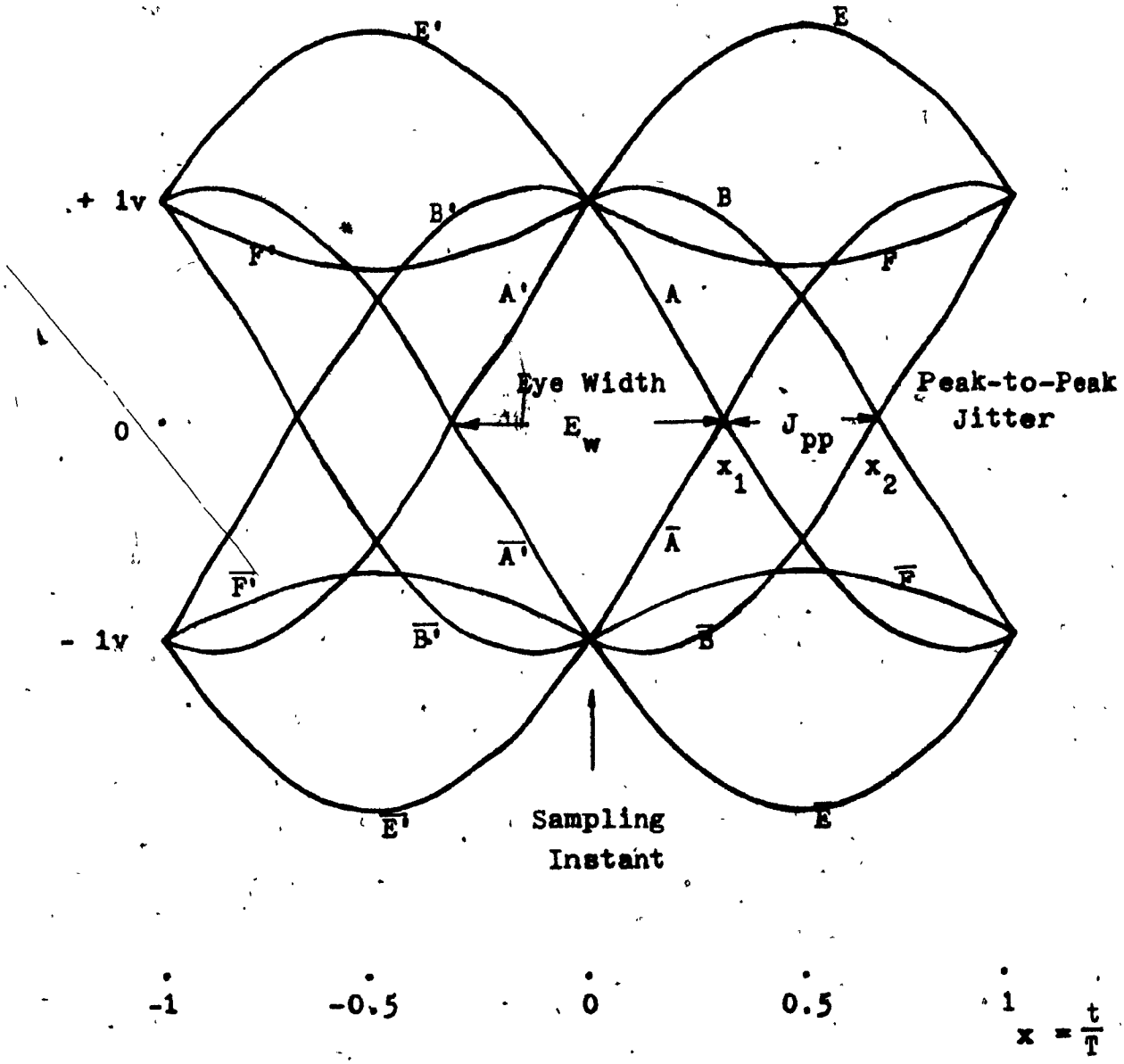

Fig. 2.5.a Eye Diagram of a Random Data Stream Using the $\alpha = 0.3$ Nyquist Pulses as Signaling Elements

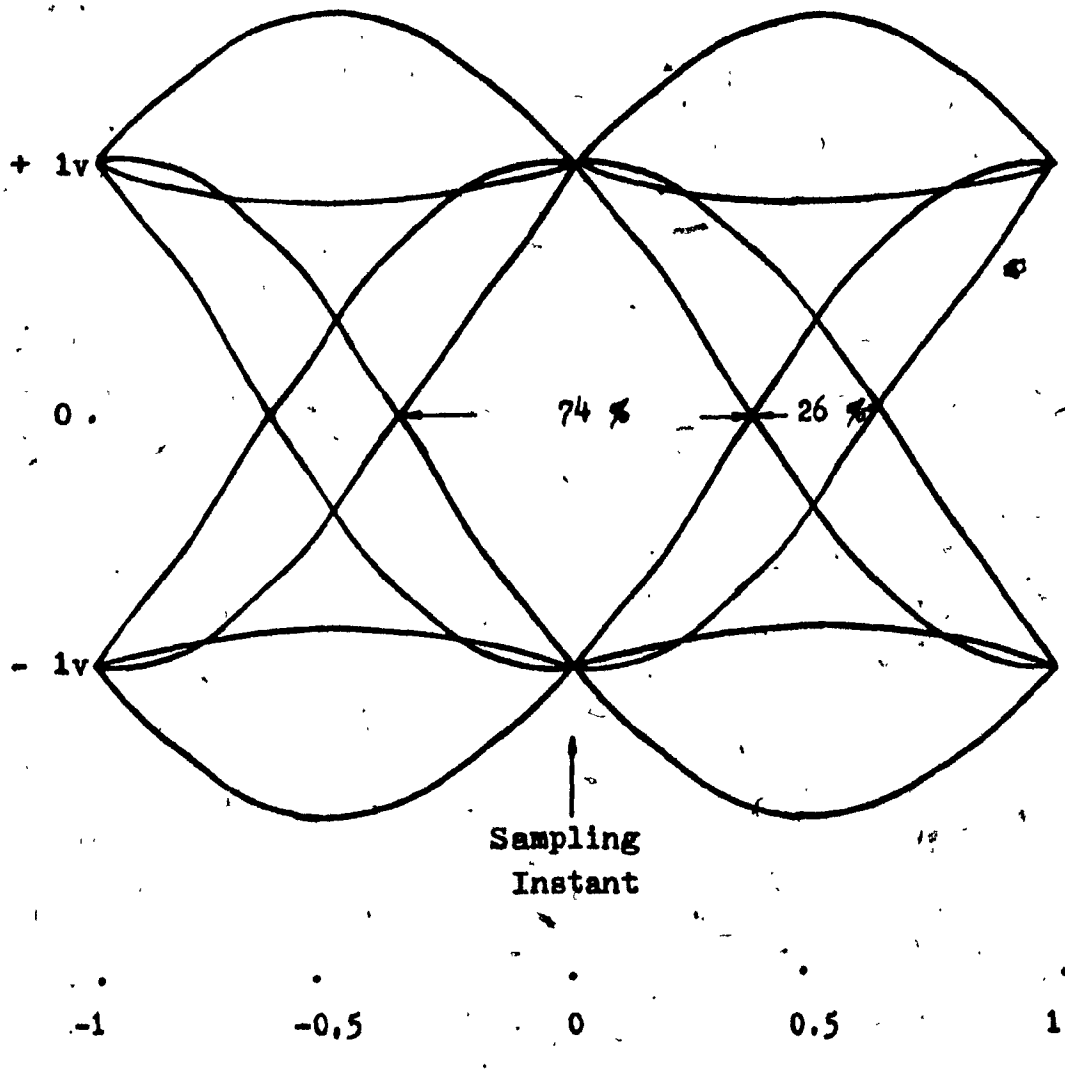

Fig. 2.5.b Eye Diagram of a Random Data Stream Using the $\alpha = 0.4$ Nyquist Pulses as Signaling Elements

of the occurrence of the worst input data pattern, such as that for curve A, will be considered first.

The input data pattern for curve A as previously defined is given by:

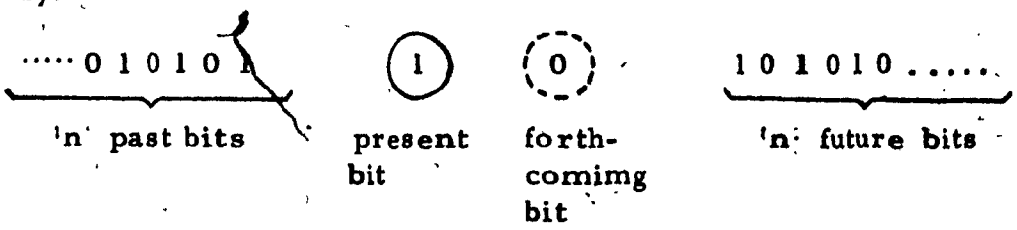

(2.5)

As in most transmission systems where scrambled data is used, the probability that symbol 1 or 0 occurs is equiprobable and is equal to $\frac{1}{2}$. Hence, the probability that the present bit is 1 and the forthcoming bit is 0, i.e., the probability of the occurrence of the pattern 1 0, becomes $\frac{1}{4}$. The probability that the first previous and the first future bits are both 1 as shown in (2.5), i.e., the probability of occurrence of the data pattern to be 1 1 0 1, is further reduced to $\frac{1}{16}$. In a similar manner, the probability for the data pattern 0 1 1 0 1 0 to occur is then $\frac{1}{64}$ and so on. Thus the probability that the data pattern shown in (2.5) will occur decreases with increasing "n". From the symmetry of the eye diagram constructed earlier in Fig. 2.5.a., it is seen that curve A is only part of the inner boundary trace. Therefore the probability of occurrence with very large n in the data pattern of Eq. (2.5) is further reduced.

Even though the probability of occurrence of the worst data pattern with very large n past and n future pulses in the data pattern of Eq. (2.5)

becomes increasingly small in a random data stream. It is worthwhile to study the convergence of the infinite series that represents the worst case. For this purpose, in the case of the $\alpha = 0$ Nyquist pulses, the behaviour of Eq. (2.6) for large n is mathematically tested for convergence or divergence. In the other cases when $\alpha \neq 0$ Nyquist pulses are used, the behaviour of Eq. (2.6) for large n is studied by computer calculation.

In the case when the $\alpha = 0$ Nyquist pulses are used, curve A from Eq. (2.6) is given by:

$$a(x) = \frac{\sin \pi x}{\pi x} - \frac{\sin \pi(x-1)}{\pi(x-1)} + \frac{\sin \pi(x+1)}{\pi(x+1)} + \frac{\sin \pi(x-2)}{\pi(x-2)} - \frac{\sin \pi(x+2)}{\pi(x+2)} + \frac{\sin \pi(x-3)}{\pi(x-3)} + \frac{\sin \pi(x+3)}{\pi(x+3)} + \frac{\sin \pi(x-4)}{\pi(x-4)} - \frac{\sin \pi(x+4)}{\pi(x+4)} + \frac{\sin \pi(x-5)}{\pi(x-5)} + \cdots\cdots \quad \text{for } 0 \leq x \leq 1 \tag{2.17}$$

In the range of interest for $0 \leq x \leq 1$ as shown in Fig. 2.3a,

$$\frac{\sin \pi(x+1)}{\pi(x+1)} = \frac{\sin \pi(x-2)}{\pi(x-2)}$$

$$\frac{\sin \pi(x+2)}{\pi(x+2)} = \frac{\sin \pi(x-3)}{\pi(x-3)}$$

Thus a(x) can be re-written as:

$$a(x) = \frac{\sin \pi x}{\pi x} - \frac{\sin \pi(x-1)}{\pi(x-1)} + 2\,\frac{\sin \pi(x+1)}{\pi(x+1)} - \frac{\sin \pi(x+2)}{\pi(x+2)} + \frac{\sin \pi(x+3)}{\pi(x+3)} + \cdots\cdots\cdots$$

$$= \frac{\sin x}{\pi}\left(\frac{1}{x} + \frac{1}{x-1}\right) - 2\left(\frac{1}{x+1} + \frac{1}{x+2} + \frac{1}{x+3} + \frac{1}{x+4} + \cdots\cdots\right) \quad \text{for } 0 \leq x \leq 1$$

Denoting:

$$T(x) = \frac{1}{x+1} + \frac{1}{x+2} + \frac{1}{x+3} + \frac{1}{x+4} + \cdots\cdots\cdots \qquad (2.17a)$$

and since for $0 \leq x \leq 1$

$$\frac{1}{x+1} \geq \frac{1}{2}$$

$$\frac{1}{x+2} \geq \frac{1}{3}$$

$$\frac{1}{x+3} \geq \frac{1}{4}$$

$$\frac{1}{x+4} \geq \frac{1}{5}$$

$$\vdots \qquad \vdots$$

Hence, $T(x) = \frac{1}{x+1} + \frac{1}{x+2} + \frac{1}{x+3} + \frac{1}{x+4} + \cdots\cdots\cdots$

$$\geq \frac{1}{2} + \frac{1}{3} + \frac{1}{4} + \frac{1}{5} + \cdots\cdots + \frac{1}{n} + \cdots$$

$$\geq \int_2^n \frac{dx}{x}$$

$$= \ln x$$

$$= \ln n - \ln 2 \qquad (2.18)$$

Hence for very large n, $T(x)$ diverges for $0 \leq x \leq 1$. In other words, in the extreme case of the data sequence shown in (2.5), curve R is shifted downwards towards $-\infty$ and has its zero crossing at $x = \pm \epsilon$,

where ϵ is infinitesimally small. In a similar manner, for the data sequence shown in (2.7), curve R is shifted upward towards $+\infty$ and has its zero crossing at $x=(1-\epsilon)$. This means that in the worst case the peak-to-peak jitter is 100%. In other words, the eye width as shown in Fig. 2.6 is zero in this extreme case.

Nevertheless, at the sampling instant (x=0), the vertical eye opening is still 100% as stipulated by Nyquist's theorem. This means that there is no ISI at the sampling instants. Any slight timing perturbation renders the system inoperable as there is zero eye width. In other words, the eye opening is closed at slight sampling time offset.

In simple terms, the margin for sampling timing error in the Nyquist minimum bandwidth system is practically zero. This means that a slight increase in the transmitted data rate through the brick-wall Nyquist channel will completely close the eye opening. Equivalently, we can say that a slight bandwidth reduction of the Nyquist filter will induce severe performance degradation to the transmission system.

In any practical transmission system, $\alpha > 0$ Nyquist filters are always used. For these filters, it is shown in the following paragraphs that the maximum shifts and overshoots do converge. For this purpose it is sufficient to show this convergence by means of computer. This approach has been taken in order to have a means of computing peak-to-peak jitter for these practical filters.

Fig. 2.7 shows the computed peak-to-peak jitter and eye width as a function of the number n shown in Eqs. (2.5) and (2.7). In this

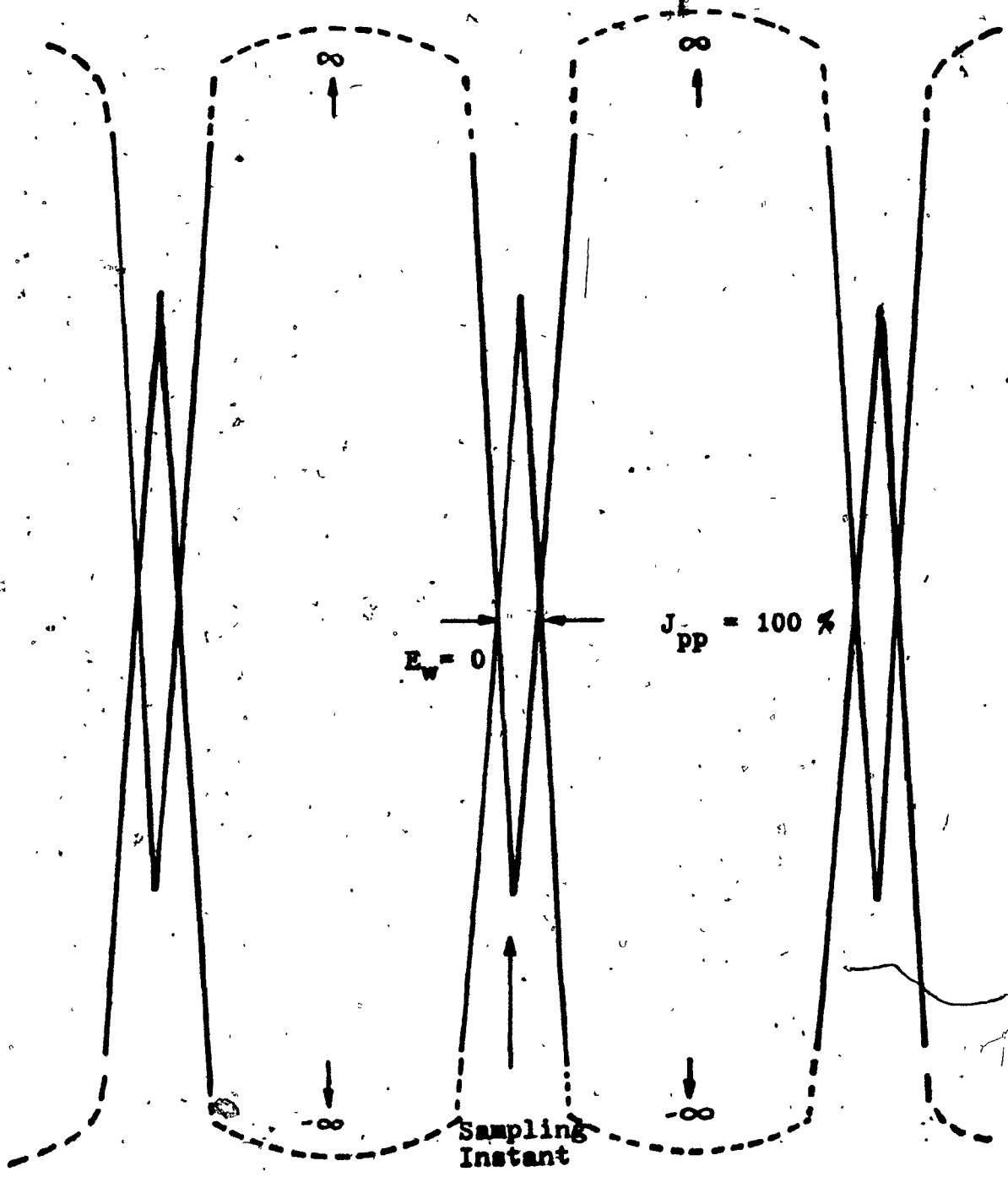

Fig. 2.8 Eye Diagram of a Random Data Stream Using the $\alpha = 0$ Nyquist Pulses as Signaling Elements

(Very Large n Assumed)

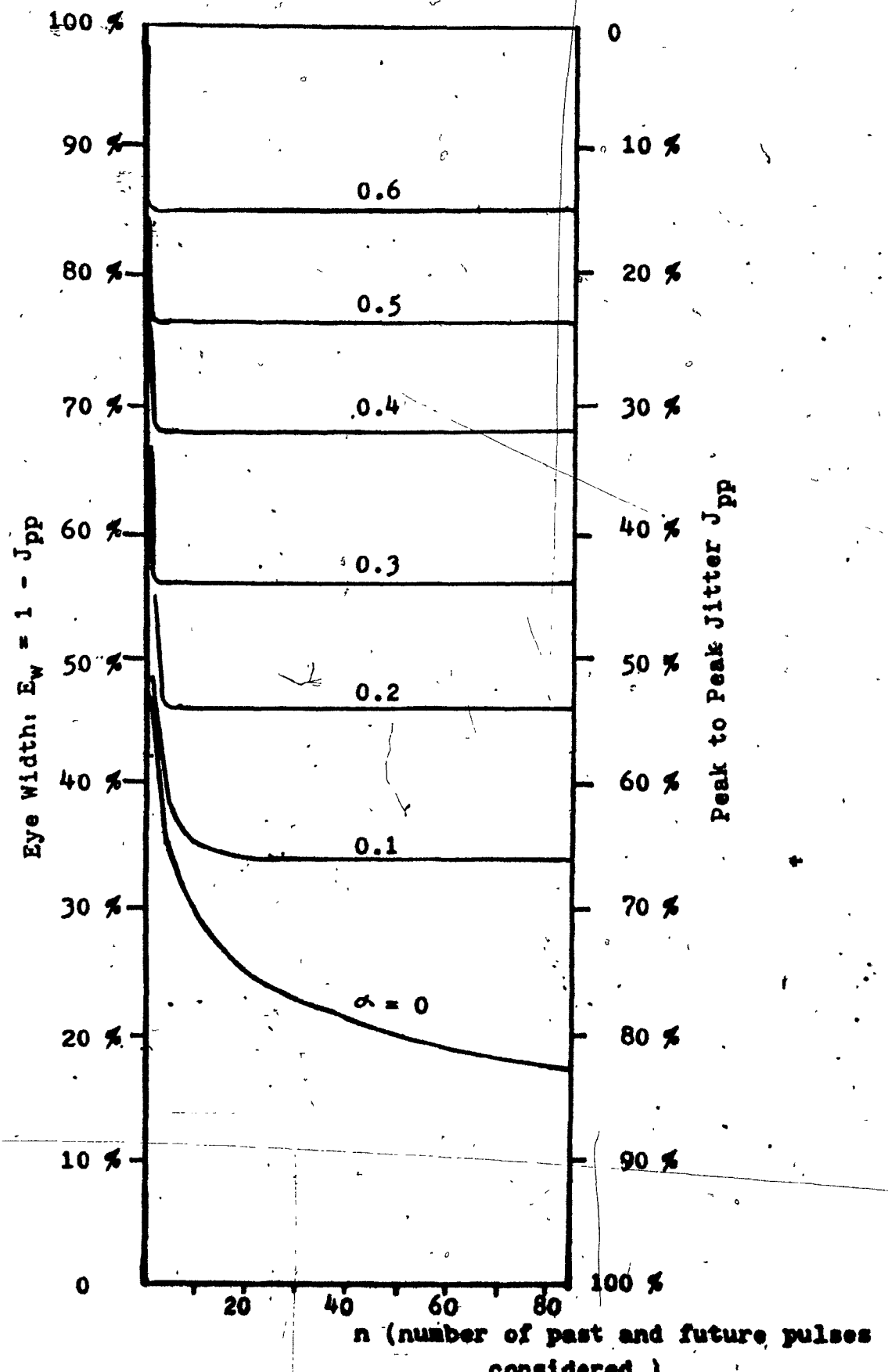

Fig. 2.7 Eye Width and Peak to Peak Jitter as a Function of n

figure, α is used as a parameter. The assumed data stream is the two worst-case sequences defined in Eqs. (2.5) and (2.7). The results represent the upper bound of the peak-to-peak jitter. We observe that the dependence of peak-to-peak jitter (or eye width) on the number 'n' diminishes with increasing α. On the other hand, for the $\alpha = 0$ Nyquist pulses, this dependence becomes quite significant. In the extreme case the peak-to-peak jitter becomes 100% as described earlier.

Fig. 2.8 shows the dependence of peak-to-peak jitter and eye width on α for different numbers of 'n'. When large 'n' is considered, the peak-to-peak jitter starts to change more significantly with decreasing α. For $\alpha > 0.5$, this dependence becomes almost unnoticeable.

The eye diagrams for the case of $\alpha = 0$ Nyquist pulses using both n=6 and n=80 are plotted in Figs. 2.9.a and 2.9.b, respectively. These two eye diagrams show the relative peak-to-peak jitter and amplitude variations of the resulting signal when the $\alpha=0$ Nyquist pulses as signalling elements. In the case of n=6, the eye diagram has a peak-to-peak jitter of 60% while in the case of n=80, the peak-to-peak jitter appearing in the eye diagram increases to 82%.

Figs. 2.10.a and 2.10.b show measured eye diagrams of two 7th order elliptical filters which approximate $\alpha=0.3$ and $\alpha=0.4$ Nyquist filters respectively.

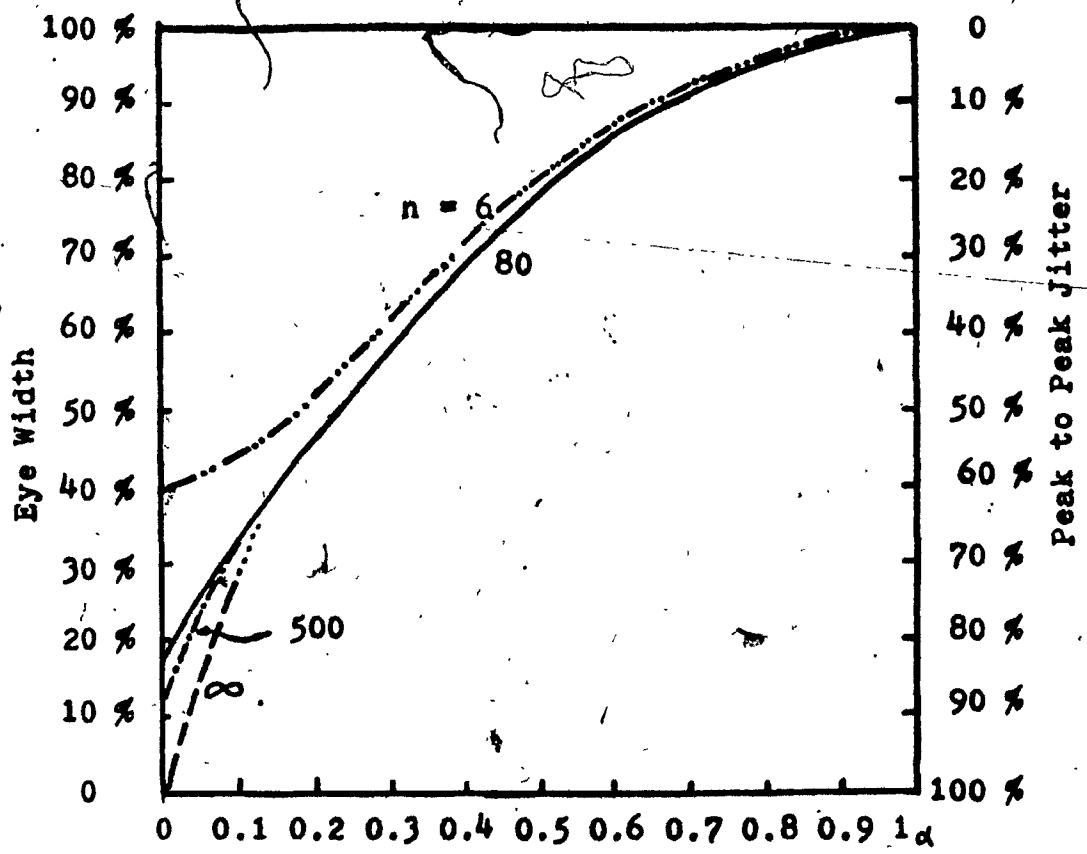

Fig. 2.8 Eye Width and Peak to Peak Jitter as a Function of α Using n as a Parameter for a Random Data Stream Having Nyquist Pulses as Signaling Elements

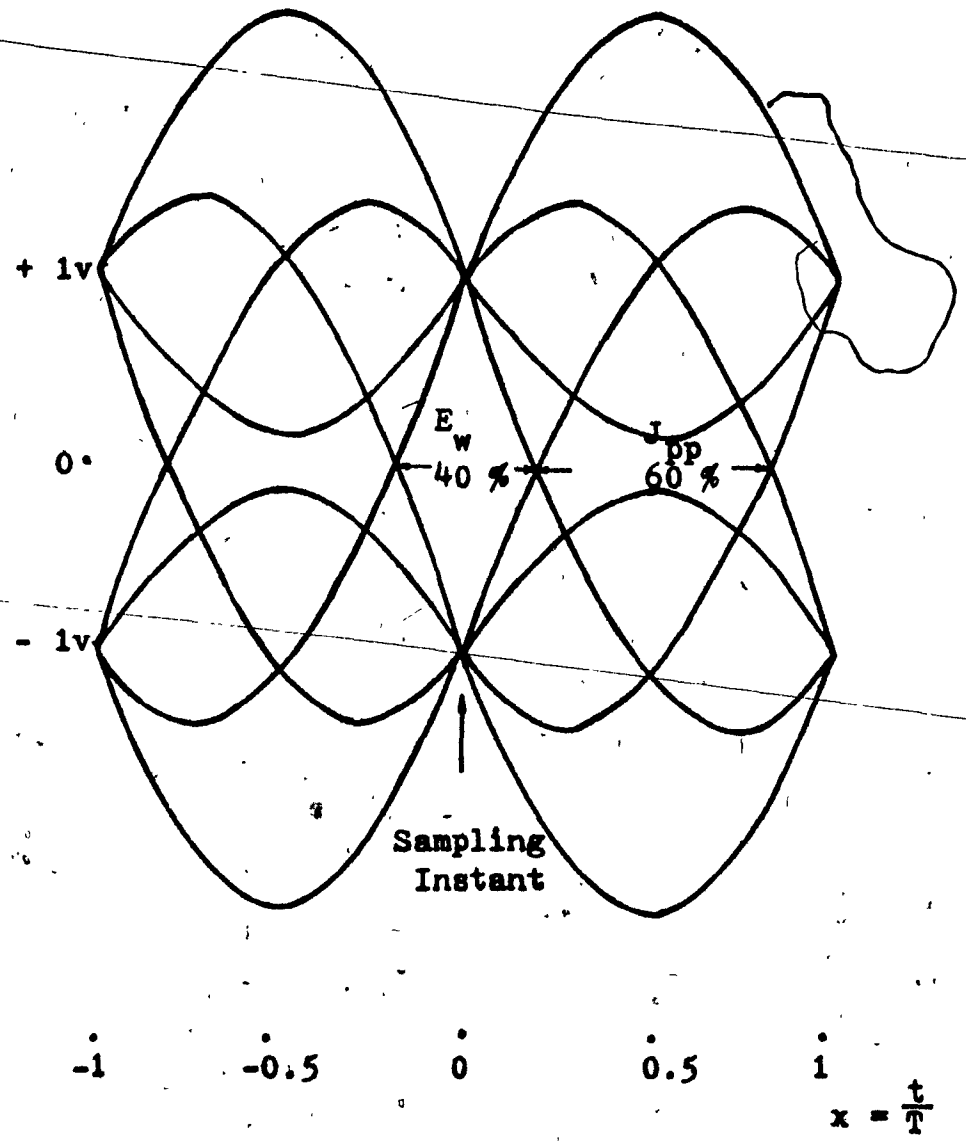

Fig. 2.9.a Eye Diagram of a Random Data Stream Having $\alpha = 0$ Nyquist Pulses as Signaling Elements (Number of Past and Future Bits Considered, n = 6)

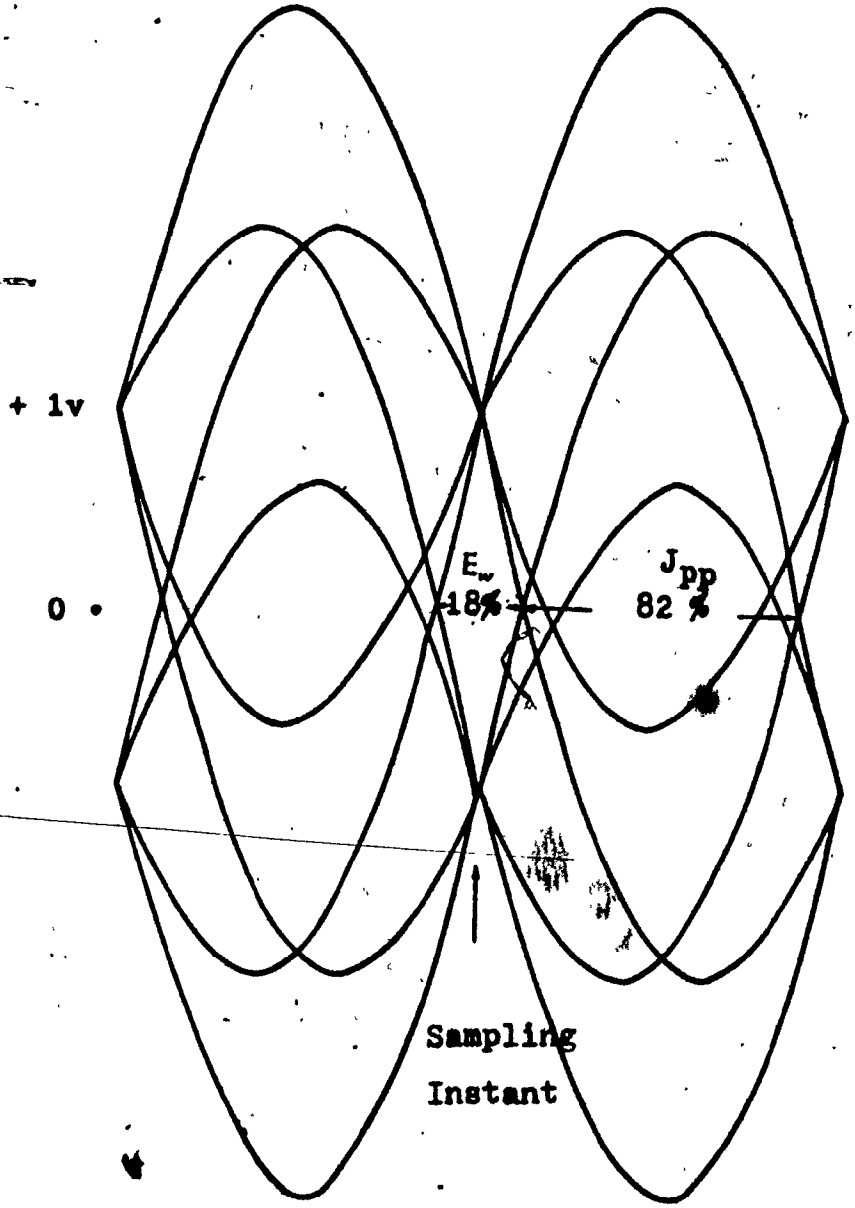

Fig. 2.9.b Eye Diagram of a Random Data Stream Having $\alpha = 0$ Nyquist Pulses as Signaling Elements (Number of Past and Future Bits Considered, n = 80)

For the $\alpha = 0.3$ Nyquist filter, the measured eye diagram shown in Fig. 2.10.a has a peak-to-peak jitter of approximately 41% while the computed peak-to-peak jitter of the eye diagram for the $\alpha = 0.3$ Nyquist pulses is 38% in the case of n=6 (Fig. 2.4.a) and 42% in the case of n=80 (from Fig. 2.7). In [El-Torky and Feher, 2.4], the computer-simulated eye diagram for $\alpha = 0.3$ Nyquist filter shows a peak-to-peak jitter of about 38%.

The laboratory measured eye diagram for the $\alpha = 0.4$ Nyquist filter, as shown in Fig. 2.10.b, has a peak-to-peak jitter of approximately 26%. In comparison, the computed eye diagram for the $\alpha = 0.4$ Nyquist pulses has a peak-to-peak jitter of 28% in the case of n=6 (Fig. 2.4.b) and 32% in the case of n=80 (from Fig. 2.7). In [2.4], the computer-simulated eye diagram for the $\alpha = 0.4$ Nyquist filter, has a peak-to-peak jitter of 30%. Thus, a good agreement between the computed and measured results is evident.

If Nyquist pulses having a rolloff factor $\alpha = 1$ are used, the computed eye diagram plotted in Fig. 2.11 shows neither ISI nor jitter. This is due to the full cosine term that appears in Eq. (2.1). Additional zero points thus exist at the middle of the bit intervals of the $\alpha = 1$ Nyquist pulses. In this case, the computed eye diagram shown in Fig. 2.11 agrees with the computer-simulated eye diagram of the $\alpha = 1$ Nyquist filter given in [2.4].

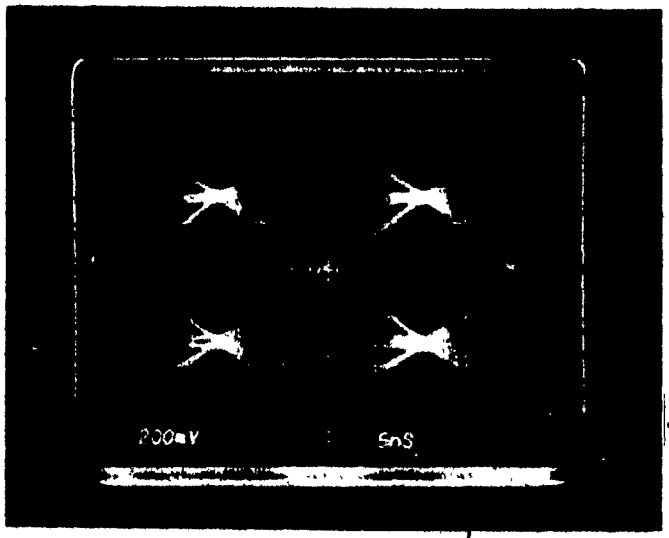

Fig. 2.10.a Laboratory-measured Eye Diagram of an $\alpha = 0.3$ Nyquist Filter

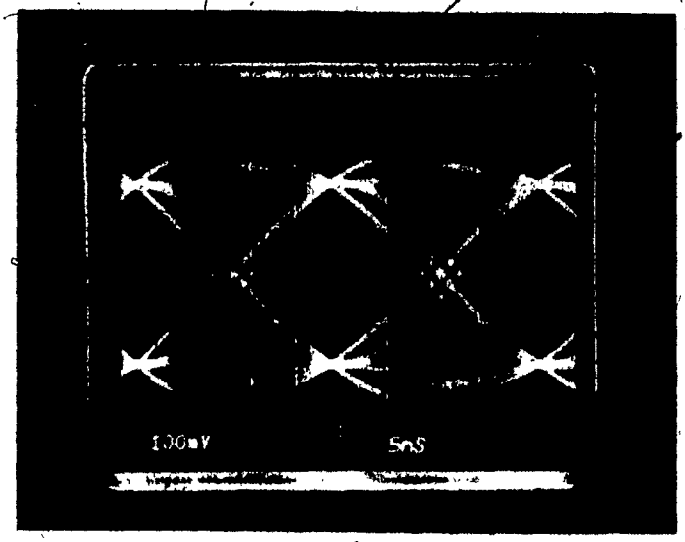

Fig. 2.10.b Laboratory-measured Eye Diagram of an $\alpha = 0.4$ Nyquist Filter

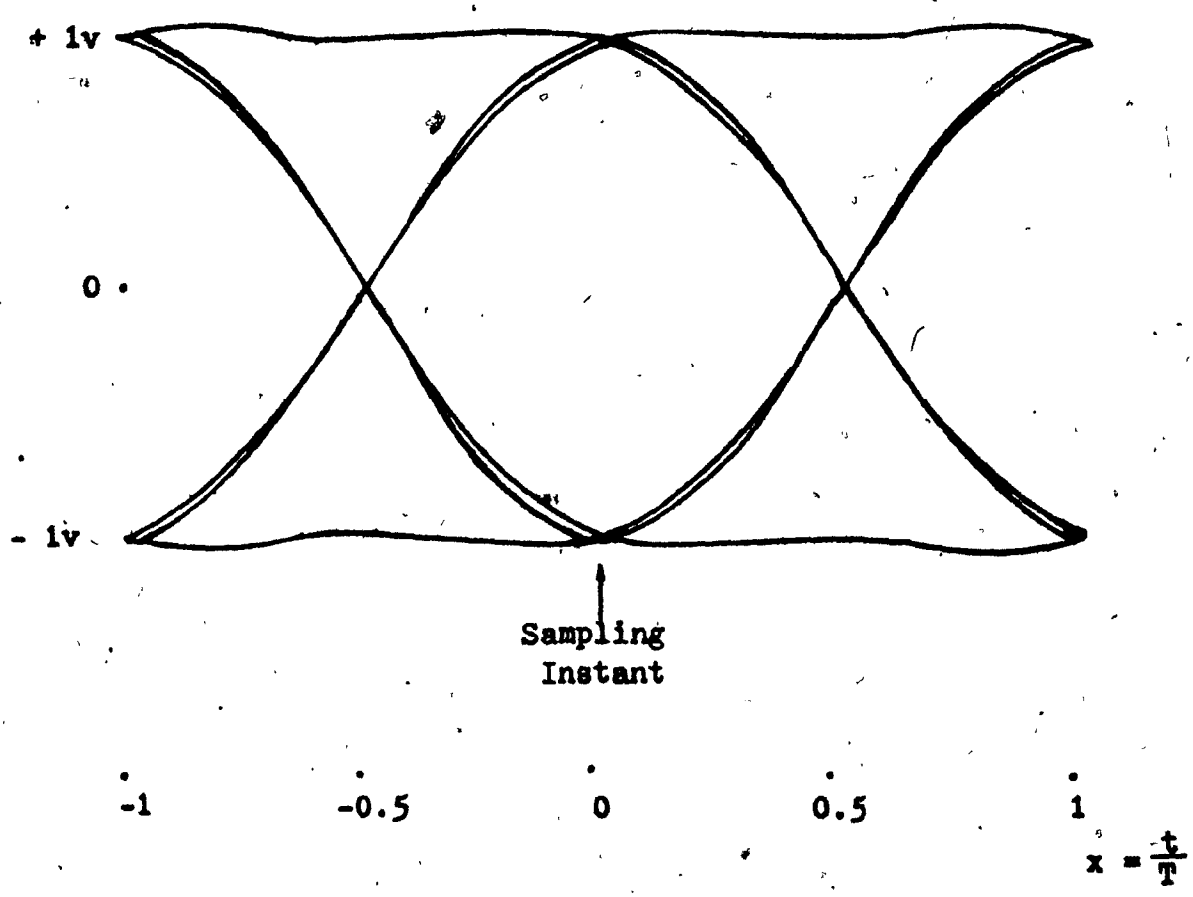

Fig. 2.11 Computed Eye Diagram of a Random Data Stream Using $\alpha = 1$ Nyquist Pulses as Signaling Elements

For this $\alpha=1$ case, it can be shown that there is no jitter by substituting $x=\frac{1}{2}$ into Eqs. (2.6) and (2.8) and noticing that both give 0 values. This means that curves A and B cross the horizontal timing axis at the same time.

In the above study, the peak-to-peak jitter is computed using theoretically ideal Nyquist pulses whose Fourier transforms have only real parts. Hence, the peak-to-peak jitter obtained in this study comes only from the amplitude function of the jitter. If there is filter phase nonlinearity, the resulting peak-topeak jitter will be increased. This can be demonstrated by considering the following experimental results.

Assume that a filter whose amplitude function is designed to have a nearly ideal approximation to that of an $\alpha=0.4$ Nyquist filter is measured to have a peak-to-peak jitter of 6 μsec. The random data stream used in this measurement has a bit rate of 32 kb/s. From Fig. 2.8 the peak-to-peak jitter which arises in a random data stream using the $\alpha=0.4$ Nyquist pulses is found to be 30%. This implies that the peak-to-peak jitter due to the amplitude function of the filter alone is at least 4.65 μsec for this 32 kb/s data stream. The portion of jitter contributed by the phase of nonlinearlity function of the designed filter is hence about 1.35 μsec.

Another factor worth considering is the peak-to-peak amplitude fluctuations of the signal which uses the Nyquist pulses as signalling elements. Fig. 2.12 shows the peak overshoot voltage of the signal as

a function of the roll off factor α. The number n of Eq. (2.12) is used as a parameter. For $\alpha > 0.2$, dependence of the peak overshoot voltage on n is not significant. For the $\alpha = 0$ case, this dependence becomes significantly noticeable. Theoretically speaking, the peak overshoot voltage for the signal using the $\alpha = 0$ Nyquist pulses could become infinitely large if the data pattern shown in Eq. (2.12) is considered. The occurrence of this large amplitude fluctuation is another serious problem in the Nyquist minimum bandwidth system. As there always exists a certain amount of nonlinearity in most of the practical transmission systems, large signal amplitude fluctuations can cause severe performance degradation.

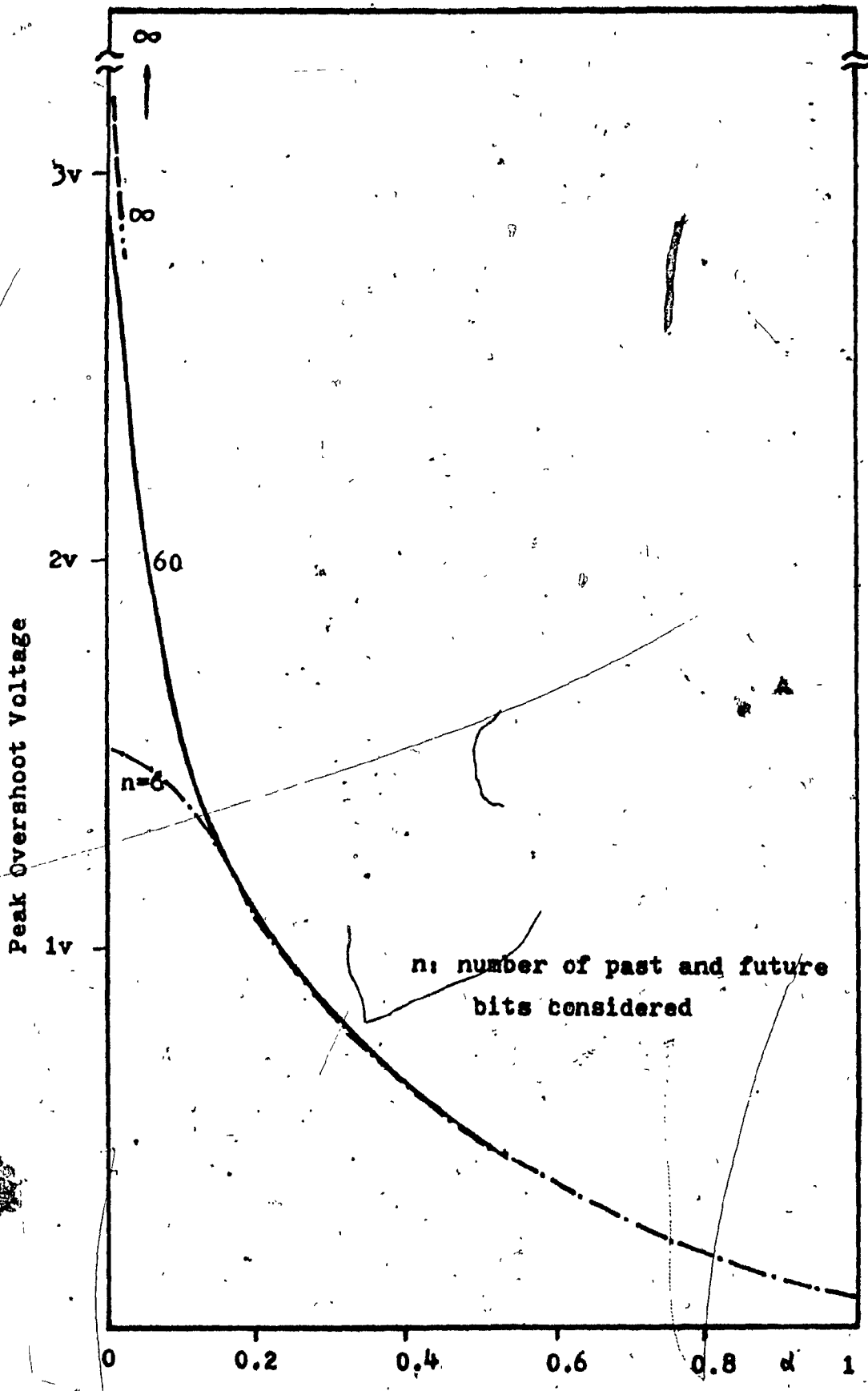

Fig. 2.12 Peak Overshoot Voltage as a Function of α for a Random Data Stream Using Nyquist Pulses as Signaling Elements

2.3 Time-limited Pulses and Spectral Shaping

For efficient utilization of the available spectrum, it is required to reduce the channel bandwidth without introducing significant amounts of intersymbol interference (ISI). This means that the filter employed to bandlimit the spectrum of a digital signal should have an equivalent Nyquist type response in order to minimize ISI.

Using conventional frequency domain synthesis techniques, it is possible to realize analog filters having an almost Nyquist type response. For example, Spaulding [2.5] approximated the magnitude of the filter frequency response by carefully positioning the zeros of the network transfer function. In the meantime, the poles of the transfer function were optimized with a computer so that nearly Nyquist response can be obtained. The final filter was then implemented by active filtering techniques. However, this filter is relatively costly.

On the other hand, the principle of a digital filter is conceived in the time domain. One type of nonrecursive digital filter which is frequently used in digital communication systems is the binary transversal filter (BTF). It can be realized by using digital integrated circuits (shift registers), weighting registors and a summing operational amplifier. Description of such a filter, having zero ISI and meeting INTELSAT SCPC* application, can be found in [de Cristofaro 2.6].

As discussed in previous sections, the Nyquist pulses, when used as information carrying elements in a random data stream, will

* Two of the INTELSAT SCPC filter specs are described on page 103.

exert a certain amount of jitter in the zero crossings of the eye patterns. From the transmission system point of view, a large amount of data pattern dependent jitter is not desirable as it might be the cause of excessive jitter in the extracted timing clock if the symbol timing circuit is not properly designed.

One method of obtaining jitter free data stream is by using time-limited pulses which occupy a single-bit or multi-bit interval. In the following sections, time-limited pulses which can be used as signaling elements to generate an ISI and also jitter free random data stream will be studied. By using appropriate time-limited pulses as signaling elements, the random data stream can have desirable spectral characteristics.

To start with, three well known single-intervaled pulses, namely, rectangular, half-cosine, and raised-cosine pulses, and their spectral properties will be described. The spectral characteristics of these pulses will then be compared with those of some known double-intervaled pulses. The spectral characteristics of some new double-intervaled pulses to be proposed in this thesis are also compared.

Double intervaled pulses are of particular interest in this thesis as their main spectral lobe is lower, and moreover, their spectral sidelobes are also lower than those of the single-intervaled rectangular pulse. In contrast to this, the single-intervaled half-cosine and

raised-cosine pulses attain lower spectral sidelobes with a widened main lobe. The purpose of this study is to search for a double-intervaled pulse which has low spectral sidelobes and narrow main lobe.

2.3.1 Time-limited Single-intervaled Pulses

A single-intervaled rectangular pulse, as defined in Chapter 1, has a duration of T. Its sin x/x shaped spectrum has a slow roll-off (Fig. 1.2.b). Because of this, for practical purposes, a NRZ coded signal, prior to transmission, requires band-limiting.

The single-intervaled half-cosine pulse [Bennett and Davey , 2.1]

$$s(t) = \cos\frac{\pi t}{T} \qquad \text{for } |t| \leq \frac{T}{2} \tag{2.19}$$

has a power spectral density given by:

$$s(f) = \left[\frac{2T}{\pi}\ \frac{\cos \pi f T}{(1-4\pi^2 f^2 T^2)}\right]^2 \tag{2.20}$$

When the half-cosine pulses are used in a random data stream, i.e., s(t) for the 1 symbol and -s(t) for the 0 symbol, the eye diagram of the resulting signal as shown in Fig. 2.13.a has zero ISI and no jitter. The spectrum of this signal shown in Fig. 2.13.b has a faster spectral rolloff than that of the rectangular pulse. One shortcoming with this signal is that the main spectral lobe is 50% wider than that of the NRZ.

The single-intervaled raised-cosine pulse [2.1]

$$s(t) = \tfrac{1}{2}\left(1 + \cos\frac{2\pi t}{T}\right) \qquad \text{for } |t| \leq \frac{T}{2}$$

has a power spectral density function given by:

$$s(f) = \left[\frac{\sin \pi f T}{\pi f T(1-\frac{1}{4} f^2 T^2)}\right]^2 \tag{2.21}$$

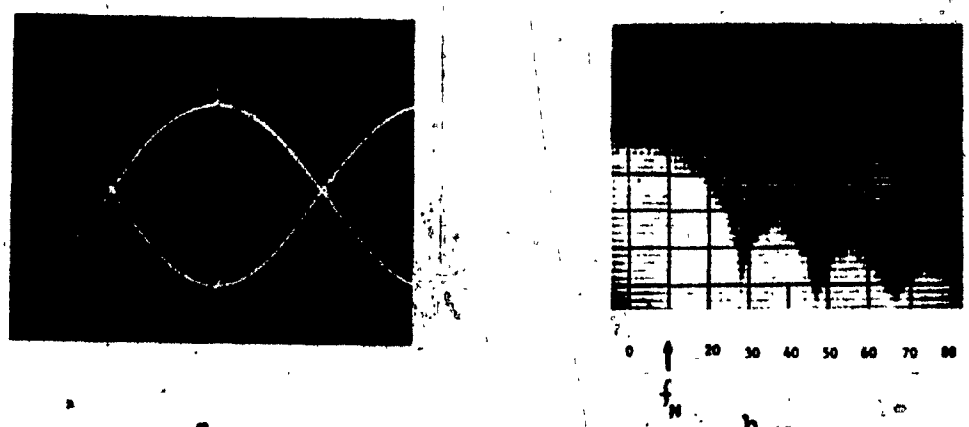

a. b.

Fig. 2.13 Measured Eye Diagram When Single-Intervaled Half-Cosine Pulses are Used in a Random Data Stream and the Corresponding Spectrum

Scale { a. V- 1 v/div H- 10 μs/div
b. V-10 dB/div H- 10 kHz/div

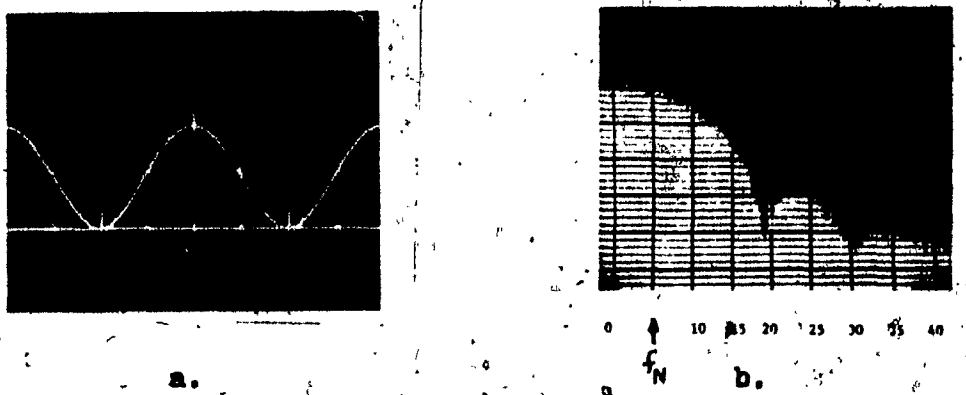

a. b.

Fig. 2.14 Measured Eye Diagram When Single-Intervaled Raised-Cosine Pulses are Used in a Random Data Stream and the Corresponding Spectrum

Scale { a. V- 1 v/div H- 20 μs/div
b. V-10 dB/div H- 10 kHz/div

(Discrete lines in Photo b. are due to clock leakage)

[Photos taken using M. Goodrum's circuit (Ref. 27)]

When the raised-cosine pulses are used in a random data stream, the eye diagram of resulting signs as shown in Fig. 2. 14. a again shows zero ISI and no jitter. The spectrum of the signal, as shown in Fig. 2. 14. b, has even lower spectral sidelobes than those of the half-cosine shaped signal. Yet, its main spectral lobe is 100% wider than that of the rectangular pulse. The spike appearing in Fig. 2. 14. b is due to clock leakage of the nonlinear switching filter used in this measurement [Gendron and Feher, 2. 7].

2.3.2 Time-limited Double-intervaled Pulses

If f in Eq. (2.2) is changed to t and $\frac{1}{T}$ is changed to T a time-limited raised cosine pulse s(t) with a rolloff factor of α is obtained:

$$s(t) = \begin{cases} 1 & |t| \leq \frac{T}{2}(1-\alpha) \\ \frac{1}{2}\left[1-\sin\frac{\pi}{\alpha T}\left(t-\frac{T}{2}\right)\right] & \frac{T}{2}(1-\alpha) \leq |t| \leq \frac{T}{2}(1+\alpha) \\ 0 & \text{elsewhere} \end{cases} \tag{2.22}$$

Thus the time-limited raised-cosine pulse defined in this manner, can be seen to be the dual of the frequency-limited pulse defined in Eq. (2.1). The Fourier transform of this pulse can thus be obtained by simply applying the principle of duality ($t \rightarrow f$ and $T \rightarrow \frac{1}{T}$) to Eq. (2.1) and is given by:

$$s(f) = \frac{\sin \pi f T \cos \alpha \pi f T}{fT\,(1-4\alpha^2 f^2 T^2)} \tag{2.23}$$

If normalized frequency 'f' is used by assuming T=1 sec, the power spectral density of the time-limited raised-cosine pulse is given by applying Eq. (2.3):

$$W_s(f) = \left[\frac{\sin \pi f \cos \alpha \pi f}{\pi f(1-\alpha^2 f^2)}\right]^2 \quad \text{for all } f \tag{2.24}$$

A time-limited raised-cosine pulse with α=0, 0.5 and 1, and its corresponding power spectral density are shown in Figs. 2.15.a and 2.15.b.

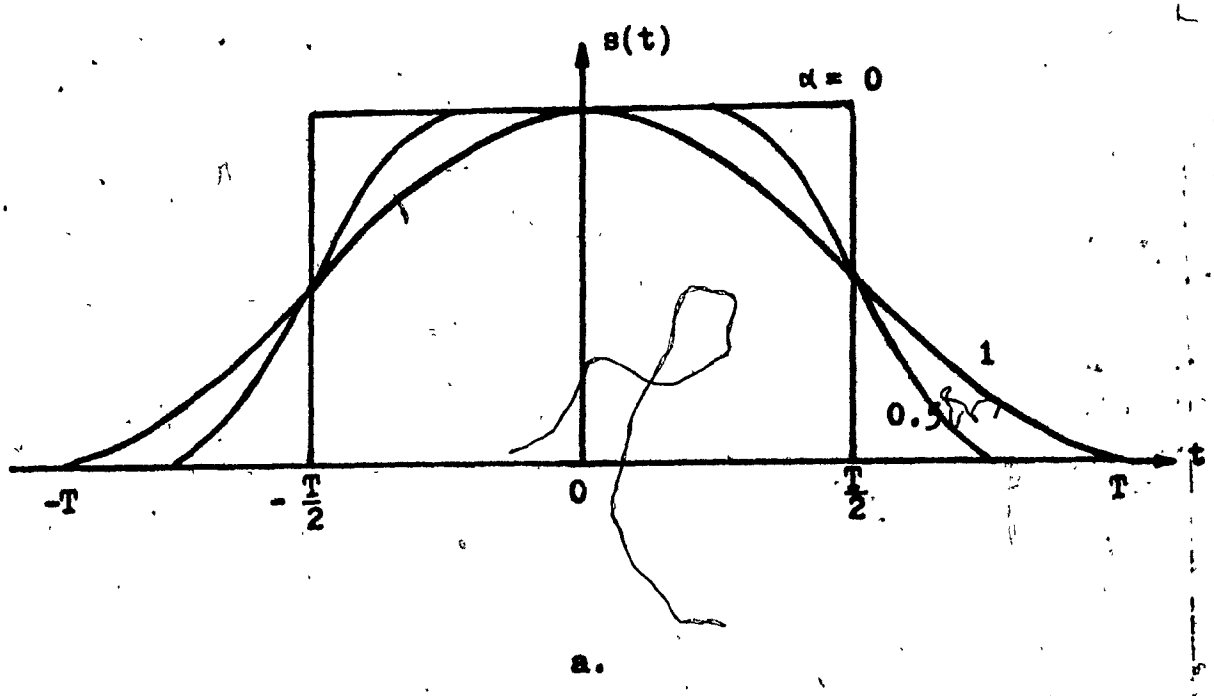

a.

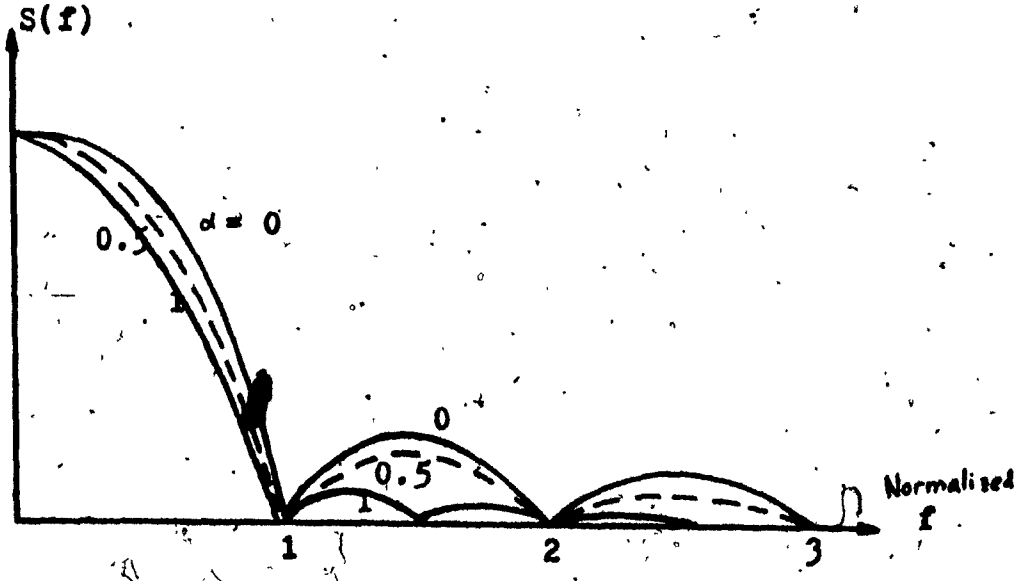

b.

Fig. 2.15 a. Time-limited Raised Cosine Pulses with $\alpha = 0, 0.5, 1$

b. Spectra of Time-limited Raised-Cosine Pulses

For $\alpha=1$, a double-intervaled raised cosine pulse is obtained:

$$s(t) = \begin{cases} \frac{1}{2}(1+\cos\frac{\pi t}{T}) & |t| \leq T \\ 0 & \text{elsewhere} \end{cases} \qquad (2.25)$$

whose power spectral density is given by:

$$W_s(f) = \left[\frac{\sin 2\pi f}{2\pi f(1-2f)(1+2f)}\right]^2 \qquad \text{for all } f \qquad (2.26)$$

The double-intervaled raised-cosine pulse s(t) defined in Eq. (2.25) can also be written as:

$$s(t) = \begin{cases} \cos^2\frac{\pi t}{2T} & |t| \leq T \\ 0 & \text{elsewhere} \end{cases} \qquad (2.27)$$

Hence it can also be obtained by squaring a double-intervaled half-cosine $\cos\frac{\pi t}{2T}$.

For $\alpha=0$, the time-limited pulse s(t) becomes a single-intervaled rectangular pulse. Assuming that the peak voltage value of the pulses shown in Fig. 2.15.a is normalized to unity, the double-intervaled raised-cosine pulse has lower spectral lobes than those of the single-intervaled rectangular pulse. As shown in Fig. 2.15.b, the first spectral null of the double-intervaled raised-cosine pulse is at the bit rate frequency. This characteristic is identical to that of the single-intervaled rectangular pulse.

By synchronously overlapping the double-intervaled raised cosine pulses, i.e., a double-intervaled pulse representing either the 1 or 0

symbol always starts at the mid-point of its previous pulse, a random data stream can be obtained which possesses the same spectral characteristics as the pulse itself. Later, it will be shown that the eye diagram of the resulting data stream also has zero ISI and is jitter free.

Before we start our search for a double-intervaled pulse that can be used to generate an ISI and jitter free data stream with desirable spectral characteristics, certain properties characteristic of the pulse shape function s(t) will be investigated. For this purpose, the double-intervaled raised-cosine will be used as an example. First, we observe that the double-intervaled raised-cosine pulse s(t) is symmetric about the center of the pulse and hence s(t) is an even function.

It also satisfies the following two conditions:

$$\begin{cases} s(t) + s(t - T) = 1 \\ s(t) - s(t - T) = f(t) = \cos\dfrac{\pi t}{T} \end{cases} \qquad \text{for } 0 \leq t \leq T \qquad (2.28)$$

where the difference function f(t) is a positive even function.

In this thesis, a positive even function is defined as one which has only positive values over $|t| \leq \frac{T}{2}$ and which is symmetric about the t=0 axis.

The two conditions shown in Eq. (2.28) are essential so that the data stream generated by synchronously overlapped double-intervaled pulses is a continuous signal with no discontinuity. In the following section, we will use two examples to demonstrate why this is the case.

A double-intervaled "complementary" raised-cosine pulse $s'(t)$ defined as

$$s'(t) = \begin{cases} 1 - s(t) & \text{for } |t| \leq T \\ 0 & \text{elsewhere} \end{cases} \qquad (2.29)$$

also satisfies the above two conditions. The only difference is that in this case, $f(t)$ is a negative even function. In this thesis, a 'negative' even function is defined as one which is symmetric about the t=0 axis but has negative values over $|t| \leq \frac{T}{2}$. In Section 2.3.5, it will be shown that a data stream generated by this type of complementary pulses is not a continuous signal.

Equation (2.28) can be easily proved by noting that for the raised-cosine pulse $s(t)$, its shifted version is

$$s(t - T) = \tfrac{1}{2}\left[1 - \cos\frac{\pi t}{T}\right] \qquad (2.30)$$

Hence, $s(t) + s(t - T) = 1$

and, $\qquad$ for $0 \leq t \leq T$ $\qquad (2.28)$

$$s(t) - s(t - T) = \cos\frac{\pi t}{T}$$

A double-intervaled triangular pulse such as defined by Bennett and Davey [2.1]:

$$s(t) = \begin{cases} 1 - \left|\frac{t}{T}\right| & |t| \leq T \\ 0 & \text{elsewhere} \end{cases} \qquad (2.31)$$

with a normalized- frequency spectrum

$$W_s(f) = \left[\frac{\sin \pi f}{\pi f}\right]^4 \qquad \text{for all } f \qquad (2.32)$$

also satisfies the above two equations (2. 28) and can be used for spectral shaping as well.

Two other important properties which are also characteristic of the double-intervaled raised-cosine pulse and triangular pulse are:

(A) The pulses have zero values at the pulse edges, $t=\pm T$

(B) The magnitude of the pulses at $t=\pm \frac{T}{2}$ are equal to one-half of the peak magnitude. The peak magnitude of the pulses occurs at mid-point of the pulses, t=0.

Property (A) is required so that the data stream generated by synchronously overlapping these double-intervaled pulses has no ISI at the sampling instants. Property (B) is essential to ensure that the data stream generated in this manner also has no data pattern dependent timing jitter.

New double-intervaled pulses that possess the afore-mentioned properties will be our subject in the following sections. As mentioned earlier, the purpose of this study is to search for double-intervaled pulses whose spectral sidelobes are low and whose main spectral lobe is confined within that of the rectangular pulse. Pulses which are found through other constraints have been well documented in [Simon, 2. 8][Kalet, 2. 9][Aulin and Sundberg, 2. 10].

2.3.2.1 Double-intervaled Raised Amoroso's Pulses

The pulse shape which has been defined by Amoroso [2.11] is given by:

$$p(t) = \begin{cases} \cos\left[\frac{\pi t}{2T} - u' \sin \frac{2\pi t}{T} \right] & \text{for } |t| \leq T \\ 0 & \text{elsewhere} \end{cases} \quad (2.33)$$

where u' is a constant ranging from 0 to $\frac{1}{2}$.

By squaring the Amoroso's pulse, the double-intervaled raised Amoroso's pulse is obtained which is given by:

$$s(t) = \begin{cases} \frac{1}{2}\left[1 + \cos \left(\frac{\pi t}{T} - u \sin \frac{2\pi t}{T} \right) \right] & \text{for } |t| \leq T \\ 0 & \text{elsewhere} \end{cases} \quad (2.34)$$

where $u = 2u'$ ranging from 0 to 1.

The double-intervaled raised Amoroso's pulse with different u are plotted in Fig. 2.16.a. For u=0, the pulse degenerates to double-intervaled raised cosine-pulse.

The power spectral density of the raised Amoroso's pulse has been derived in Appendix A by taking the Fourier transform of the pulse and using the Bessel expansions of the trigonometric function such as [Abramowitz and Stegun, 2.12]:

$$\cos (u \sin at) = J_0(u) + 2 \sum_n J_{2n}(u) \cos (2nat) \quad (2.35)$$

and

$$\sin (u \sin at) = 2 \sum_n J_{2n-1}(u) \sin (2n-1)at \quad (2.36)$$

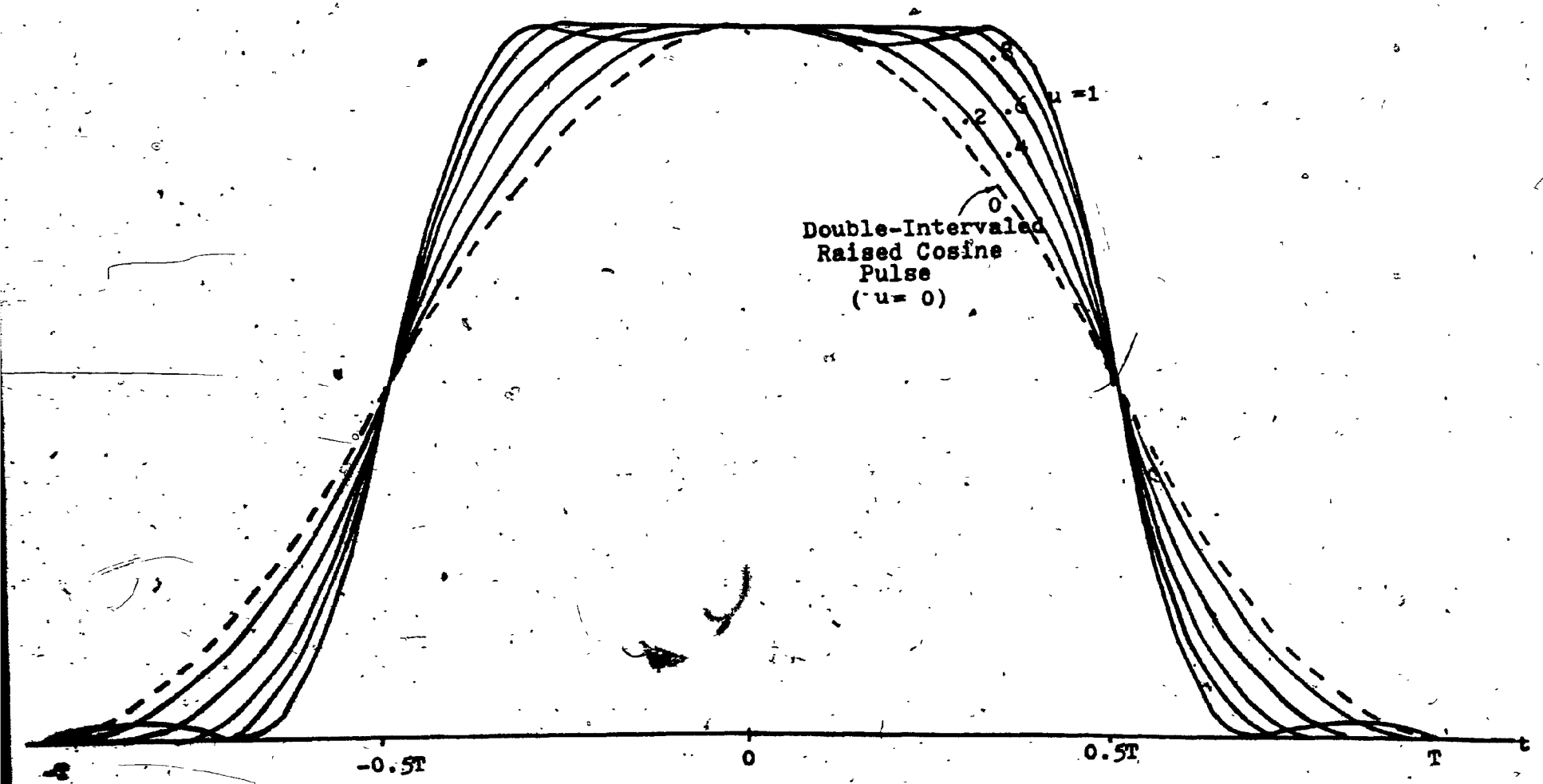

Fig. 2.16.a Double-Intervaled Raised Amoroso's Pulses

where, for computational purposes, the Bessel-function expansions are truncated to the N-th term.

The power spectral density of the class of pulses defined by Eq. (2.34) is given by:

$$W_s(f) = A(f) + J_o(u)\, A_o(f) + 2\sum_{n=1} J_{2n}(u)\, B_{2n}(f) + 2\sum_{n=1} J_{2n-1}(u)\, B_{2n-1}(f) \qquad (2.37)$$

where f is the normalized frequency by assuming T=1 sec and

$$A(f) = \left(\frac{\sin 2\pi f}{2\pi f}\right)$$

$$A_o(f) = \tfrac{1}{2} A(f + \tfrac{1}{2}) + \tfrac{1}{2} A(f - \tfrac{1}{2})$$

$$A_{2n}(f) = \tfrac{1}{2} A(f + 2n) + \tfrac{1}{2} A(f - 2n) \qquad (2.38)$$

$$B_{2n}(f) = \tfrac{1}{2} A_{2n}(f + \tfrac{1}{2}) + \tfrac{1}{2} A_{2n}(f - \tfrac{1}{2})$$

$$A_{2n-1}(f) = \tfrac{1}{2} A(f + (2n - 1)) - \tfrac{1}{2} A(f - (2n - 1))$$

$$B_{2n-1}(f) = \tfrac{1}{2} A_{2n-1}(f - \tfrac{1}{2}) - \tfrac{1}{2} A_{2n-1}(f + \tfrac{1}{2})$$

The power series representation of $J_n(x)$ [Jahnke and Emde, 2.15]:

$$J_n(x) = \frac{(\frac{1}{2}x)^n}{0!n!} - \frac{(\frac{1}{2}x)^{n+2}}{1!\,(n+1)!} + \frac{(\frac{1}{2}x)^{n+4}}{2!\,(n+2)!} - \frac{(\frac{1}{2}x)^{n+6}}{3!\,(n+3)!} + \cdots \qquad (2.39)$$

for $n = 0, 1, 2, \ldots$

in the interval of interest $(0 \leq x \leq 1)$ is an alternating series with monotomically decreasing term. A useful upper bound on the series truncation error in Eq. (2.37) is obtained by considering the dominance of the above power series by its leading term.

Thus,

$$\left| J_n(x) \right| \leq \frac{(\frac{1}{2}x)^n}{n!} \tag{2.40}$$

and,

$$\sum_{}^{\infty} \left| J_n(x) \right| \leq \frac{(\frac{1}{2}x)^n}{n!}$$

which is a bound on the truncation error as $|A_o(f)|$, $|B_{2n}(f)|$ and $|B_{2n-1}(f)|$ never exceed unity.

It is easy to prove that

$$\sum_{}^{\infty} \frac{(\frac{1}{2}x)^n}{n!} < \frac{(\frac{1}{2}x)^m}{m!} \; e^{\frac{1}{2}x} \tag{2.41}$$

The upper bound of the truncation error, by using only up to the N-th term, is thus

$$2 \frac{(\frac{1}{2}u)^{2n+1}}{(2n+1)!} \cdot e^{\frac{1}{2}u} \tag{2.42}$$

According to Eq. (2.42), for n=3 and $0 \leq u \leq 1$, the truncation error in the spectrum computation is found to be down to -100 db. The spectra for the class of the raised Amoroso's pulses for different u are thus computated by using only up to the n=3 terms. As shown in Fig. 2.16.b, we observe that the raised Amoroso's pulses ($u \neq 0$) have higher spectral sidelobes than those of the raised cosine pulses (u=0). Hence, little gain is achieved by using the raised Amoroso's pulses. This is contrary to the much lower spectral sidelobes attained by the original Amoroso's pulses [2.11]. The main drawback with the original Amoroso's pulses is that they have their first spectral null at 1.5 times

the bit rate frequency or even at higher frequency. On the other hand, the first spectral null of the raised Amorosols pulses are located at the bit rate frequency.

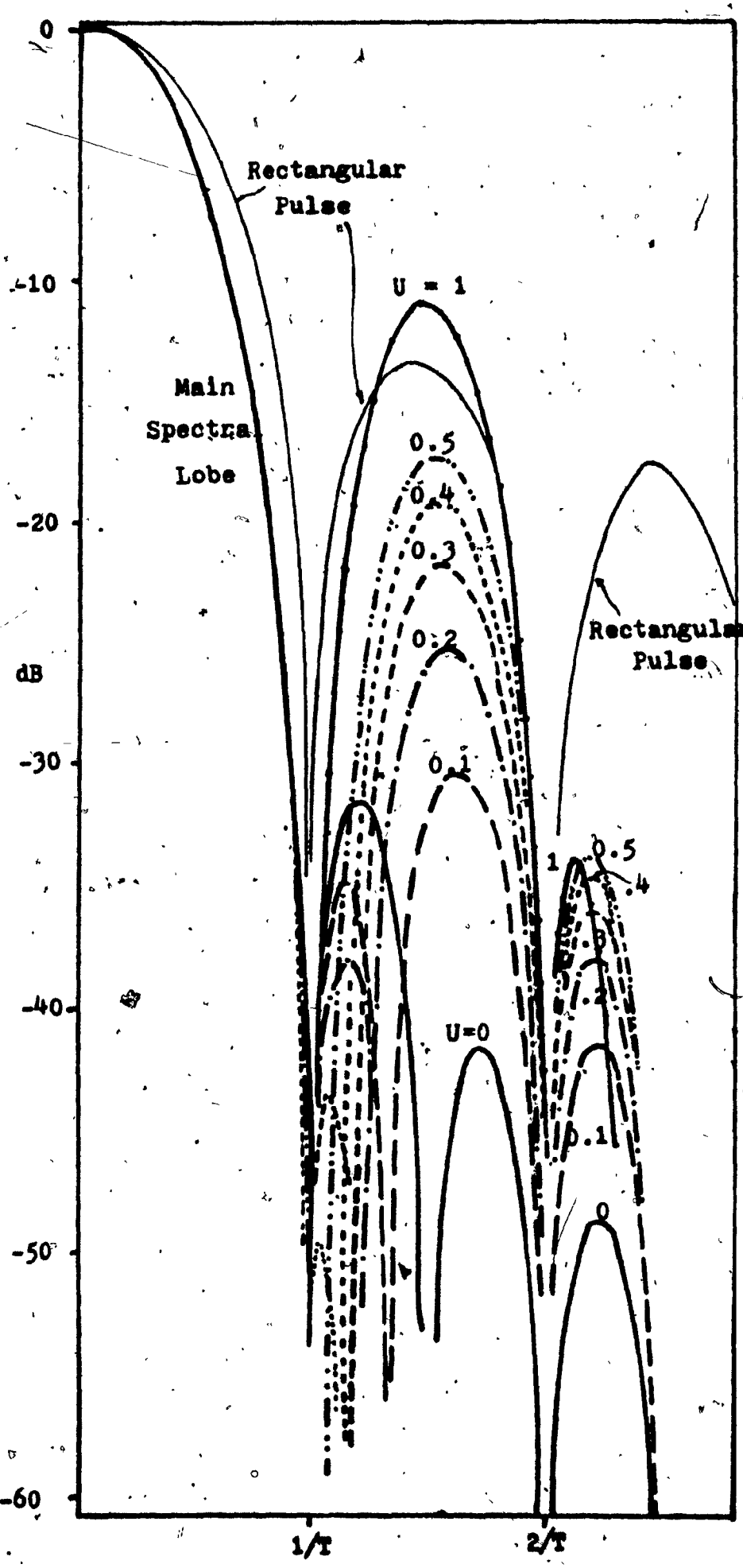

Fig. 2.16.b .

Power Spectra of Raised Amoroso' Pulses

2.3.2.2 Double-intervaled Raised Kalet's Pulses

The raised Kalet's pulses are obtained in a similar manner to the method used in the previous section. As shown in Table 2.1, the raised Kalet's pulses are obtained by squaring the Kalet's pulses [2.9]

	Kalet's Pulses f(t)	Raised Kalet's Pulses $f(t)^2$
$s_1(t)$	$\cos\left[\frac{1}{2}\left(\frac{\pi}{2} - \frac{\pi}{2}\cos\frac{\pi t}{T}\right)\right]$	$\frac{1}{2}\left[1+\sin\left(\frac{\pi}{2}\cos\frac{\pi t}{T}\right)\right]$
$s_2(t)$	$\cos\left[\frac{1}{2}\left(\frac{\pi}{2} - \cos\frac{\pi t}{T} + \left(1-\frac{\pi}{2}\right)\cos^3\frac{\pi t}{T}\right)\right]$	$\frac{1}{2}\left[1+\sin\left(\cos\frac{\pi t}{T} - \left(1-\frac{\pi}{2}\right)\cos^3\frac{\pi t}{T}\right)\right]$
$s_3(t)$	$\left(.5+.75\cos\frac{\pi t}{T} - .25\cos^3\frac{\pi t}{T}\right)^{\frac{1}{2}}$	$\left(.5+.75\cos\frac{\pi t}{T} - .25\cos^3\frac{\pi t}{T}\right)$
$s_4(t)$	$\left(.5+.9375\cos\frac{\pi t}{T} - .625\cos^3\frac{\pi t}{T} + .1875\cos^5\frac{\pi t}{T}\right)^{\frac{1}{2}}$	$\left(.5+.9375\cos\frac{\pi t}{T} - .625\cos^3\frac{\pi t}{T} + .1875\cos^5\frac{\pi t}{T}\right)$
$s_5(t)$	$\left(.5+1.09375\cos\frac{\pi t}{T} - 1.09375\cos^3\frac{\pi t}{T} + .65625\cos^5\frac{\pi t}{T} - .15625\cos^7\frac{\pi t}{T}\right)^{\frac{1}{2}}$	$\left(.5+1.09375\cos\frac{\pi t}{T} - 1.09375\cos^3\frac{\pi t}{T} + .65625\cos^5\frac{\pi t}{T} - .15625\cos^7\frac{\pi t}{T}\right)$

Table 2.1 Kalet's and Raised Kalet's Pulses

The five raised Kalet's pulses are plotted in Fig. 2.17. a. It is found that No. 1 and No. 3 raised Kalet's pulses are approximately identical.

The spectra of the five raised Kalet's pulses, have been described in Appendix A and are summarized below:

1. $$W_{s_1}(f) = \left[A(f) + 2\sum (-1)^{n-1} J_{2n-1} \frac{\pi}{2} C_{2n-1}(f) \right]^2 \qquad (2.43)$$

where $A(f) = \frac{\sin 2\pi f}{2\pi f}$ as in Eq. (2.38)

$$C_{2n-1}(f) = \tfrac{1}{2}A\left[\frac{(2n-1)}{2} - f\right] + \tfrac{1}{2}A\left[\frac{(2n-1)}{2} + f\right]$$

and $J_{2n-1}(.)$ is again the Bessels function defined in Eq. (2.39)

2. $$W_{s_2}(f) = \Bigg\{ A(f) + 2J_o \frac{(1-\frac{\pi}{2})}{4} \sum_K (-1)^{k-1} J_{2n-1}\left[\frac{(1+\frac{3\pi}{2})}{4}\right] \frac{A_{2k-1}}{2}(f)$$

$$-2J_o \frac{(1+\frac{3}{2}\pi)}{4} \sum_K (-1)^k J_{2k-1}\left[\frac{(1-\frac{\pi}{2})}{4}\right] \frac{A_{3(2k-1)}}{2}(f)$$

$$+\sum_1 \sum_K (-1)^{1+k-1} J_{2k-1}\left[\frac{(1+\frac{3\pi}{2})}{4}\right] J_{21-1}\left[\frac{(1-\frac{\pi}{2})}{4}\right]$$

$$\cdot \left[\frac{A_{2k+61-1}}{2}(f) + \frac{A_{2k-61-1}}{2}\right](f) \qquad (2.44)$$

$$-\sum_1 \sum_K (-1)^{1+k-1} J_{2k-1}\left[\frac{(1-\frac{\pi}{2})}{4}\right] J_{21-1}\left[\frac{(1+\frac{3\pi}{2})}{4}\right]$$

$$\cdot \left[\frac{A_{6k+21-3}}{2}(f) + \frac{A_{6k-61-3}}{2}(f)\right] \Bigg\}^2$$

where $A(f)$ and $A_{2n}(f)$ are defined as before.

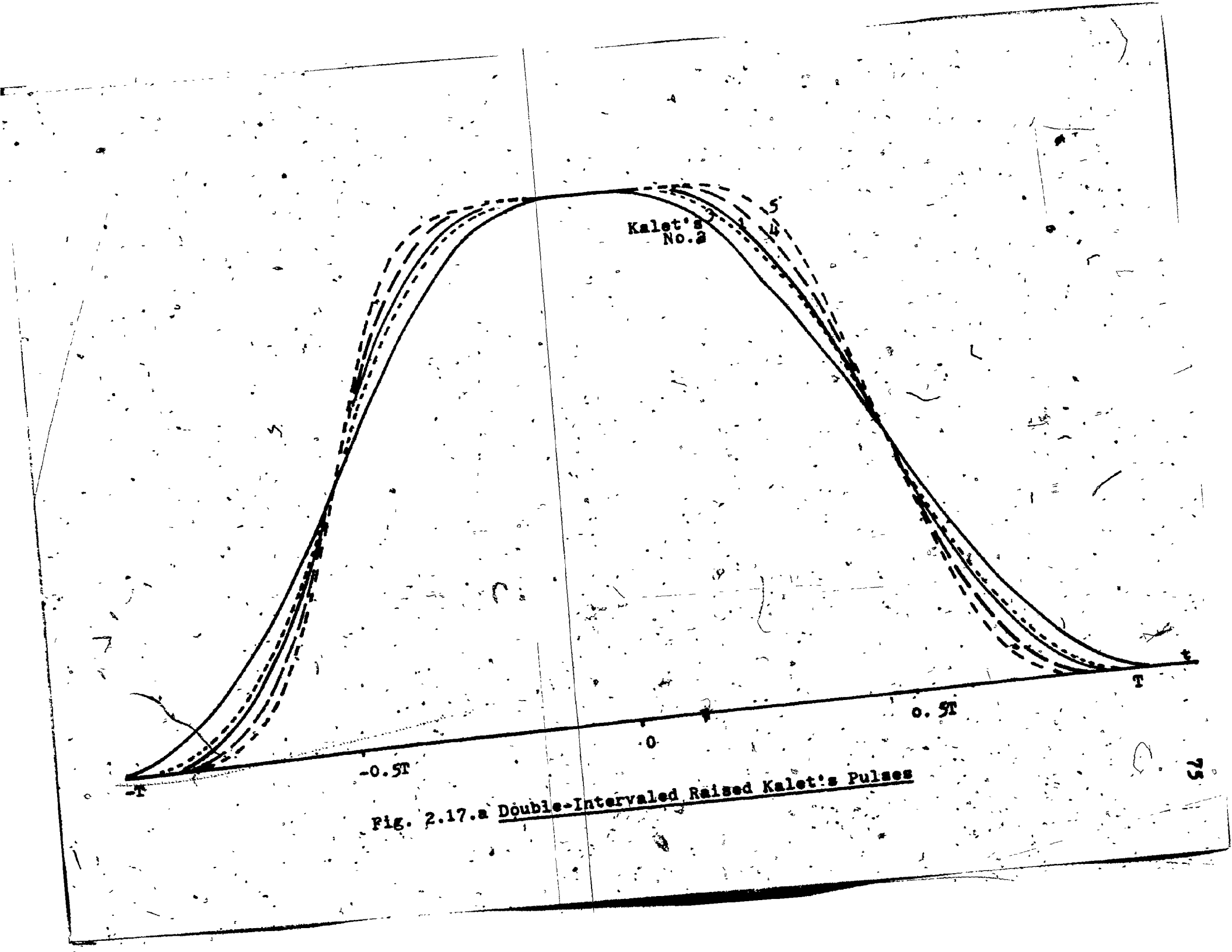

Fig. 2.17.a Double-Intervaled Raised Kalet's Pulses

$$3.\ W_{s_3}(f) = \left[\frac{\sin 2\pi f}{2\pi f} + \frac{2.25 f \sin 2\pi f}{4\pi(\frac{1}{2}-f)(\frac{1}{2}+f)} - \frac{0.25 f \sin(2\pi\frac{f}{3})}{4\pi(\frac{3}{2}-f)(\frac{3}{2}+f)} \right]^2 \quad (2.45)$$

$$4.\ W_{s_4}(f) = \left[\frac{\sin 2\pi f}{2\pi f} + \frac{2.34375 f \sin 2\pi f}{4\pi(\frac{1}{2}-f)(\frac{1}{2}+f)} - \frac{0.390625 f \sin(2\pi\frac{f}{3})}{4\pi(\frac{3}{2}-f)(\frac{3}{2}+f)} + \frac{0.046875 f \sin(2\pi\frac{f}{5})}{4\pi(\frac{5}{2}-f)(\frac{5}{2}+f)} \right]^2 \quad (2.46)$$

$$5.\ W_{s_5}(f) = \left[\frac{\sin 2\pi f}{2\pi f} + 2.392578 \frac{f \sin 2\pi f}{4\pi(\frac{1}{2}-f)(\frac{1}{2}+f)} - 0.485152 \frac{f \sin(2\pi\frac{f}{3})}{4\pi(\frac{3}{2}-f)(\frac{3}{2}+f)} + 0.0957 \frac{f \sin(2\pi\frac{f}{5})}{4\pi(\frac{5}{2}-f)(\frac{5}{2}+f)} - 0.00976 \frac{f \sin(2\pi\frac{f}{7})}{4\pi(\frac{7}{2}-f)(\frac{7}{2}+f)} \right]^2 \quad (2.47)$$

The spectra of these double-intervaled raised pulses, (excluding pulse No. 2) are plotted in Fig. 2.17.b. Although the spectra of these pulses did not have as fast a rolloff as that of the double-intervaled raised-cosine pulse, the suggested pulses again maintain the characteristic of an unwidened main spectral lobe. This is an improvement over the original Kalet's pulses whose main spectral lobe is wider than that of a single-intervaled rectangular pulse.

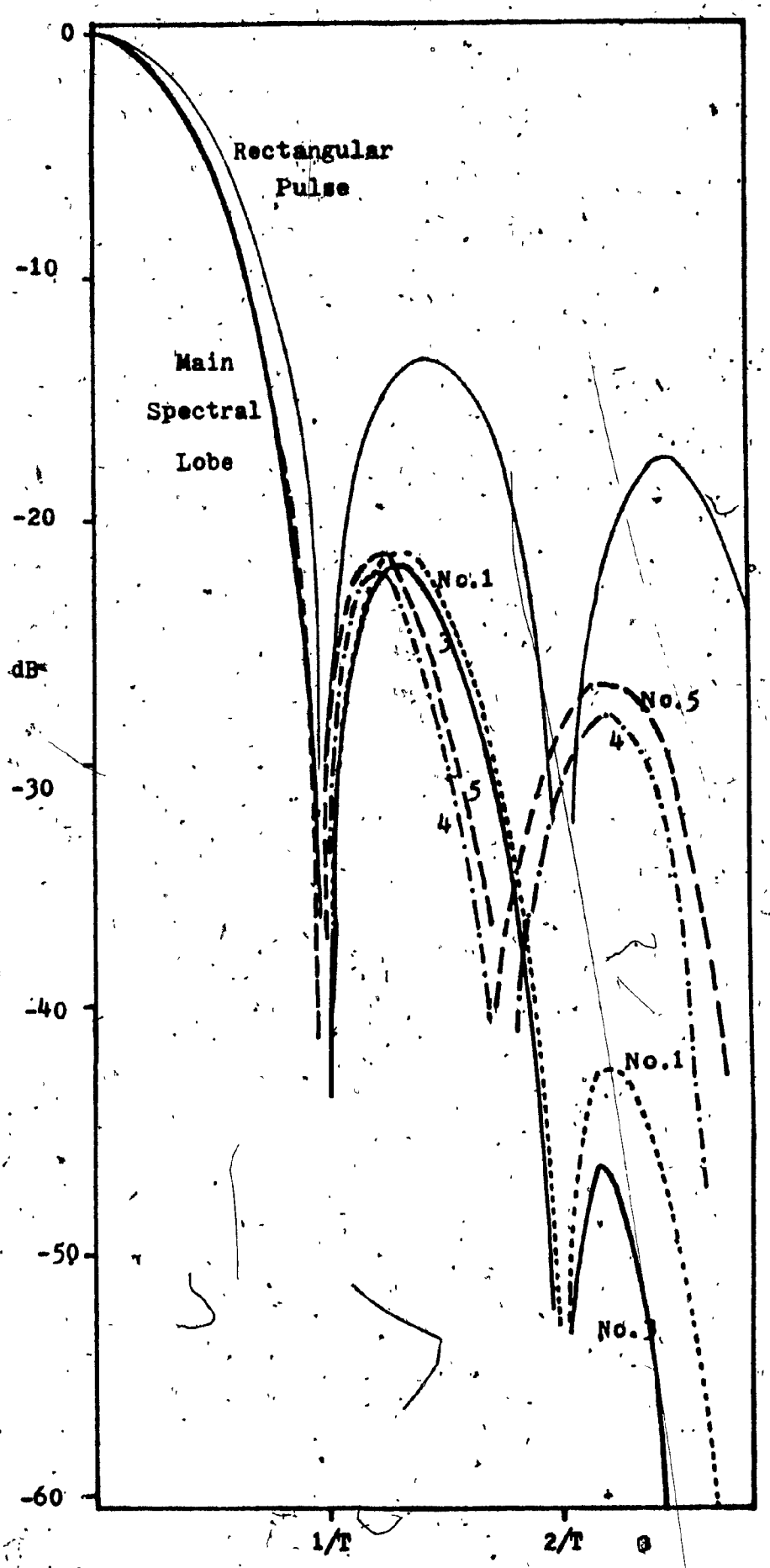

Fig. 2.17.b

Power Spectra of Raised Kalet's Pulses

2.3.2.3 Double-intervaled Modified Raised-Cosine Pulses

As described in the previous two sections, double-intervaled raised Amoroso's pulses and some of the raised Kalet's pulses contain the $\cos\frac{\pi t}{T}$ term which is characteristic of the raised-cosine pulse. In the following, the effect of the magnitude of this term on the spectrum of the resulting pulse shape is analyzed.

The raised-cosine pulse as given by Eq. (2.25) is:

$$s(t) = \begin{cases} \frac{1}{2}\left(1 + \cos\frac{\pi t}{T}\right) & \text{for } |t| \leq T \\ 0 & \text{elsewhere} \end{cases} \qquad (2.25)$$

By modifying the $\cos\frac{\pi t}{T}$ term with different coefficients, the modified (or shifted) raised-cosine pulse is given by:

$$s(t) = \begin{cases} \frac{1}{1+k}\left(1 + k\cos\frac{\pi t}{T}\right) & \text{for } |t| \leq T \\ 0 & \text{elsewhere} \end{cases} \qquad (2.48)$$

where k is a positive constant. The normalizing coefficient $\frac{1}{1+k}$ is added in Eq. (2.48) so that s(t) has a unity value at t=0.

Negative k is not considered here as it would give the complementary type of pulses. For example, if k=-1, Eq. (2.48) becomes the complementary raised-cosine pulse mentioned earlier. (For negative k Eq. (2.48) is to be modified as follows:

$$s(t) = \frac{1}{1+|k|}\left(1 + k\cos\frac{\pi t}{T}\right)$$

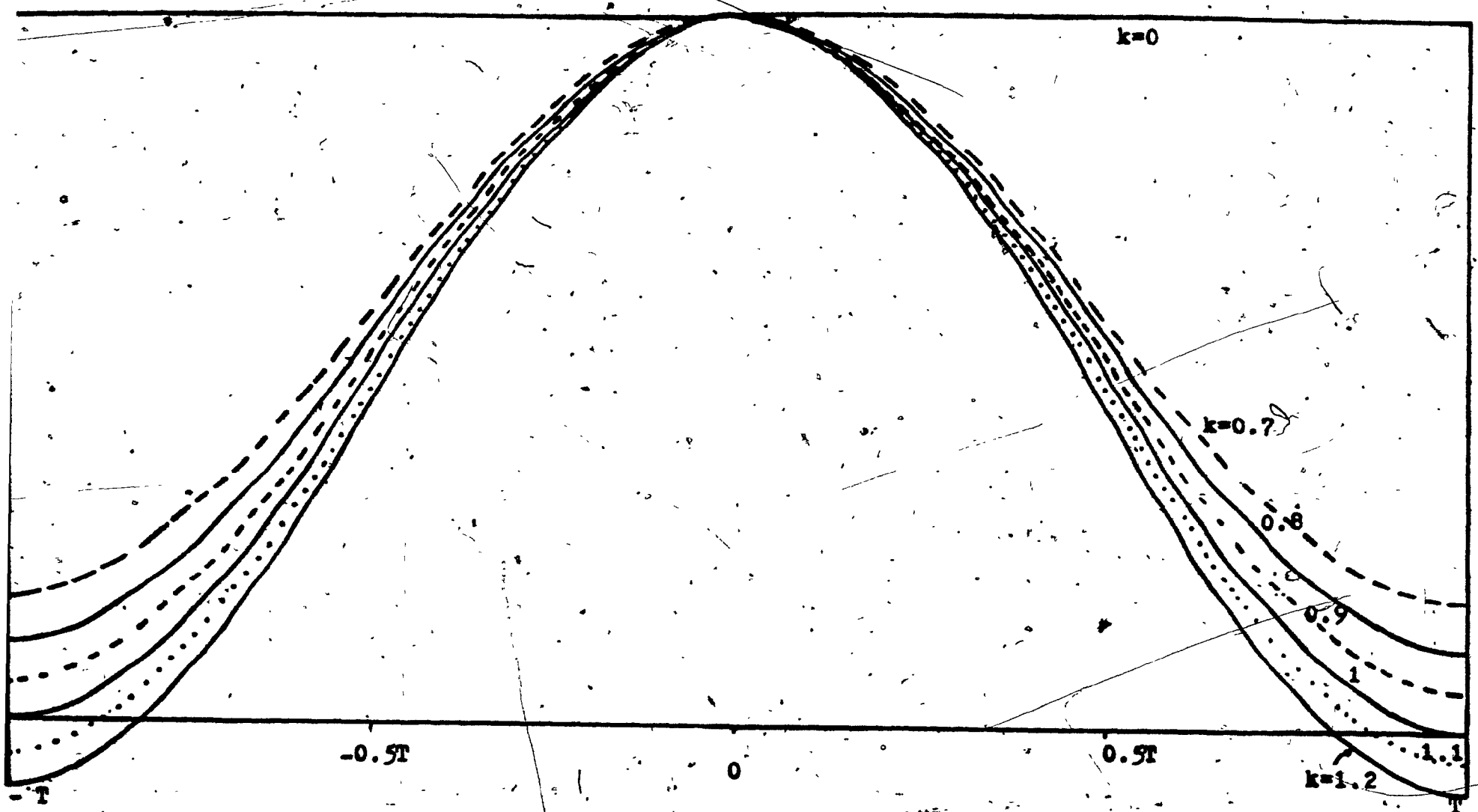

Fig. 2.18.a Double-Intervaled Modified Raised-Cosine Pulses

The subject of the complementary raised-cosine pulse will be covered in more detail in Section 2. 3. 3. 4.

For k=0, s(t) in Eq. (2. 48) becomes the double-intervaled rectangular pulse as shown in Fig. 2. 18. a. For k=1, it becomes the double-intervaled raised-cosine pulse.

For $0 < k < 1$, s(t) becomes the double-intervaled 'over-raised' cosine pulse, and for $1 < k$, s(t) becomes the double-intervaled 'under-raised' cosine pulse.

The power spectral density of the modified raised-cosine pulse s(t) of Fq. (2. 48) is derived similarly as in the previous sections and is given by:

$$W_s(f) = \left[\frac{1}{1+k} \left(\frac{\sin 2\pi f}{\pi f} + \frac{4kf \sin 2\pi f}{\pi (1-2f)(1+2f)} \right) \right]^2 \qquad (2.49)$$

where f again is the normalized frequency by assuming T = 1sec.

The spectra of the k=0. 7, 0. 8, 0. 9, 1, 1. 2 pulses are shown in Fig. 2. 18. b. The k=0. 8 pulse, which is an over-raised cosine pulse, has the lowest spectral sidelobes. For this reason, it is studied further in the following paragraphs.

As shown in Fig. 2. 18. b, the k=0. 8 pulse has non-zero values at the pulse edges ($t = \pm T$). Also its magnitudes at $t = \pm \frac{T}{2}$ are not equal to 0. 5. Recall conditions (A) and (B) in Section 2. 3. 2., p. 66. As a signaling element in the generation of a random data stream, the non-zero values at the pulse edges introduce ISI while the not-equal-to-0. 5

values at $t = \pm \frac{T}{2}$ exert timing jitter in the zero crossings of the eye patterns.

Shown in Fig. 2.18. c, the eye diagram exhibits a peak ISI of 22% at the sampling instants. The peak-to-peak jitter is 8% over one bit interval.

Due to the inherent ISI in this data stream, the resulting system requires a higher signal-to-noise ratio (SNR) to attain the same error rate as in an ideal binary system. This is similar to the Tamed FM (TFM) system which uses a baseband coding scheme involving the correlation of three consecutive bits to achieve spectral shaping at the expense of higher SNR requirement [de Jagar and Debkar, 2.13]. In a number of bandwidth-restricted systems, where sufficient SNR is available, this k=0.8 pulse might be used to generate a bandwidth efficient data stream.

A method that can be used to generate this data stream will be described in the following section.

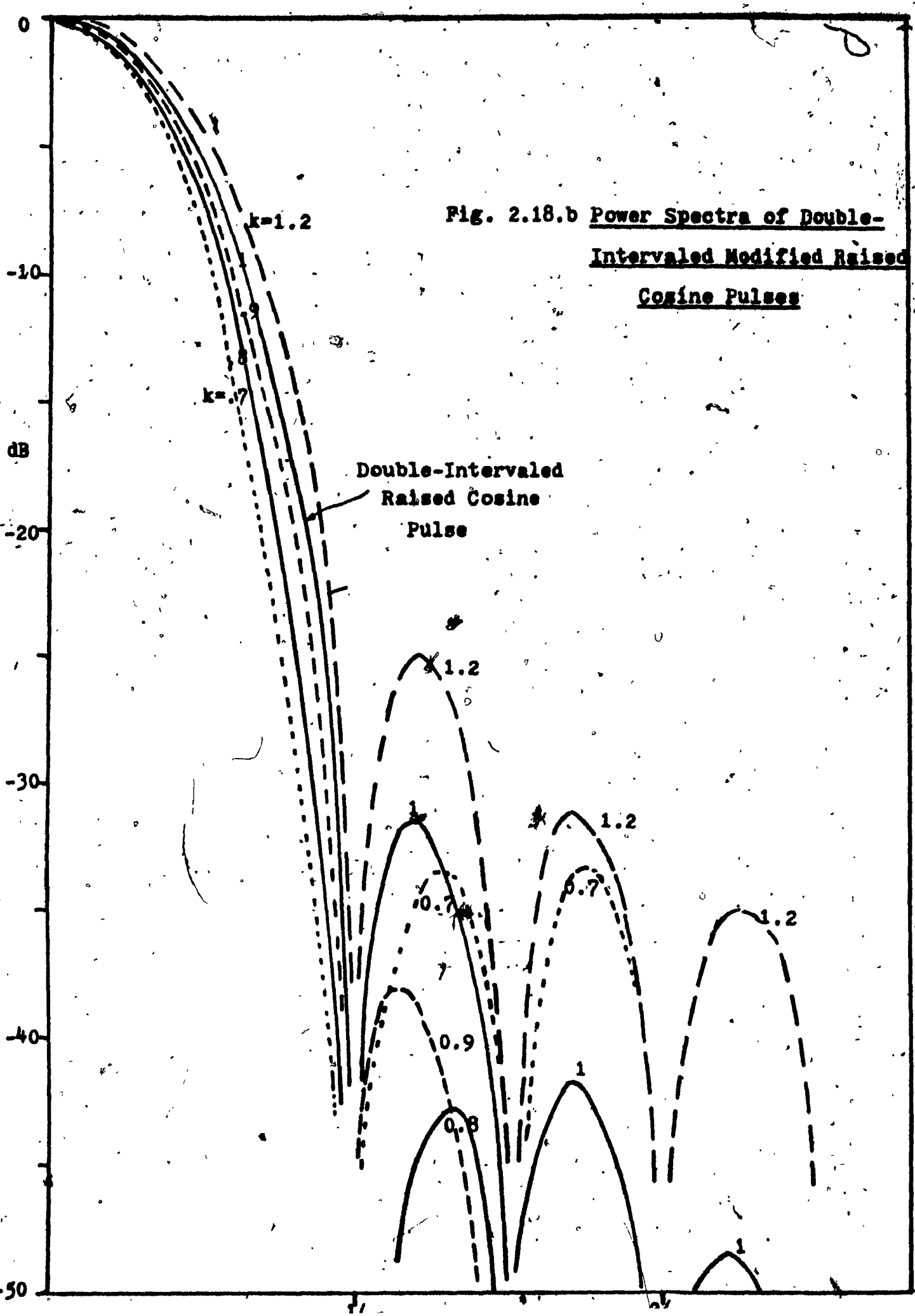

Fig. 2.18.b Power Spectra of Double-Intervaled Modified Raised Cosine Pulses

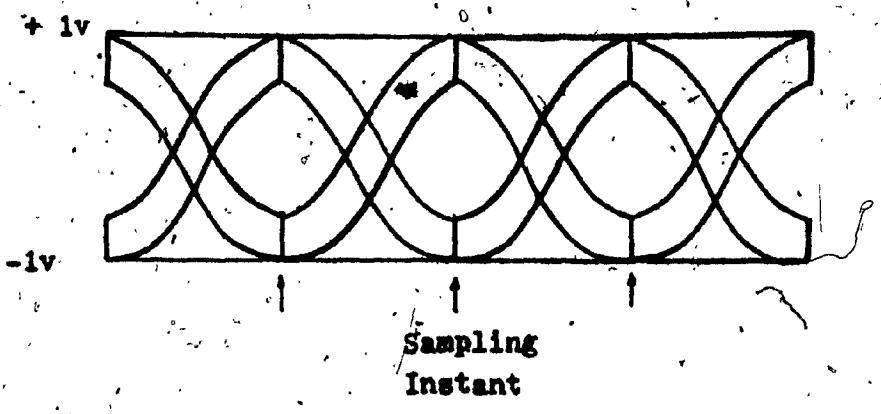

Fig. 2.18.c Eye Diagram of a Random Data Using Doulbe-Intervaled k=0.8 Modified Raised Cosine Pulses as Signaling Elements

2.3.2.4 Complementary Double-intervaled Pulses

As mentioned earlier, a complementary double-intervaled pulse $s'(t)$ is defined as:

$$s'(t) = \begin{cases} 1 - s(t) & \text{for } |t| \leq T \\ 0 & \text{elsewhere} \end{cases} \qquad (2.50)$$

where $s(t)$ is any of the double-intervaled pulses studied earlier.

For example, the double-intervaled complementary raised-cosine $s'(t)$, shown in Fig. 2.19.a, is given by:

$$s'(t) = \tfrac{1}{2}\left(1 - \cos \frac{\pi t}{T}\right) \qquad (2.51)$$

When $s'(t)$ is used as a signaling element to generate a random data stream, the resultant signal waveform has discontinuities as shown in Fig. 2.19.b. Its eye diagram is closed at the sampling instants as shown in Fig. 2.19.c. Hence, for this type of pulse, we do not foresee practical applications. It is included here only as it forms part of the entity in our study of the double-intervaled pulses. Description for the generation of the random data stream using double-intervaled pulses such as shown in Fig. 2.19.b will be covered in the next section.

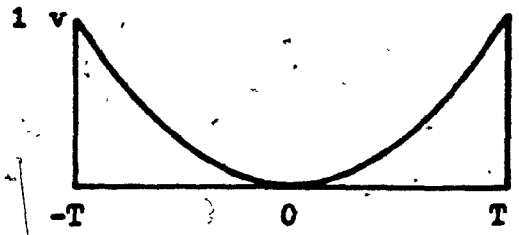

a.

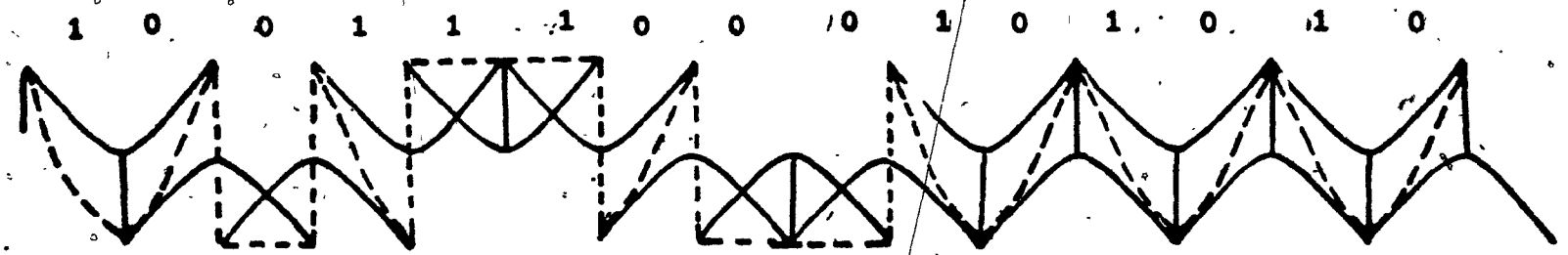

Dotted Line: Resultant Signal Waveform

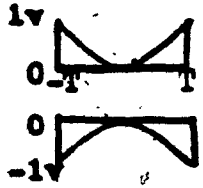

— Definition of 1

— Definition of 0

b.

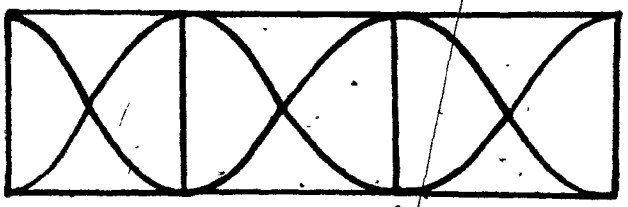

Sampling Instants

c.

Fig. 2.19 a. Complementary Raised-Cosine Pulse s(t)

b. Random Data Stream Formed of s(t) shown in (a)

c. Resulting Eye Diagram

2.4 Generation of ISI and Jitter-Free Data Streams by Pulse Overlapping

In the previous sections, double-intervaled pulses and their spectral properties were studied. In this section, one method that can generate a random data stream using double-intervaled pulses as signaling elements is described. One important feature of the random data stream generated by this technique is that it has the same spectral shape as that of the original double-intervaled pulse element itself [Bennett and Davey, 2.1]. Hence, a bandlimited signal can be generated by choosing a suitable pulse shape for the signaling elements in the data stream. Another important feature of the random data stream generated in this manner is that it has no ISI and is jitter free.

Since a double-intervaled pulse occupies a two-bit interval, for ISI and jitter free transmission, it has to synchronously overlap with its adjacent pulses. This means that each pulse starts at the mid-point of its preceding pulses as shown in the two examples given in Fig. 2.20. As signaling elements, a double-intervaled pulse $s(t)$ representing a 1 symbol is switched on for a two-bit duration; for a 0 symbol, an inverted double-intervaled pulse $-s(t)$ is switched on for the same duration. For the NRZ data stream consisting of the 1 0 0 1 1 1 0 0 0 1 0 1 0 1 0 pattern, example 1 shows the resultant signal waveform when double-intervaled raised cosine pulses are used.

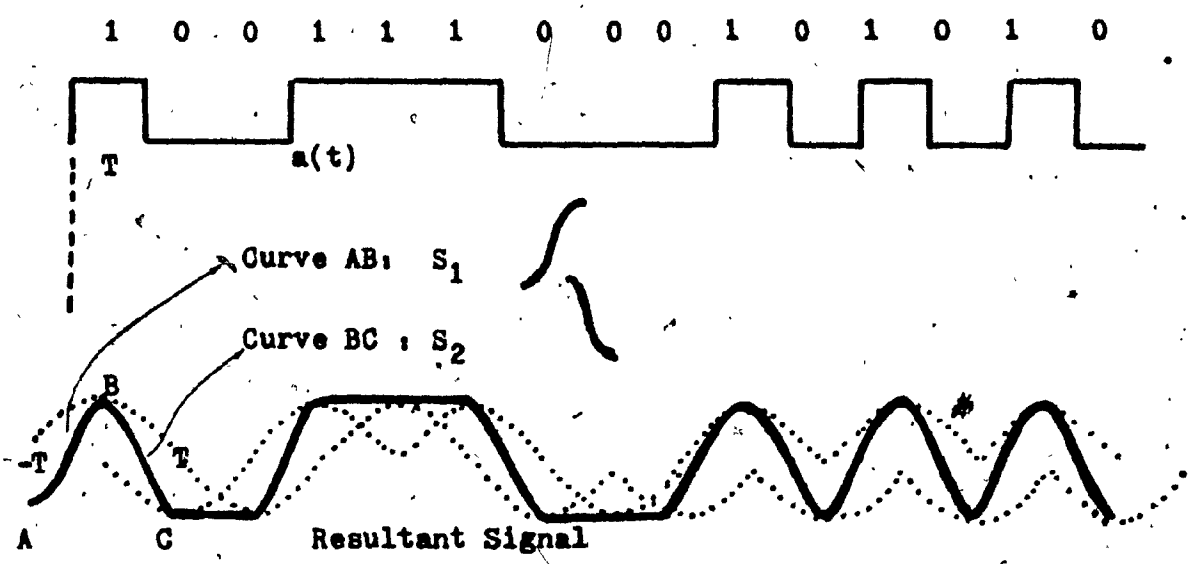

EXAMPLE 1

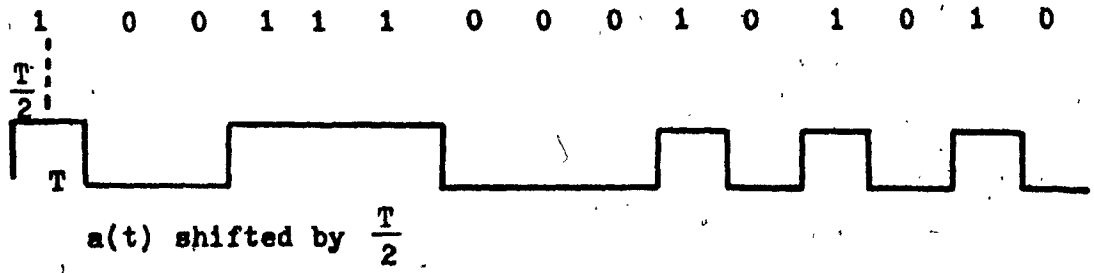

a(t) shifted by $\frac{T}{2}$

Resultant Signal

EXAMPLE 2

Fig. 2.20 Examples Illustrating Generation of a Random Data Stream Using Overlapped Double-Intervaled Pulses

For the same data pattern, Example 2, shows the resultant signal waveform when double-intervaled triangular pulses are used.

In our earlier discussion (Eq. 2.28), it was established that the double-intervaled pulses to be studied in this thesis have the following properties: the sum of the pulse $s(t)$ and its shifted pair $s(t - T)$ at any instant over one bit interval has unity value while the difference of $s(t)$ and $s(t - T)$ over the bit interval is a positive even function. The first condition implies that if there is no transition between the present and the previous bits, then a constant $\pm$ 1 volt prevails in the overlapping region. The second condition is required so that if there is a transition between the present and previous bits, the positive even function is to connect the $\pm$ 1 volt dc without any discontinuity.

For a periodic data stream such as the 1 0 1 0 1 0 pattern shown in the latter segment of the data sequence used in Fig. 2.20.a, the resultant signal waveform is part of a sine wave in Example 1 and part of a triangular wave in Example 2.

Based on the principle of pulse overlapping, one method that can generate a random data stream using double-intervaled pulses is described below.

As shown in Fig. 2.21, the input NRZ data stream is first series-to-parallel converted into two data streams by assigning the odd numbered bits into one channel and the even numbered bits into another channel.

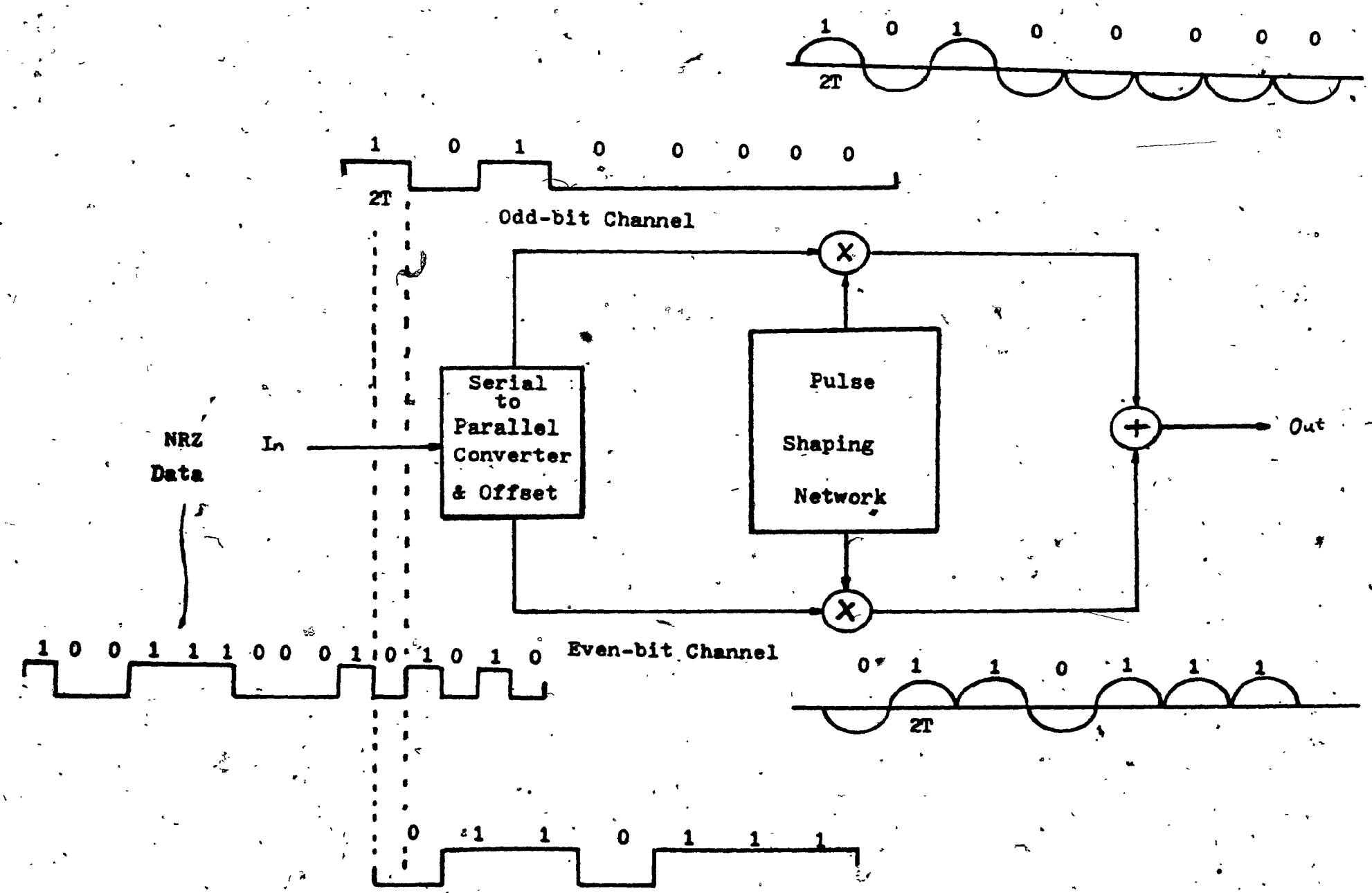

Fig. 2.21 Block Diagram of a Random Data Stream Generator Using Double-Intervaled Pulses

The bit duration of these two new data streams are also lengthened to twice that of the original NRZ data stream. The even channel data is also delayed by one bit interval in comparison with the odd channel data. These two data streams are then pulse shaped by any pre-chosen double-intervaled pulse. If a double-intervaled raised-cosine pulse is used, the sum of these two pulse-shaped data streams becomes the signal waveform depicted in Example 1 of Fig. 2.20. If a double-intervaled triangular pulse is used, the signal waveform depicted in Example 2 of Fig. 2.20 is obtained.

2.5 Nonlinear Switching Filter

As mentioned in Section 2.4, the two conditions specified in Eq. (2.28) are to ensure that when there is no transition between the present and the previous bits a constant 1 volt prevails in the overlapping region and when there is a transition between the present and the previous bits a positive even function connects the 1 volt dc without any discontinuity. By observing the signal waveforms shown in the two examples of Fig. 2.20, we find that they can also be generated in the following manner:

(1) When there is a positive transition from 0 to 1 in the input data stream, waveform S_1 is connected to the output during one bit interval.

(2) When there is a negative transition from 1 to 0 in the input data stream, waveform S_2 is connected to the output during one bit interval.

(3) When there is no transition, a positive or negative dc level is connected according to the logic levels of the input data (1 or 0). The switching-on time also is one bit interval.

Similar nonlinear switching concept was briefly described in Manley's paper on timing noise [2.14] in which he defined the following four signaling conditions:

(i) only the leading edge of a pulse present

(ii) only the trailing edge of a pulse present.

(iii) overlapping pulse present

(iv) no pulse present

Conditions (i) and (ii) in Manley's paper correspond to cases (1) and (2) listed above, respectively. Conditions (iii) and (iv), on the other hand, correspond to the two possibilities of case 3.

Even though the basic concept was described in Manley's paper, no implementation of the system was presented. In [2.7], Gendron and Feher presented circuit implementation of a class of nonlinear switching filters. In this section, a different version of implementing the nonlinear switching filter is described. This modified scheme has the advantage that the filtered signal is not fed back to the input for comparison with the input data stream. This approach avoids the instability problem that might occur in the circuit implementation shown in [2.7]. It also reduces the amount of the clock leakage in the filtered signal.

In the design of the nonlinear switching filter, we define the following four functions. For descriptive purpose, Example 1 of Fig. 2.20 is used. In this example, waveforms S_1 and S_2 are segments of a sine wave.

At time kT, the input NRZ data bit d(kT) is compared with the previous data bit d(kT - T) to produce one of the following waveforms:

1. If d(kT) and d(kT-T) differ and d(kT) = 1, waveform S_1 is generated.

2. If d(kT) and d(kT-T) differ and d(kT) = 0, waveform S_2 is generated.

(2.52)

3. If d(kT) is the same as d(kT-T) and d(kT) = 1, a positive dc level is generated.

4. If d(kT) is the same as d(kT-T) and d(kT) = 0, a negative dc level is generated.

The dc level is equal to the peak value of the sine wave so that the resultant signal waveform will be smooth and continuous.

The timing clocks used in the nonlinear switching filter are derived from the sine wave. These timing clocks and the analog waveforms shown in Fig. 2.22 are obtained in the clock generator and function generator inside the filters. Description of these two generators will be presented later on.

From the above description [(Eq. (2.51) and timing clocks shown in Fig. 2.23], the following four logic signals are defined:

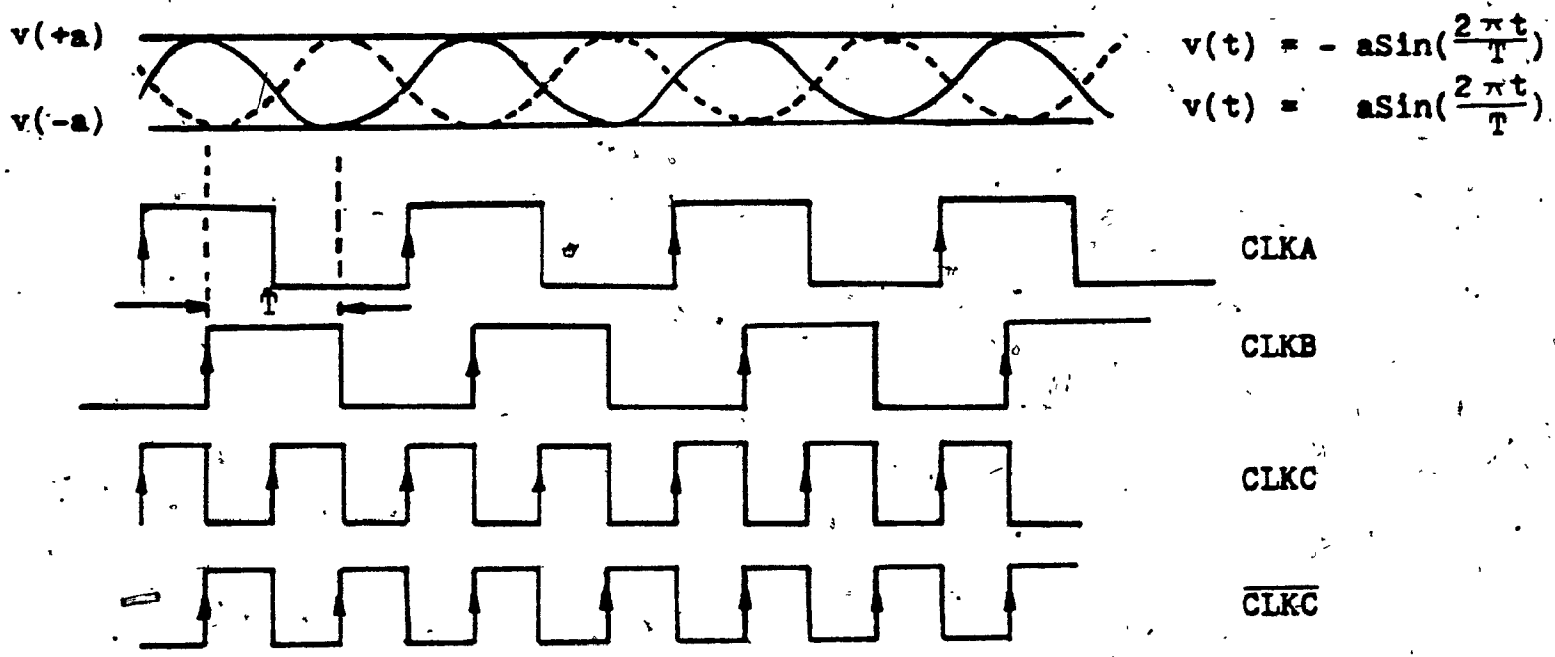

Fig. 2.22 Timing Clocks and Analog Waveforms Used in the Nonlinear Switching Filter

$$A = A(kT) = (d(kT) \oplus d(kT - T)) \cdot (d(kT) \oplus CLKA)$$

$$B = B(kT) = (d(kT) \oplus d(kT - T)) \cdot \overline{(d(kT) \oplus CLKA)}$$

$$C = C(kT) = \overline{(d(kT) \oplus d(kT - T))} \cdot d(kT) \qquad (2.53)$$

$$D = D(kT) = \overline{(d(kT) \oplus d(kT - T))} \cdot \overline{d(kT)}$$

where the $\oplus$ sign stands for Exclusive OR.

Assuming that the four signals $v(t)$, $\overline{v(t)}$, $v(+a)$ and $v(-a)$ are provided, then based on the description given in Eqs. (2.51) and (2.53), one of these waveforms is chosen according to the states of the logic signals:

If A = 1, B=C=D=0, $\overline{v(t)}$ is chosen.

If B = 1, A=C=D=0, $v(t)$ is chosen. (2.54)

If C = 1, A=B=D=0, + a is chosen

If D = 1, A=B=C=0, - a is chosen.

These logic states are clocked by $\overline{CLKC}$ to ensure that the logic produces the right portion of the chosen waveforms (S_1 and S_2) at the right time. A smooth and continuous signal can then appear at the filter output.

The block diagram for the implementation of the nonlinear switching filter consists of the following blocks (Fig. 2.23):

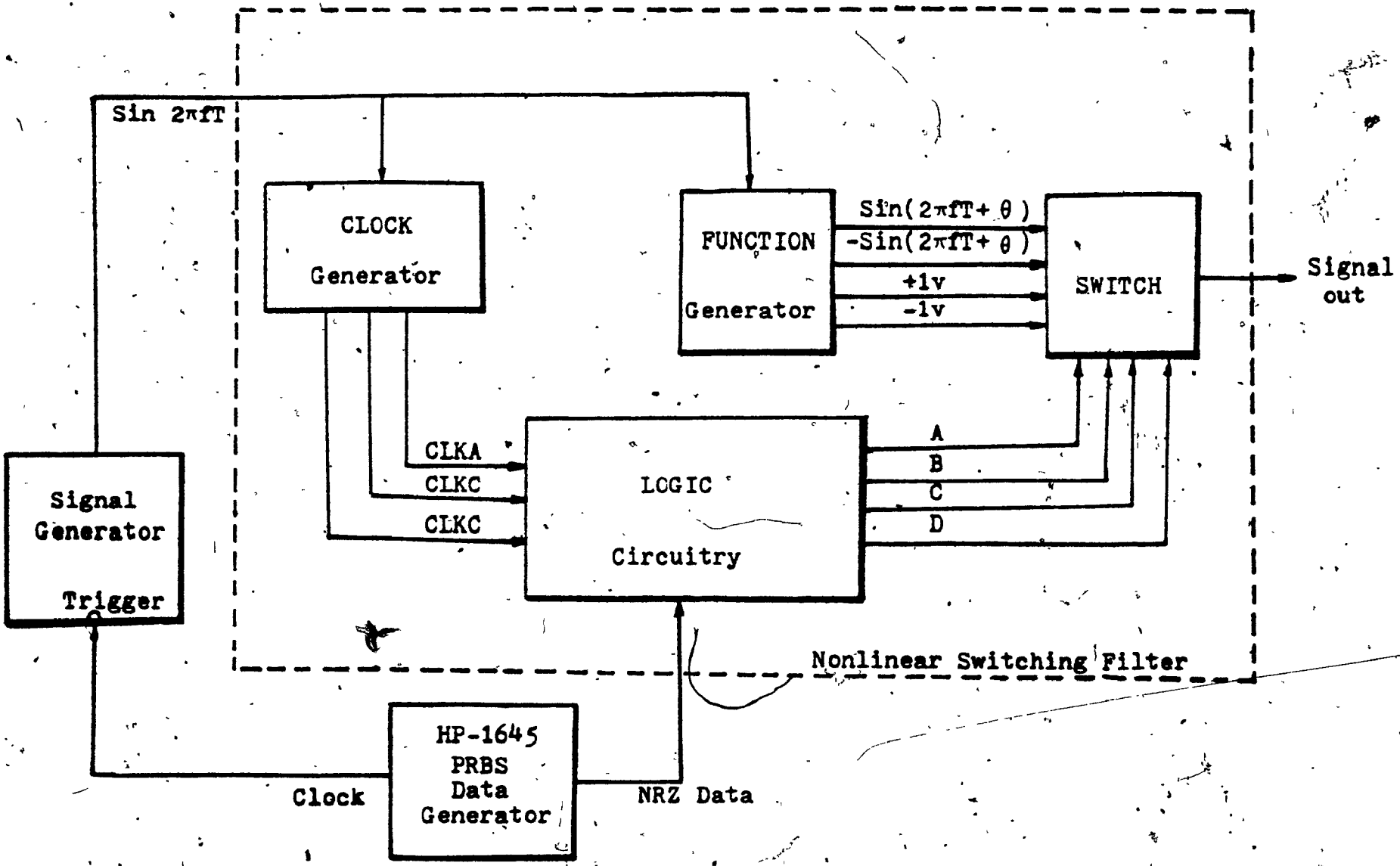

Fig. 2.23 Block Diagram of Nonlinear Switching Filter

a. Clock generator: producing clock waveforms from a periodic signal source v(t).

b. function generator: producing waveforms v(t) $\overline{v(t)}$, + a, and -a from v(t).

c. logic circuit: producing signals at A, B, C and D based on the Boolean logic equations discussed above.

d. Switch: connecting and disconnecting a desired waveform (v(t), $\overline{v(t)}$, + a or -a) depending on the signal from A, B, C and D.

In Fig. 2.24, the clock from the Pseudo-Random Binary Sequence (PRBS) Data Generator is used to trigger the Signal Generator, whose output, sin $2\pi ft$, is employed to produce the timing clocks. These timing clocks and the PRBS data are then applied to the logic circuitary which produces the logic signals, A, B, C and D. The sine wave from the Signal Generator is also applied to the Function Generator which produces the four analog waveforms. Segments of these four analog waveforms are connected and disconnected at the Switch output according to the logic signals A, B, C and D.

The schematic diagram of the circuit of the nonlinear switching

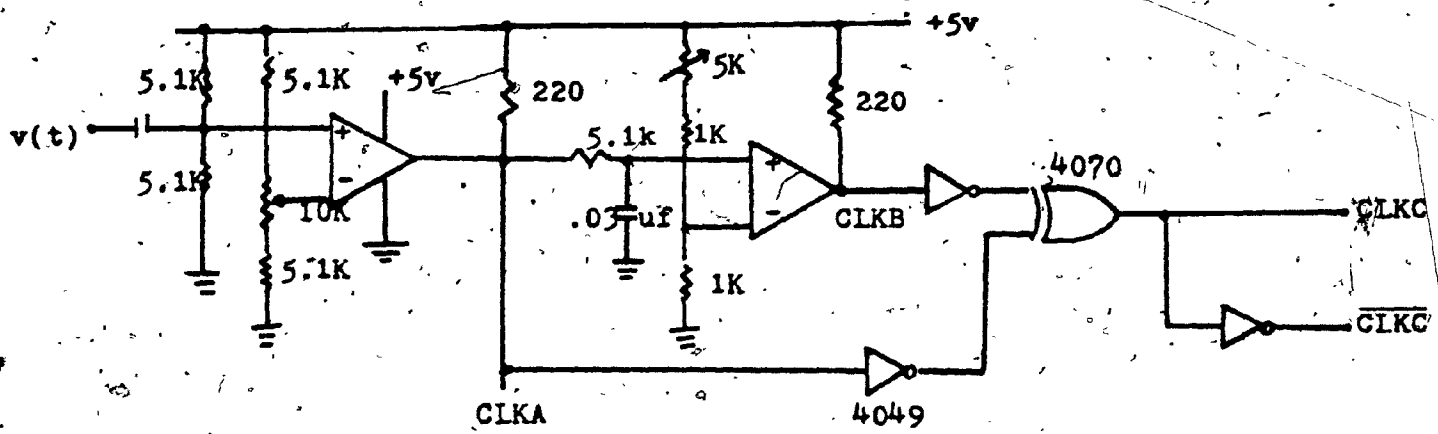

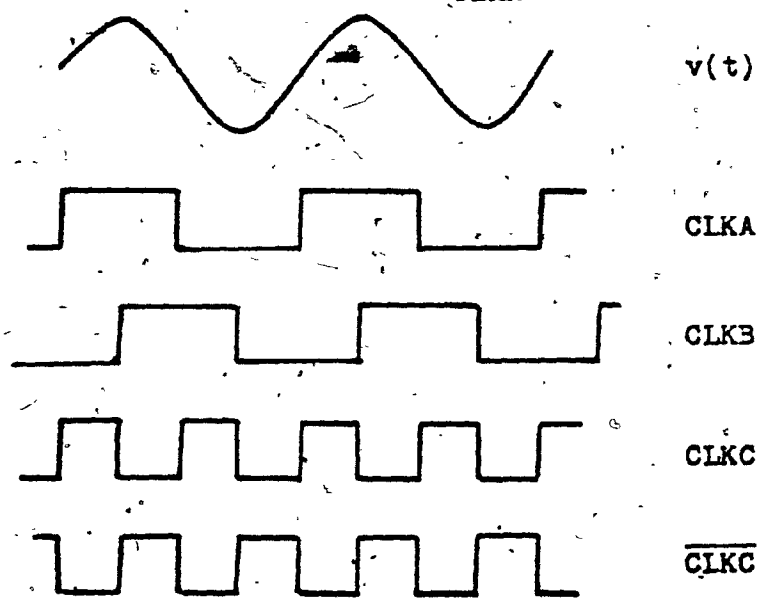

Fig. 2.24.a CLOCK Generator

filter consisting of the four functional blocks is shown in Fig. 2.24.

In the clock generator, the sine wave v(t) having a period of 2T is used to generate at its positive-going edge the timing clock CLKA. This clock and its shifted version CLKB are then exclusively OR-ed to produce CLKC and its inversion $\overline{\text{CLKC}}$. The period of these two new timing clocks is T.

At the input of the logic circuit, the PRBS data bit d(kT) and its delayed version d(kT - T) are modulo-two added. The data bit d(kT) is also modulo-two added with CLKA. From Eq. (2.53) we can see that during any bit interval only one of the four D flip-flops has a high output state. Synchronism is assured by parallel clocking of the flip-flops.

The analog waveform v(t), its inversion $\overline{v(t)}$ as well as the $\pm$ dc signals v(+a) and v(-a), which are generated at the output of the function generator, are then connected or disconnected by the analog switch (in this case, a CMOS integrated circuit CD4066).

In Fig. 2.25 the experimental set-up for measuring the eye diagram and the spectrum of the signal at the output of the nonlinear switching filter is shown. The HP 1645 Data Generator transmits a 32 kb/s PRBS data stream. It also generates a clock which is used to produce a 16 kHz sine wave. This sine wave is then used to produce the four auxiliary analog waveforms v(t), $\overline{v(t)}$, v(+a) and v(-a) as

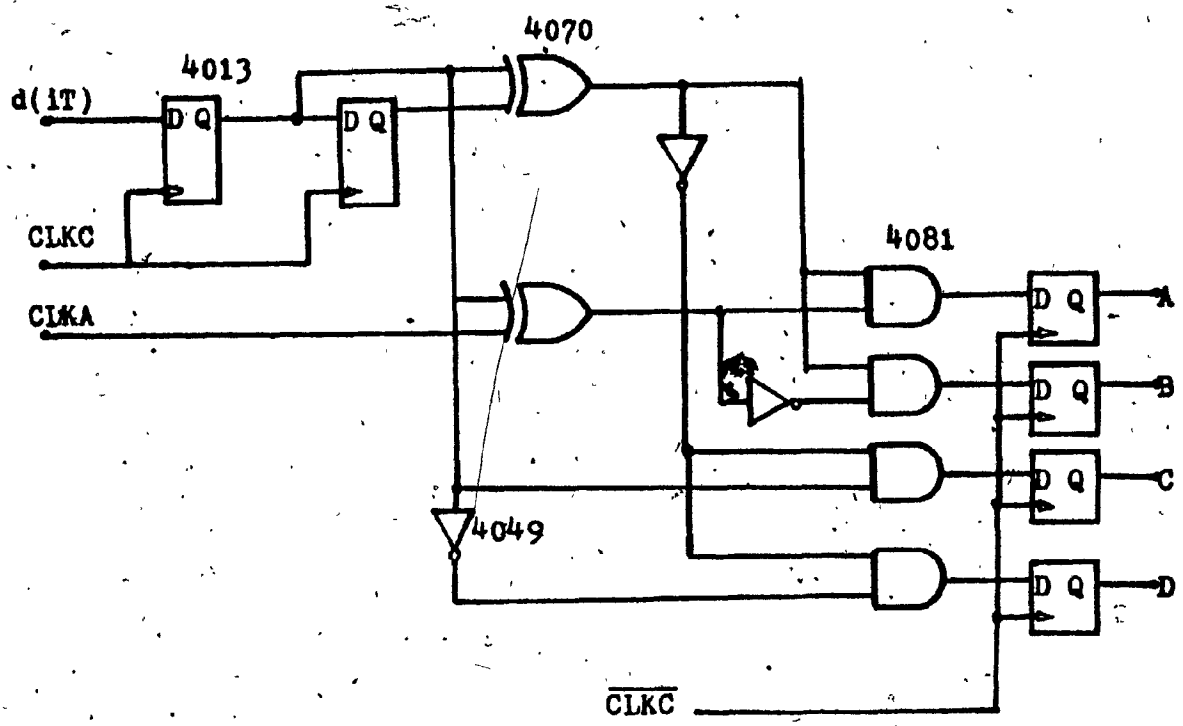

Fig. 2.24.b LOGIC Circuitry

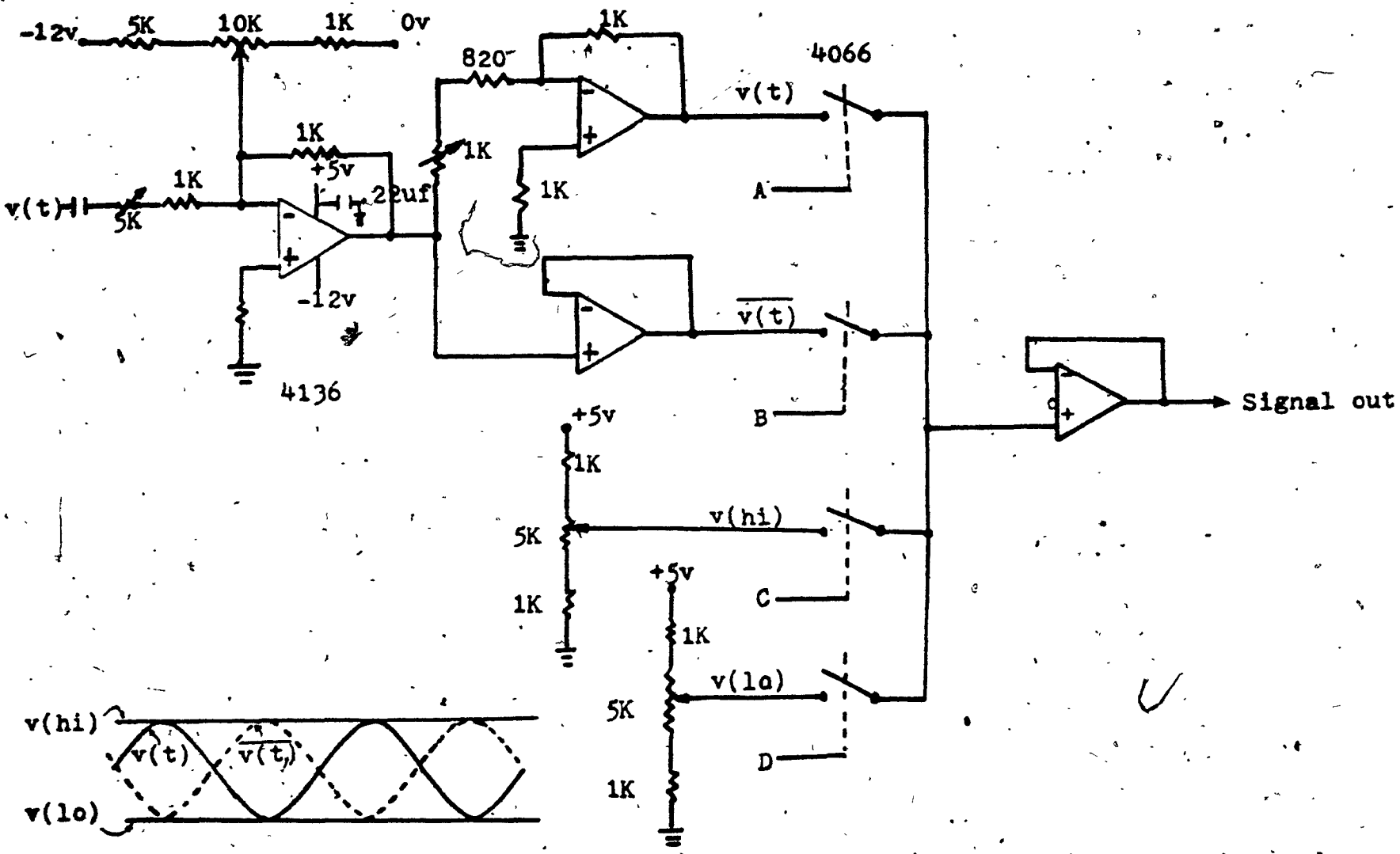

Fig. 2.24.c Function Generator and Multiplexer

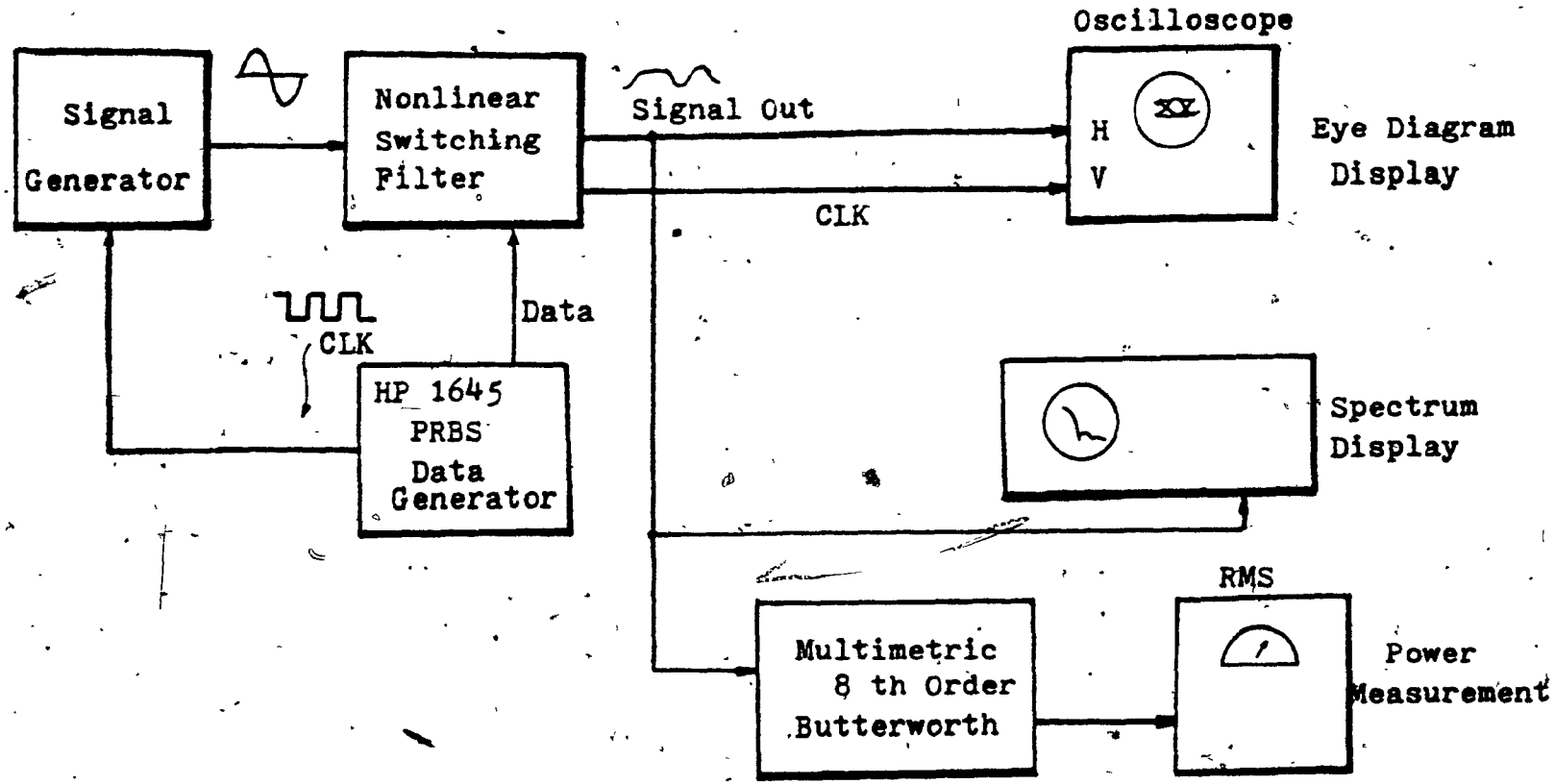

Fig. 2.25 Experimental Set-up for Measuring the Eye Diagram, Spectrum and Out-of-band and In-band Power of a Filtered Signal

described earlier. The eye diagram of the filtered signal at the output of the non-linear switching filter is then observed on an oscilloscope which is triggered by the CLK signal. The spectrum of the filtered signal is displayed on a spectrum analyzer.

The eye diagram of the filtered signal as shown in Fig. 2. 26. a, has no ISI and is also jitter free. The spectrum as shown in Fig. 2. 27. b. is identical to that of the double-intervaled raised-cosine pulse given in Eq. (2. 26). In comparation the spectrum of the NRZ signal is also shown in Fig. 2. 26. b.

The original objective of designing this nonlinear switching filter is to see if it meets the INTELSAT Single Channel per Carrier (SCPC) satellite system requirements. The jitter free characteristic of this nonlinear switching filter obviously meets the 14% peak-to-peak jitter requirement. Another important SCPC specification is that the out-of-band signal power at 1. 4 times the Nyquist frequency should be more than 26dB down from the in-band signal power. This specification is required to reduce the adjacent channel interference.

To measure the in-band and out-of-band power of the filtered signal, a Multimetric active filter is used. In order to have sufficient attenuation, the two 4-pole Butterworth filters in the Multimetric are cascaded to form an 8-pole filter. The 6dB corner frequency of the cascaded 8-pole Butterworth high pass filter is set at 22. 4 kHz

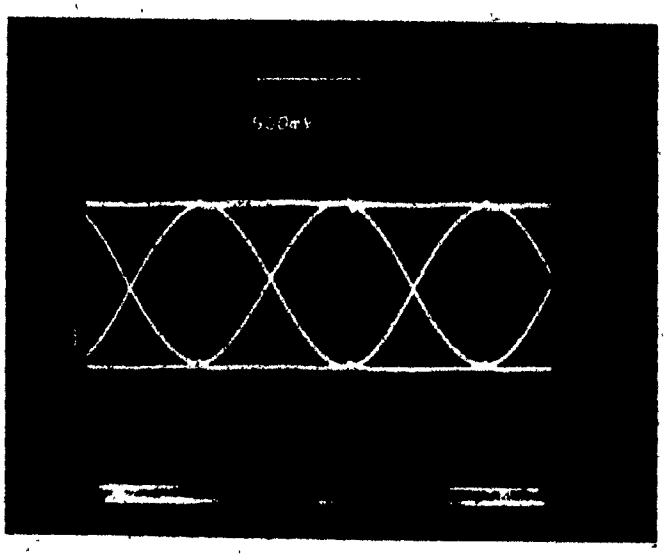

V: 500 mv/div

H: 10μs/div

Fig. 2.26.a Eye Diagram of the Output Signal of Nonlinear Switching Filter when a Sine Wave is Used

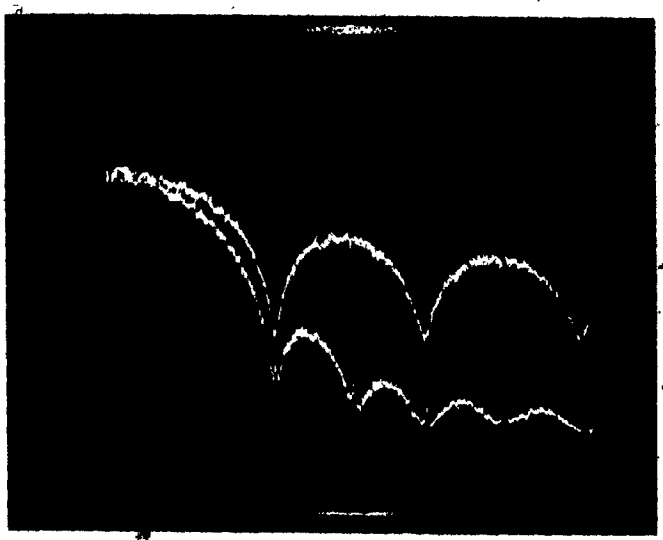

NRZ

Signal of Fig. 2.26.a

V: 10 dB/div.

H: 10 kHz/div

Fig. 2.26.b Spectrum of Signal Shown in Fig. 2.26.a in Comparison with that of NRZ

which is equal to 1.4 Nyquist frequency for the 32 kb/s data stream. The out-of-band power was measured to be -22 dBm at the RMS voltmeter. By removing the Multimetric filter, the in-band signal power was measured to be -1.2dBm. The in-band signal power can also be measured by using the 8-pole Butterworth low pass filter setting at the corner frequency of 22.4 kHz. The error between these two measurements is very small as most of the signal power is contained in the main spectral lobe.

The measured in-band to out-of-band power ratio of the signal at 1.4 times the Nyquist frequency is hence about 20dB. Using Eq. (2.26), the in-band to out-of-band energy ratio at 1.4 times the Nyquist frequency is calculated to be also 20dB. Thus this filter does not meet the SCPC 26 dB rejection requirement. Only at 1.6 times the Nyquist frequency was the in-band to out-of-band power measured to be 26dB.

If the sine wave from the signal generator is changed to a triangular wave, the signal at the output of the nonlinear switching filter becomes that shown in Example 2 of Fig. 2.20. The eye diagram of this signal as shown in Fig. 2.27.a is also ISI and jitter free. Its spectrum in comparison with that of the NRZ signal is shown in Fig. 2.27.b. The measured in-band to out-of-band power ratio in this case was 22.4 dB at 1.4 times the Nyquist frequency.

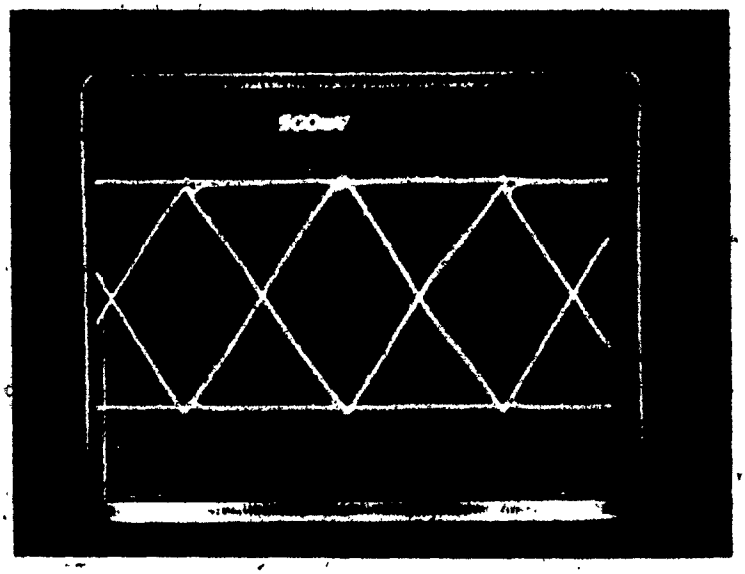

V: 500 mv/div

H: 10 μs/div

Fig. 2.27.a Eye Diagram of the Output Signal of Nonlinear Switching Filter when a Triangular Wave is Used

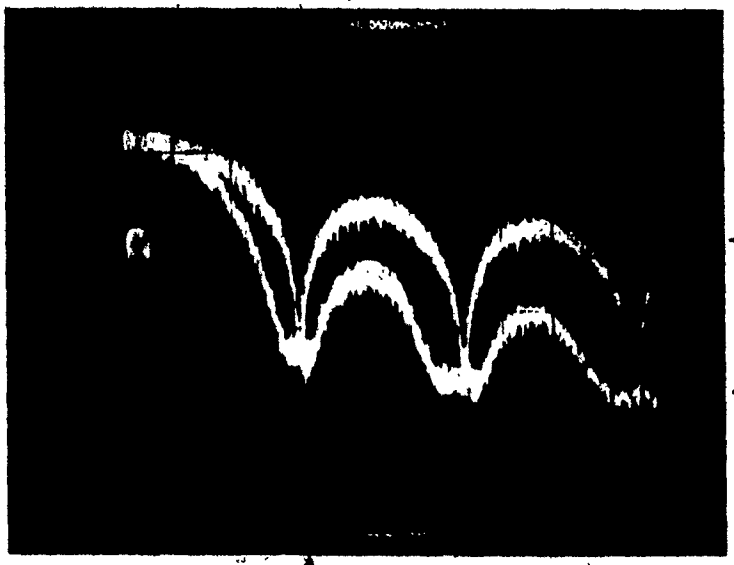

NRZ

Signal of Fig. 2.27.

V: 10 dB/div

H: 10 kHz/div

Fig. 2.27.b Spectrum of Signal Shown in Fig. 2.27.a in Comparison with that of NRZ

The performance of a digital baseband system using this nonlinear switching filter in a white gaussian noise environment was given in Ref. [2.7]. For a baseband system in a coloured gaussian noise environment, Feher and Huang [2.17] demonstrated that the error rate performance is identical to that in a white gaussian noise environment if the SNR at the regenerator input is the same.

Another important characteristic of the jitter free signal obtained by either the nonlinear switching method of the pulse overlapping method is that, after it is passed through an analog filter, the jitter-free property still prevails even if the analog filter starts to cause ISI on the signal. This can be seen from Figs. 2.28.a and 2.28.b. In contrast to this, most conventional analog filters causing ISI to the signal also introduce jitter.

Although this nonlinear switching filter does not meet all the SCPC specifications, it is expected that it might still find applications in other low bit rate satellite communication systems because of its ISI- and jitter-free characteristics.

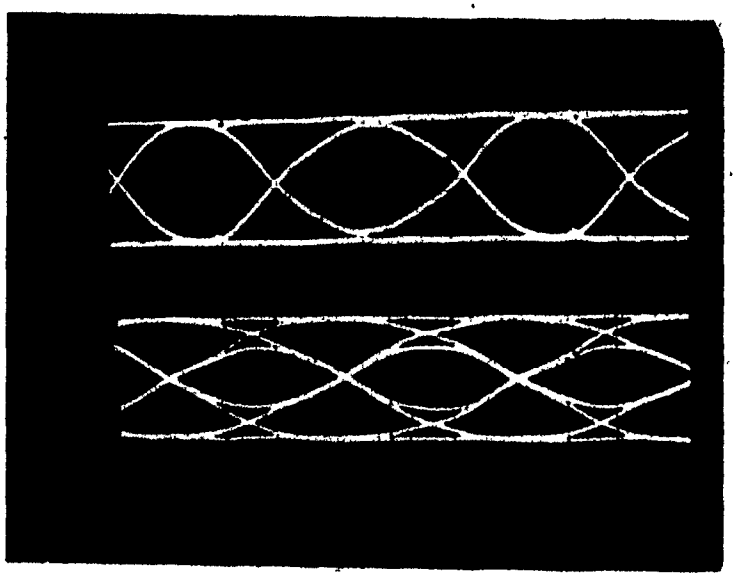

V: 500 mv

H: 10 μs

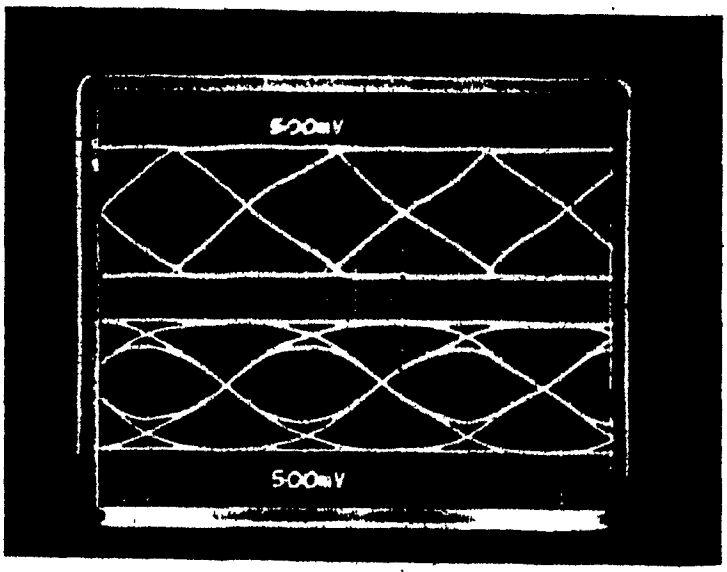

V: 500 mv

H: 10 μs

Upper Photo: Raised-cosine Pulse-shaped Signal before and after Passing through an 8 Pole Butterworth LPF (f_{3dB} at 20 kHz)

Lower Photo: Triangular Pulse-shaped Signal beore and after Passing through an 8 Pole Butterworth LPF (f_{3dB} at 20 kHz)

Fig. 2.28 Eye Diagrams Showing the Jitter-free Property of the Nonlinear Switching Filtered Signal

2. Summary of Chapter 2

As stipulated by the Nyquist theorem, a random data stream using synchronous time-domain Nyquist pulses as signaling elements has no ISI. Due to the oscillating tails of the Nyquist pulses, jitter exists in the zero crossings of the eye patterns of the random signal. An analytical method was presented in this chapter which can be used to calculate the peak-to-peak jitter and to plot the boundary traces of the resulting eye pattern. Results obtained from this study can be used to study the system tolerance caused by the imperfections of the designed filter.

It is shown that a random data stream using synchronous double-intervaled pulses as signaling elements exerts zero ISI and no jitter. The spectral characteristics of double-intervaled pulses were studied. Random data streams generated by overlapping double-intervaled pulses are shown to have low spectral lobes.

Two methods that can generate the ISI-and jitter-free bandlimited signal were described. The first method uses the concept of pulse overlapping. The second method employs the concept of nonlinear switching.

A circuit design of nonlinear switching filter was presented. Measured results from this circuit agree with our theoretical predictions. It is expected that this nonlinear switching filter might find applications in the low bit rate satellite communication systems.

CHAPTER 3

Chapter 3

Partial Response Signaling Techniques and Their Applications in QPRS Radio Systems

3.1 Introduction

As described in Chapter 1, an ideal brick-wall Nyquist filter allows a binary system to transmit at the Nyquist rate of 2 b/s/Hz without intersymbol interference (ISI). For practical purposes, the ideal Nyquist filter is not realizable because of the infinite delay involved. Our study on jitter in Chapter 2 also shows that the resulting system is intolerant to any slight sampling errors. On the other hand, the raised cosine filter, whose impulse response maintains zero crossings at the sampling instants for ISI free transmission, is realizable. This is made possible at the expense of wider bandwidth and consequently the transmission spectrum efficiency is reduced. For example, the full raised-cosine filter ($\alpha=1$) can only transmit binary data at a rate of 1 b/s/Hz. Thus, the Nyquist rate of transmission cannot be achieved with the Nyquist type of filter which has zero memory in the sampling instants.

One way to increase the data rate is to use multi-level PAM (Pulse Amplitude Modulation) systems where the pulse amplitudes can take any one of M levels. If M levels per symbol are used, the bit rate is increased by a factor of k relative to that of the binary system where

$$k = \log_2 M \qquad (3.1)$$

For a given bandwidth, the transmission speed of the multi-level PAM systems therefore becomes k times higher than that of the binary system. This is achieved at the expense of a higher signal-to-noise ratio (SNR) requirement for the same error rate in comparison with that of the binary system. The error rate performance of the binary, 4 and 8 level PAM systems is presented in Figure 3. 1 [Lucky et al, 3. 1] .

However, there is a practical limit as to how much the binary source rate may be increased using the PAM technique. With levels increasing, it becomes more difficult to make a correct decision at the receiver as the noise margin is reduced. The hardware complexity also becomes more involved. In practice, PAM systems with higher than sixteen levels have not yet found applications.

Another method of achieving Nyquist, or even higher, rate of transmission with realizable filters, is to introduce prescribed amounts of ISI into the binary system.

Due to the correlation of the data bits, i. e., the existence of finite memory, spectral reshaping of the binary or PAM systems, permits transmission at the Nyquist rate or even higher with more gentle filters. Originated by Lender [3. 2] in 1963, the first correlative system was called duobinary as this new system can achieve the Nyquist rate of transmission. Higher level correlative system is

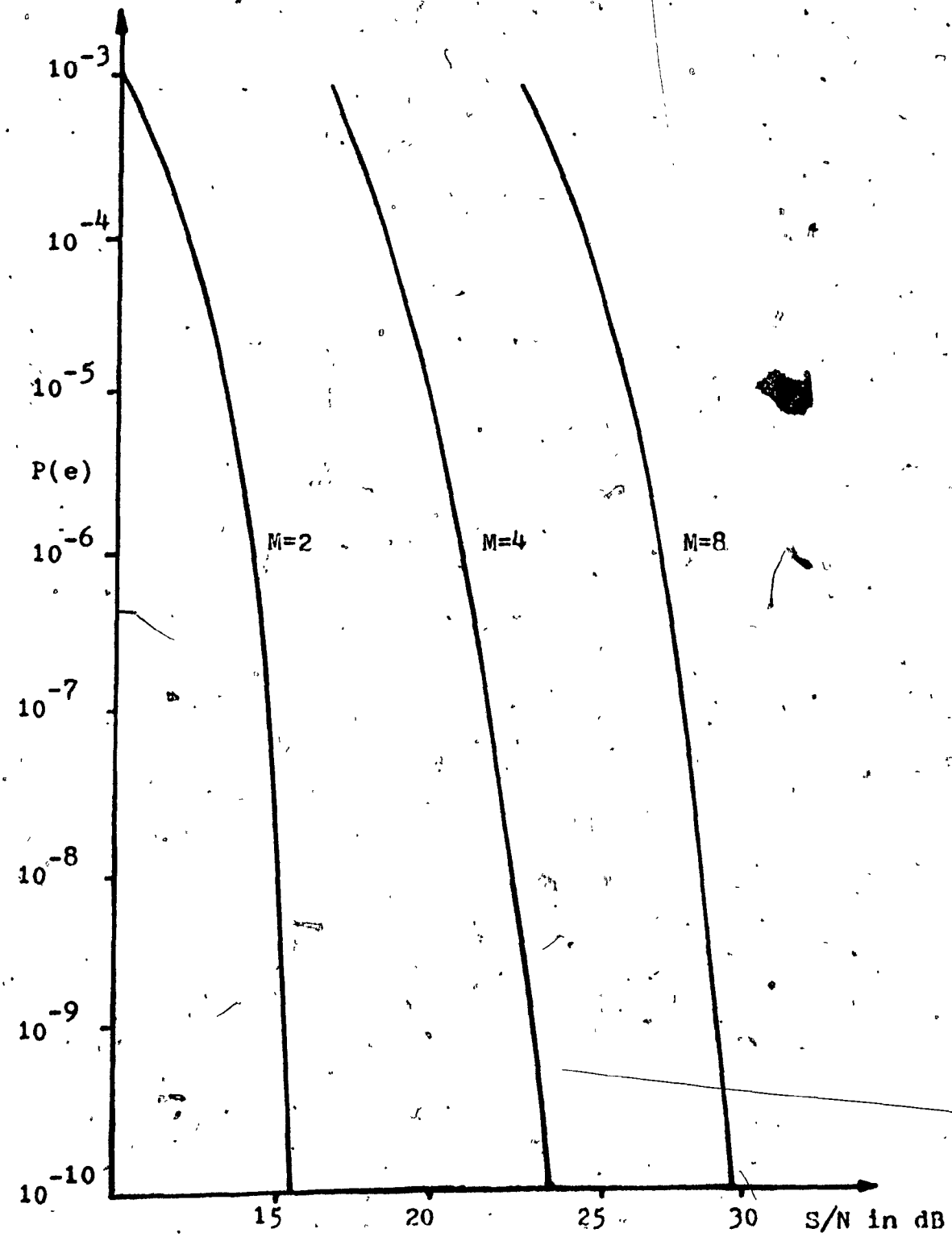

Fig. 3.1 Probability of Error, P(e), of M-level PAM Baseband Systems

(The rms S/N is specified in the Nyquist bandwidth)

generally known as polybinary [Lender, 3.3]. Subsequently, in 1965, Kretzmer [3.5] used the term Partial Response for more generalized correlative systems. Nowadays, both terms are used in the literature. For convenience, we use the term Partial Response (PR) in this thesis.

Some of the PR filtered signals have no DC component and little energy at low frequency end. This feature might be useful for transmission systems where service channel is to be inserted at the low frequency end [Lender, 3.7]. One other important feature of the PR scheme is that it has an inherent advantage that it can also detect transmission errors without the need of introducing any redundant bits into the original data stream [Lender, 3.2][Pasupathy 3.4].

PR technique has been applied to various modulation schemes such as FM and SSB as well as baseband systems. For digital transmission over existing analog microwave radio systems, Bell Telephone System in the U.S.A. introduced the Data Under Voice system where baseband data, encoded as a 7-level PR signal, is placed under the FDM voice channels in a hybrid mode of operation [Feher, 3.13]. GTE Lenkurt has also applied the duobinary FM and 7 level correlative FM techniques for transmission over existing analog systems., [3.6][3.7]. For digitalized telephone signal voice transmission,

GTE Lenkurt has developed a modified duobinary repeater which doubles the capacity of the T1 carrier from 24 to 48 channels [3.8].

The PR technique has also been adopted in a Quadrature Amplitude Modulation system known as Quadrature Partial Response System (QPRS). For example, Bell-Northern Research has developed a high capacity digital radio system using QPRS with a spectrum efficiency of 2.25 b/s/Hz [3.9]. This system has a radio frequency of 8GHz and is intended for a Trans-Canada telephone network. In Japan, Fujitsu has developed a 2 GHz digital radio using QPRS with a spectrum efficiency of 2 b/s/Hz [3.10]. In the U.S.A., Avantek has manufactured a 2 GHz QPRS digital radio which attains a spectrum efficiency of 1.8 b/s/Hz [3.11].

In this Chapter, we will first review the basic schemes of PR signaling. The principle of superposition of time-domain $\alpha=0$ Nyquist pulses introduced in Chapter 2, will be used in our presentation. This approach has the advantage that the amount of ISI introduced intentionally, can be identified in resulting PR pulses [Kretzmer, 3.5]. The transfer functions of the PR filters can then be obtained from the Fourier transforms of these PR pulses.

The concept of pulse overlapping presented in Chapter 2, can also be applied to the generation of multilevel PR signals. It will be shown that pulse overlapping is equivalent to introducing correlation into a binary random data stream. The ratio of the Fourier

transform of the multi-bit intervaled pulse to that of the uni-bit intervaled rectangular pulse, results in a transfer function identical to that of the digital filter which performs the transformation of the binary signal into the multilevel signal. The transfer function of the partial response filter is the transfer function of the digital filter in cascade with that of a brick-wall Nyquist filter. It is shown that the spectrum of the multi-level signal prior to the Nyquist filter can also be computed from the Fourier transform of the overlapping pulse. Our presented method provides an alternate derivation of the power spectrum of the correlative-coded data stream. It is expected that our derivation presents additional insight into the physical interpretation of these signaling techniques.

The SNR degradation for PR signaling in comparison to a binary system can be calculated for the two system models discussed in detail in [3. 12]. We will call these two system models Model 1 and Model 2 in this chapter. In the experimental 7-level correlative FM radio system [3. 7], Lender used a different model for the implementation of the modified-duobinary filter. In this chapter, Lender's model will be analyzed and extended to other PR systems. Results for this third system model will then be compared with the two other system models. Based on design and application considerations, the merits of each system model will also be assessed.

The realization of a practical PR filter shape and its effect on the performance of a transmission system have not been documented in sufficient detail in the literature. Also, the performance of PR modulated systems operating through a nonlinear device such as a Travelling Wave Tube amplifier (TWT) or an IMPATT Diode amplifier has not yet been published. To study these effects, a computer simulation program for a QPRS digital radio link was developed. The effects of imperfect filtering in a linear channel will be presented first. Afterwards, the study of the TWT nonlinearity effect will be divided into AM/AM conversion alone and AM/AM and AM/PM conversions combined.

Based on references [3.19][3.20], a simple guideline for evaluating the performance of a digital radio system will be presented. Using this simple guideline, the performance of some digital radio systems using QPRS will be compared and summarized in a table.

The listing of the QPRS computer simulation program is given in Appendix B.

3.2 Partial Response Signaling by Superposition of Nyquist Pulses

In this section, time domain PR pulses are obtained from the superposition of $\alpha_s=0$ Nyquist pulses. These PR pulses have spectra that satisfy the Nyquist minimum bandwidth requirement. As such, the resulting PR system permits transmission at the Nyquist rate with more gentle filters. If even more efficient bandwidth compression is desired, an adaptive decision feedback technique can be applied for the elimination of excessive ISI. This approach was adopted in the design of the Bell-Northern Research's DRS-8 radio system to achieve the 2.25 b/s/Hz spectral efficiency [3.9].

3.2.1 Class 1 PR System

The simplest and most widely used PR system is obtained from the superposition of two Nyquist pulses with their peaks positioned at $\pm$ T/2, where T is the bit duration of the binary system. As shown in Figure 3.2.a, the resulting pulse (dotted line) has two non-zero samples, at the sampling instants. Following Kretzmer's notation [3.5], this pulse is called the class 1 PR pulse (or duobinary pulse if Lener's notation is adopted (3.2)). The class 1 partial PR pulse such as shown in Figure 3.2.a is given by:

$$h(t) = \frac{\sin\frac{\pi}{T}(t-\frac{T}{2})}{\frac{\pi}{T}(t-\frac{T}{2})} + \frac{\sin\frac{\pi}{T}(t+\frac{T}{2})}{\frac{\pi}{T}(t+\frac{T}{2})} \qquad (3.2)$$

$$= \frac{4T^2}{\pi} \quad \frac{\cos \frac{\pi t}{T}}{(T^2 - 4t^2)} \tag{3.2}$$

from which it may be easily shown that if the response sampling time t_o is chosen to be $-T/2$, then

$$h_n = h(nT + t_o) = \begin{cases} 1 & n = 0, 1 \\ 0 & \text{otherwise} \end{cases} \tag{3.3}$$

As there are two non-zero samples at the sampling instants, there is intersymbol interference (ISI) from the previous symbol. This controlled amount of ISI can be removed by using either decision feedback equalized at the receiver or precoding at the transmitter [Lender, 3.2 and 3.3].

The class 1 PR pulse has the same shape as the impulse response of the class 1 PR filter whose transfer function is given by:

$$H(f) = \begin{cases} 2T \cos \pi fT & \text{for } 0 \leq f \leq \frac{1}{2}t \\ 0 & \text{elsewhere} \end{cases} \tag{3.4}$$

and is plotted in Figure 3.2.b.

A class 1 PR sequence (P_n) can be realized by adding algebraically the present bit a_n of a binary sequence to its previous bit a_{n-1} as given below:

$$P_n = a_n + a_{n-1} \tag{3.5a}$$

where $\{a_n\}$ represents the input binary sequence. A segment of the binary sequence and its corresponding 3 level PR sequence are

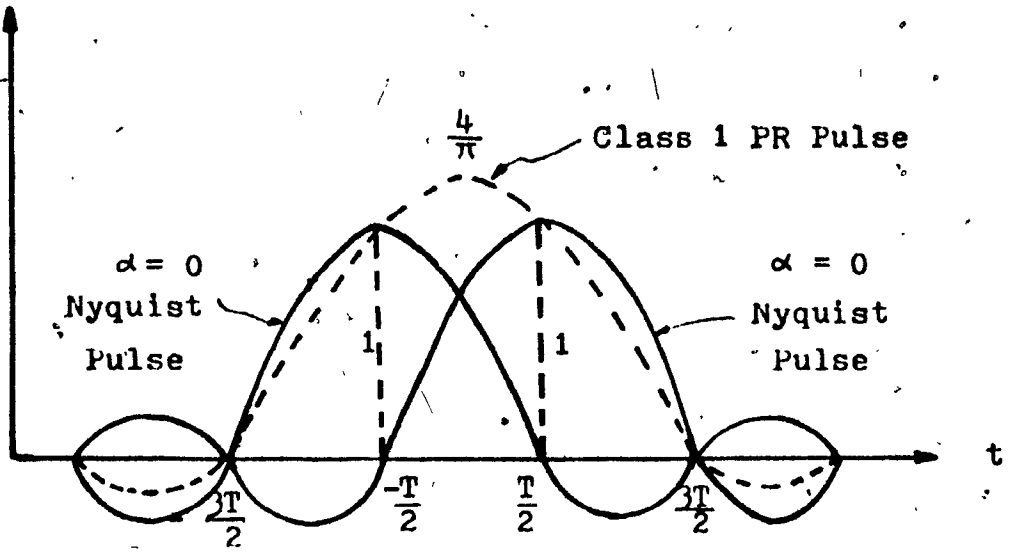

a. Class 1 PR Pulse from the Superposition of Two $\alpha = 0$ Nyquist Pulses

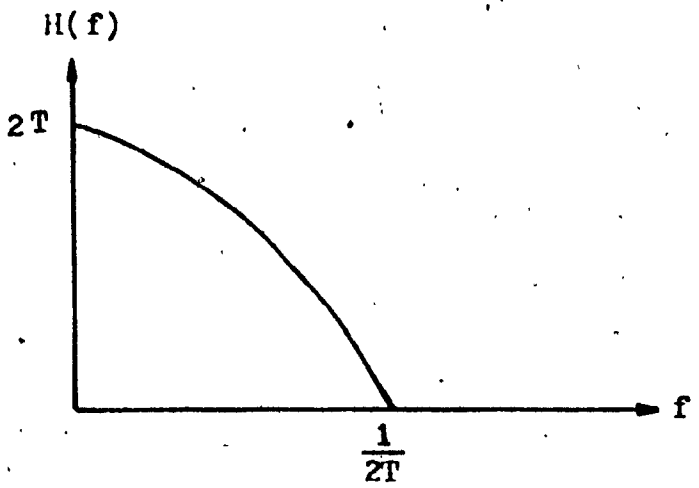

b. Class 1 PR Filter (Duobinary)

Fig. 3.2 Generation of a Class 1 PR Pulse and Its Corresponding Fourier Transform

shown in Figure 3.3.

One drawback of this system is that errors, once made, tend to propagate, i.e., if a_{n-1} is in error, then a_n is likely to be in error also. To eliminate this error propagation problem, Lender [3.2] introduced the precoding scheme at the transmitter. It involves transformation of the input binary data stream $\{a_n\}$ into a new binary data stream $\{b_n\}$ by modulo-2 addition as follows:

$$b_n = a_n \oplus b_{n-1} \tag{3.5.b}$$

The new binary data stream $\{b_n\}$ is then transformed into the 3 level class 1 PR pulse train $\{b_n\}$ using Eq. (3.5.a).

At the receiver, the binary data stream $\{a_n\}$ can now be detected independently. For example, if a_n is 0, then $b_n = b_{n-1}$ and p_n is either +2d or -2d, if the bit sequence $\{b_n\}$ uses the level $\pm$d for 1 or 0 respectively. On the other hand, if a_n is 1, then b_n is always the reverse of b_{n-1} and the received level p_n is always 0. Hence, a_n, in the absence of noise, can be described by the following rule:

$$\begin{aligned} a_n &= 0 \quad \text{if} \quad p_n = \pm 2d \\ a_n &= 1 \quad \text{if} \quad p_n = 0 \end{aligned} \tag{3.5.c}$$

This rule involves rectification of p_n and a simple threshold binary

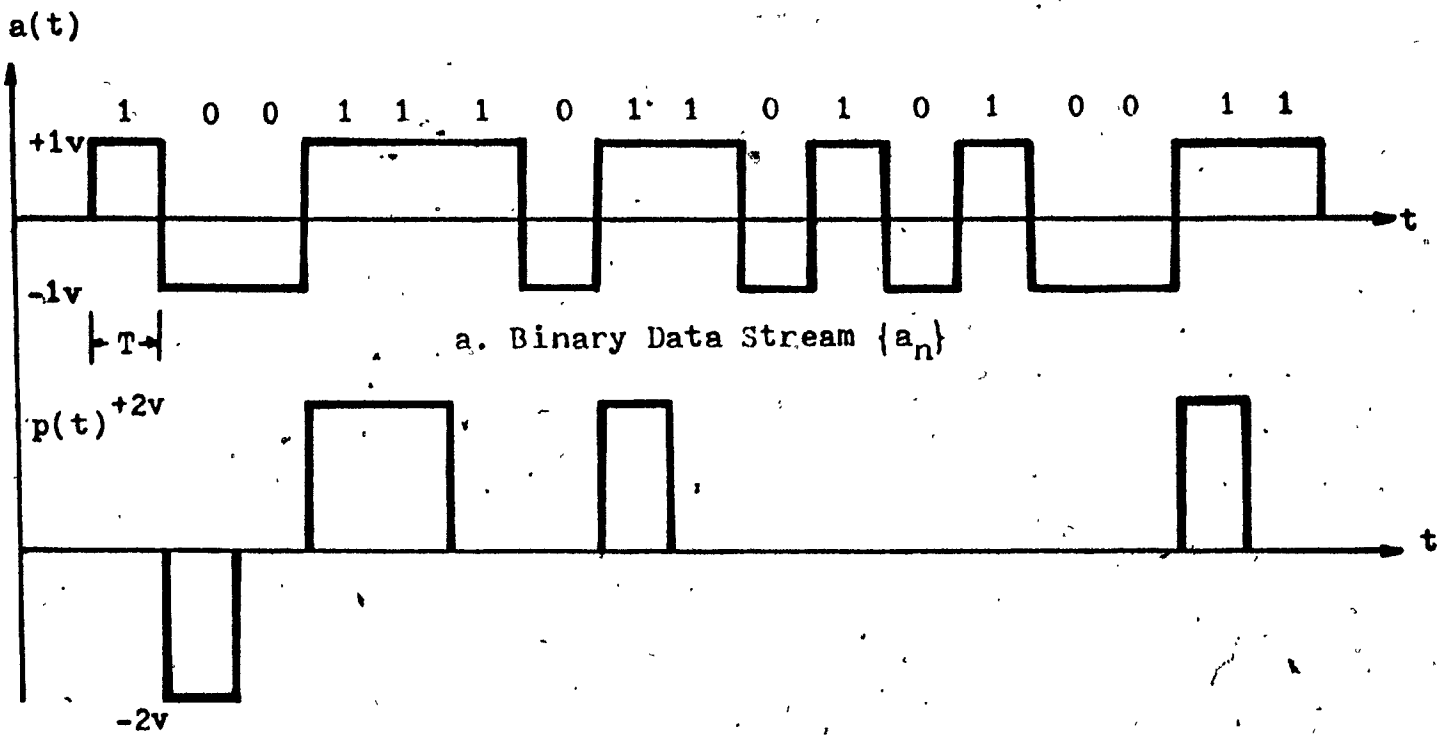

Fig. 3.3 Generation of a 3-level Class 1 PR Pulse Train from a Binary Data Stream

decision. As no prior knowledge of any symbol other than p_n is required in deciding a_n in the precoding scheme, no error propagation will occur.

Based on Eq. (3.5.a), a class 1 PR filter can be realized as shown in Figure 3.4.a. The cascade of the digital filter and the ideal brick-wall Nyquist filter can be shown as follows to give the transfer function of the class 1 PR filter.

The delay element has a transfer function of $e^{-j2\pi ft}$. Hence, the transfer function of the digital filter is $1 + e^{-j2\pi ft}$, i.e.,

$$\begin{aligned} H_1(f) &= 1 + e^{-j2\pi ft} \\ &= e^{-j\pi ft} \cdot (e^{j\pi ft} + e^{-j\pi ft}) \\ &= e^{-j\pi ft}\,(2T\cos\pi fT) \end{aligned} \tag{3.6}$$

and,

$$|H_1(f)| = 2T\cos\pi fT \qquad \text{for all } f \tag{3.7}$$

The brick-wall Nyquist filter is then used to remove the transfer function beyond the Nyquist frequency. The overall transfer function of Figure 3.4.a is thus that given in Eq. (3.4).

Figure 3.4.b. shows circuit implementation of the class 1 PR baseband system. This circuit design follows the block diagram shown in Figure 3.4.a where the PR filter transfer function is obtained by synthesizing a hybrid digital/analog filter. The input data stream

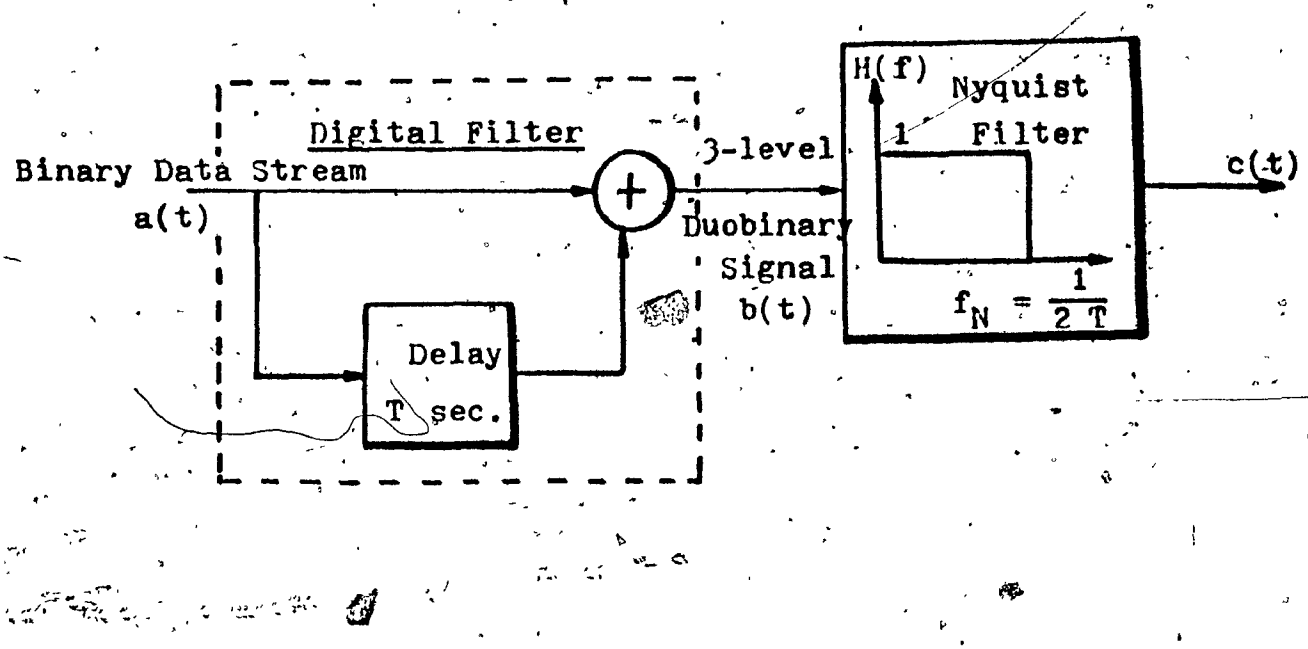

Fig. 3.4.a Generation of A Duobinary Data Stream Using a Digital Delay Element

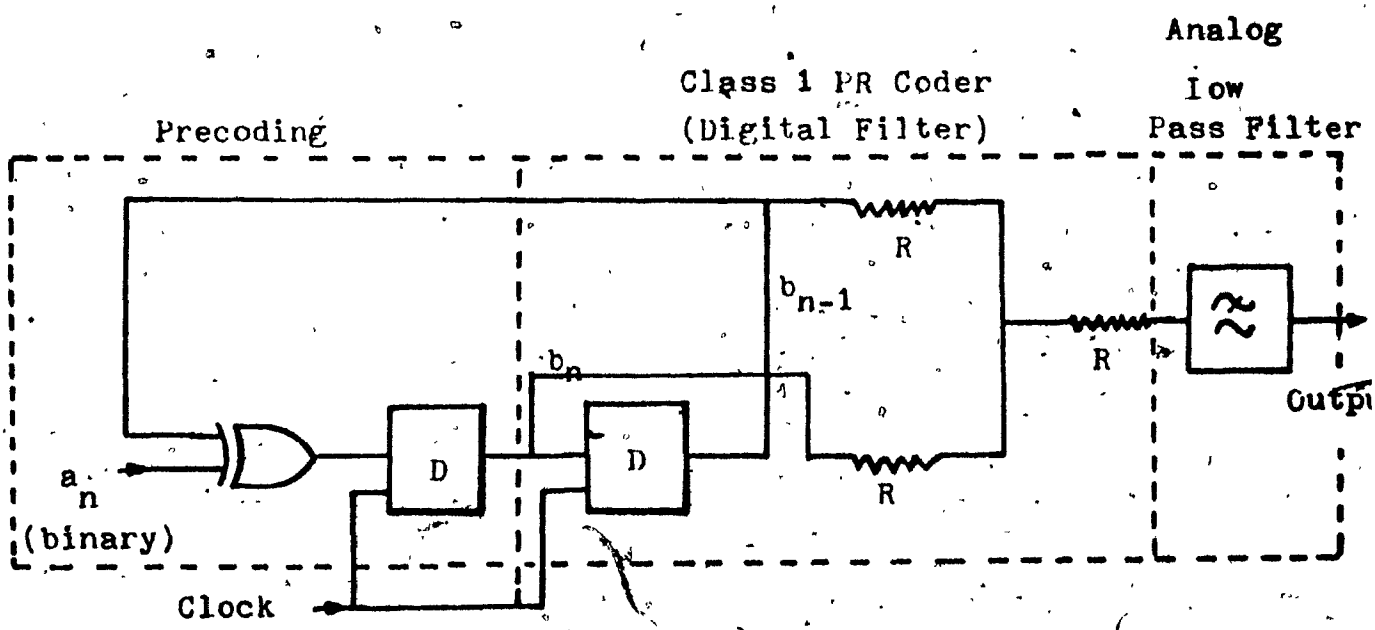

Fig. 3.4.b Combined Analog/Digital Realization of a Class 1 PR Signal with Precoding

$\{a_n\}$ is first precoded into a new data stream $\{b_n\}$. The digital filter performs the transformation of the binary stream $\{b_n\}$ into the class 1 PR pulse train at the summing network output. The analog lowpass filter is then used to attenuate the transfer function beyond the Nyquist frequency.

Figure 3.5.a shows the eye diagrams of a 10 kb/s binary NRZ signal and a 10kb/s class 1 3-level PR signal after they both pass through an f_{3dB} = 5kHz lowpass filter (4th order Butterworth). The corresponding spectra for equiprobable random data are shown in Figure 3.5.b.

For this case, the eye diagram of the binary signal shows a $20 \log_{10}(1 - \frac{1}{4})$ = 2.5dB ISI degradation while the 3 level PR signal has an ISI degradation of $20 \log_{10}(1 - \frac{1}{6})$ = 1.58 dB. The spectrum of the 3 level PR signal has its first null at the Nyquist frequency (5kHz in this case), whereas the first null of the binary signal is located at the bit rate frequency (10 kHz for a 10kb/s signal). The significant attenuation of the PR filtered signal beyond the Nyquist frequency is clearly demonstrated.

Figures 3.5.c and 3.5.d show the corresponding eye diagrams and spectra of the binary and 3-level PR signal after they pass through the Butterworth filter whose f_{3dB} frequency is now changed from

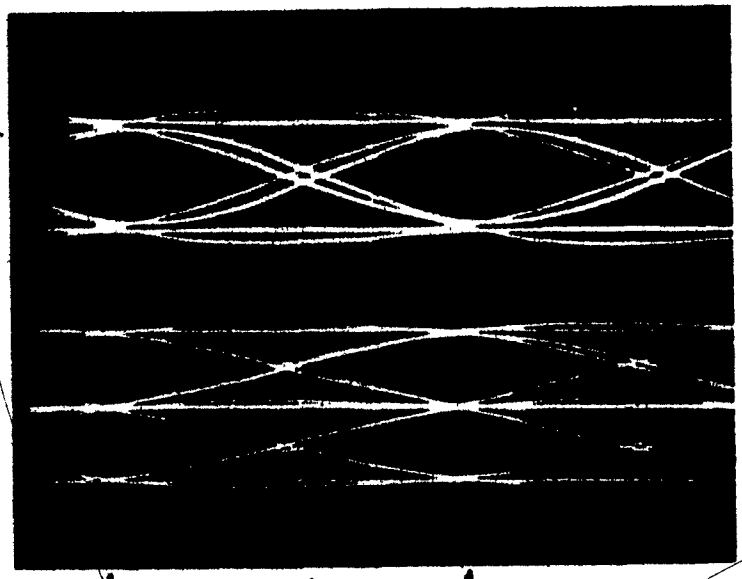

Fig. 3.5.a Measured Eye Diagrams of a Binary NRZ Signal and a Class 1 3-level Signal (Both at 10 kb/s and passing through an f_{3dB} = 5 kHz LPF)

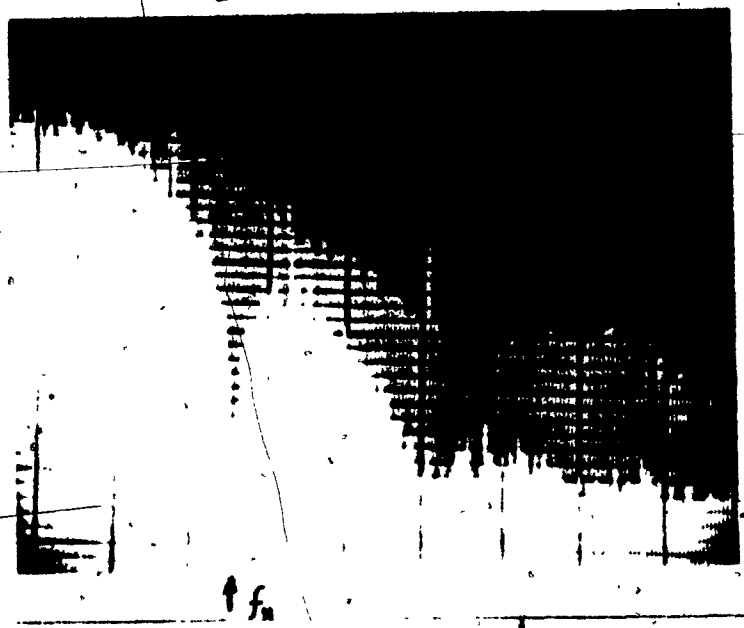

Fig. 3.5.b Spectra of the Binary Signal and the Class 1 3-level Signal after Filtering

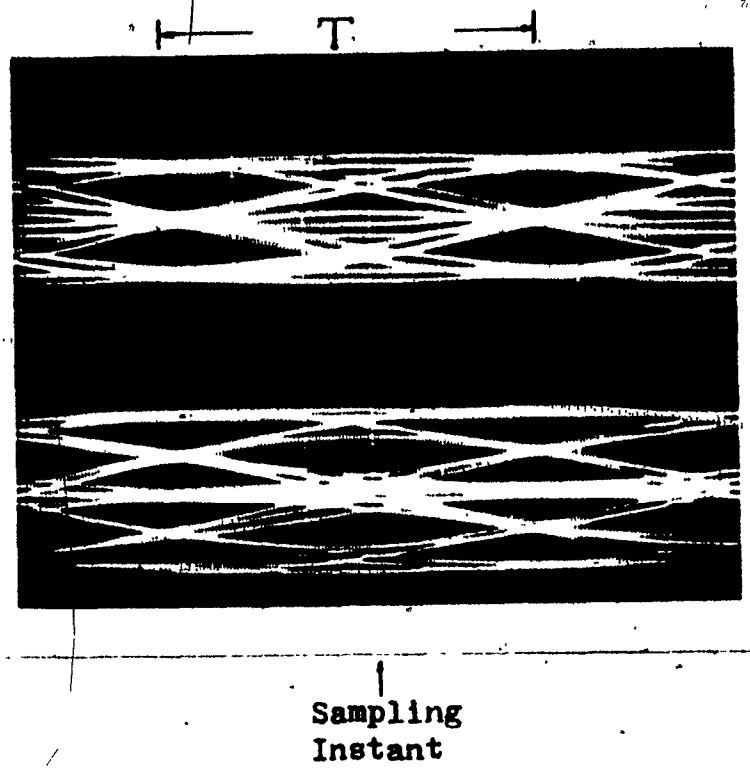

Fig. 3.5:c Measured Eye Diagrams of a Binary NRZ Signal and a Class 1 3-level PR Signal Passing through an f_{3dB} = 3 kHz LPF

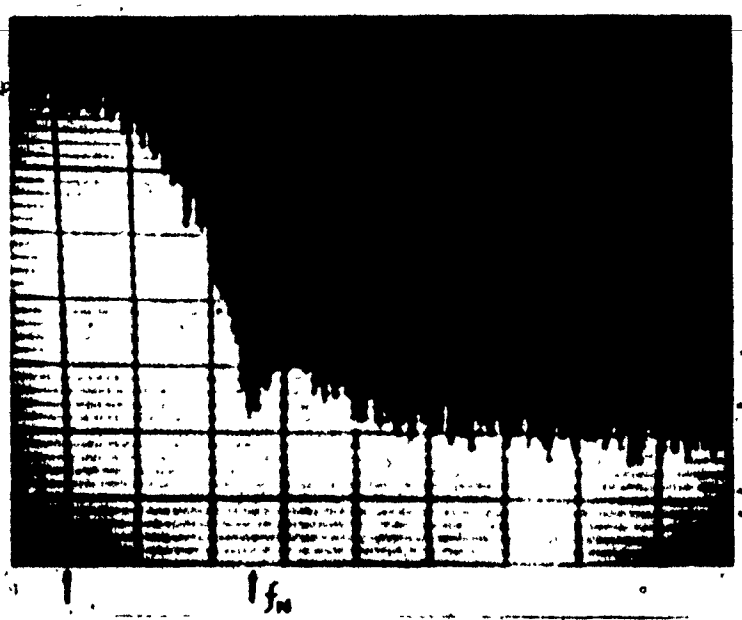

Fig. 3.5.d Spectra of the Filtered Binary Signal and the Class 1 3-level PR Signal

5kHz to 3kHz.

The eye of the binary signal is almost closed while that of the PR signal is still half open. The spectral attenuation of the PR signal beyond the Nyquist frequency again, for this case, demonstrates the advantage of using the PR scheme over the binary.

The computer simulated eye diagrams plotted in Figure 3.5.e provide, for a design engineer, a useful tool to analyze the tolerance of a digital communication system due to the imperfect filtering effect [Feher, 3.13]. From these two eye diagrams, it is easy to see that the 3 level PR signal suffers less filtering distortion effect than the binary signal.

3.2.2 Class 4 PR System

Another PR scheme, which is also frequently adopted in digital communication systems, is the class 4 PR scheme. The class 4 PR pulse, shown as the dashed line in Figure 3.6.a, is obtained by the superposition of the Nyquist pulse $S(t+\frac{T}{2})$ and the inverted / shifted Nyquist pulse $-S(t+\frac{3T}{2})$. The class 4 PR pulse is therefore given by:

$$h(t) = \frac{\sin\frac{\pi}{T}(t+T)}{\frac{\pi}{T}(t+T)} - \frac{\sin\frac{\pi}{T}(t-T)}{\frac{\pi}{T}(t-T)} \qquad (3.8)$$

$$= \frac{2T^2}{\pi}\,\frac{\sin\frac{\pi t}{T}}{t^2-T^2}$$

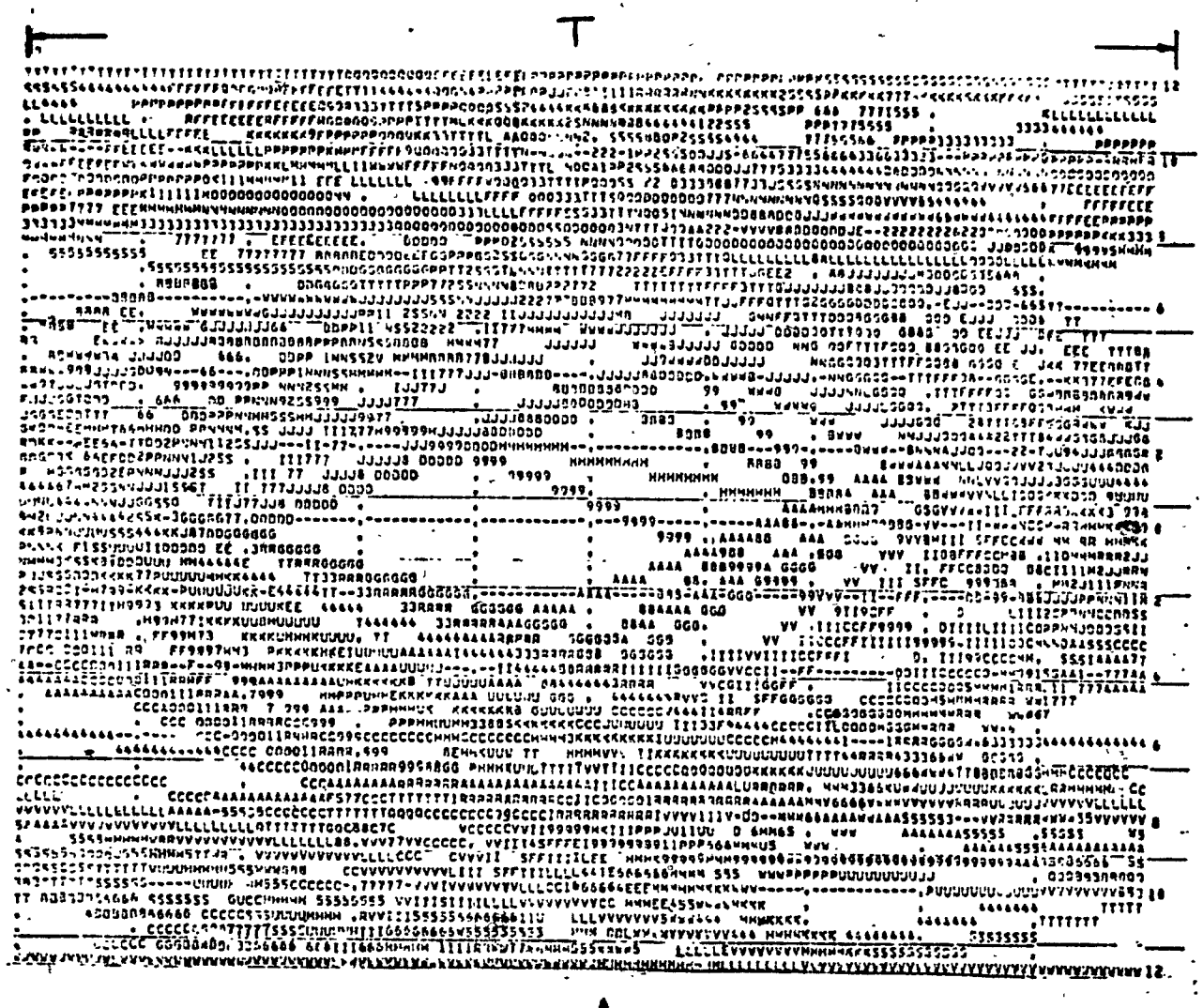

Sampling Instant

Fig. 3.5.e Computer-simulated Eye Diagram of a 1.3 Mb/s Random Data Stream Passing through an $f_{3\ dB}$ = 650 kHz LPF

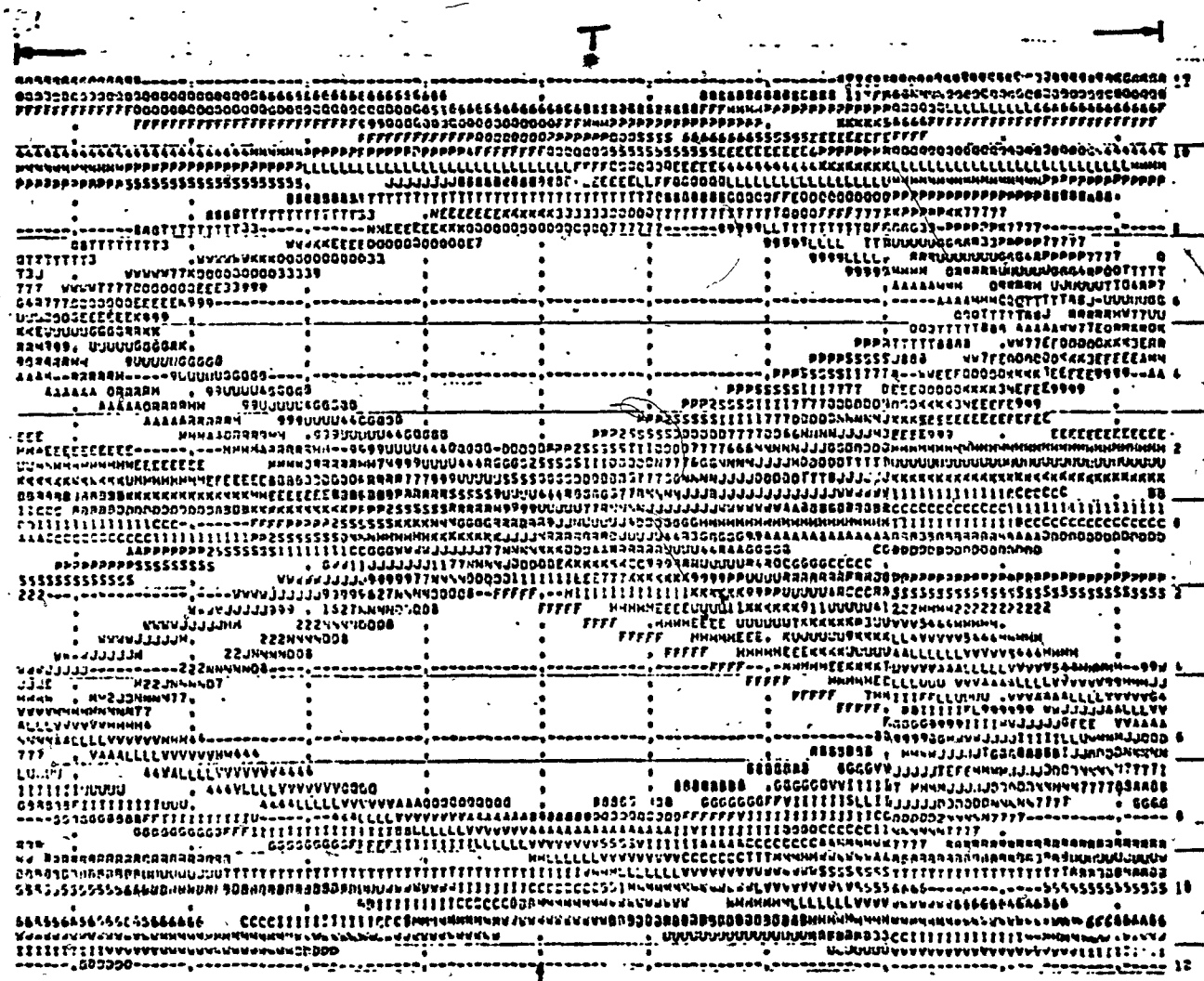

Fig. 3.5.e' Computer-simulated Eye Diagram of a 1.3 Mb/s Class 1 PR Signal Also Passing through an f_{3dB} = 650 kHz LPF

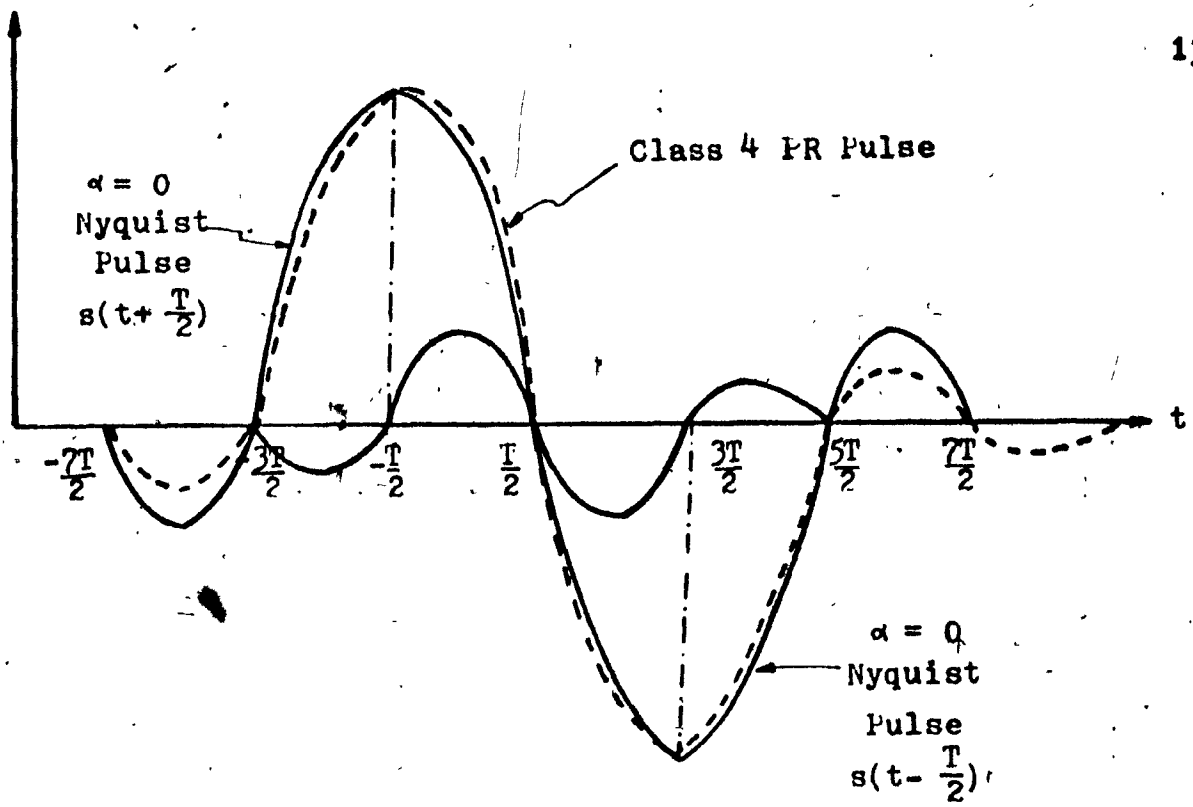

a. Class 4 PR Pulse from Superposition of Two $\alpha = 0$ Nyquist Pulses

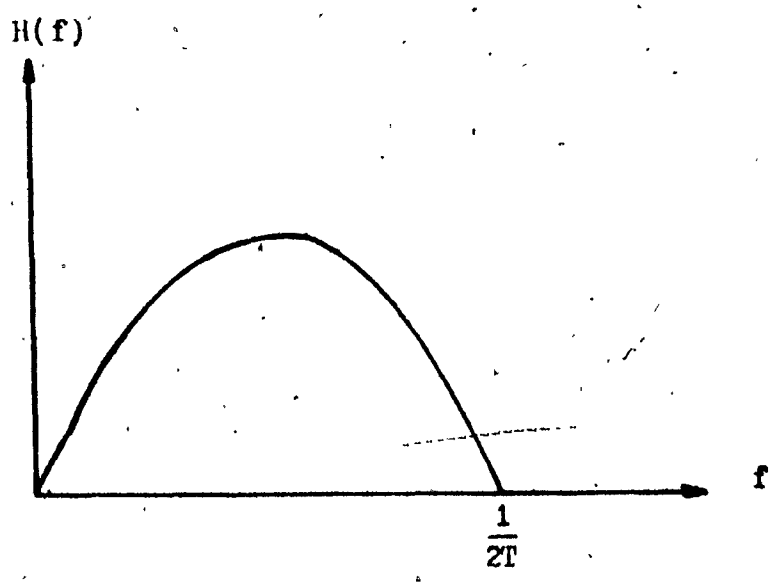

b. Class 4 PR Filter (Modified Duobinary)

Fig. 3.6 Generation of a Class 4 PR Pulse and Its Corresponding Fourier Transform

This PR pulse has the same shape as the impulse response of the filter whose transfer function is given by:

$$H(f) = \begin{cases} j2T \sin 2\pi fT & \text{for } 0 \leq f \leq \frac{1}{2T} \\ 0 & \text{elsewhere} \end{cases} \qquad (3.9)$$

The transfer function, $|H(f)|$, as depicted in Figure 3.6.b, has no DC component. This feature can be useful for insertion of service channel in the low frequency end. For example, in the GTE Lenkurt's 7-level correlative FM radio system [3.7], a band of 10 kHz is removed from the baseband spectrum for this purpose. This has almost no effect on the digital signal as there is no energy at DC and negiligible amount of energy at low frequencies.

The class 4 PR filter can be realized by a digital filter in cascade with a brick-wall Nyquist filter as shown in Figure 3.7.a. The digital filter performs the following operation:

$$p_n = a_n - a_{n-2} \qquad (3.10.a)$$

where a_n is the present bit of the binary data stream and a_{n-2} is the second previous bit. In the literature, the class 4 PR signal is also known as the modified duobinary.

Figure 3.7.b shows the circuit realization of the class 4 PR filter. The input binary data stream $\{a_n\}$ is first precoded as discussed earlier to form a new binary data stream $\{b_n\}$ using the following relationship:

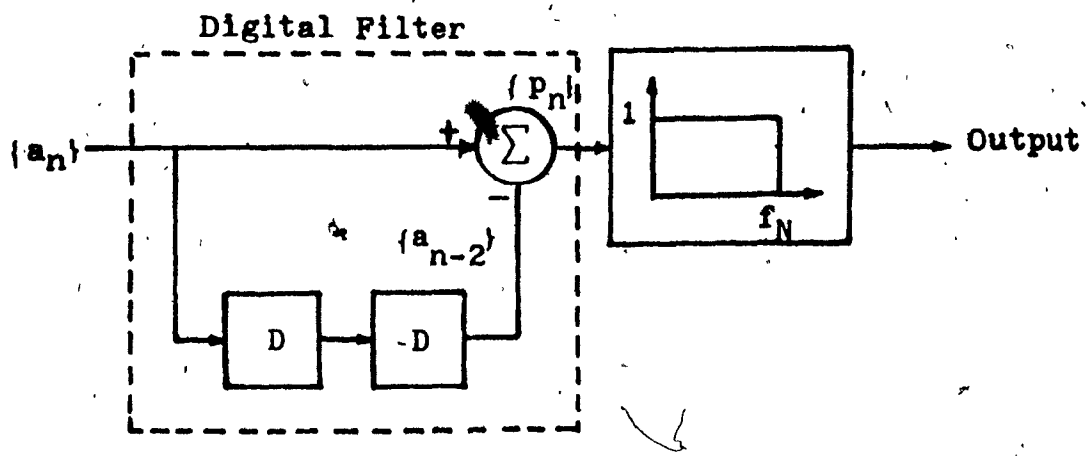

Fig. 3.7.a Class 4 PR Signaling Method

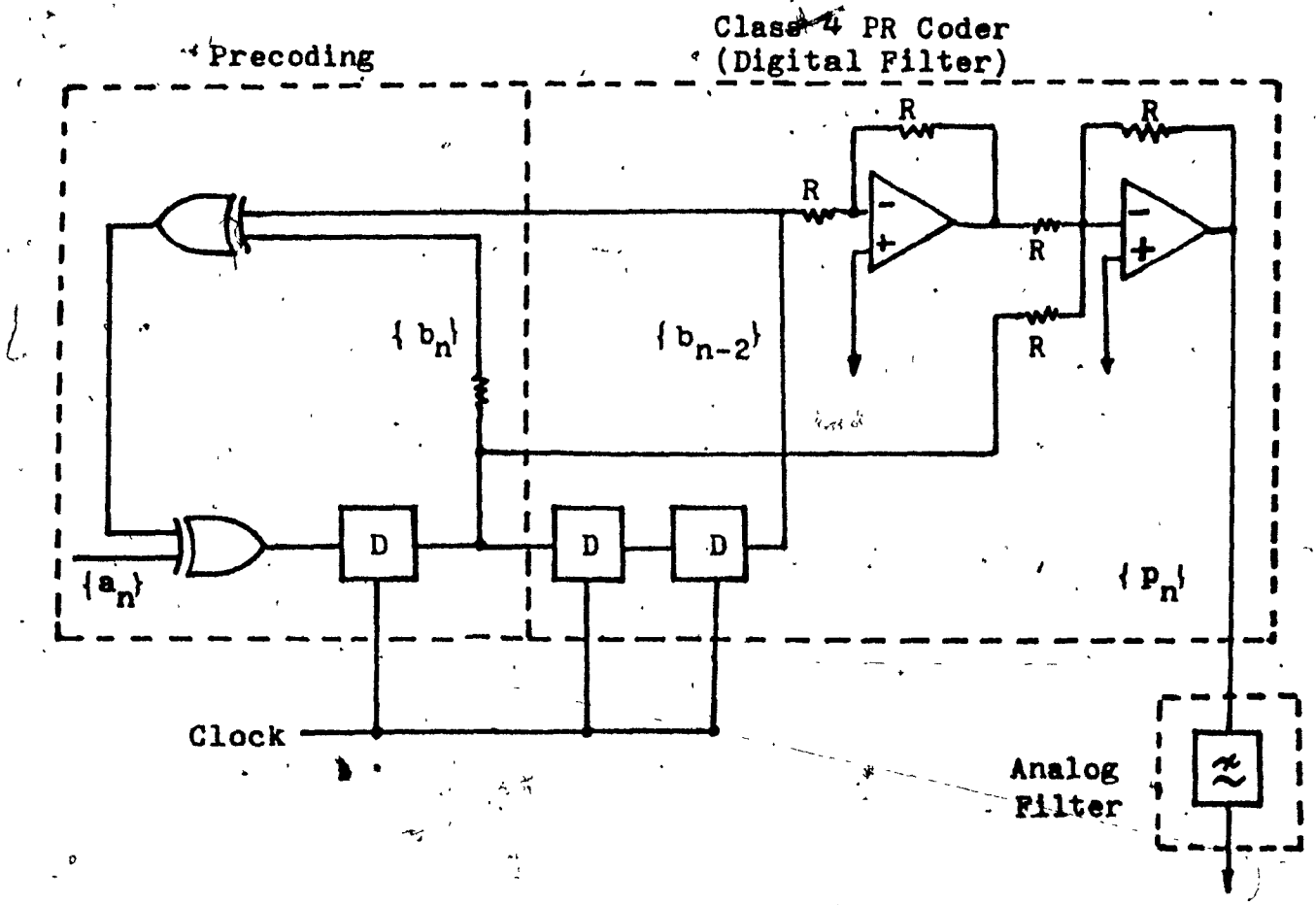

Fig. 3.7.b Combined Analog/Digital Realization of Class 4 PR Filter

$$b_n = a_n + b_{n-2} \qquad (3.10.b)$$

The precoded binary data stream $\{b_n\}$ is passed through the digital filter which transforms $\{b_n\}$ into the 3 level class 4 PR pulse train $\{p_n\}$ (Eq. 3.9). An analog lowpass filter is then used to approximate the brick-wall Nyquist filter.

3.2.3 Other PR Systems

In general, a PR pulse can be written as [Kabal et al, 3.12]:

$$h(t) = \sum_{n=0}^{N-1} f_n \frac{\sin \frac{\pi}{T}\left(t - \frac{(n-1)T}{2}\right)}{\frac{\pi}{T}\left(t - \frac{(n-1)T}{2}\right)} \qquad (3.11)$$

where $\{f_n\}$ represents the N nonzero sample values.

Expressed in terms of the delay polynomials, the PR system can be written as:

$$F(D) = \sum_{n=0}^{N-1} f_n D^n \qquad (3.12)$$

where D is the delay operator.

If, for binary inputs, the numberof output levels is restricted to be less than 5 and the Fourier transform of h(t) is also constrainted to have neither nulls nor severe ripples in the Nyquist minimum bandwidth, then there are only seven other PR systems of practical interest. The nine PR pulses and the transfer functions of these nine PR filters are summarized in Table 3.1. They are reproduced here from Ref. [Kabal et al, 3.12] for our study on pulse overlapping to be presented in the following section.

F(D)	|H(f)|	h(t)
$1 + D$ (Class 1-Duobinary)	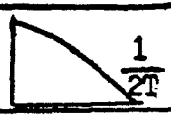 $2\,T\,\cos \pi fT$	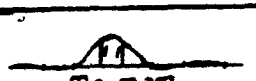 $\frac{4T^2 \cos(\pi t/T)}{\pi \quad T^2 - 4t^2}$
$1 - D$ (Dicode)	 $j2\,T \sin \pi fT$	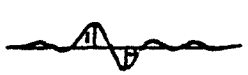 $\frac{8Tt \cos(\pi t/T)}{\pi \quad 4t^2 - T^2}$
$1 - D^2$ (Class 4-Mod. Duo.)	 $j4\,T \sin 2\pi fT$	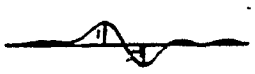 $\frac{2T^2}{\pi} \frac{\sin(\pi t/T)}{t^2 - T^2}$
$(1 + D)^2$ (Class 2)	 $4\,T \cos^2 \pi fT$	 $\frac{2T^3}{\pi t} \frac{\sin(\pi t/T)}{T^2 - t^2}$
$1 + D - D^2 + D^3 = (1+D)^2(1-D)$	 $j4\,T \cos \pi fT \sin \pi fT$	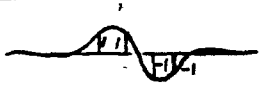 $-\frac{64\,T^3 t \cos(\pi t/T)}{\pi (4t^2-9T^2)(4t^2-T^2)}$
$1 - D - D^2 + D^3 = (1+D)(1-D)^2$	 $-4\,T \sin \pi fT \sin 2\pi fT$	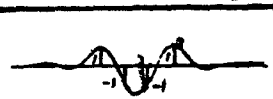 $\frac{16\,T^2}{\pi} \frac{\cos(\pi t/T)(4t^2-3T^2)}{(4t^2-9T^2)(4t^2-T^2)}$
$1 - 2D^2 + D^4$ (Class 5)	 $-4T \sin^2 2\pi fT$	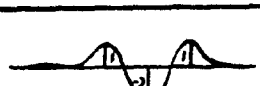 $\frac{8\,T^3}{\pi t} \frac{\sin(\pi t/T)}{t^2 - 4T^2}$
$2 + D - D^2$ (Class 3)	 $T(1 + \cos 2\pi fT + j3 \sin 2\pi fT)$	 $\frac{T^2}{\pi t} \sin(\pi t/T)\left(\frac{3t-T}{t^2 - T^2}\right)$
$2 - D^2 - D^4$	 $-T(1 - \cos 4\pi fT - j3 \sin 4\pi fT)$	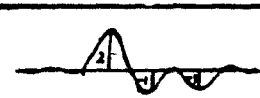 $\frac{2T^2}{\pi t} \sin(\pi t/T)\left(\frac{2T-3t}{t^2 - 4T^2}\right)$

Table 3.1 Transfer Functions of Partial Response Filters and Their Impulse Responses

3.3 Generation of Partial Response Signals by Pulse Overlapping

In Chapter 2, the concept of pulse overlapping was used to generate an ISI and jitter-free bandlimited random data stream. This concept can also be applied to the generation of the PR signals. In this section, we will show that overlapping of the multi-intervaled pulses can also be viewed as to introduce correlation into the data bits of the binary random sequence. Multi-intervaled pulses that can generate different classes of partial response signals are obtained, based on the coefficients used in the polynomial representation of the partial response filters. It is found that the ratio of the Fourier transforms of the multi-intervaled pulse to that of the single-intervaled rectangular pulse is equivalent to the transfer function of the digital filter that performs the transformation of the binary signal into the multilevel signal. This digital filter in cascade with a brick-wall Nyquist filter gives the partial response filter. The transfer function of this filter is derived by this method. The spectrum of the multilevel signal prior to the Nyquist filter is obtained from the Fourier transform of the multi-intervaled pulse. This method elliminates the considerable effort required in finding the spectrum of the multilevel signal from the autocorrelation of the signal [Wachira, 3.14]. In addition, we note that the power spectrum density derivation of the correlative coded data prior to the Nyquist filter was not given in the literature.

3.3.1 Generation of Duobinary and Polybinary Signals and Derivation of their Spectra.

The polybinary technique, as originated by Lender [3.3], involves the transformation of a precoded NRZ random data stream into a polybinary pulse stream by adding algebraically the present digit of the binary data stream to the (b-2) preceding digits where b is the number of signal levels in the polybinary pulse stream. For b=3, the polybinary pulse stream becomes the duobinary pulse stream or the class 1 partial response signal [Lender, 3.2][Kretzamer, 3.5].

As described earlier in Section 3.2.1, for binary random data stream having a bit duration T the corresponding 3-level duobinary signal is obtained by adding the present bit to its preceding bit. An alternate method to generate the 3-level duobinary pulse train by means of pulse overlapping is proposed next.

The binary random data stream $\{d_n\}$, such as shown in Fig. 3.2, is divided into the odd data stream $\{a_n\}$ and even data stream $\{b_n\}$, as shown in Fig. 3.8. The unit symbol duration of these two new data streams is made twice that of the source bit duration. The even bit data stream is also delayed by half a symbol duration (equaling to one bit duration) in respect to the odd bit data stream. Adding the two data streams, the resultant signal is found to be identical to the 3-level duobinary signal obtained as the output of the digital filter

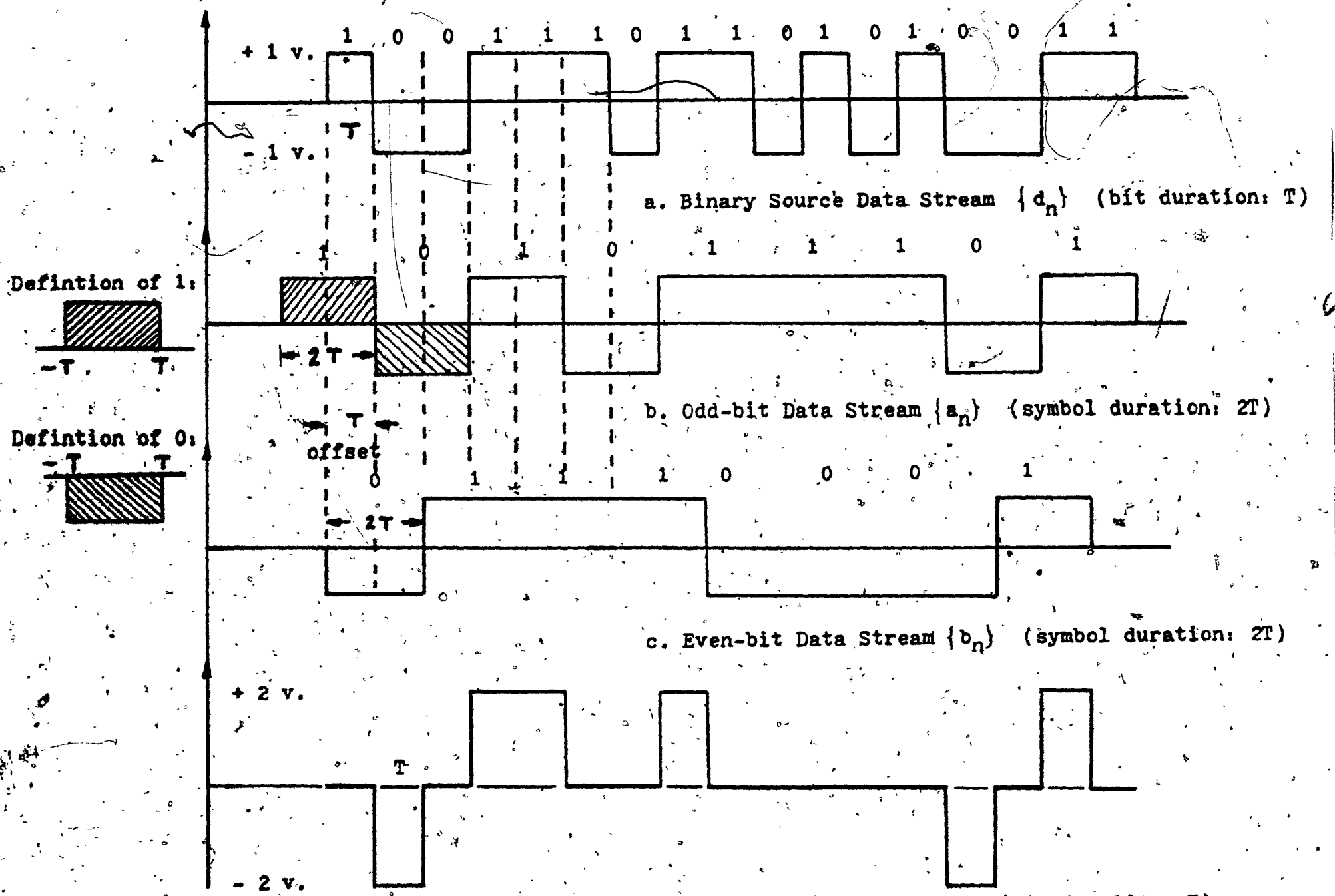

Fig. 3.8 Generation of Duobinary Signal by Pulse Overlapping Method.

shown earlier in Figs. 3. 3. a and 3. 4. a. From Figure 3. 8, it is easy to see that in the generation of the 3-level duobinary signal, pulse overlapping between the odd bit and even bit data streams prevails over each bit interval. Overlapping of the double-intervaled rectangular pulses is thus equivalent to introduction of correlation between the present bit and its previous bit. As the double-intervaled rectangular pulse occupies a two-bit interval, synchronous pulse overlapping is essential. In other words, the double-intervaled rectangular pulse representing the present bit starts at the mid-point of the double-intervaled rectangular pulse that represents the previous bit. The double-intervaled rectangular pulse having a peak magnitude of +1 volt over a two-bit duration is used to represent the 1 symbol while the one having a peak magnitude of -1 volt over the same duration is used to represent the 0 symbol.

As the odd bit and even bit random data streams are statistically independent, the spectrum of the 3-level duobinary signal shown in Fig. 3. 8 is simply the sum of the spectra of the odd bit and even bit data streams. The unit-symbol duration of these two data streams is 2T, hence the spectrum of either the odd bit or even bit data stream is given by [Feher, 3. 15]:

$$S_{2T}(f) = 2T\left(\frac{\sin 2\pi fT}{2\pi fT}\right)^2 \qquad (3.13)$$

where the subscript 2T denotes the unit symbol duration. Thus the spectrum of the 3-level 1/T rate duobinary signal is given by:

$$S_D(f) = 4T \left(\frac{\sin 2\pi fT}{2\pi fT}\right)^2 \qquad (3.14)$$

where the subscript D denotes "duobinary".

This is identical to equation (7) in Lender's paper [3.2] if the probability of occurrence of the 1 or 0 symbol is assumed equi-probable.

The spectrum of the binary random data stream having a bit duration T is given by [Feher, 3.15]:

$$S_T(f) = T \left(\frac{\sin \pi fT}{\pi fT}\right)^2 \qquad (3.15)$$

The ratio of $S_D(f)$ to $S_T(f)$ is defined as $|H_1(f)|^2$:

$$|H_1(f)|^2 \triangleq \frac{S_D(f)}{S_T(f)} = \left(\frac{\sin 2\pi fT}{\sin \pi fT}\right)^2 \qquad (3.16.a)$$

or

$$|H_1(f)| = \frac{\sin 2\pi fT}{\sin \pi fT} = 2 \cos \pi fT \quad \text{for all } f \qquad (3.16.b)$$

Notice that the product of $S_T(f)$ and $|H_1(f)|^2$ given by equations (3.15) and (3.16.a) is equal to $S_D(f)$, equation (3.14.) This means that the spectrum of the 3-level duobinary pulse train can be simply obtained from the spectrum of the binary data stream and the transfer function

of the digital filter that transforms the binary into 3-level signal.

In most transmission systems, the spectrum of the signal given in Fig. 3. 8. d is bandlimited by a filter which has been designed to approximate a brick-wall Nyquist filter having an $f_N=\frac{1}{2}T$ as shown in Fig. 3. 4. a. The transfer function of $H_1(f)$ in cascade with the Nyquist filter is then the overall transfer function of the class 1 partial response filter $H_1(f)$ shown in Eq. (3. 4).

The transfer function of the digital filter H(f) can also be obtained directly from the ratio of the Fourier transforms of the double-intervaled rectangular pulse and the single-intervaled rectangular pulse. This can be explained by taking into account that the former pulse functions as the signaling element in the generation of the 3-level signal and the latter pulse is used as the signaling element in the binary random data stream.

The block diagram illustrating the implementation concept of pulse overlapping for the generation of the 3-level duobinary signal is shown in Fig. 3. 9. The input binary random data stream is first serial-to-parallel converted into the odd bit and even bit data streams. The two data streams also have a lengthened symbol duration of 2T. The even data stream is then delayed by half a symbol duration in relation to the odd data streams. The addition of these two offset data streams gives the 3-level duobinary pulse train shown in Fig. 3. 8.

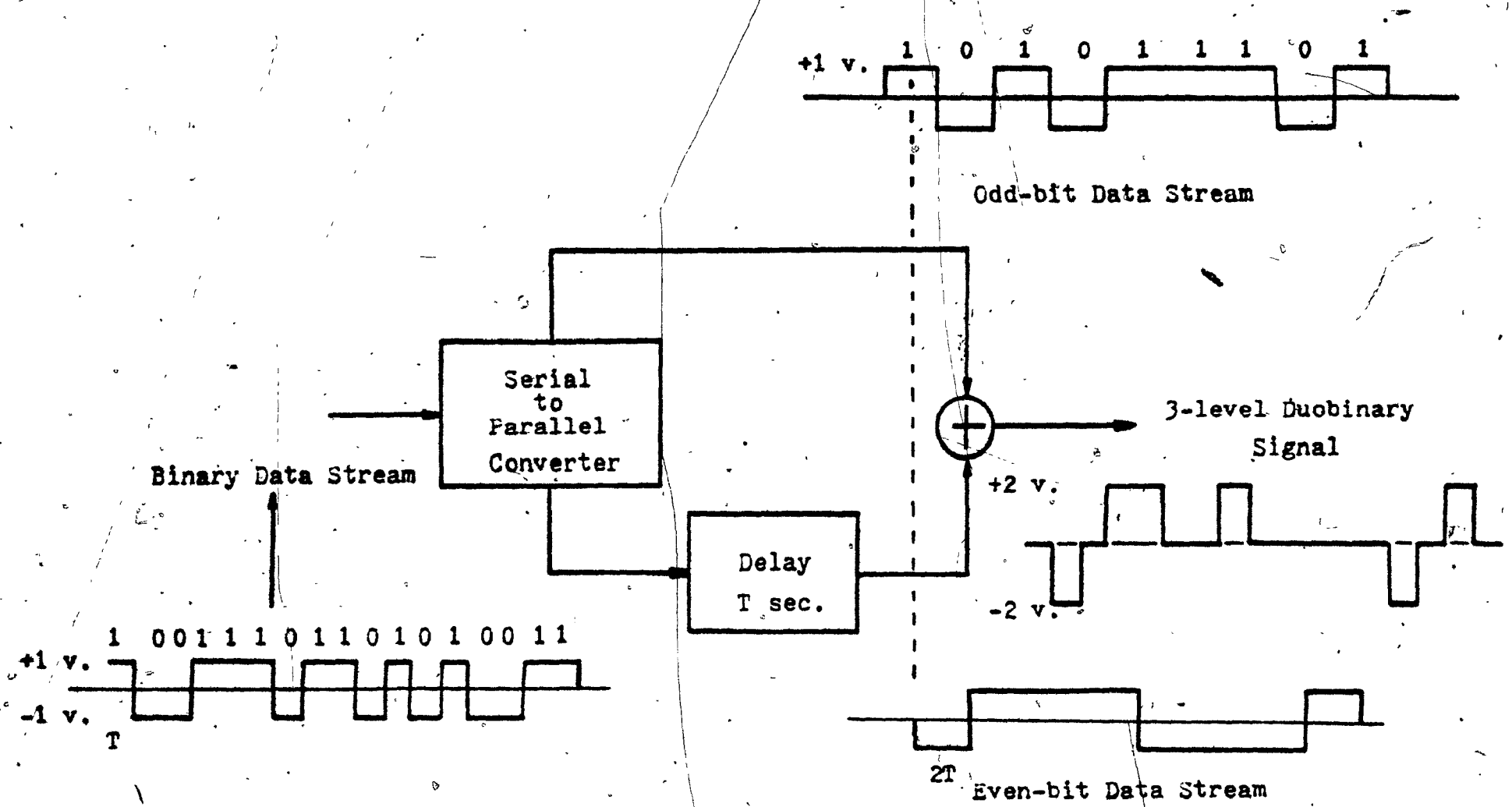

Fig. 3.9 Generation of Duobinary Signals by Means of Pulse Overlapping

In order to extend the previously presented concept to more complex partial response systems in the following paragraphs, it is required to analyze the spectra of the individual pulses.

The Fourier transform of the double-intervaled rectangular pulse $F_{2T}(f)$ shown in Fig. 3.10.a is given by:

$$F_{2T}(f) = 2T \left(\frac{\sin 2\pi fT}{2\pi fT}\right) \tag{3.17}$$

The Fourier transform of the single-intervaled rectangular pulse $F_T(f)$ shown in Fig. 3.10.b is given by:

$$F_T(f) = T \left(\frac{\sin \pi fT}{\pi fT}\right) \tag{3.18}$$

while $H_1(f)$ is the same as in equation 3.16.b, that is:

$$H_1(f) = \frac{F_{2T}(f)}{F_T(f)} = \left(\frac{\sin 2\pi fT}{\sin \pi fT}\right) = 2\cos \pi fT \quad \text{for all } f. \tag{3.19}$$

For the generation of a polybinary signal, a rectangular pulse occupying nT-intervals such as shown in Fig. 3.11.a can be used as the unit signaling element. For synchronous transmission, as shown in Fig. 3.11, b, if the nT-intervaled rectangular pulse $S_{nT}(t)$ representing the present bit is used as the reference, then the nT-intervaled rectangular pulse $S_{nT}(t-T)$ representing the forthcoming bit is delayed by a bit duration relative to $S_{nT}(t)$. The nT-intervaled

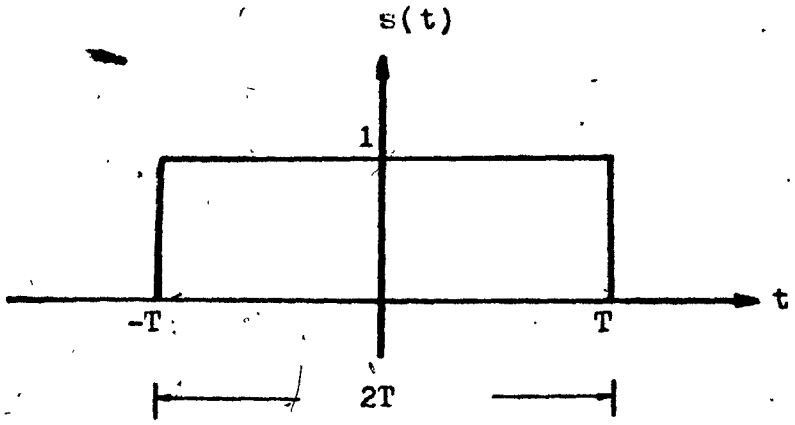

a. Double-Intervaled Rectangular Pulse

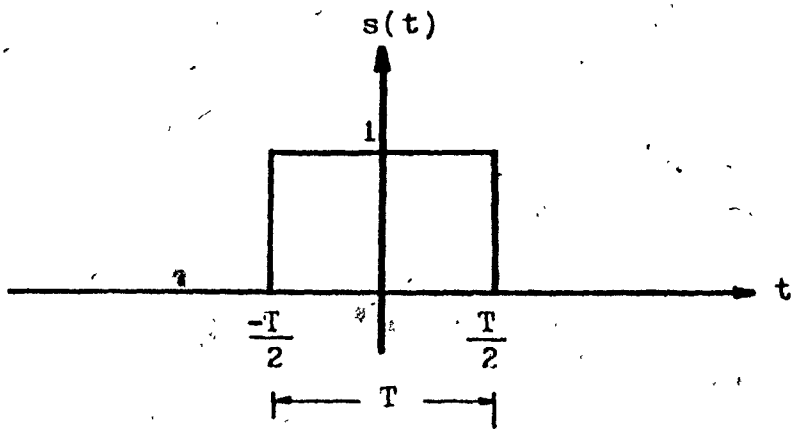

b. Single-Intervaled Rectangular Pulse

Fig. 3.10 Definition of Double-Intervaled and Single-Intervaled Pulses

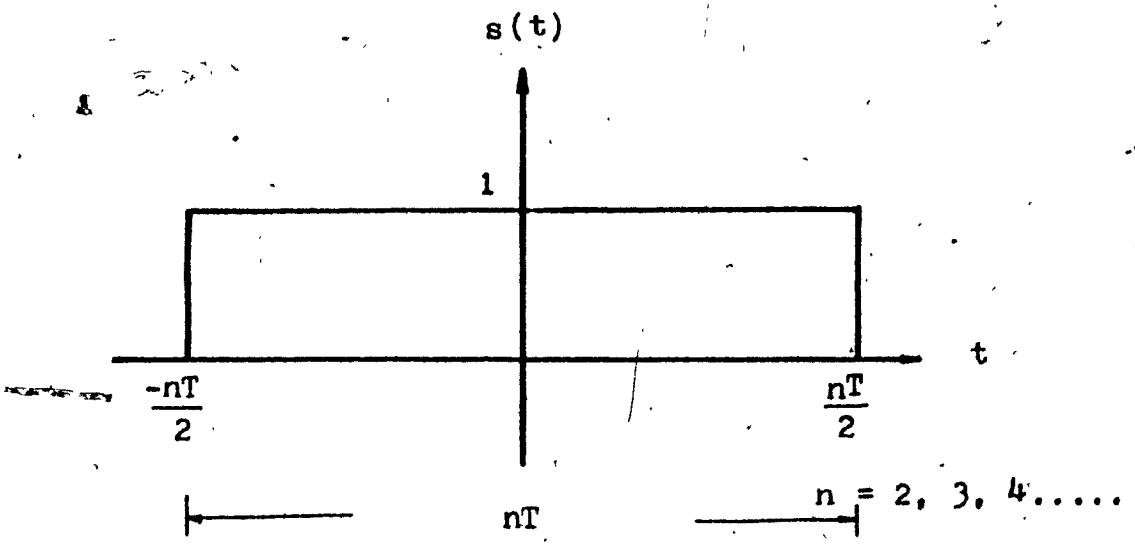

a. nT-Intervaled Rectangular Pulse

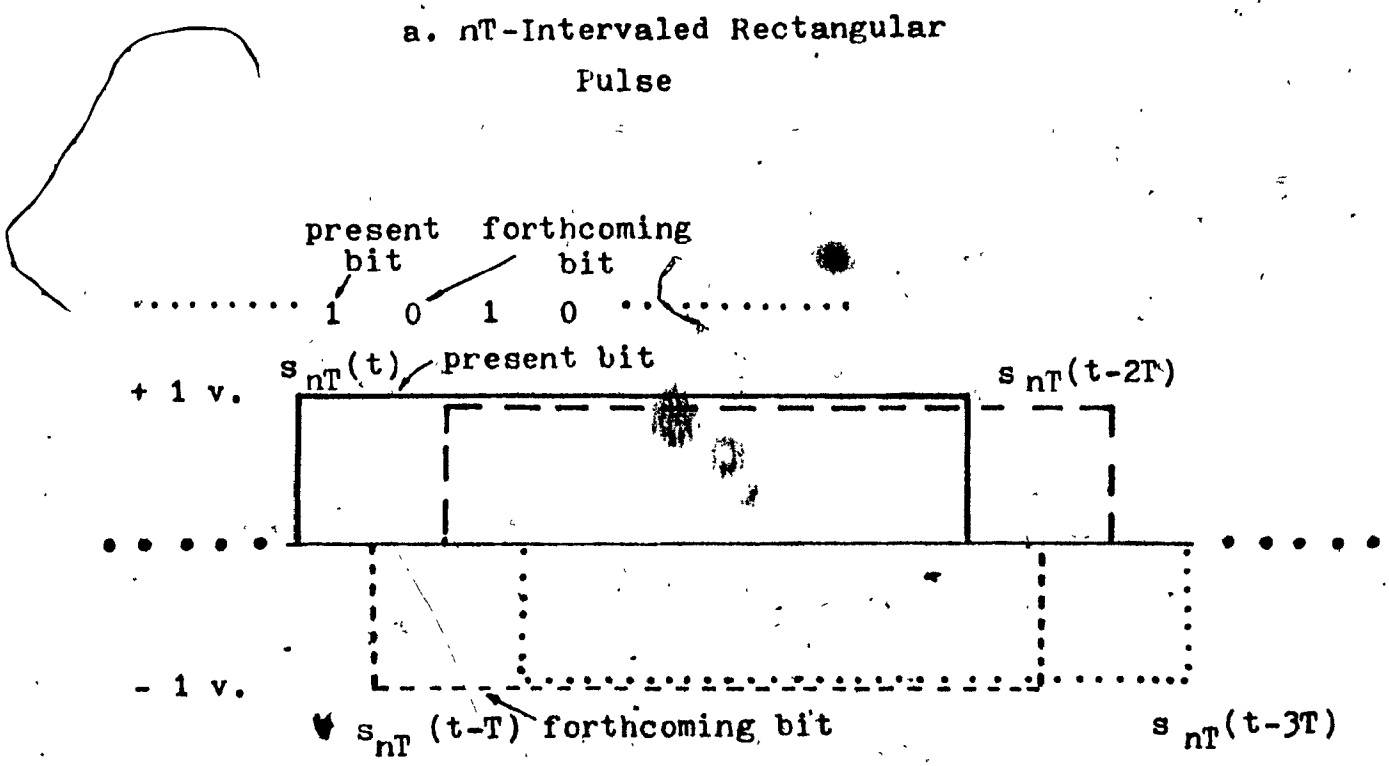

b. Overlapping of nT-Intervaled Rectangular Pulses

Fig. 3.11 Time-Domain Representation of an nT-Intervaled Pulse and Generation of Polybinary Signal by Pulse Overlapping

rectangular pulse $S_{nT}(t-2T)$ representing the second forthcoming bit is also delayed by a bit duration in relation to $S_{nT}(t-T)$. Hence, $S_{nT}(t-2T)$ is delayed by two-bit duration in relation to $S_{nT}(t)$ and so on. As a signaling element, the nT-intervaled rectangular pulse having a value of +1 volt is used to represent the 1 symbol while the 0 symbol is represented by the nT-intervaled pulse having a value of -1 volt. The resultant signal of these synchronously overlapped pulses is the (n+1) - level polybinary signal.

The Fourier transform of the nT-intervaled rectangular pulse is given by:

$$F_{nT}(f) = nT\left(\frac{\sin n\pi fT}{n\pi fT}\right) \qquad (3.20)$$

The ratio of $F_{nT}(f)$ over the Fourier transform of the single-intervaled rectangular pulse $F_T(f)$ is defined as:

$$|H_n(f)| \triangleq \frac{F_{nT}(f)}{F_T(f)} = \left(\frac{\sin n\pi fT}{\sin \pi fT}\right) \text{ for all } f \qquad (3.21)$$

As in the case of the duobinary signal, this ratio represents the transfer function of the digital filter that transforms the binary signal into the polybinary signal. If a brick-wall Nyquist filter is cascaded with this digital filter, the overall transfer function $H_p(f)$ of a polybinary filter is obtained. The transfer function of the polybinary filter is therefore:

$$H_p(f) = \begin{cases} T\,\dfrac{\sin n\pi fT}{\sin \pi fT} & \text{for } 0 \leq f \leq \dfrac{1}{2T} \\ 0 & \text{elsewhere} \end{cases} \qquad (3.22)$$

The absolute value of the transfer functions for n=3 (four levels) and n=4 (five levels) are plotted in Fig. 3.12. The same transfer functions have been obtained by a different technique by [Kretzmer 3.5]. The four level polybinary transfer function has a discontinuity at the Nyquist frequency and therefore, this four level, or any other even level polybinary filter, is not used in practice [3.5]. The extra null that appears within the Nyquist frequency band in the transfer function of the polybinary filter for the cases of n=3 and n=4 as shown in Figure 3.12 does not mean that the bandwidth requirement can be further reduced to less than the Nyquist frequency. It has been shown by [Howson, 3.16] that no further advantage is achieved by using higher orders of polybinary schemes.

One approach to improve the spectral compression capability of partial response systems is to convert the binary source information into a multi-level PAM pulse train and, afterwards, to apply the duobinary filtering technique to the PAM pulse train.

The spectrum of the polybinary signal prior to the Nyquist filter is obtained, in a similar way as the duobinary case, as follows:

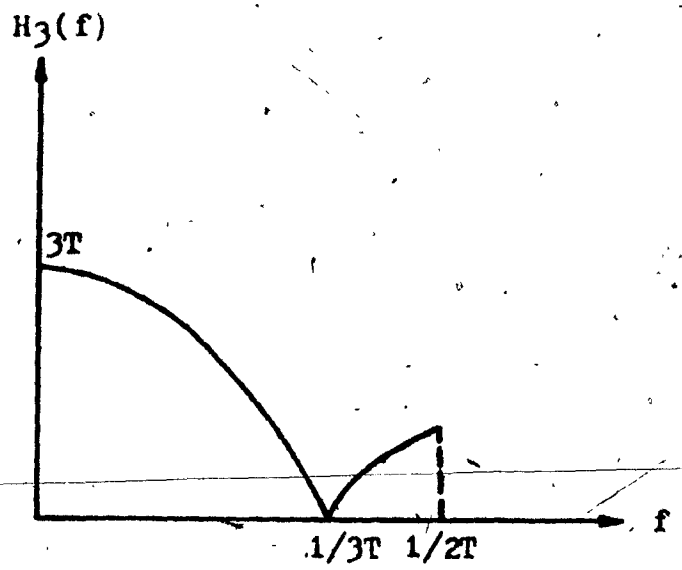

a. n = 3 Polybinary Filter

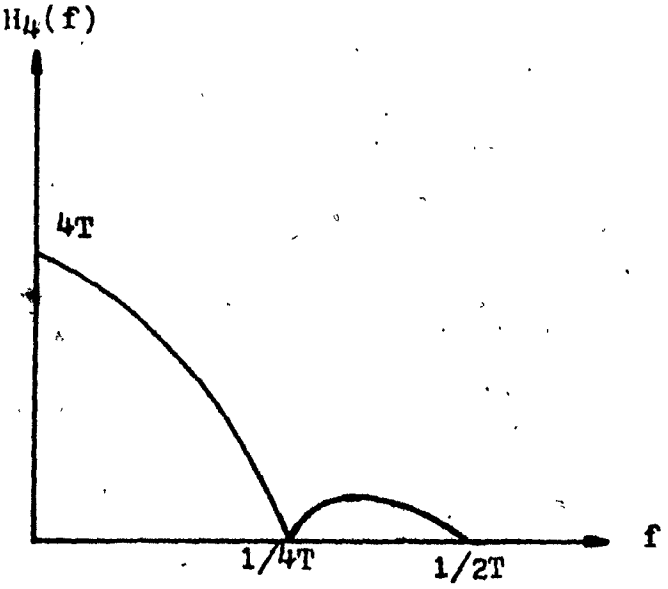

b. n = 4 Polibinary Filter

Fig. 3.12 Polybinary Filter Transfer Functions

$$S_{nT}(f) = S_T(f)\,|H_n(f)|^2$$
$$= T\left(\frac{\sin \pi fT}{\pi fT}\right)^2 \left(\frac{\sin n\pi fT}{\sin \pi fT}\right)^2 \qquad (3.23)$$
$$= n^2 T \left(\frac{\sin n\pi fT}{n\pi fT}\right)^2$$

Even though our power spectrum derivation is completely different to that of Lender's [3.2], we confirmed the validity of both derivations by obtaining the same final equations.

3.3.1.1 Generation of 3-level Duobinary Signal by Nonlinear Switching Method

In Chapter 2, it was mentioned that the nonlinear switching method was equivalent to the pulse overlapping method in that both methods can generate the same ISI and jitter free signal. In the previous section, the pulse overlapping technique was employed to generate the 3-level Duobinary signal. In this section, we will show that the nonlinear switching method can also be used to generate the 3-level Duobinary signal.

If there is a transition between the present and the previous bits in the binary random data stream, no signal (0 dc voltage) appears at the output of the nonlinear switching filter. If there is no transition, a +2V or -2V dc voltage is produced at the output depending on if the present and previous bits are both 1 or both 0, respectively. In this manner, for the input data pattern used in

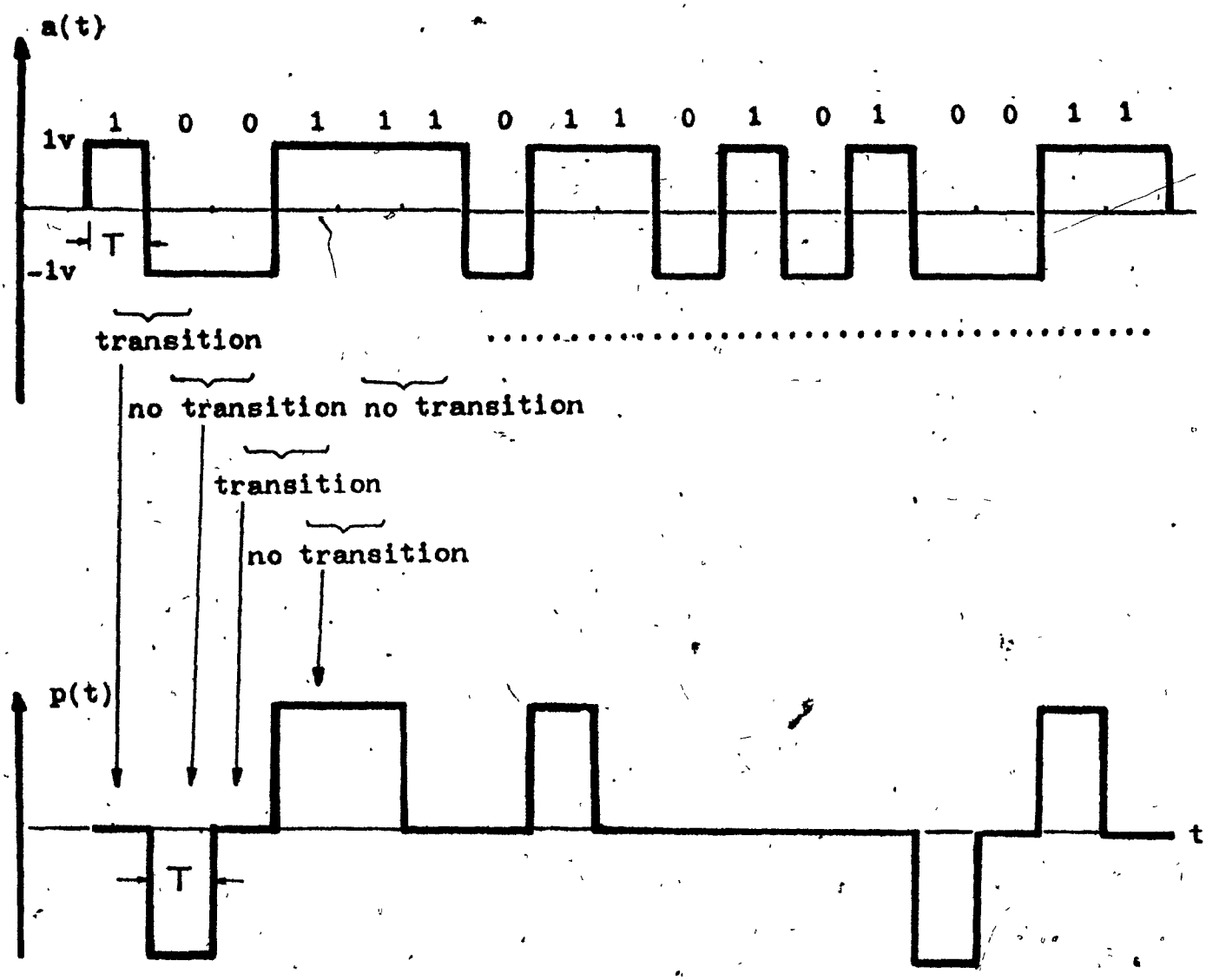

a(t): Binary Data Stream $\{a_n\}$

p(t): 3-level Class 1 PR Pulse Train $\{p_n\}$

Fig. 3.13 Generation of a 3-level Class 1 PR Pulse Train by Nonlinear Switching Method

Rules { No transition–0 v is switched on for T sec
Transition — ± 2 v is switched on for T sec

Fig. 3. 8. a the resultant signal shown in Fig. 3. 13 is the same as that of the 3-level class 1 PR signal which is generated by the pulse overlapping method (Fig. 3. 8. c).

3. 3. 2 Generation of Other Partial Response Signals By Overlapping Pulses

The concept of pulse overlapping used in the generation of the duobinary and polybinary signals can also be extended to the generation of other partial response signals by using suitable multi-intervaled synchronously overlapped pulse. In this section a systematic method of finding these multi-intervaled pulses is described. The multi-intervaled pulse found suitable for the generation of the 3-level dicode signal (1-D) from a binary random data stream is used as an example. As in the cases of duobinary and polybinary, the ratio of the Fourier transforms of the multi-intervaled pulses and the single-intervaled rectangular pulses is, again, the transfer function of the digital filter that performs the transformation of the signal levels. Cascading this digital filter with a brick-wall Nyquist filter gives the dicode filter. The spectrum of the multi-level signal can also be obtained from the Fourier transform of this multi-intervaled pulse.

For example, in the duobinary case, which is represented by (1+D) in [Kabal et al, 3. 12], where D denotes the delay operator, the

pulse is the double-intervaled rectangular pulse such as shown in Fig. 3. 3. If the pulse in the -T to 0 interval represents the present bit denoted by the 1 in (1+D) then the part of this pulse from 0 to T is the previous bit denoted by the +D in (1+D). This designation is adopted for the front part of the present double-intervaled pulse as it must overlap the end part of the previous double-intervaled pulse as shown in Figs. 3. 8. a and 3. 8. b. Thus for the dicode case, which is represented by (1+D) in [Kabal et al, 3. 12], the suitable double-intervaled pulse would be as shown in Fig. 3. 14. a. In this case again, the part of the pulse from -T to 0 having a peak magnitude +1 volt represents the 1 in (1-D) while the part of the pulse from 0 to T having a peak magnitude of -1 volt represents the -D in (1-D).

In a similar manner to the generation of the duobinary signal, the binary random data stream shown in Fig. 3, 14. b is first divided into the odd bit and even bit data streams. The symbol duration of the odd bit and even bit data stream is also lengthened to 2T as shown in Figs. 3. 14. c and 3. 14. d. An offset of half a symbol duration is then introduced between these two data streams. The pulses adapted as a signaling element in these two data streams are the dicode pulses shown in Fig. 3. 14. a. The resultant signal of these data streams is the 3-level dicode signal (Fig. 3. 14. e)

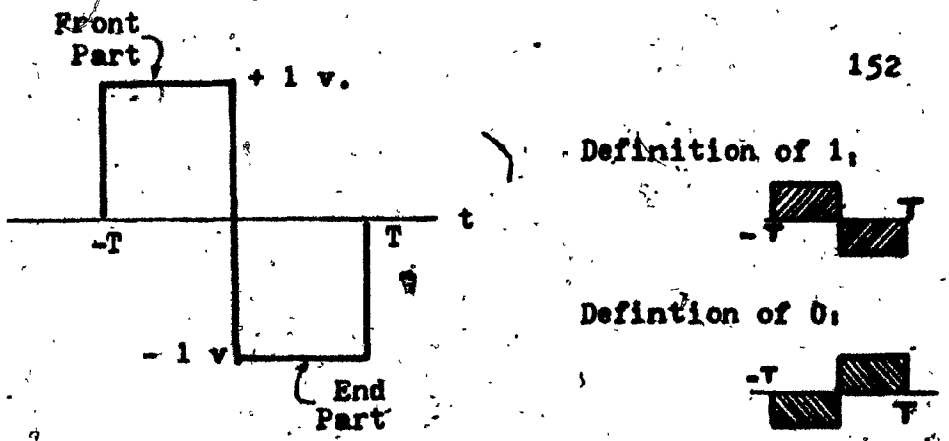

a. Double-Intervaled Dicode Pulse

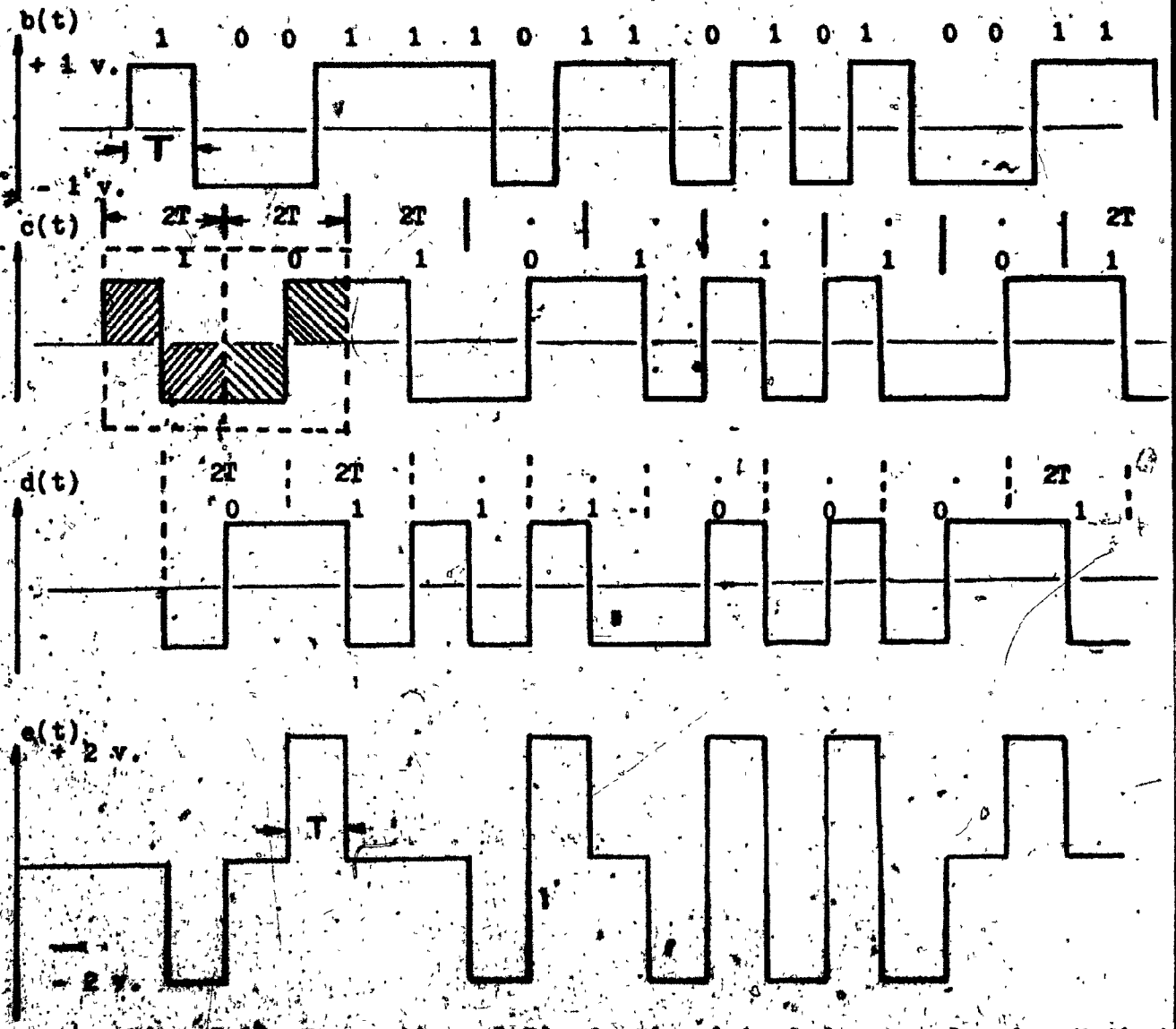

Fig. 3.1 Generation of Dicode Signal by Pulse Overlapping Method

b(t): Binary Data Stream c(t): Odd-bit Data Stream

d(t): Even-bit Data Stream e(t): Dicode Signal

Following the same approach, the second column of Table 3.2 shows the multi-intervaled pulses corresponding to the polynomial representations of the partial response filters listed in the first column. The Fourier transforms of these pulses are listed in the third column. The spectra of the resulting multilevel signals, prior to filtering, are obtained from the Fourier transforms of these multi-intervaled pulses and are listed in the fourth column. The ratio of the Fourier transforms of these pulses and the signle-intervaled rectangular pulse corresponds to the transfer function of the digital filters that perform the transformation of signaling levels. Cascading these digital filters into a brick-wall Nyquist filter gives the partial response filters whose transfer functions are listed in the last column of Table 3.2. The transfer functions derived from the method of overlapping pulses are found to be identical to those listed in Table 3.1.

Polynominal Representation (F(D))	Multi-Intervaled Pulse s(t)	Fourier Transform of s(t) S(f)	Spectrum of the Multi-level Partial Resp. Prior to Filtering	Transfer Function of the Partial Response Filter ($0 \leq f \leq 1/2T$)
$1 - D$ (Dicode)	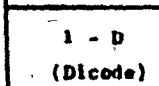	$j\,2T\,(\frac{\sin^2 \pi fT}{\pi fT})$	$4\,T\,(\frac{\sin^2 \pi fT}{\pi fT})^2$	$j\,2T \sin \pi fT$
$1 - D^2$ (Class 4-Mod.Duo)	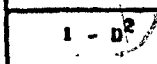	$j\,4T(\frac{\cos \pi fT \sin^2 \pi fT}{\pi f T})$	$16T(\frac{\cos \pi fT \sin^2 \pi fT}{\pi f T})^2$	$j\,2T \sin 2\pi fT$
$1 + 2D + D^2$ (Class 2)	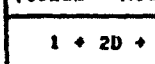	$4T \cos^2 \pi fT(\frac{\sin \pi fT}{\pi fT})$	$16T(\frac{\sin \pi fT \cos^2 \pi fT}{\pi f T})^2$	$4T \cos^2 \pi fT$
$1 + D - D^2 - D^3$	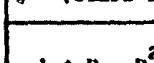	$j\,2T(\frac{\sin^2 2\pi fT}{\pi fT})$	$16T(\frac{\sin \pi fT}{\pi fT})^2 \cdot \sin^2 2\pi fT \cos^2 \pi fT$	$j\,4T \sin 2\pi fT \cos \pi fT$
$1 - D - D^2 + D^3$	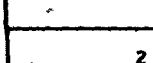	$-4T(\frac{\sin^2 \pi fT \sin^2 \pi fT}{\pi fT})$	$16T(\frac{\sin \pi fT}{\pi fT})^2 \cdot \sin^2 2\pi fT \sin^2 \pi fT$	$-4T \sin 2\pi fT \cos \pi fT$
$1 - 2D^2 + D^4$ (Class 5)	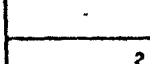	$-4T(\frac{\sin \pi fT \sin^2 2\pi fT}{\pi fT})$	$16T(\frac{\sin \pi fT}{\pi fT})^2 \sin^4 2\pi fT$	$-4T \sin^2 2\pi fT$
$2 + D - D^2$ (Class 3)	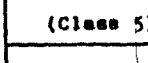	$T(\frac{\sin \pi fT}{\pi fT})^2(1+\cos 2\pi fT + j3 \sin 2\pi fT)$	$T(\frac{\sin \pi fT}{\pi fT})^2(1+\cos 2\pi fT + (3 \sin^2 2\pi fT)^2$	$T(1 + \cos 2\pi fT + j3 \sin 2\pi fT)$
$2 - D^2 - D^4$	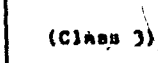	$T(\frac{\sin \pi fT}{\pi fT})(-1+\cos 4\pi fT + j3 \sin 4\pi fT)$	$T(\frac{\sin \pi fT}{\pi fT})^2(-1+\cos 4\pi fT + (3 \sin 4\pi fT)^2)$	$-T(1 - \cos 4\pi fT - j3 \sin 4\pi fT)$

Table 3.2 Generation of Partial Response Signals by Pulse Overlapping Method

3.4 PR System Models in Linear Channels

In order to calculate the S/N degradation of PR systems due to the increased number of output levels in comparison with a binary system, it should be specified how the filtering is apportioned between the transmitter and the receiver. To begin with, two existing models discussed in [Kabal et al, 3.12] will be studied. Afterwards, a third system model will be presented. Merits of each system model will also be assessed.

a. Model 1

Kretzmer distributed equal apportionment of the transfer function of a PR filter between the transmitter and the receiver (3.5). This arrangement is depicted in Fig. 3.15.a and will be called Model 1. In an additive white gaussian noise environment, for a specified P(e), this filtering requires the smallest SNR. Thus, this system model is considered to be optimum.

In practical implementation, it might be difficult to distribute exactly equal apportionment of the PR filtering between the transmitter and the receiver. [Lender, 3.2] and [Fish et al, 3.18] have shown that it is possible to generate PR filtering by first designing a transmit filter using frequency domain concepts, which then, together with the corresponding receive filter give the desired PR

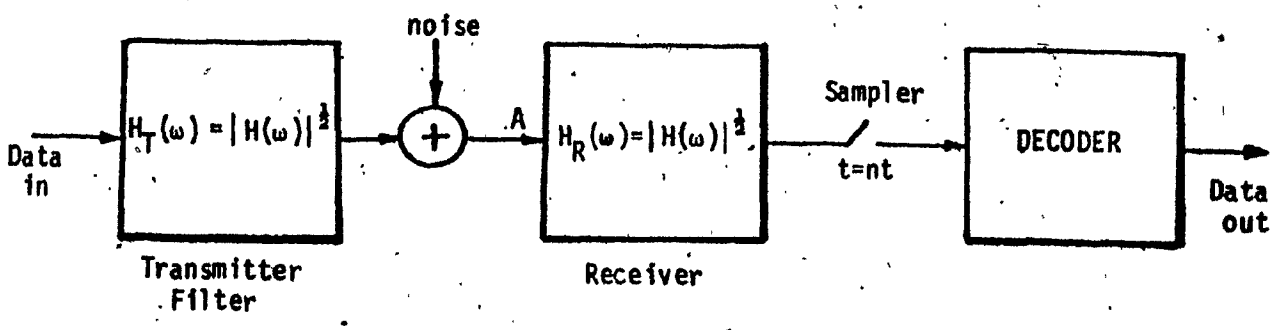

(a) Model 1 [Kretzmer]

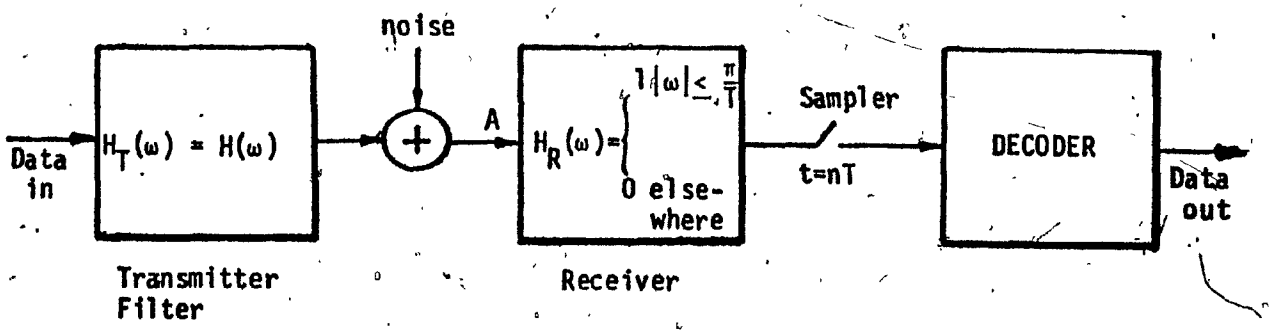

(b) Model 2 [Qureshi and Newhall]

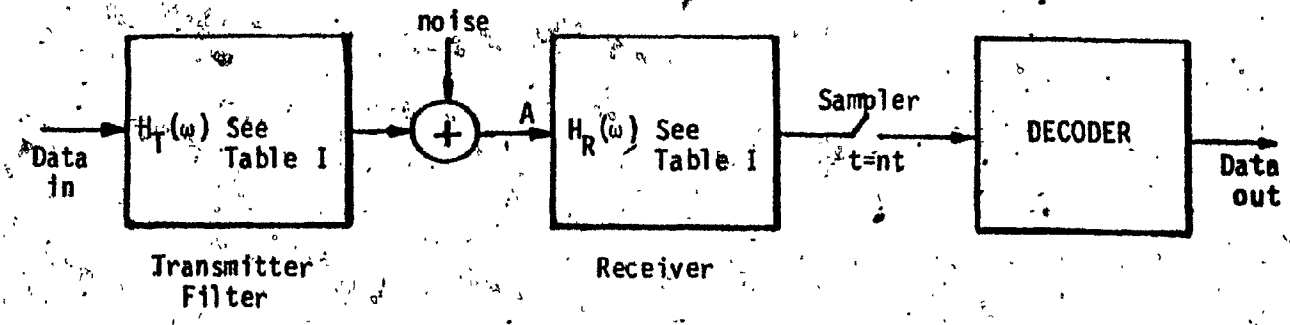

(c) Model 3 [Lender]

Fig. 3.15 Partial Response System Models

characteristic. Any imperfection due to filtering can then be compensated at the receiver by using a decision feedback equalizer and, if properly designed, can result in higher than the Nyquist rate of transmission. Using this approach, Bell-Northern Research's 8 GHz digital radio has succesfully achieved its design objectives [Barber and Anderson, 3.9].

b. Model 2

Qureshi and Newhall used a discrete channel model as depicted in Fig. 3.15.b [Qureshi et al, 3.18]. In this model, the transmit filter determines the essential spectral shaping while the receive filter merely bandlimits the noise. Even though the receive filter is a brick-wall filter, it does not shape the overall spectrum. The transmit shaping filter modifies the spectrum and has an infinite attenuation at and beyond the Nyquist frequency.

Model 2 is a straightforward method of generating a PR signal by using baseband coding to achieve the desired spectrum shaping. The signal processing required for Model 2 might be achieved by synthesizing the transmitter transfer function using a combined digital analog method. The digital circuit first generates a multilevel signal with a spectrum extending indefinitely in the frequency domain, which can then be sharply cutoff at the Nyquist frequency by an analog filter.

c. Model 3

In this model, Lender [3.7] partitioned the modified duo-binary filter into $H_T(\omega) = 4T \sin \frac{\omega T}{2}$ for the transmitter and $H_R(\omega) = \cos \frac{\omega T}{2}$ for the receiver as shown in Fig. 3.15. c. Both $H_T(\omega)$ and $H_R(\omega)$ are zero for $|\omega| > \frac{\pi}{T}$. This way of apportionment can result in a digital implementation to convert the binary input into a multi-level signal at the transmitter. According to Lender, this digital conversion assures a high degree of precision in forming the multi-level signal and is superior to the analog conversion method. It can also result in a filtering technique that has more gradual attenuation beyond the Nyquist frequency for both the transmit and receive filters.

In Table 3.3, Lender's model having the $1-D^2$ polynomial was extended to systems having other polynomials. These polynomials have been chosen in accordance with the restrictions specified in [Kabal et al, 3.12]. It is noted that for binary inputs the 1+D, 1-D and $1-D^2$ polynomials are the ones which have 3-level output signals while the others have higher numbers of signaling states. Theoretically the bandwidth of all system polynomials, with the exception of the 1-D system, is limited below the Nyquist frequency. However, only systems 1+D and $1-D^2$ have been implemented.

System Polynomial	$H(\omega)$ for $\lvert\omega\rvert < \frac{\pi}{T}$, 0 elsewhere	$H_T(\omega)$	$H_R(\omega)$	No. of Output Levels
$1+D$	$2T \cos \frac{\omega T}{2}$	$2T(\cos \frac{\omega T}{4} - \sin \frac{\omega T}{4})$	$(\cos \frac{\omega T}{4} + \sin \frac{\omega T}{4})$	$2m-1$
$1-D$	$j2T \sin \frac{\omega T}{2}$	$j4T \sin \frac{\omega T}{4}$	$\cos \frac{\omega T}{2}$	$2m-1$
$1-D^2$	$j2T \sin \omega T$	$j4T \sin \frac{\omega T}{2}$	$\cos \frac{\omega T}{2}$	$2m-1$
$1+2D+D^2$	$4T \cos^2 \frac{\omega T}{2}$	$4T \cos \frac{\omega T}{2}$	$\cos \frac{\omega T}{2}$	$4m-3$
$1+D-D^2-D^3$	$j4T \cos \frac{\omega T}{2} \sin \omega T$	$j4T \sin \omega T$	$\cos \frac{\omega T}{2}$	$4m-3$
$1-D-D^2+D^3$	$-4T \sin \frac{\omega T}{2} \sin \omega T$	$-4T \sin \omega T$	$\sin \frac{\omega T}{2}$	$4m-3$
$1-2D^2+D^4$	$-4T \sin^2 \omega T$	$-4T \sin \omega T$	$\sin \omega T$	$4m-3$
$2+D-D^2$	$T+T \cos \omega T + j3T \sin \omega T$	$2T \cos \frac{\omega T}{2} + j6T \sin \frac{\omega T}{2}$	$\cos \frac{\omega T}{2}$	$4m-3$
$2-D^2-D^4$	$-T+T \cos 2\omega T + j3T \sin 2\omega T$	$-2T \sin \omega T + j6T \cos \omega T$	$\sin \omega T$	$4m-3$

m: No. of Input Levels

TABLE 3.3 A List of Transmitter and Receiver Filters for Model 3

3.4.1 SNR Degradation of Model 3

In this section, following the methodology presented by Kabal et al as in [3.12], the SNR degradation for the three system models will be derived.

In general, the error probability for PR systems (including those with precoding) can be written as:

$$P(e) = K\,Q\,(d/\sigma_N) \tag{3.24}$$

where the value of K is suitably σ_N, is the rms value of the noise at the decoder input, d is the decision distance, and

$$Q(x) \triangleq \frac{1}{\sqrt{2\pi}} \int_{x}^{\infty} e^{-u^2/2}\, du \tag{3.25}$$

The noise variance at the decoder input is given by:

$$\sigma_N^2 = \frac{N_o}{2\pi} \int_{-\infty}^{\infty} \left| H_R(\omega) \right|^2 d\omega \tag{3.26}$$

where N_o is the noise power spectral density and $H_R(\omega)$ is the receive filter as defined in Fig. 3.15.

The SNR of interest at the receive input (prior to the receive filter filter, point A in Fig. 3.15) in the Nyquist band is given by:

$$SNR = \frac{\dfrac{\sigma_x^2}{2\pi T} \displaystyle\int_{-\infty}^{\infty} \left| H_T(\omega) \right|^2 d\omega}{\dfrac{N_o}{T}} \tag{3.27}$$

where T is the bit duration, σ_x^2 is the variance of the input symbol and is equal to $(m^2-1)/3$, where m is the number of input levels to $H_T(\omega)$ and N_o/T is the received double sided noise power in the Nyquist band.

The SNR required to achieve a given probability of error P(e) is obtained from Eqs. (1), (3) and (4):

$$SNR = \frac{\sigma_x^2}{2\pi d} \cdot Q^{-1}\left[(P(e)/k)^2\right] \int_{-\infty}^{\infty} |H_T(\omega)|^2 d\omega \int_{-\infty}^{\infty} |H_R(\omega)|^2 d\omega \tag{3.28}$$

where $Q^{-1}(P)$ is the solution x_p of $p = Q(x_p)$.

Our interest is in Lender's Model 3. We will therefore apply the generalized formula equation (5) to Model 3 (denote it by SNR) and compare the SNR degradation with the ideal binary Non-Return to-Zero signaling system which has an SNR_b related to P(e) as:

$$\begin{aligned} P(e) &= Q(\sqrt{SNR_b}) \\ \text{or,} \quad \sqrt{SNR_b} &= Q^{-1}(P(e)) \\ \text{hence,} \quad SNR_b &= Q^{-1}(P(e))^2 \end{aligned} \tag{3.29}$$

The noise power of the binary system is computed in the received double sided Nyquist bandwidth. The SNR degradation of Model 3 is B_3 and will be SNR_3 over SNR_b. We note that the SNR degradation varies with the bit error rate (BER) unless K in Eq. (1) is equal to unity. The effect of K on the SNR degradation vanishes for low

BER, i.e., $Q^{-1}(P(e)/K)$ approaches $Q^{-1}(P(e))$ as P(e) approaches zero Kabal et al, 3.12. This approximation is valid if the BER is better than 10^{-5}. The SNR degradation B_3 therefore becomes asymptotically independent of P(e).

$$B_3 = \frac{SNR_3}{SNR_b} \geq \lim_{P(e)\to 0} \frac{SNR_3}{SNR_b} \tag{3.30}$$
$$= \frac{\sigma_x^2}{2\pi d} \int_{-\infty}^{\infty} |H_T(\omega)|^2 \, d\omega \int_{-\infty}^{\infty} |H_R(\omega)|^2 \, d\omega$$

The asymptotic expression for the SNR degradation of Model 1 is [3.12]:

$$B_1 = \frac{\sigma_x^2}{2\pi d} \left| \int_{-\infty}^{\infty} H(\omega) \, d\omega \right|^2 \tag{3.31}$$

From Schwarz's Inequality, it can be easily shown that B_1 is less than B_3. In a similar way, B_1 can be shown to be less than B_2 of Model 2. This means that Model 1 has the minimal S/N degradation.

The computed values of the SNR degradation for these models are given in Table 3.4. From these results we confirmed the already known result that Model 2 has a higher SNR requirement than Model 1 [Kabal et al, 3.12]. Due to the unequal filtering between the transmitter and the receiver, Model 3 also has a higher SNR requirement than Model 1.

System	No. of Output Levels	S/N Degradation (No Precoding) dB		
		Model 1	Model 2	Model 3
$1 + D$ $1 - D$ $1 - D^2$	3	2.1	3	6
$1 + 2D + D^2$ $1 - 2D^2 + D^4$	5	6	7.8	6
$2 + D - D^2$ $2 - D^2 - D^4$	5	1.2	1.8	3.97
$1 + D - D^2 - D^3$ $1 - D - D^2 + D^3$	5	4.6	6	6

TABLE 3.4 S/N Degradation for Binary Inputs of the Three System Models

3.5 Computer Simulation of QPRS Radio System

A computer simulation program* of a QPRS radio communication link, such as shown in Fig. 3.16, was developed to study the effects of non-ideal PR filtering and of the channel non-linearities on the overall system performance. Channel nonlinearity arises from the use of a traveling wave tube amplifier (TWT) at the transmitter output which exhibits both AM/AM and AM/PM conversions.

In the simulation, two pseudo-random binary sequences of the quadrature channels were first modulo-2 precoded separately and then passed through a class-1 PR coder. The precoding is employed so that error propagation arising from PR coding scheme can be avoided [Lender, 3.2]. The resultant 3-level signals were quadrature modulated and passed through a transmit bandpass filter for spectral shaping. This modulation method is called Quadrature Partial Response System (QPRS) and is one of the modulation techniques being adopted for digital microwave radio transmission [Feher, 3.20].

Theoretically, the above mentioned transmit bandpass filter should have an equivalent low pass characteristic that approaches the ideal brick-wall Nyquist filter. Also, at the receiver, an ideal Nyquist filter should be employed to bandlimit the thermal noise and adjacent channel interference. The effect of using non-ideal

* For description of the simulation program, refer to Appendix C2.

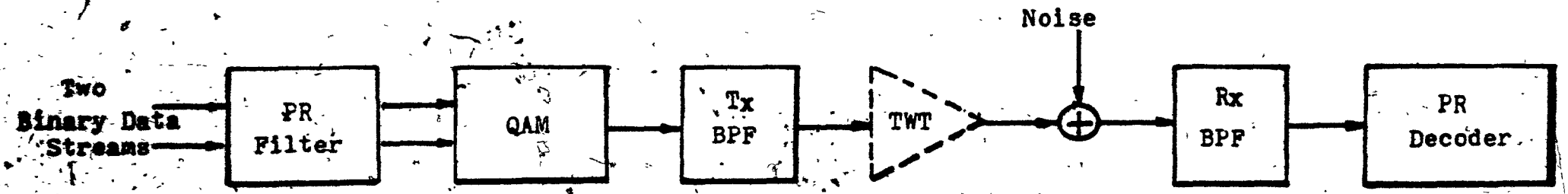

a. Model of Computer Simulation for the Study of Filtering Effect without TWT. If TWT is Included, Severe Degradation Results.

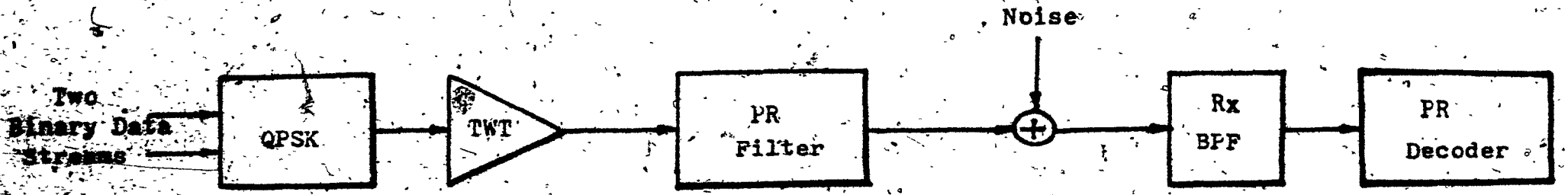

b. Model of Computer Simulation for the Study of the TWT Nonlinearity Effect.

Fig. 3.16 Block Diagrams of a Simplified QPRS Radio System

practical filters at the transmitter and the receiver is to degrade the overall system performance from that of the ideal situation and is the first subject of our computer simulation.

Our interest in using QPRS is to utilize its inherent property of transmission at the Nyquist rate or even at higher rate. The frequently employed product of the filter double sided 3 dB bandwidth B and the symbol interval T is used in our simulations [Feher, 3.15]. First it is set to unity (for a spectrum efficiency of 2 b/s/Hz) and then to 0.833 (for a spectrum efficiency of 2.4 b/s/Hz).

In order to check the accuracy of the simulation program, a brick-wall Nyquist filter was used at both the transmitter (for spectral shaping) and the receiver (for bandlimiting the noise and adjacent channel interference). This resembles Model 2 discussed in previous sections. The results for this ideal case shows that an SNR of 14.6 dB is required if a $P(e) = 10^{-4}$ is specified. This compares favorably to the theoretical value of 14.4 dB of Model 2. For Model 1, the theoretical value is 13.5 dB. This close agreement demonstrates the accuracy of the simulation.

3.5.1 Filtering Effects

Chebychev filters are frequently used in digital microwave systems. The overall performance of a radio system therefore depends not only on the filter bandwidth and the number of poles of the filter, but also on the filter passband ripples.

3.5.1.a Filter Passband Ripple Effect

To separate the contribution of the P(e) performance degradation of the transmit and receive filters, an ideal brick-wall Nyquist filter was assumed at the transmitter while at the receiver, a 4-pole Chebychev filter having a variable passband ripple was used. This allows one, in this and in the following case, to study the effect of the filter passband ripples on the overall system performance. Results for this case are presented in Fig. 3.17. In this figure, the BT=1 curves represent, for example, a 90 MB/s data rate transmitted through a double-sided RF bandwidth (3dB point) of 45 MHz/s (2 b/s/Hz).

Next, the ideal Nyquist filter at the transmitter was substituted by an identical Chebychev filter as that used at the receiver. Results for this situation are given in Fig. 3.18.

Since the ideal class 1 PR filter has a linear phase function, it is worthwhile to study the effect of the phase function on the performance of the QPRS signal. The results shown in Fig. 3.19, indicate

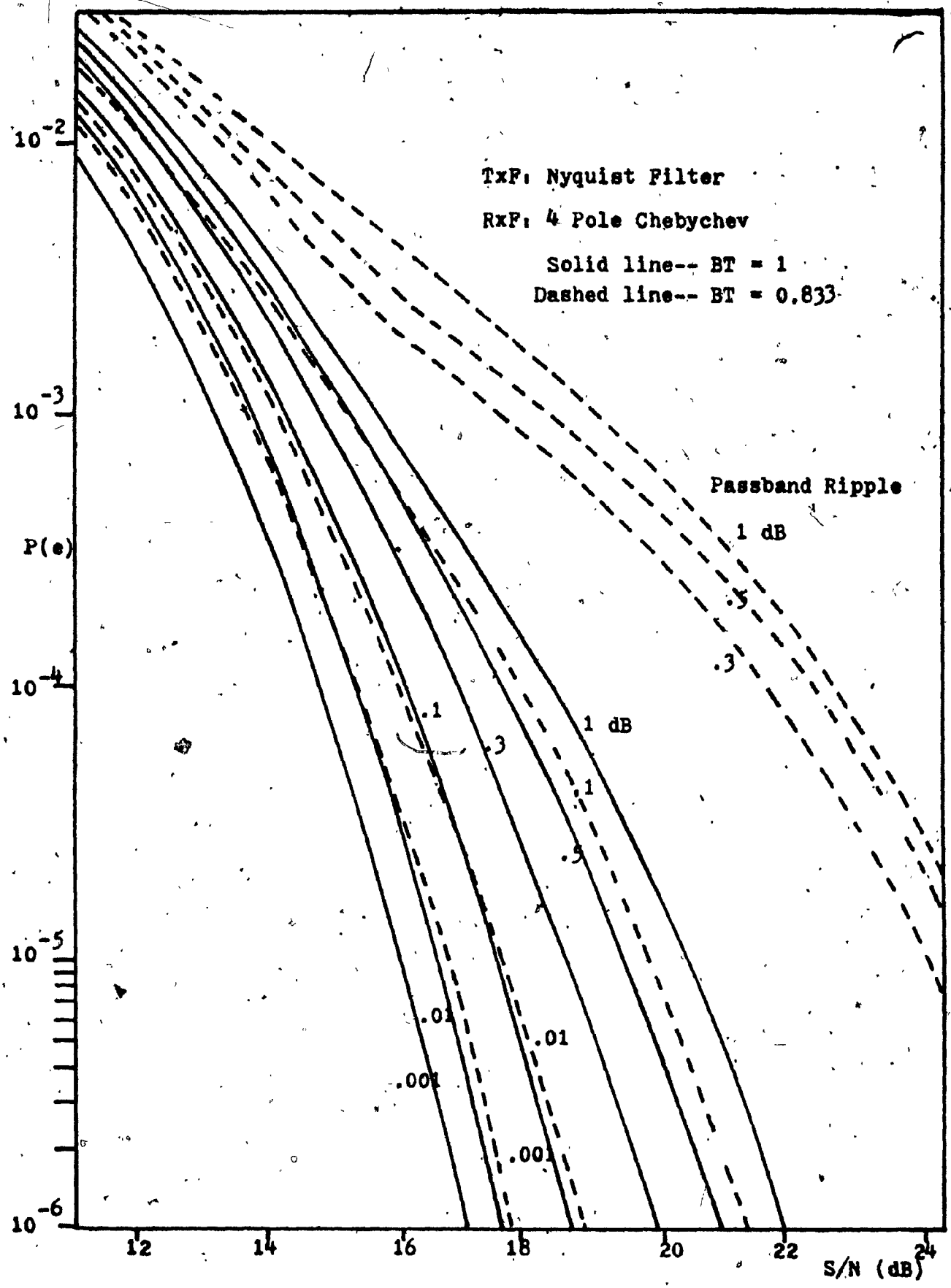

Fig. 3.17 Filter Passband Ripple Effect on QPRS

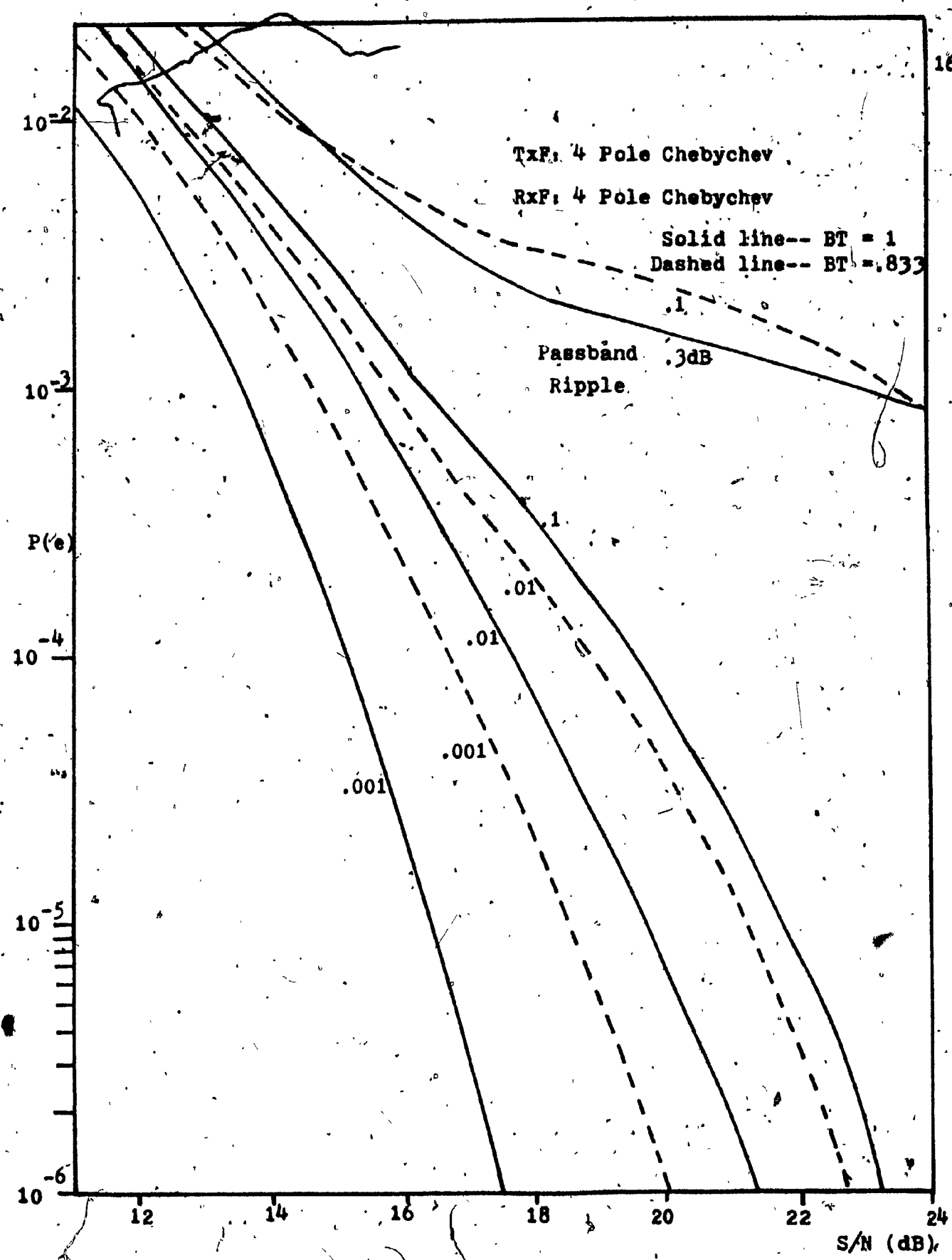

Fig. 3.18 Filter Passband Ripple Effect on QPRS

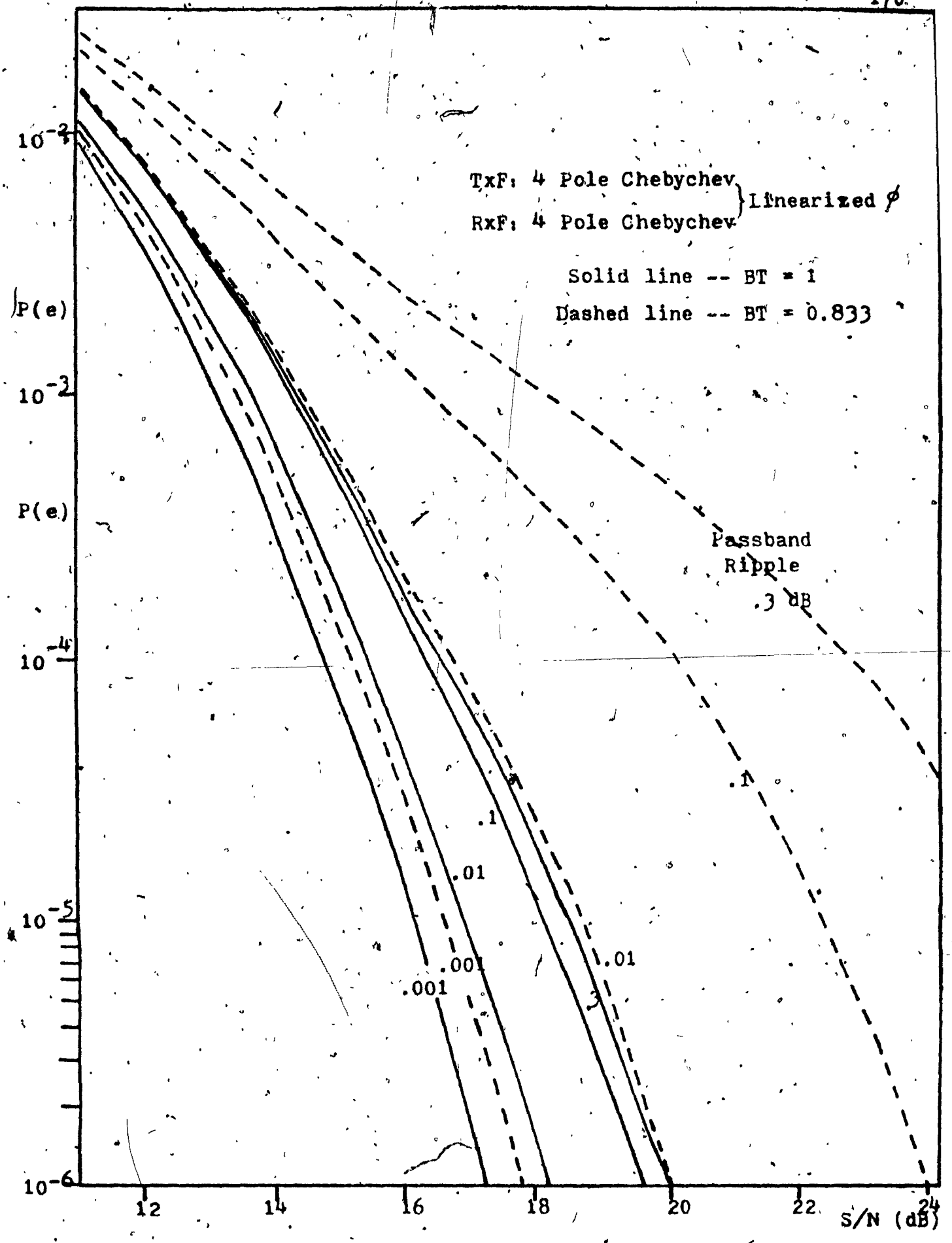

Fig. 3.19 Filter Passband Ripple Effect on QPRS

that some significant improvements were made with the linearized Chebychev filters for the case BT=1 at the transmitter and the receiver. For the case BT=0.833, the amplitude function of the Chebychev filters with passband ripples larger than 0.1 dB still causes severe degradation.

3.5.1.b Effect due to Number of Poles of the Chebychev Filters

To study the effect of the number of poles of the Chebychev filters on the system performance, for the first situation in which the ideal Nyquist filter was again assumed at the transmitter, a 3, 4 or 5 pole Chebychev filter with 0.01 dB passband ripples was used. Results are plotted in Fig. 3.20.

Again, the ideal Nyquist filter at the transmitter was replaced by a 3, 4 or 5 pole Chebychev filter with 0.01 dB passband ripples. Results for this situation are given in Fig. 3.21.

If the phase functions of the Chebychev's filters were linearized as before, significant improvements were made as shown in Fig. 3.22. This is especially so in the case of BT=1.

From these simulation results, it can be concluded that the phase function of the Chebychev filter degrades the performance of the QPRS signal for the case BT=1. In both situations of BT=1 and BT=0.83, we find that a steeper amplitude slope degrades the performance more than a gentler slope. This P(e) performance degradation is caused by increased ISI.

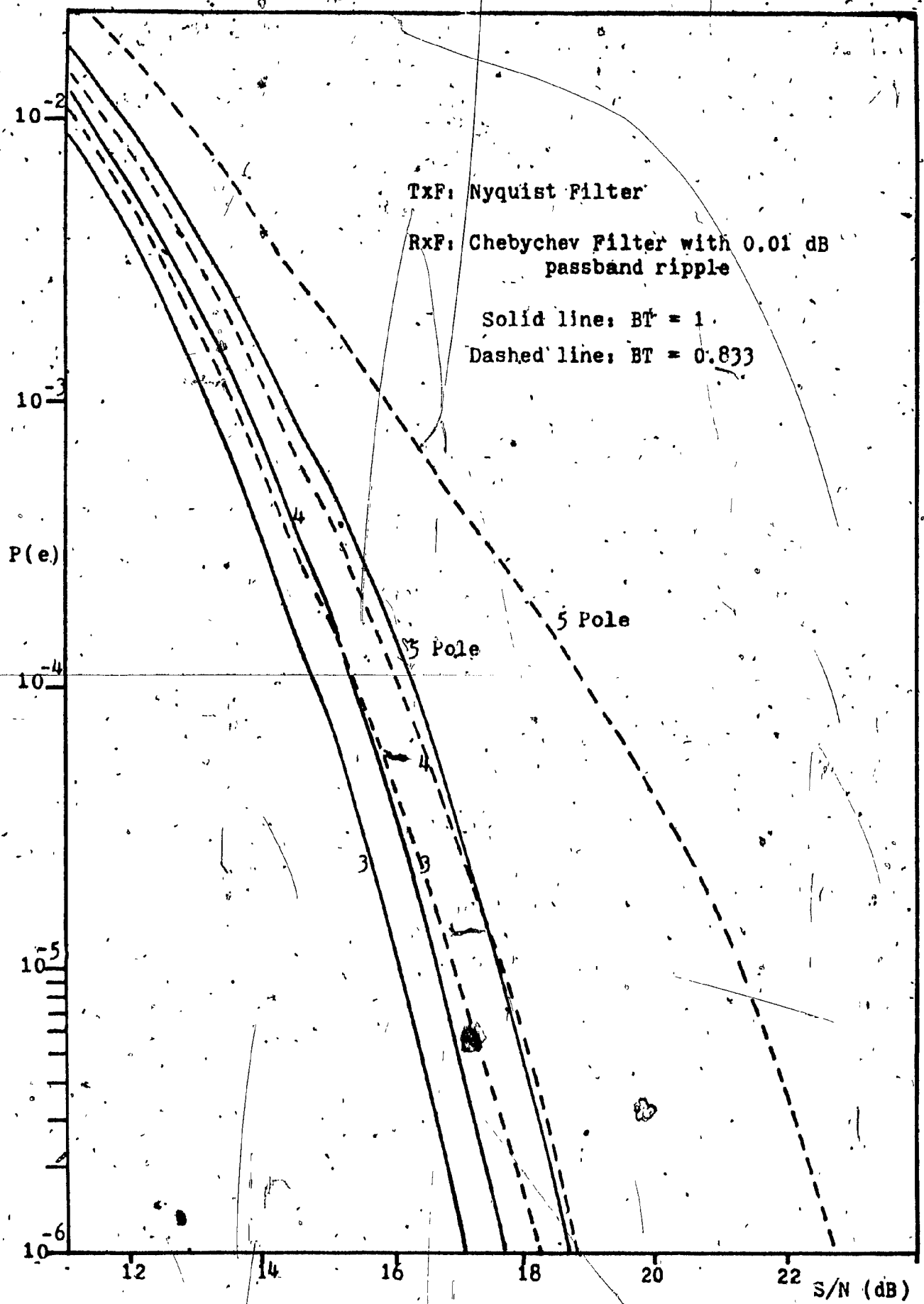

Fig. 3.20 Effect of Number of Filter Poles on QPRS

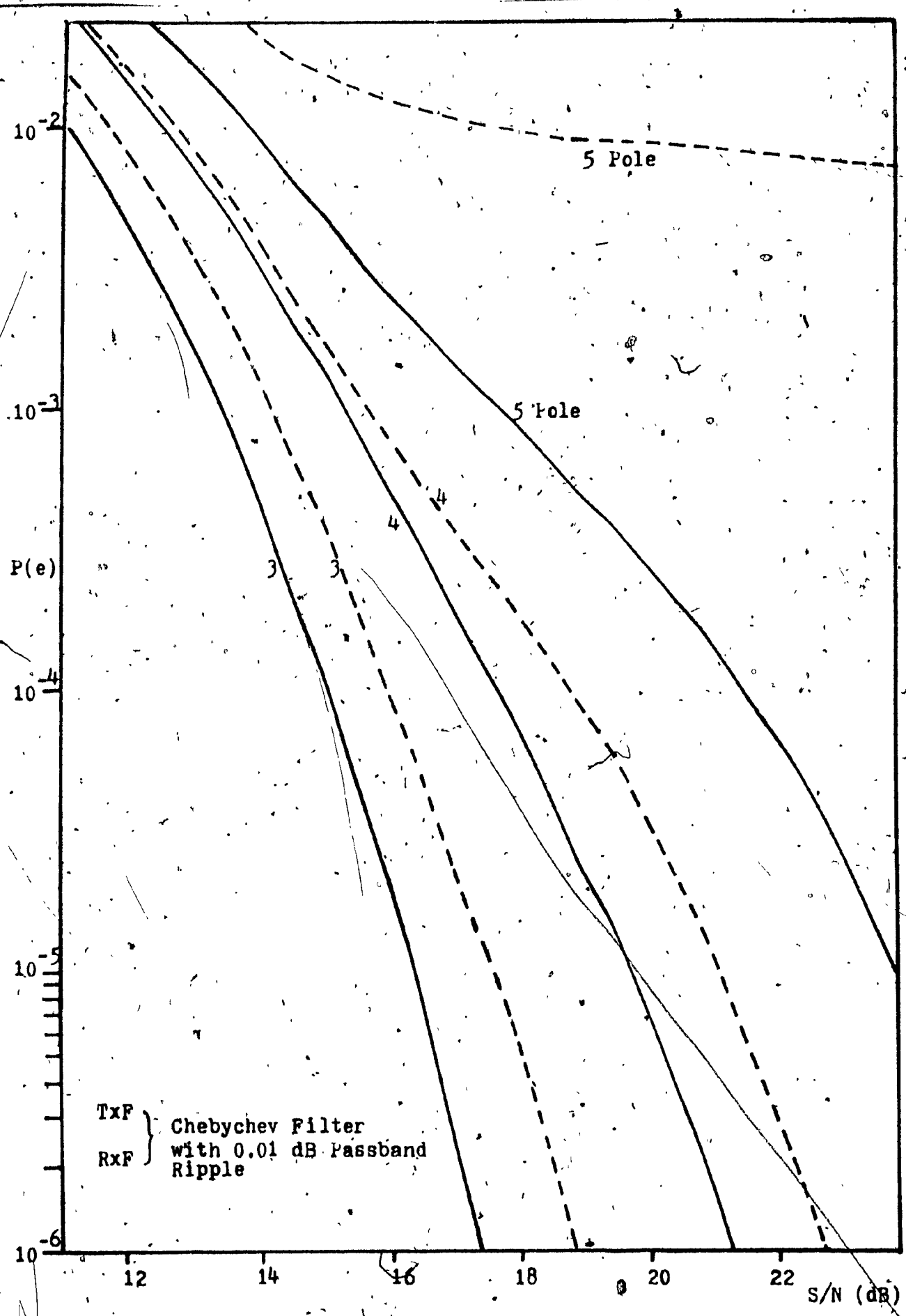

Fig. 3.21 Effect of Number of Filter Poles on QPRS

Solid line: BT = 1 ; Dashed Line : BT = 0.833

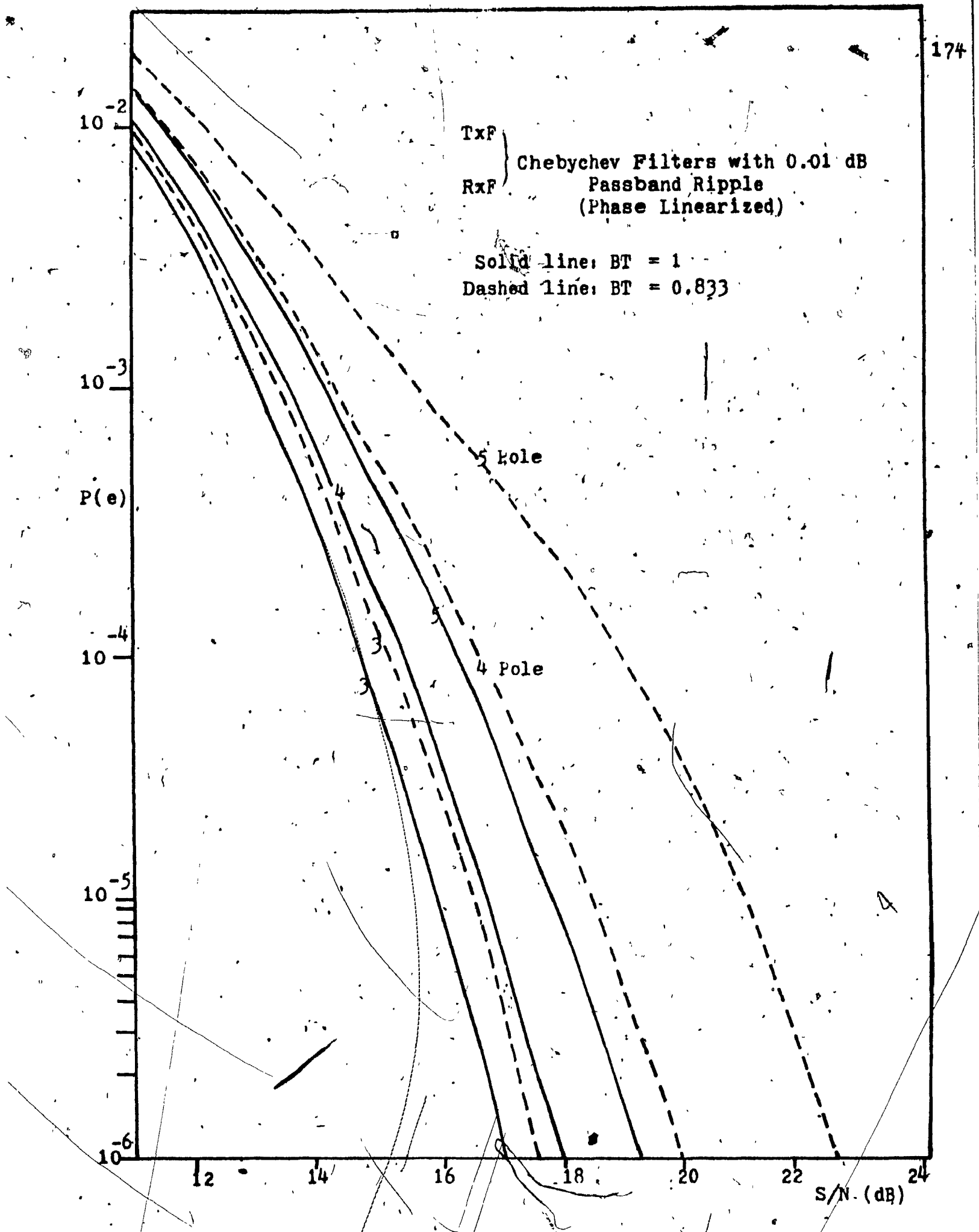

Fig. 3.22 Effect of Number of Filter Poles on QPRS

3.5.2 Channel Nonlinearity Effect

In this study, the characteristics of a typical TWT, such as a Hugher 261-H TWT, were used. The AM/AM and AM/PM curves of this TWT are given in Fig. 3.23.

The TWT was first placed after the transmit bandpass filter. It was found that under this situation the QPRS signal suffers severe degradation because of its multi-level nature.

The TWT was then placed before the PR filter. In this mode of operation, the signal at the TWT input was the undistorted QPSK signal. Hence, for the 3 level QPRS, filtering should be employed after the power amplifier.

3.5.2.A AM/AM Conversion Effect

To separate the effect of the AM/AM and AM/PM conversion on the QPRS signal, the TWT was first assumed to exert only the AM/AM conversion. At the transmitter, the ideal Nyquist filter was assumed and at the receiver, a 4 pole Chebychev filter with 0.01 dB passband ripples was used. Results for different TWT input backoffs are given in Fig. 3.24. From the input power back-off and Fig. 9, the nonlinear coefficients of the TWT can be obtained, [Eric, 3.21].

Next, the Nyquist filter at the transmitter was replaced by identical 4 pole Chebychev filter with 0.01 dB passband ripple. Results for this situation are plotted in Fig. 3.25.

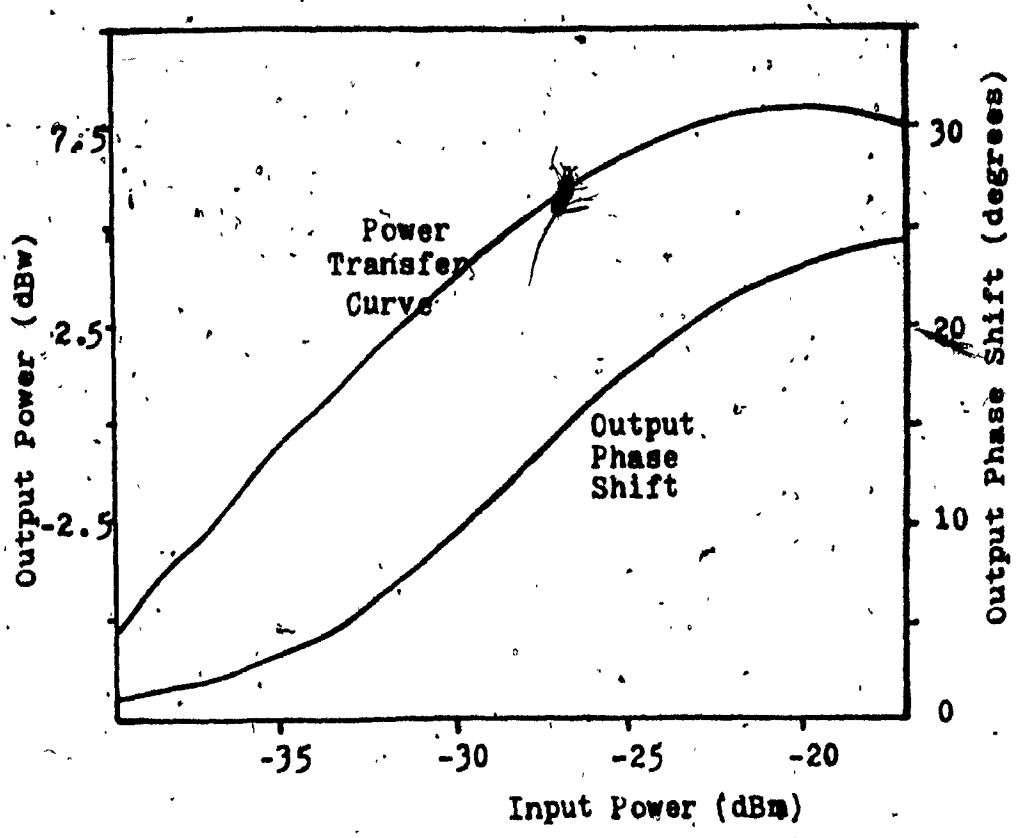

Fig. 3.23 The Single-Carrier Characteristics of an Hughes 261-H TWT

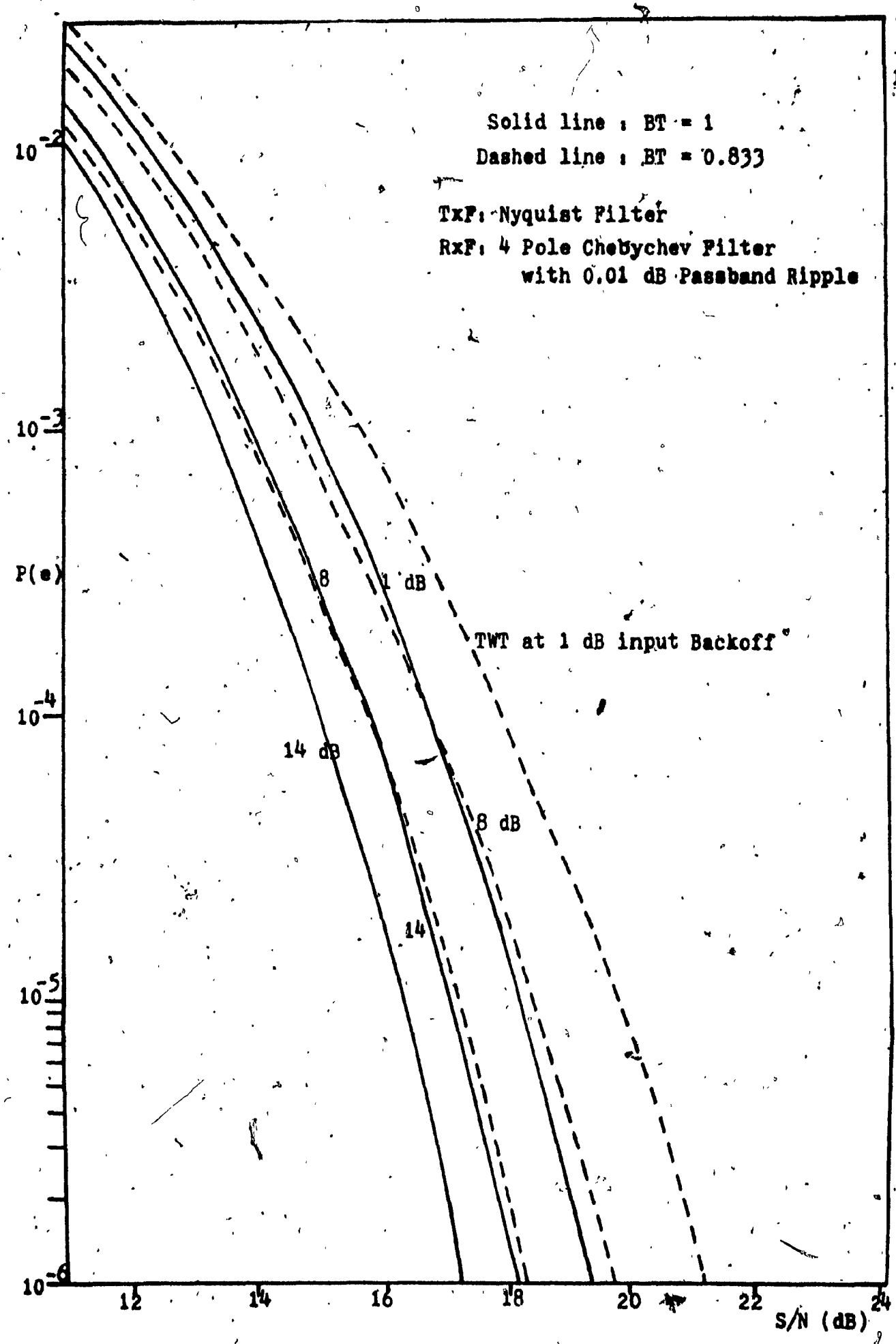

Fig. 3.24 Effect of TWT AM/AM Conversion on QPRS

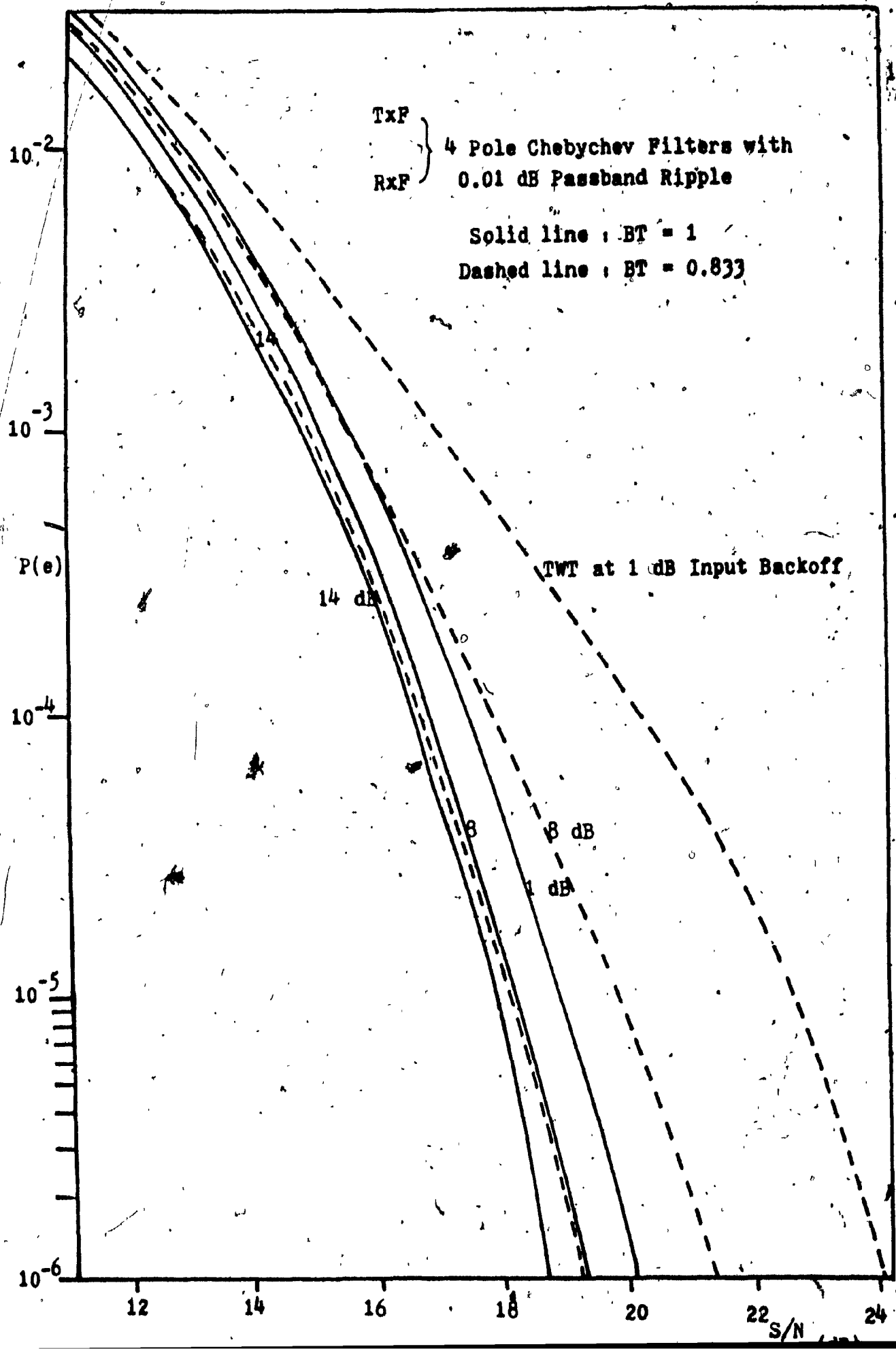
TxF
RxF
4 Pole Chebychev Filters with
0.01 dB Passband Ripple
Solid line : BT = 1
Dashed line : BT = 0.833
TWT at 1 dB Input Backoff
P(e)
10^{-2}
10^{-3}
10^{-4}
10^{-5}
10^{-6}
14 dB
8 dB
4 dB
12
14
16
18
20
22
24
S/N

3. 5. 2. B AM/AM and AM/PM Conversion Effect

Finally, both the AM/AM and AM/PM conversions of the TWT were assumed in the simulation. Results for the first situation, when the Nyquist filter was assumed at the transmitter and the 4 pole Chebychev filter with 0.01 dB passband ripples at the receiver, are shown in Fig. 3.26.

Then the Nyquist filter at the transmitter was again replaced by a 4 pole Chebychev filter with 0.01 dB ripples. Results for this situation with the TWT operating at different input backoffs are shown in Fig. 3.27.

Above results demonstrate, when both the AM/AM and AM/PM conversions of the TWT are considered, the drastic effect of the AM/PM conversion, on the performance of the QPRS signal. On the other hand, the AM/AM conversion effect alone only slightly degrades the system performance.

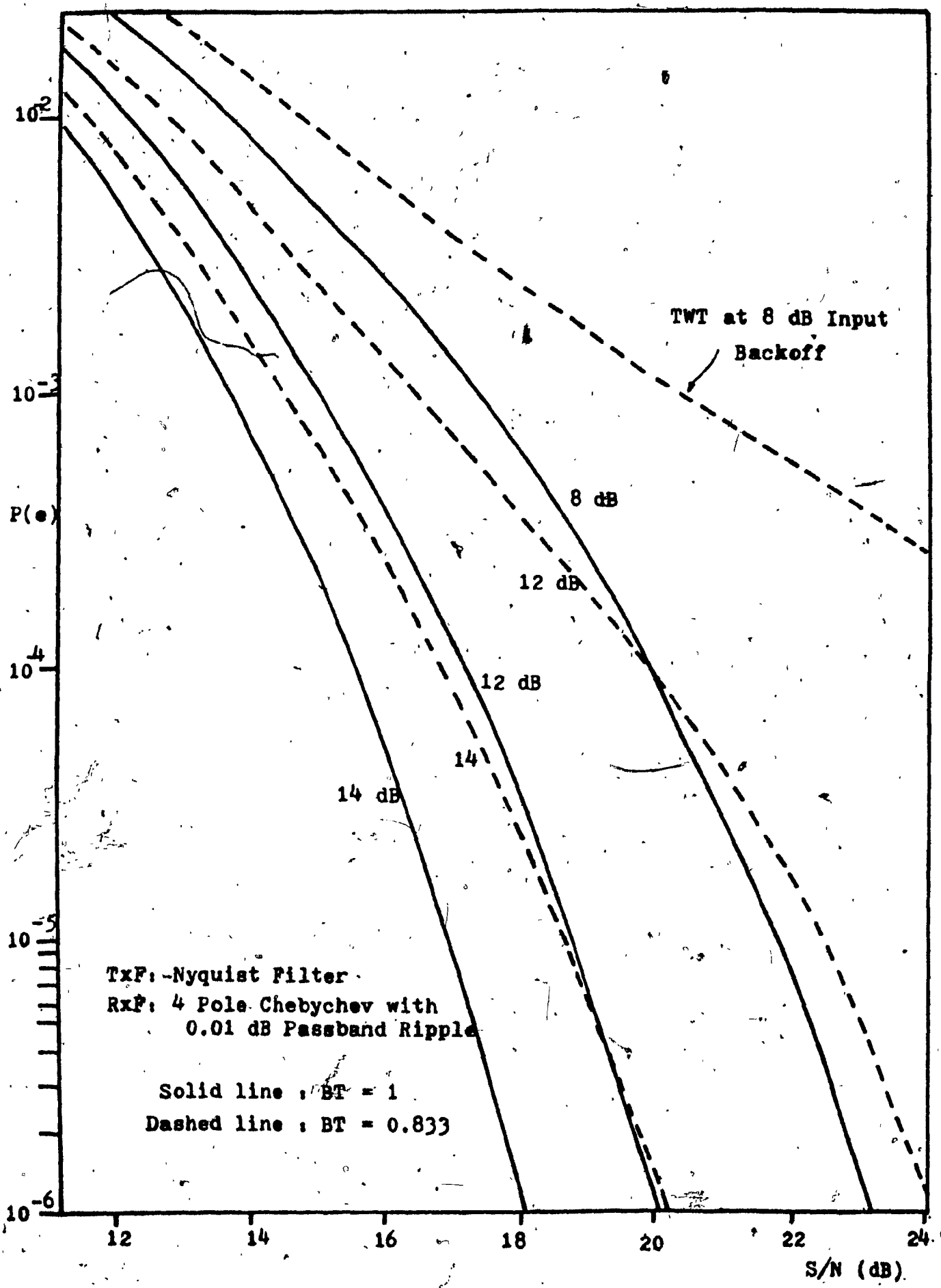

Fig. 3.26 Effect of TWT AM/AM and AM/PM Conversion on QPRS

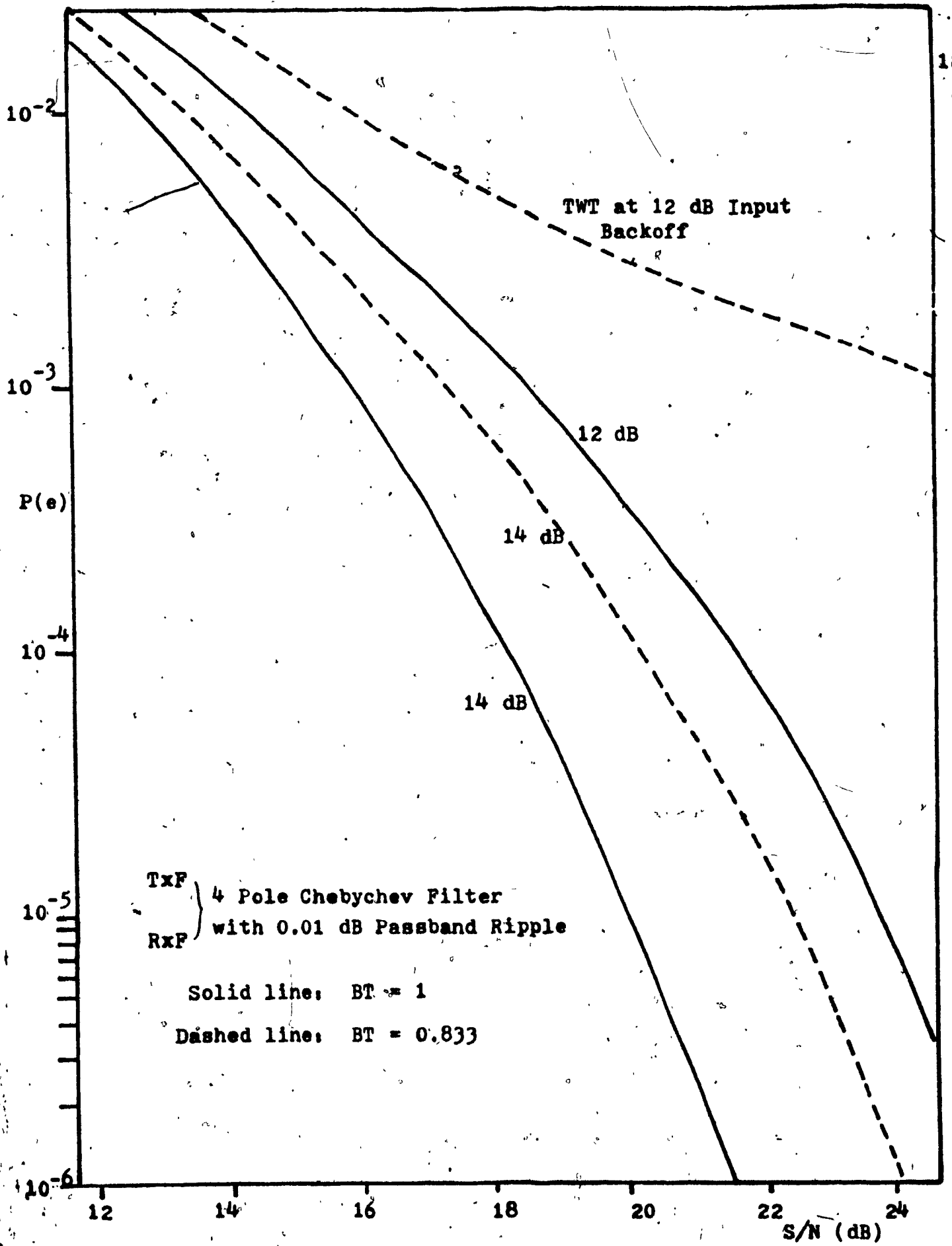

Fig. 3.27 Effect of TWT AM/AM and AM/PM Conversion on QPRS

3.6 System Evaluation of a PR Digital Radio

As described in the introduction, the PR scheme is a promising technique for efficient utilization of the available bandwidth in digital radio transmission. In this section, a simple guideline that allows one to study and compare the performance of a digital radio system based on the Bit Error Rate (BER) and bandwidth utilization efficiency, will be described.

In a radio system, the noise power N_b in the bit rate bandwidth at room temperature is defined as [Gill, 3.19], [Morais, 3.20]:

$$N_b = (-174 + 10 \log_{10} BR + NF) \qquad (3.32)$$

where BR is the bit rate, and NF is the noise figure.

For a specified BER, the carrier to noise ratio (C/N) can be obtained from the received carrier power and then compared with the theoretical predictions.

For example, if the received threshold of a radio system is specified at -82 dBm for a BER of 10^{-6} and the noise figure is 6dB, then at the operating bit rate of 6.313 Mb/s [Feher, 3.15]:

$$N_b = -174 + 10 \log_{10} 6.313 \times 10^6 + 6 = -100 \text{ dBm} \qquad (3.33)$$

and

$$C/N = -82 - (-100) = 18 \text{ dB} \qquad (3.34)$$

For a QPRS system, the theoretical C/N requirement for a BER of 10^{-6} is 15.6 dB. Therefore, this radio has a 2.5 dB degradation from theory. Also, since the transmit filter has a bandwidth of 3.2 MHz, the spectrum efficiency is approximately 2 b/s/Hz.

Table 3.5 lists the performance of some digital radio systems using the QPRS modulation method. The Fujitsu QAM2G-10R seems to have the closest performance to the theoretical prediction. The GTE Lenkurt 9120A is a 3 level FM whose theoretical SNR requirement for a $P(e) = 10^{-6}$ performance is listed as 15.9 dB. It is assumed that a correction factor of 0.3 dB exists between the baseband system and the FM system [Lender, 3.7].

Manufacturer	Avantek DR2C-96	GTE Lenkurt 9120A	Fujitsu QAM2G-10R	Northern Telecom DRS-8
Frequency Band	2 GHz	2 GHz	2 GHz	8 GHz
Modulation Technique	QPRS	3-level FM	QPRS	QPRS
Bit Rate (Mbit/s)	6.313	3.1	6.302	91.040
Transmitter Bandwidth	3.5 MHz	3.5 MHz	3.5 MHz	40.74 MHz
Bit Rate to Bandwidth Ratio	1.8 b/s/Hz	0.88 b/s/Hz	1.8 b/s/Hz	2.25 b/s/Hz
Required Received Signal Power for BER of 10^{-6}, S dBm	-82	-75	-82.7	* -69 for 10^{-4}
Transmitter Power Output, P dBm	27	36	27	40
System Gain, (P-S) dB	109	111	109.7	109
Receiver Noise Figure, NF dB	6	9	5	8 (est.)
Noise Power N_b = -174 +10log BR + NF	100	-99.5	-101	-86.4
Carrier to Noise Ratio C/N in Bit Rate Bandwidth, (dB)	18	24.5	17.3	17.4
Theoretical C/N for 10^{-6}	15.6	15.8	15.6	* 13.5 (for 10^{-4})

Table 3.5 Performance Comparison of Digital Radio Systems Using QPRS

3.7 Summary of Chapter 3

The pulse overlapping concept has been applied to the generation of different types of partial response signals. Multi-intervaled pulses suitable for this purpose were found from the coefficients of the polynominal representations of the partial response filters. By overlapping these multi-intervaled pulses in a synchronous fashion, it was demonstrated how correlation was introduced into a binary system for transformation into a multilevel correlative system. The spectra of the multilevel correlative signals were derived from the Fourier transforms of these multi-intervaled pulses. The ratios of the Fourier transforms of these pulses and the single-intervaled pulse were shown to equal to the transfer function of the digital filters that perform the signaling level transformations. Cascading each of these digital filters with a brick-wall Nyquist filter gives the partial response filter whose transfer function was then derived.

Lender's PR model was analyzed and extended to other PR systems. It was also compared with the models of Kretzmer and Qureshi.

A computer simulation was developed to study the effect of filtering and nonlinearity on the performance of the QPRS radio systems. Results showed that, if degradation less than 2dB from

theory is required, the filter passband ripple should be less than 0.01dB and the phase of the filter linearized. To reduce the AM/PM conversion degradation, the power amplifier should be placed before the PR filter and it should be operated in the linear mode.

CHAPTER 4

Chapter 4

Performance of Bandlimited QPSK, OKQPSK and MSK Signals Through Cascaded Nonlinearities

4.1 Introduction

In Chapter 3, a computer simulation program was used to study the effects of filtering and nonlinearity on the performance of a QPRS digital radio system. Because of power constraint and channel bandwidth restriction, a satellite communication system suffers similar or even more degradating effects of bandlimiting and cascaded nonlinearities. In this chapter, the QPRS computer program will be modified to study these effects on the performance of QPSK, OKQPSK and MSK signals through a satellite channel. Due to their inherent characteristics, these three types of modulation schemes have been frequently mentioned in the literature as possible candidate techniques suitable for a nonlinear satellite channel [Wolejzsa, 4.1], [Murakami, 4.2] [Gronemeyer et al, 4.3] [Feher, 4.4].

Fig. 4.1 shows a typical satellite channel model. The satellite link considered, consists of the earth transmitting station, the satellite transponder and the earth receiving station. At the earth transmitting station, the transmit bandpass filter (F_1), used to bandlimit the spectrum, causes intersymbol interference (ISI); the high power amplifier (HPA), operated near saturation, causes both the AM/AM and AM/PM conversions of the signal and degrades the system

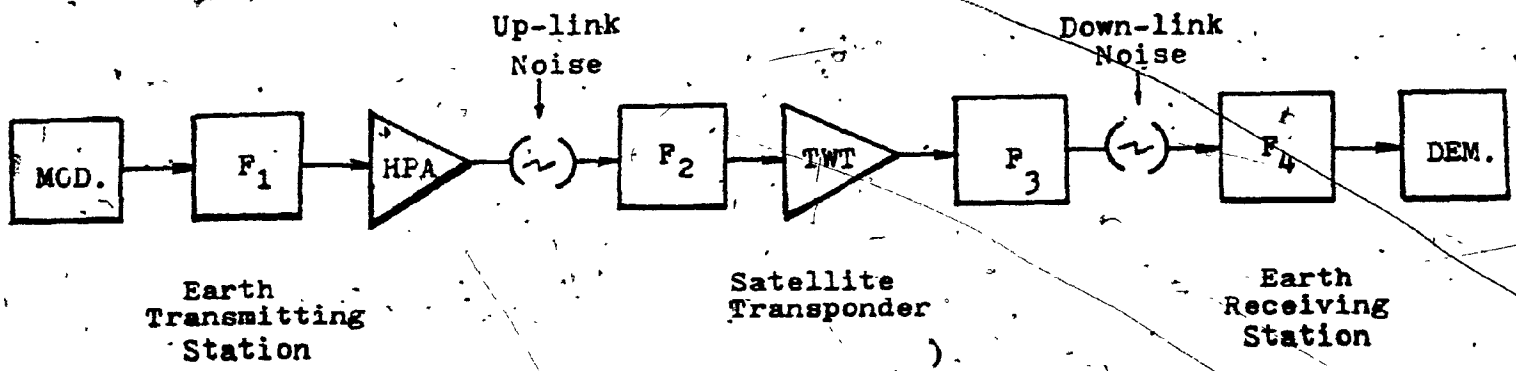

Fig. 4.1 Digital Satellite Communication System Model

performance. The satellite input and output MUX filters (F_2 and F_3) which are used to bandlimit the signal and reduce the spectrum spreading caused by the TWT, induce also ISI. Due to the power constraint on board the satellite transponder, the TWT is usually operated near saturation and causes AM/AM and AM/PM conversion degradation At the earth receiving station, the receive filter, which is used to bandlimit the thermal noise and reduce the adjacent channel interference, also degrades the system performance.

The HPA at the earth station and the TWT at the satellite transponder are operated close to saturation in order that maximum power conversion efficiency can be achieved. The DC to RF power conversion efficiency of these nonlinear devices is the highest when they are operated near saturation. In this mode of operation, these two devices exhibit the nonlinear effects of AM/AM and AM/PM conversion [Bell Blue Book, 4.5]. The AM/AM conversion causes spectral spreading of the filtered signal which will then interfere with signals in the neighbouring channels (adjacent channel interference). In the case of M-ary PSK (Phase Shift Keying) modulated signals, substantial AM/PM conversion will also deteriorate the system performance.

Because of the ever increasing demand in communication traffic, the channel bandwidth available for the satellite communication system is usually narrowband. For example, the Intelsat V system will be

operating at 60 Mb/s using only 36 MHz of bandwidth. To avoid the adjacent channel interference, the channel allocation is 40 MHz [Murakami, 4.2]. Tight filtering is therefore required so as to reduce the adjacent channel interference while maintaining manageable intersymbol interference so that optimum performance can still be achieved.

Digital modulation techniques suitable for the nonlinear satellite channel therefore, must meet the following two requirements.

1. Bandwidth efficient with optimal bandlimiting filters for minimal intersymbol and adjacent channel interference.
2. Optimal system gains from the HPA and TWTA with little spectrum spreading and distortion degradation from their AM/AM and AM/PM conversions.

Based on these two constraints, three modulation techniques, namely, conventional QPSK, OKQPSK and MSK, have frequently been considered for such a nonlinear satellite channel. The basic schemes for these three modulation techniques will be reviewed in section 4.2.

To study and compare the performance of these three signals in a bandlimited nonlinear satellite channel, the first part of this chapter is devoted to analyzing the envelope fluctuations of these signals which arise when they are bandlimited. Understanding of the envelope fluctuations is essential in the study of the spectrum spreading which occurs

when these filtered signals pass through a nonlinear device.

Two types of envelope fluctuations are considered. The first type is the overall envelope fluctuation of the filtered signal. The second type is the envelope fluctuation at the sampling instants. The latter type of envelope fluctuation is more important as the performance of the system is determined by what occurs to the signal at the sampling instants.

Next, spectrum spreading which occurs when a filtered PSK signal passes through a power amplifier is studied. Two types of spectrum spreading are experimentally demonstrated. The first type, defined as complete spectrum restoration, occurs when a jitter free signal is hardlimited. The second type, defined as spectrum restoration with modification, is partly attributed to the timing jitter of the filtered signal.

Finally, to study the overall system performance of these three signals through a typical satellite link, computer simulation program similar to that used in the QPRS study but more involved, has been developed. Results from this simulation are then analyzed and compared with those available in the literature.

The working versions of the simulation programs and the instruction manual are listed in Appendix G2. Although they are not optimized for faster computation times, they will, nevertheless, provide a useful tool in the system design of a satellite communication link.

4.2 Conventional QPSK, Offset QPSK and MSK

As mentioned in the previous section, three modulation techniques, namely, conventional QPSK, offset QPSK and MSK, have been frequently considered for signal transmission through a nonlinear satellite channel. In this section, the basic schemes of these three modulation techniques are described.

In conventional QPSK (Quaternary Phase-Shift Keying), the in-phase and the quadrature phase data streams, as shown in Fig. 4.2.a, are aligned coincidently.

In OKQPSK (Offset QPSK) and MSK(Minimum Shift Keying), one data stream is delayed by half a symbol interval in comparison with the other data stream (Figs. 4.2.b and 4.2.c). The difference between OKQPSK and MSK lies in the extra pulse shaping networks which shape the rectangular pulses of OKQPSK into the half cosine pulses of MSK.

Simplified block diagrams of these three modulation schemes are shown in Fig. 4.3. The binary input random data stream having a bit interval T is first serial to parallel converted into two data streams. These two data streams have a symbol duration of 2T as shown in Fig. 4.2.

In the case of conventional QPSK, they are then quadrature modulated by a carrier. To obtain OKQPSK from QPSK, one of the two parallel data streams is first delayed by a bit interval relative to the other data stream. Afterwards, they are then quadrature modulated

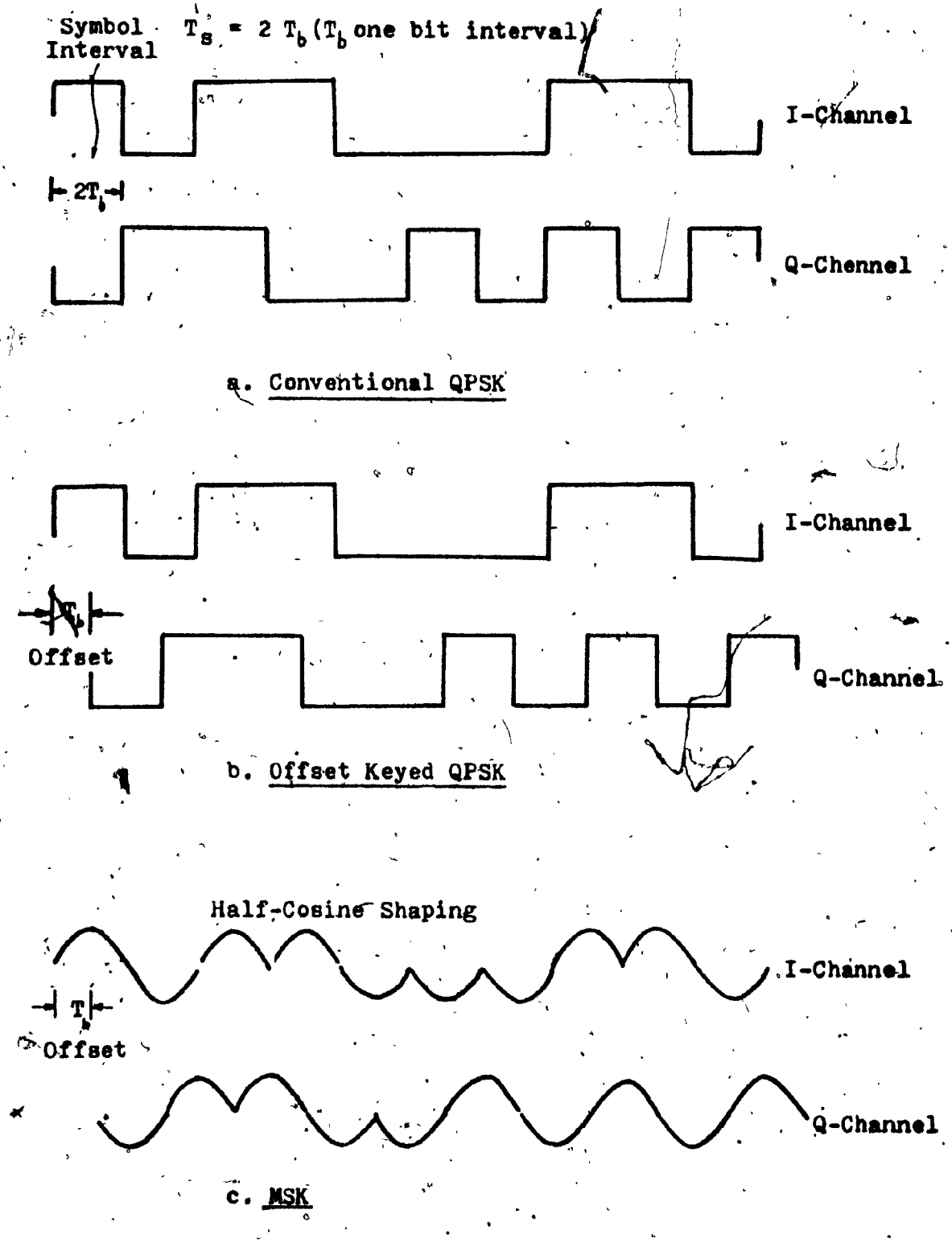

Fig. 4.2 Signaling Format of Conventional QPSK, OKQPSK and MSK

as in conventional QPSK. MSK is similar to OKQPSK except that a pulse shaping network modifies the rectangular pulses of OKQPSK into half cosine pulses in these two parallel data streams before they are quadrature modulated. In all three cases, the bandpass filter F_1 after the modulator is used for spectrum shaping purpose.

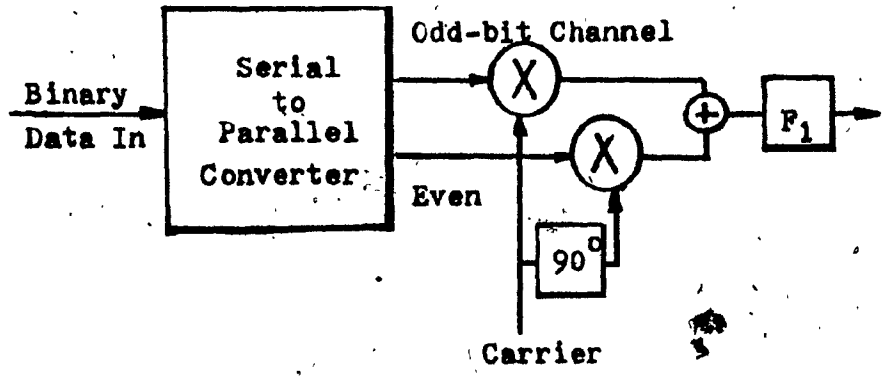

a. Conventional QPSK

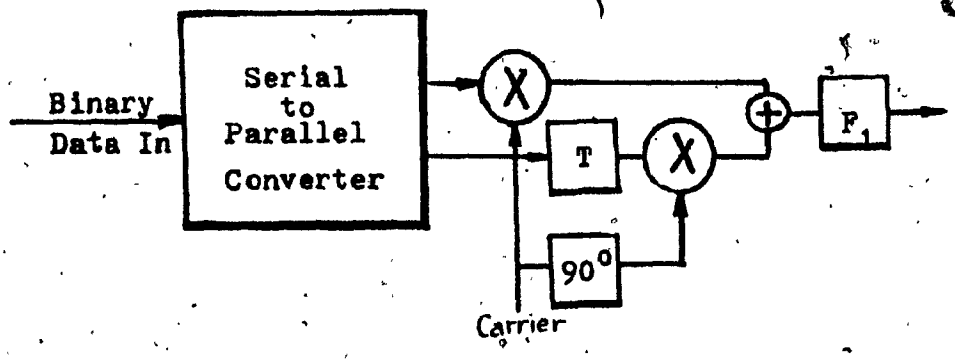

b. Offset Keyed QPSK

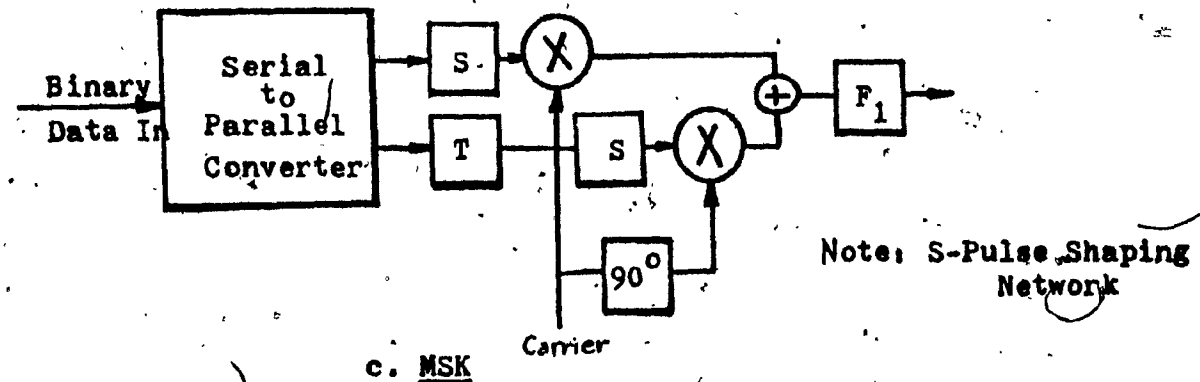

c. MSK

Fig. 4.3 Block Diagrams of Conventional QPSK, OKQPSK and MSK

4.2.1 FFSK View of MSK

MSK can also be viewed as one type of the general Continuous Frequency Shift Keying (CFSK) modulation schemes. In this sense, it is called Fast Frequency Shift Keying (FFSK) [de Buda, 4.6]. As indicated in Fig. 4.4, the frequency deviation in FFSK $\Delta f = \frac{f_1 - f_2}{2}$ is exactly equal to $\pm \frac{1}{4} T$, where f_1 is the frequency of the signal representing the 1 symbol and f_2 is the frequency of the signal representing the 0 symbol.

This view of looking at MSK as FFSK can easily be demonstrated as follows:

For a frequency shifted keying signal,

$$s(t) = A \cos\left[2\pi(f_c \pm \Delta f)t\right] \qquad (4.1)$$

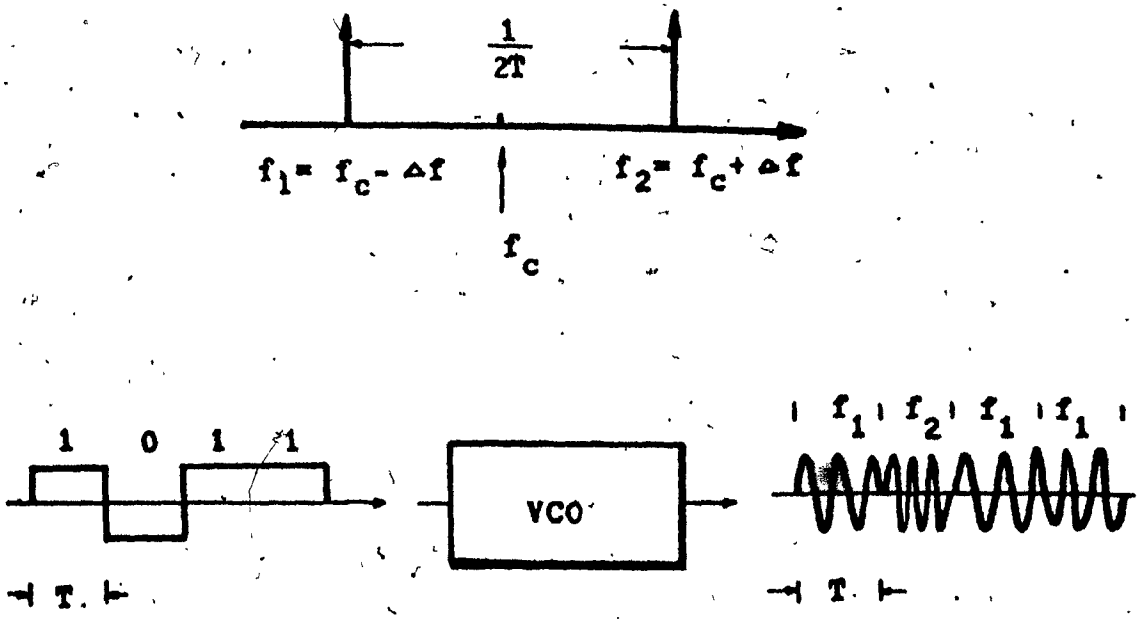

Fig. 4.4 FFSK View of MSK

which can be considered as the transmission of a sinusoid whose frequency is shifted between the following two frequencies:

$$f_1 = f_c - \Delta f$$

and (4. 2)

$$f_2 = f_c + \Delta f$$

The FSK signal $s(t)$ in Eq. (4. 1) can then be expanded as:

$$A \cos (\pm 2\pi \Delta f t) \cos 2\pi f_c t - A \sin (\pm 2\pi \Delta f t) \sin 2\pi f_c t \quad (4. 3)$$

Now, if the frequency deviation is

$$\Delta f = \tfrac{1}{2}(f_2 - f_1) = \pm 1/4T \quad (4. 4)$$

where T is the unit bit duration of the input random data stream.

Then,

$$s(t) = A \cos (\pm \pi t/2T) \cos 2\pi f_c t - A \sin (\pm \pi t/2T) \sin 2\pi f_c t \quad (4. 5)$$

Thus, $s(t)$ is an offset quadrature carrier signal with half a cosine pulse shaping in its baseband signals. The baseband signals are:

$$x(t) = A \cos (\pm \pi t/2T)$$

and (4. 6)

$$y(t) = A \sin (\pm \pi t/2T).$$

It is important to notice that,

$$x^2(t) + y^2(t) = A^2 \tag{4.7}$$

This feature is characteristic of the baseband signaling waveform suitable for applications in CFSK. This signaling format is also known as MSK-formatted signal [Kalet, 4.7], or MSK-type signal [Simon, 4.8].

4.2.2 Spectra of QPSK, OKQPSK and MSK

The spectra of conventional QPSK (hereafter abbreviated as QPSK), OKQPSK and MSK are shown in Fig. 4.5. The power spectrum of OKQPSK is identical to that of the QPSK. Both have the (sin x/x) shape centered at the carrier frequency. Mathematically, the spectra of both the QPSK and OKQPSK are given by [Gronemeyer, 4.3]:

$$S_{\substack{QPSK \\ OKQPSK}}(f) = 2 P_c T \left(\frac{\sin 2\pi fT}{2\pi fT}\right)^2 \qquad (4.8)$$

where f = frequency offset from carrier, P_c = power of the modulated waveform, T = unit bit duration. (In Appendix C1, the Power Spectrum of the filtered OKQPSK signal will be derived and shown to be identical to that of QPSK signal).

The spectrum of a MSK signal is given also by 4.3 :

$$S_{MSK}(f) = \frac{8 P_c T(1 + \cos 4\pi fT)}{\pi^2 (1 - 16f^2 T^2)^2} \qquad (4.9)$$

Eqs. (4.8) and (4.9) can easily be obtained from the well-known fact that the power spectrum density of a PSK signal with a baseband signaling waveform s(t) has the same spectral shape as that of s(t) itself. The only difference is that the spectrum of the PSK signal is double-sided and centered at the carrier frequency [Bennett and Davey, 4.9].

Comparing the spectrum of MSK with that of QPSK (or OKQPSK) we find that the main lobe width of MSK is 50% wider than that of QPSK (or OKQPSK). The sidelobes of MSK, on the other hand, are much lower than those of QPSK (or OKQPSK).

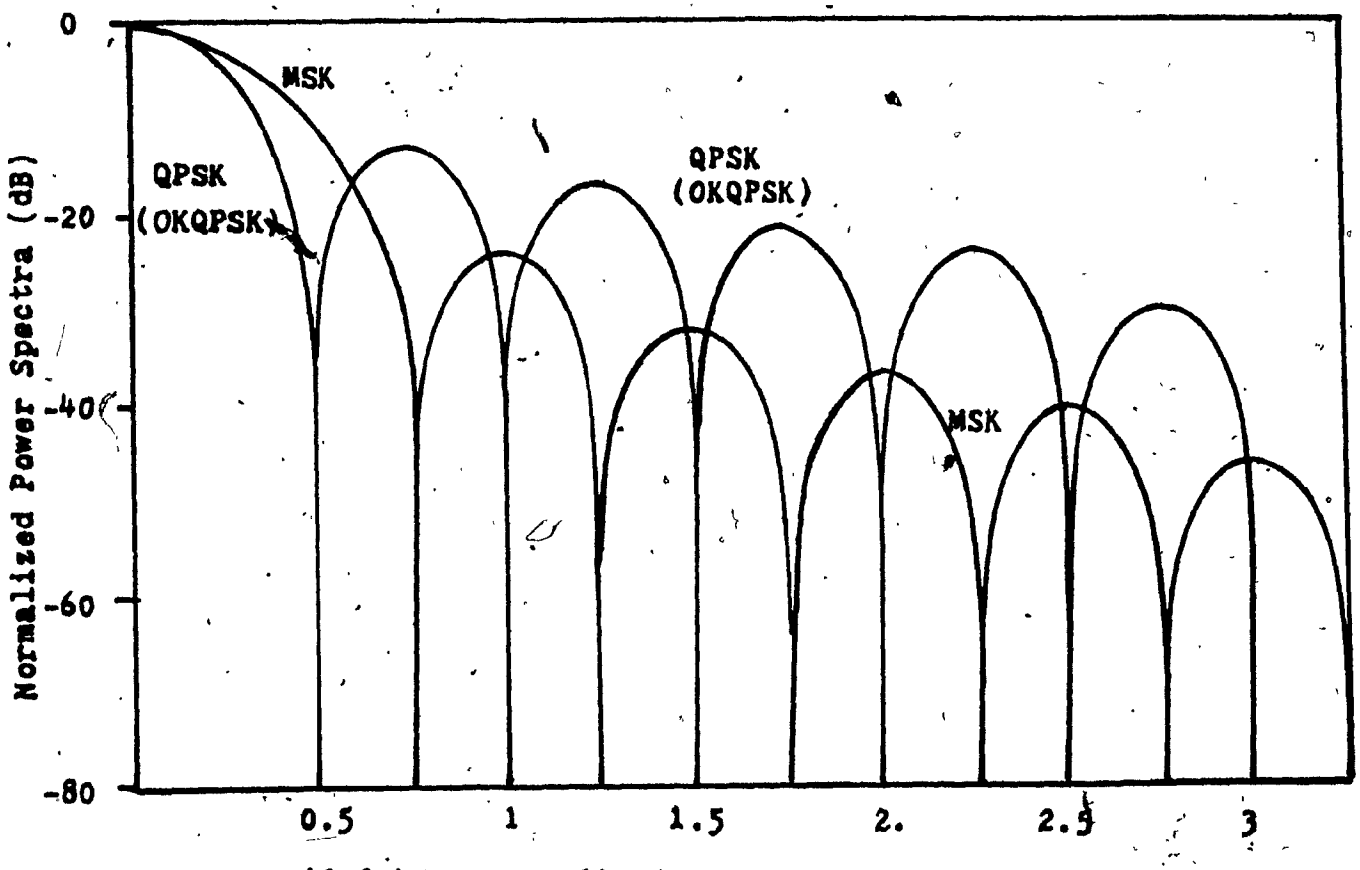

Fig. 4.5 Power Spectra for MSK and QPSK (OKQPSK)

($T = 1$ sec. $P_c = 1$ W.)

4.3 Overall Envelope Fluctuations of QPSK, OKQPSK and MSK Signals

Due to the time coincidence of the two data streams in QPSK, phase transitions of 0°, $\pm 90^{\circ}$, and 180° can occur. Fig. 4.6.a shows the RF amplitudes and phases of the filtered QPSK signal. At the 180° instantaneous phase transitions, which arise when both the in-phase channel data and the quadrature channel data change phase simultaneously, the envelope goes through zero amplitude. At the $\pm 90^{\circ}$ phase transitions, which occur when only one channel data change phase at the keying instant, there is a 3dB envelope fluctuation.

In OKQPSK, because of the one bit (half a symbol) duration delay between the two data channels, the 180° phase transitions are avoided. Only $\pm 90^{\circ}$ phase transitions arise with maximum 3 dB envelope fluctuations as shown in Fig. 4.6.b. The overall envelope fluctuations of OKQPSK are thus smaller than those of QPSK.

In MSK, the data waveforming pulses are of half cosine shape as shown in Fig. 4.6.c. According to Eq. (4.7), the signal has a constant envelope. Another important feature of MSK is that the phase transitions are linear and continuous [de Buda, 4.6].

The overall envelope fluctuations of QPSK, OKQPSK and MSK can also be studied from the signal space diagrams, as shown in Fig. 4.7. Fig. 4.7.a shows the signal space diagrams of those three signals using computer simulation. Fig. 4.7.b shows the signal space diagrams

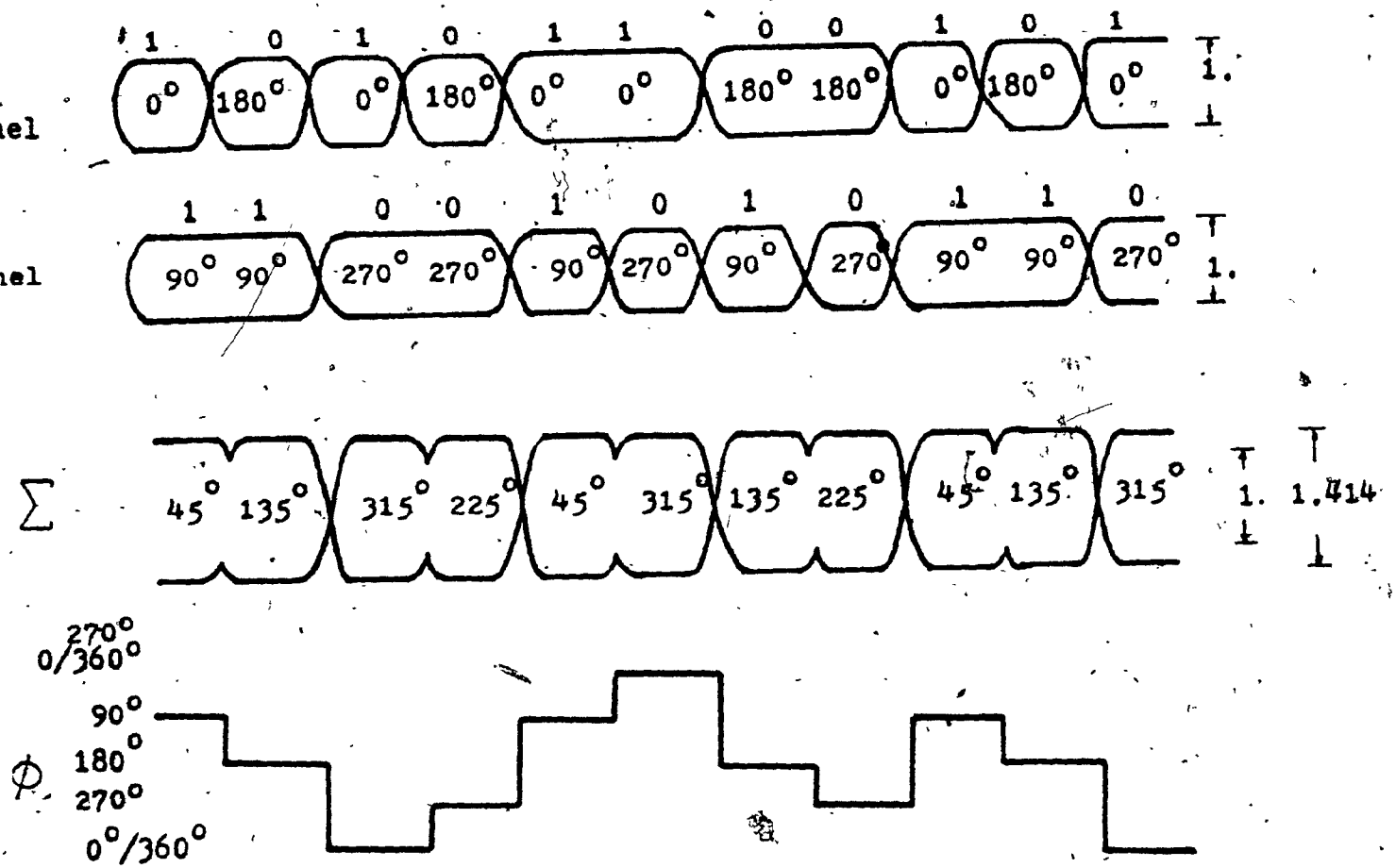

Fig. 4.6.a RF Amplitude and Phase of Conventional QPSK Signal

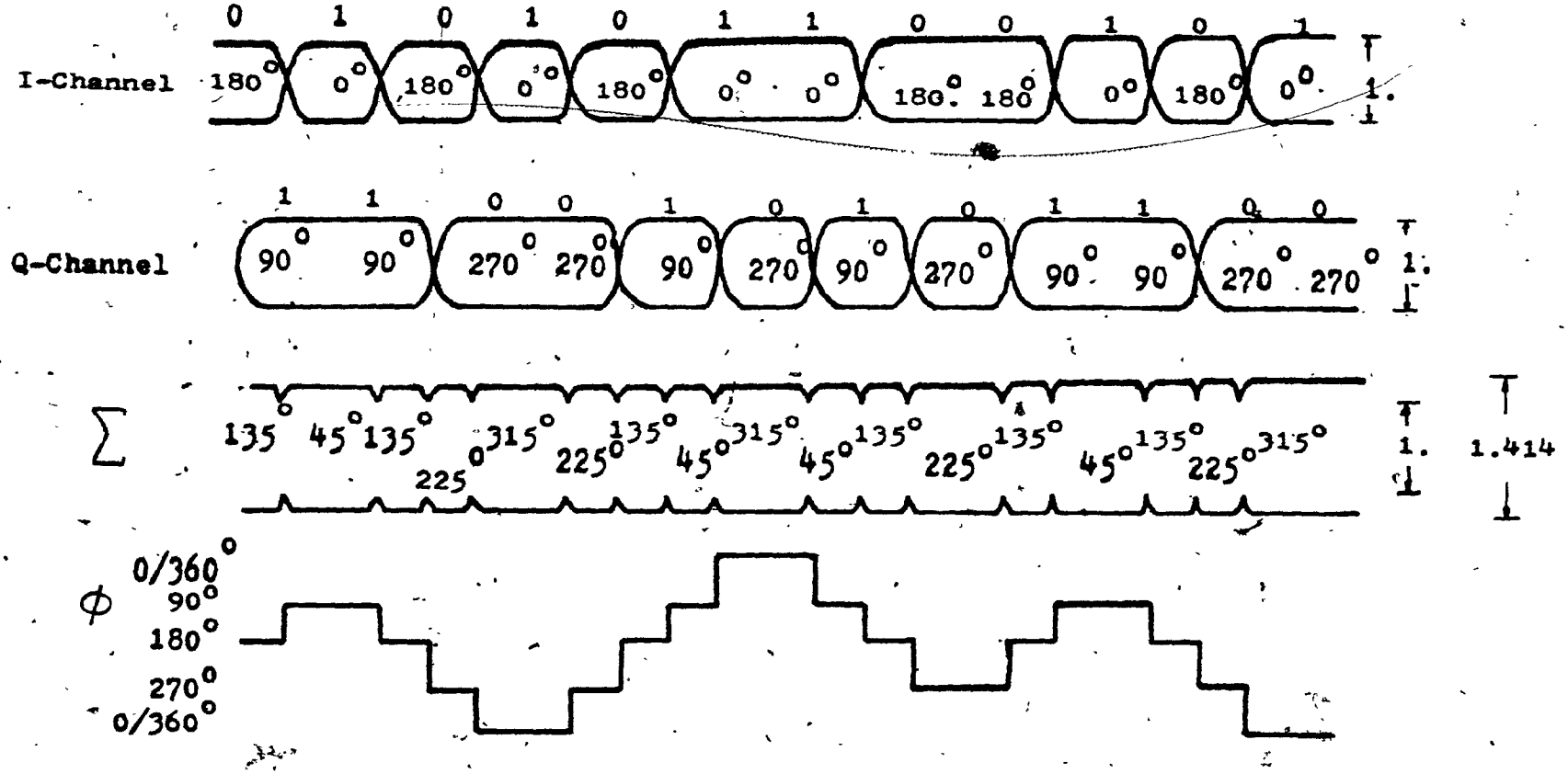

Fig. 4.6.b RF Amplitude and Phase of OKQPSK Signal

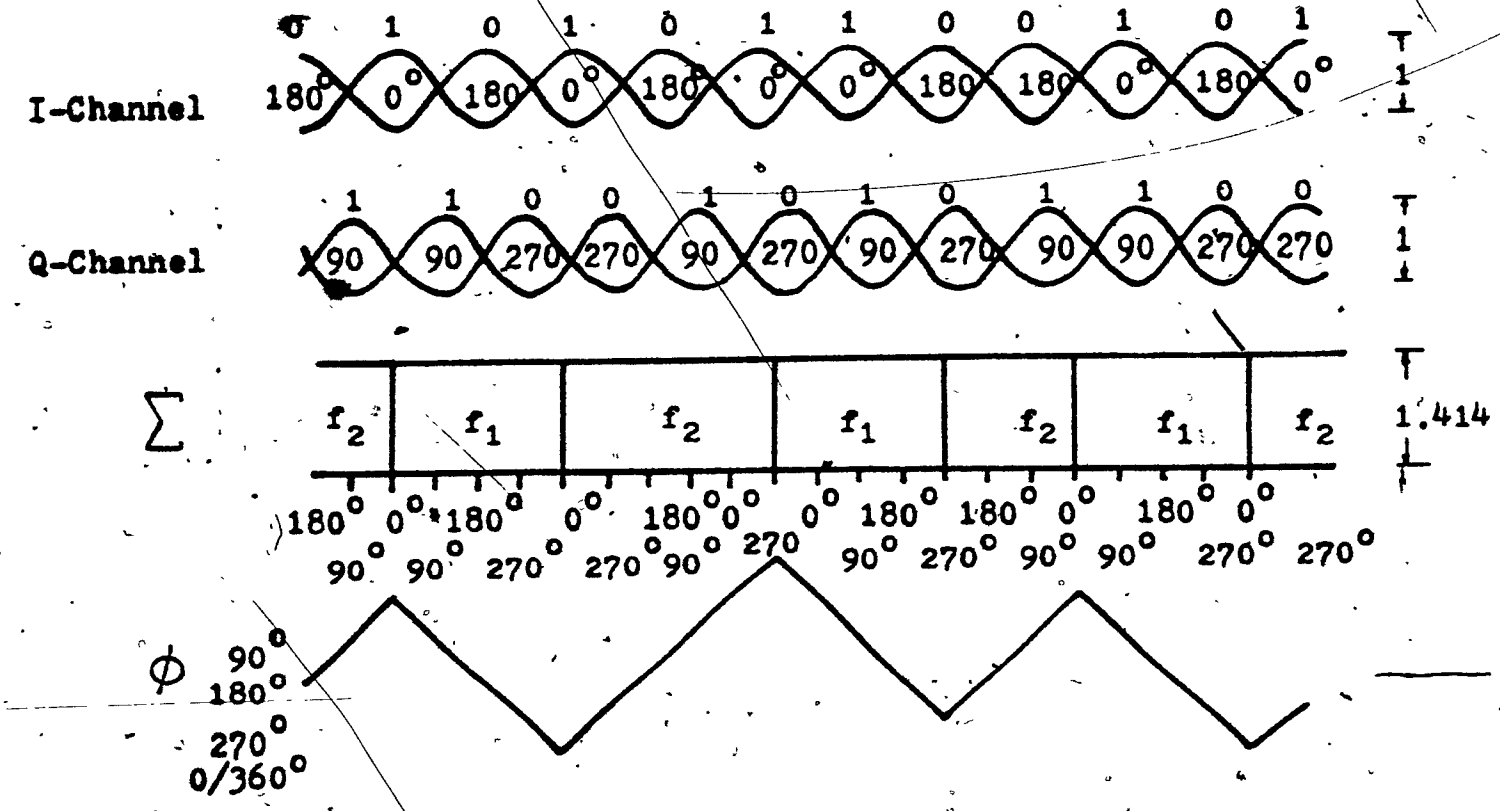

Fig. 4.6.c RF Amplitude and Phase of MSK Signal

Bit Rate 90 Mb/s

$F_1 = F_4 = 54$ MHz

$F_2 = F_3 = 125$ MHz

(f_{3dB} of the 4 pole Chebychev filters)

HPA and TWT at 1 dB input backoff

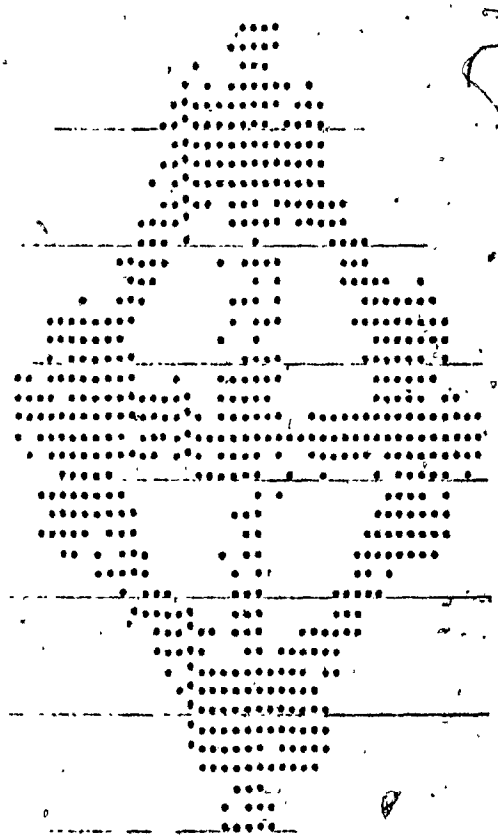

a. QPSK

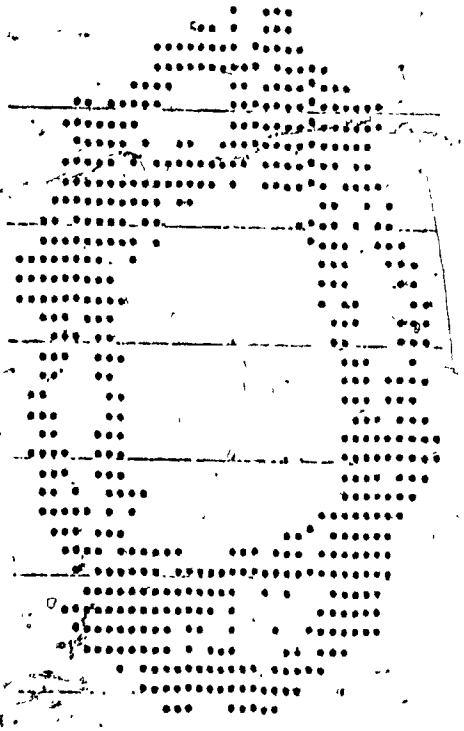

b. OKQPSK

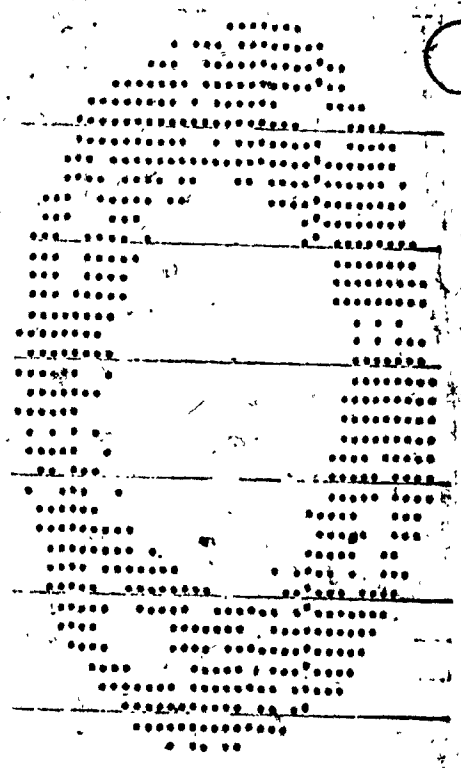

c. MSK

Fig. 4.7 Computer-Simulated Signal Space Diagrams

Fig. 4.7.d Signal Space Diagram of QPSK

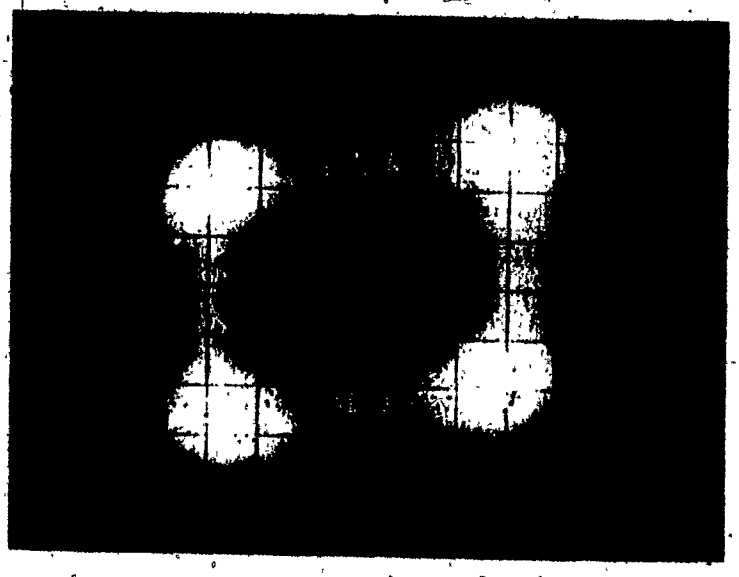

Fig. 4.7.e Signal Space Diagram of OKQPSK

(Blurred Traces due to Circuit Malfunction)

of the QPSK and OKQPSK signals from laboratory measurements. These space diagrams are obtained by feeding the demodulated in-phase and quadrature baseband signals to the x-(vertical) input and the y-(horizontal) input of the oscilloscope, respectively.

In computer simulation, the received quadrature signals were assigned to quadrature components of a two-dimensional matrix and stored in the memory. At the end of the simulation, the signal space diagram was then plotted from the computer memory of the final matrix.

The signal space diagrams show that whenever the in-phase and quadrature channel data change states simultaneously, the QPSK signal goes through the origin (zero amplitude). In OKQPSK and MSK, because of the time delay between the two parallel channel data, this does not occur.

The inherent envelope fluctuation of QPSK therefore causes distortion and more spectrum spreading when it passes through a nonlinear amplifier. The spectrum spreading of QPSK and OKQPSK will be demonstrated and compared experimentally in section 4.5.

In the following we will analyze the overall envelope variations of the filtered QPSK and OKQPSK signals. This analysis, in conjunction with the pictorial description of Fig. 4.6, will also be used in our discussion on the envelope fluctuations of the filtered QPSK and OKQPSK signals at the sampling instants.

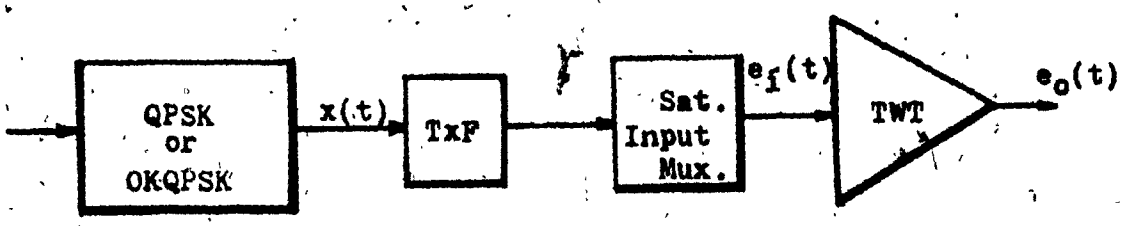

Fig. 4.8 Simplified Digital Satellite Channel Model

To simplify our discussion, the quadrature carrier communication system model shown in Fig. 4. 1 will be assumed to include only the transmit filter and the TWT input MUX filter and the TWT itself as depicted in Fig. 4. 8. This simplified model is adopted because we are only interested in the envelope fluctuations caused by the bandlimiting filters and one nonlinear device. A similar model has also been used by Robinson, et al in their theoretical analysis on spectrum spreading of QPSK [4. 10] and by McMaster University in their comparative performance study by computer simulation [4. 11]. The initial part of the analysis on QPSK follows [4. 10] which is then extended to OKQPSK.

The QPSK or OKQPSK signal x(t) at the transmit filter TXF input can be written as:

for QPKS

$$x(t) = \sum_{-\infty}^{\infty} \left[a_k\, s(t - kT_s) \cos 2\pi f_c t\right] + \sum_{-\infty}^{\infty} \left[b_k\, s(t - kT_s) \sin 2\pi f_c t\right] \tag{4.10}$$

for OKQPSK,

$$x(t) = \sum_{-\infty}^{\infty} \left[a_k\, s(t - kT_s) \cos 2\pi f_c t\right] + \sum_{-\infty}^{\infty} \left[b_k\, s(t - T_s/2 - kT_s) \sin 2\pi f_c t\right] \tag{4.11}$$

where a_k, $b_k = \pm 1$ with equal probability of occurrence.

f_c is the carrier frequency, T_s is the symbol interval (T_s=2T)

and

$$s(t) = \begin{cases} \text{rectangular pulse for } |t| \leq T_s/2 \\ 0 \qquad\qquad\qquad \text{otherwise} \end{cases}$$

x(t) can be rewritten as:

QPSK,

$$x(t) = \mathrm{Re}\left\{ e^{j2\pi f_c t} \cdot (a_k + j\, b_k)\, s(t - kT_s) \right\} \tag{4.12}$$

OKQPSK,

$$x(t) = \mathrm{Re}\left\{ e^{j2\pi f_c t} \left[a_k\, s(t - kT_s) - j\, b_k\, s(t - T_s/2 - kT_s) \right] \right\} \tag{4.13}$$

where Re stands for the real part of a complex variable.

Assuming h(t) is the low-pass equivalent of the impulse response of the filters between the quadrature carrier modulator and the TWT, then, the filtered equivalent baseband signal at the input of the TWT is [Lucky et al, 4.12]:

for QPSK,

$$e_i(t) = \sum_k \overbrace{\left[a_k\, R(t - kT_s) - b_k\, I(t - kT_s) \right]}^{y(t)} \cos 2\pi f_c t - \sum_k \underbrace{\left[a_k\, I(t - kT_s) + b_k\, R(t - kT_s) \right]}_{z(t)} \sin 2\pi f_c t \tag{4.14}$$

and

for OKQPSK,

$$e_i(t) = \sum_k \overbrace{\left[a_k\, R(t - kT_s) - b_k\, I(t - T_s/2 - kT_s) \right]}^{y(t)} \cos 2\pi f_c t - \sum_k \underbrace{\left[a_k\, I(t - kT_s) + b_k\, R(t - T_s/2 - kT_s) \right]}_{z(t)} \sin 2\pi f_c t \tag{4.15}$$

where $R(t) = \frac{1}{2} \mathrm{Re}\left[s(t) * h(t) \right]$

$I(t) = \frac{1}{2} \mathrm{Im}\left[s(t) * h(t) \right]$

and (4.16)

$R(t - kT_s) = \frac{1}{2} \mathrm{Re}\left[s(t - kT_s) * h(t) \right]$

$I(t - kT_s) = \frac{1}{2} \mathrm{Im}\left[s(t - kT_s) * h(t) \right]$

with * denoting convolution.

The IF signal $e_i(t)$ can be written for both QPSK and OKQPSK as

$$e_i(t) = y(t) \cos 2\pi f_c t + z(t) \sin 2\pi f_c t$$
$$= \sqrt{y^2(t) + z^2(t)} \cos\left(2\pi f_c t + \tan^{-1}\left[y(t)/z(t) \right] \right) \quad (4.17)$$

The amplitude of $e_i(t)$ is:

for QPSK,

$$A(t) = \sqrt{y^2(t) + z^2(t)} = \sqrt{2 \sum_K \left[R^2(t - kT_s) + I^2(t - kT_s) \right]} \quad (4.18)$$
$$= \sqrt{\tfrac{1}{2} \sum_K v^2(t - kT_s)}$$

and

for OKQPSK,

$$A(t) = \sqrt{y^2(t) + z^2(t)} \quad (4.19)$$
$$= \sqrt{2 \sum_K \left\{ \left[R^2(t - kT_s) + I^2(t - kT_s) \right] + \left[R^2(t - T_s/2) + I^2(t - T_s/2 - kT_s) \right] \right\}}$$
$$= \sqrt{\frac{1}{4} \sum_K \left[v^2(t - kT_s) + v^2(t - T_s/2 - kT_s) \right]}$$

where $v(t)$ is the envelope of the filtered signal and $v^2(t) = R^2(t) + I^2(t)$.

The envelope signal $v(t - kT_s)$ generally looks as shown in Fig. 4.9.a. So for QPSK, the envelope has zero amplitudes when both data channels change transitions simultaneously. The overall envelope fluctuations of QPSK can change from maximum to zero.

For OKQPSK, because of the time delay between $v(t - T_s/2 - kT_s)$ and $v(t - kT_s)$, there are no zero crossings and the overall envelope fluctuations are smaller than QPSK as shown in Fig. 4.9.b.

If the amplitude distortion (AM/AM) and the phase distortion (AM/PM) functions are assumed to be $g(.)$ and $f(.)$, respectively, then the signal at the output of the TWTA is:

$$e_o(t) = g(A(t)) \cos(2\pi f_c t + \tan^{-1} y/z + f(A(t))) \qquad (4.20)$$

Large amplitude variations will hence induce more signal distortions due to the nonlinearity effect of the TWTA. Depending on the $g(.)$ and $f(.)$ functions, the spectrum spreading effect can be computed using the methods described in [Robinson et al, 4.10][Palmer et al, 4.13].

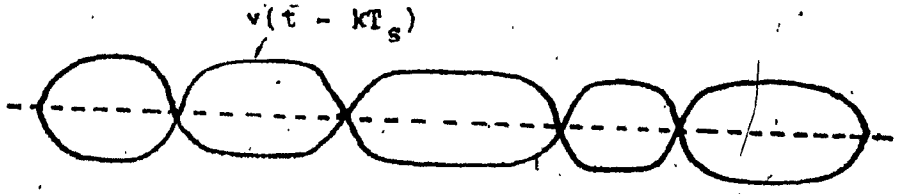

a. QPSK

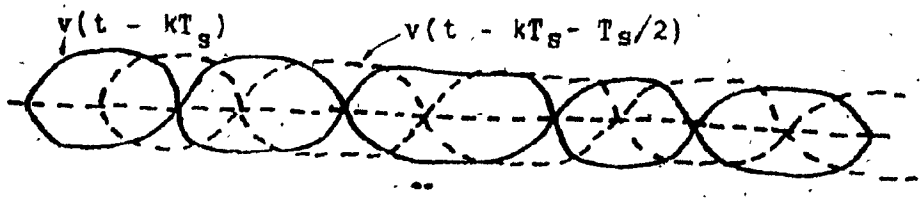

b. OKQPSK

Fig. 4.9 Overall Envelope Fluctuations of QPSK and OKQPSK Signals

4.4 Envelope Fluctuations of Filtered QPSK, OKQPSK and MSK Signals at the Sampling Instants

It was shown in the previous section that by delaying one channel data by a bit interval in respect to the other channel data, OKQPSK and MSK have much smaller overall envelope fluctuations than those of QPSK. They therefore suffer less spectrum spreading than QPSK when passing through a nonlinear power amplifier. The subject of spectrum spreading will be covered in section 4.5.

On the other hand, in a bandlimited satellite channel, the OKQPSK (and MSK) signal will be shown to have larger envelope fluctuation at the sampling instants than those of QPSK. As these three modulation schemes belong to four phase modulation, a multiply by four method is frequently employed for carrier recovery [Feher, 4.4]. The larger amplitude fluctuations of OKQPSK (and MSK) at the sampling instants imply much larger variations in the fourth powered signal for carrier recovery. If baseband impulses are assumed instead of the rectangular pulse, then the QPSK signal and its signal space diagram are as shown in Fig. 4.10.a, while the OKQPSK signal and its signal space diagram are shown in Fig. 4.10.b. Clearly, because of the offsetting in the two parallel data streams in OKQPSK, when the in-phase channel (I-channel) is sampled, there is no signal in the quadrature channel (Q-channel) and vice versa. In the case of QPSK, there are always signals at the sampling instants at both channels.

When both QPSK and OKQPSK are bandlimited, the impulses become shaped pulses as shown in Fig. 4. 11. b. For QPSK, the signal amplitudes at the sampling points do not change too much if no large intersymbol interference effect from the filter is assumed. For OKQPSK, the signal envelope at the sampling points is no longer only a function of the sampled channel. This is because sampling points in one channel are transition points in the other channel and vice versa. The signal states of OKQPSK(and MSK), as shown in Fig. 4. 11, lie on a line.

The signal states of QPSK on the other hand, as shown in Fig. 4. 11, are still located near the four points of Fig. 4. 9. a without too much variation.

To verify that this is indeed the case, computer simulation was used to plot the signal scatter diagrams at the sampling instants. The signal scatter diagrams of QPSK, OKQPSK and MSK, as shown in Fig. 4. 12, are obtained by sampling the received QPSK signal once per symbol and the received OKQPSK and MSK signal twice per symbol. These scatter diagrams agree with those described in Fig. 4. 11.

When fourth powered, the four signal states of QPSK will converge to one point as shown in Fig. 4. 13. This is because the received signal,

$$s(t) = \cos (2\pi f_c t + \theta) \qquad (4.21)$$

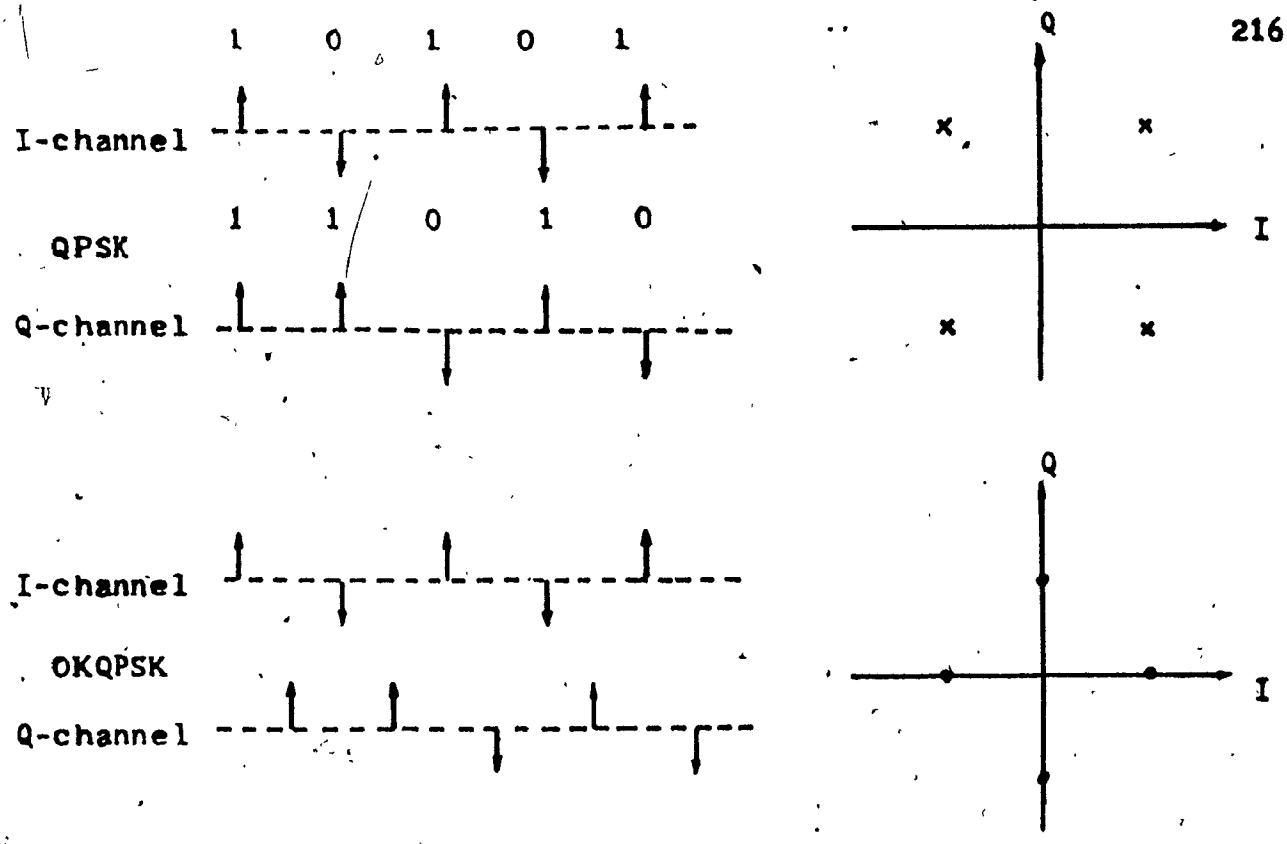

Fig. 4.10 Impulsed QPSK and OKQPSK Signals and Corresponding Signal Space Diagrams

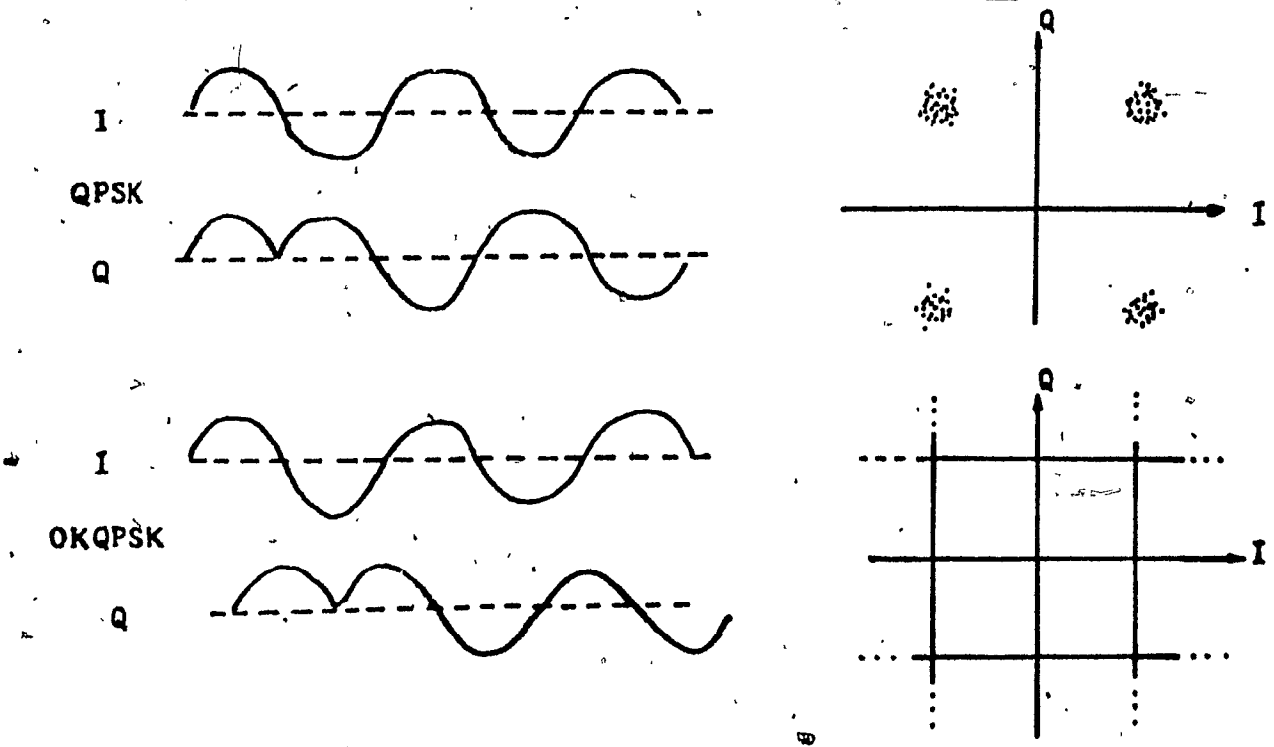

Fig. 4.11 Pulsed QPSK and OKQPSK Signals and Corresponding Scatter Diagrams

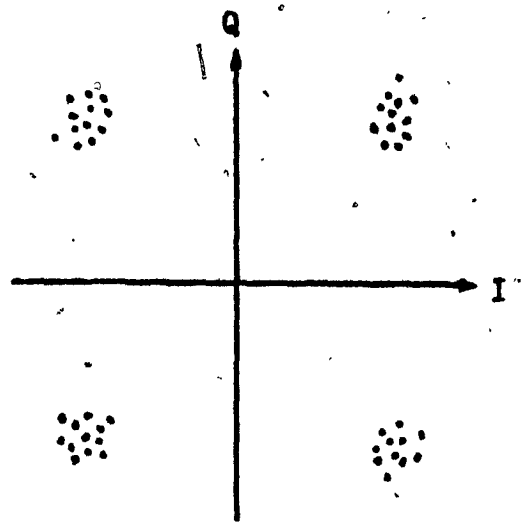

a. QPSK

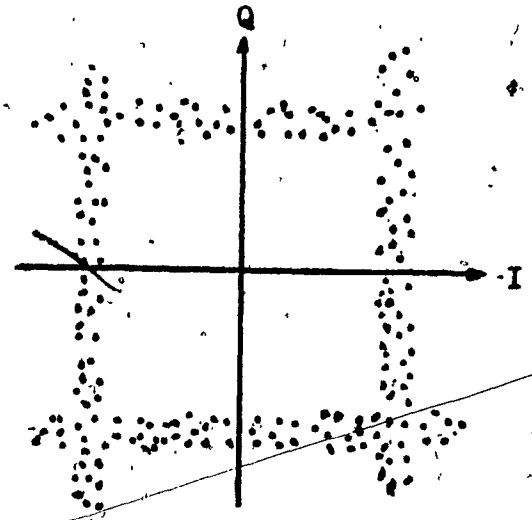

b. OKQPSK

Fig. 4.12 Computer-Simulated Signal Scatter Diagram of QPSK and OKQPSK at the Sampling Instants

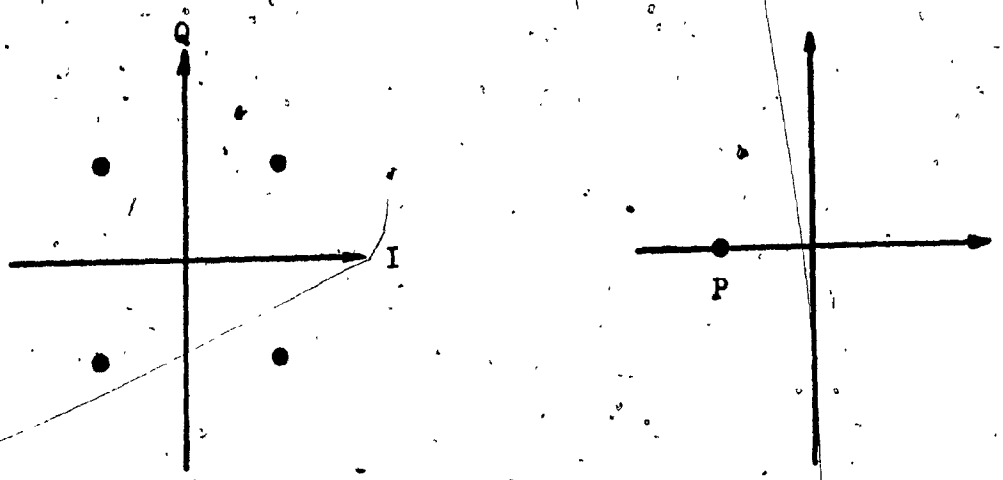

QPSK Signal Space Diagram Fourth-Powered Signal

Fig. 4.13 QPSK and Its Fourth-Powered Signal

with $\theta = \pm 45^{\circ}$, or $\pm 135^{\circ}$. When fourth powered, this signal becomes,

$$\cos (8\pi f_c t + 4\theta) \qquad (4.22)$$

and $4\theta = \pm 180^{\circ}$ or $\pm 540^{\circ}$, sq it converges to one point.

For OKQPSK, the signal states lie on a line (Fig. 4.12), and the fourth powered signal will then lie on the curve as shown in Fig. 4.14. In this figure, it is shown that the vertical line AB of the signal scatter diagram of the filtered OKQPSK (or MSK) signal, when fourth powered, will not only be a point (P in Fig. 4.14) at the four times carrier frequency, but also a continuous curve. The same curve is also obtained when the horizontal line CD is fourth powered. In other words, the fourth-powered signal of OKQPSK at the sampling instants lie on a curve as shown in Fig. 4.14. c.

To demonstrate that this is the case, Fig. 4.14. a is used as an example.

Line AB can be written in polar coordinates as:

$$\overline{AB} = \sqrt{a^2 + y^2} \, \angle \tan^{-1} \frac{y}{a} \qquad (4.23)$$

when fourth-powered, it becomes:

$$\overline{AB}^4 = (a^2 + y^2)^2 \, \angle 4 \tan^{-1} \frac{y}{a} \qquad (4.24)$$

For point 1 on line AB, it can be represented by a $\angle 0^{\circ}$ when fourth-powered, it becomes $a^4 \angle 0^{\circ}$ and is indicated as point Q_1 in Fig. 4.14. a.

For point 3 on line AB, the ordinate y is equal to a. It can be represented by $\sqrt{2}a \angle 45^{\circ}$. When fourth-powered, it becomes $2a^4 \angle 180^{\circ}$ as indicated by P in Fig. 4. 14. a. Any point along $\overline{AB}$ between point 1 and point 3 when fourth-powered, lies on the curve $\overset{\frown}{P Q_2 Q}$. In a similar way, any point along point 1 and point 3', when fourthed powered, lies on the curve $\overset{\frown}{P Q_2' Q_1}$. Point P is the degenerate point for points 3 and 3'.

Any point on AB beyond point 4 and point 4', when fourthed powered, can be shown to lie on curve $\overset{\frown}{Q_4 P Q_4'}$.

This fourth – powered signal can be computed using Eq. (4. 19). Due to the variational nature of this signal at the sampling instants, computer simulation was used. Shown in Fig. 4. 14. d, the shape of the computer simulated signal resembled that plotted in Fig. 4. 14. c, except that Fig. 4. 14. d shows also the distribution pattern of the variation of the fourth-powered signal. Fig. 4. 14. d was obtained by sampling the received signal at the receiver using the simulation programs described in Appendix C2.

If the shaped pulses are of the (sin x/x) shape, then theoretically this fourth powered signal in OKΩPSK can have infinite envelope fluctuations for one channel at the sampling instants of the other channel. This situation occurs when a data pattern like :

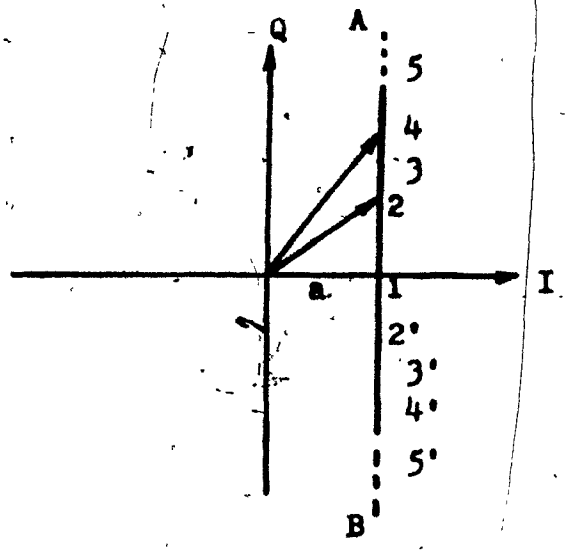

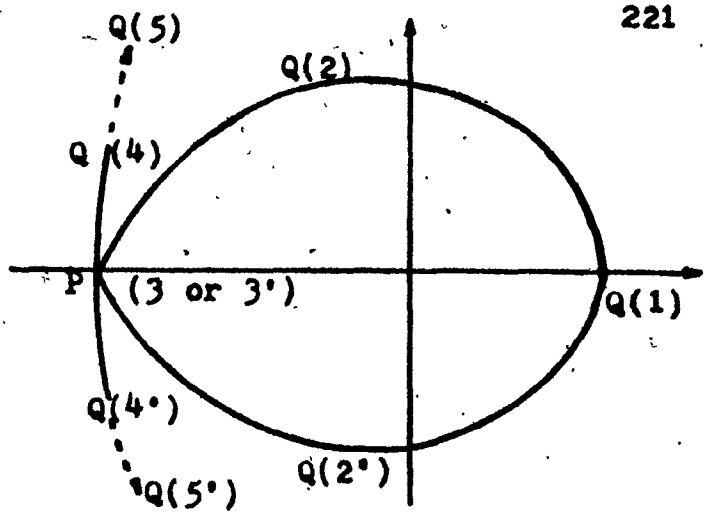

a. Line AB Fourth Powered

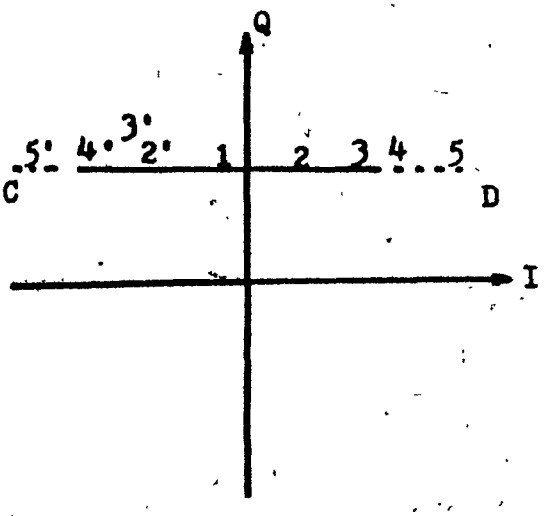

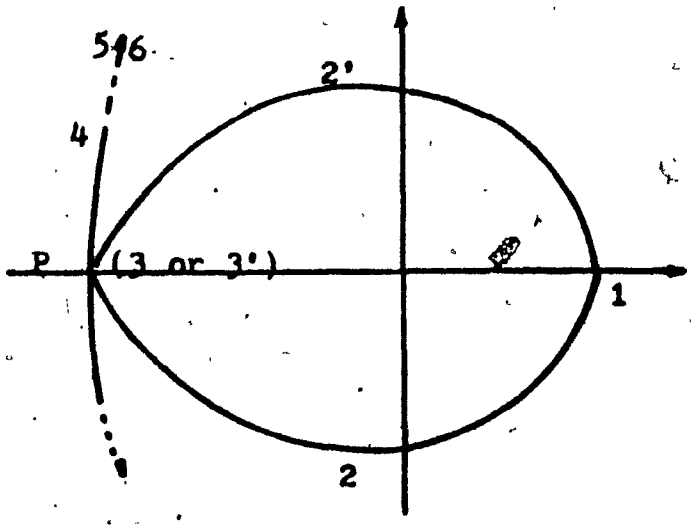

b. Line CD Fourth Powered

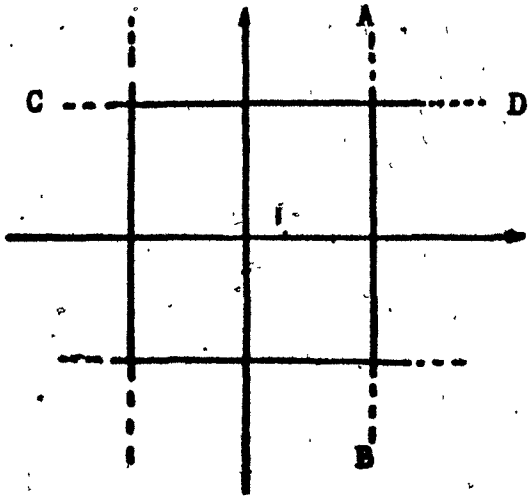

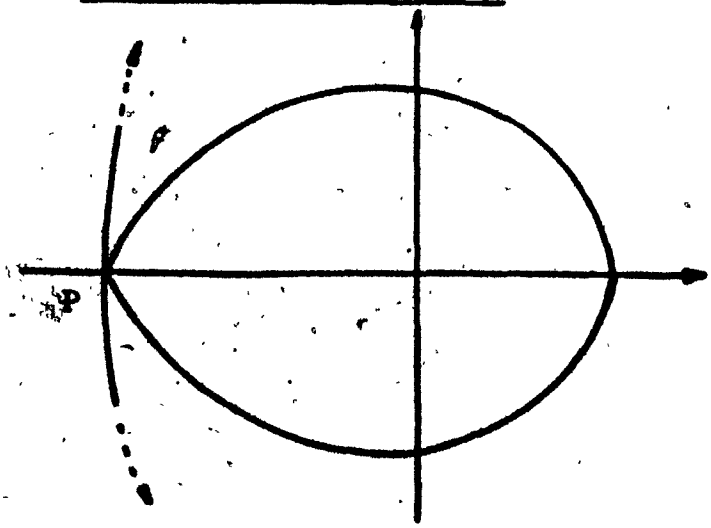

c. Fourth Powered Signal

Fig. 4.14 Fourth Powered OKQPSK

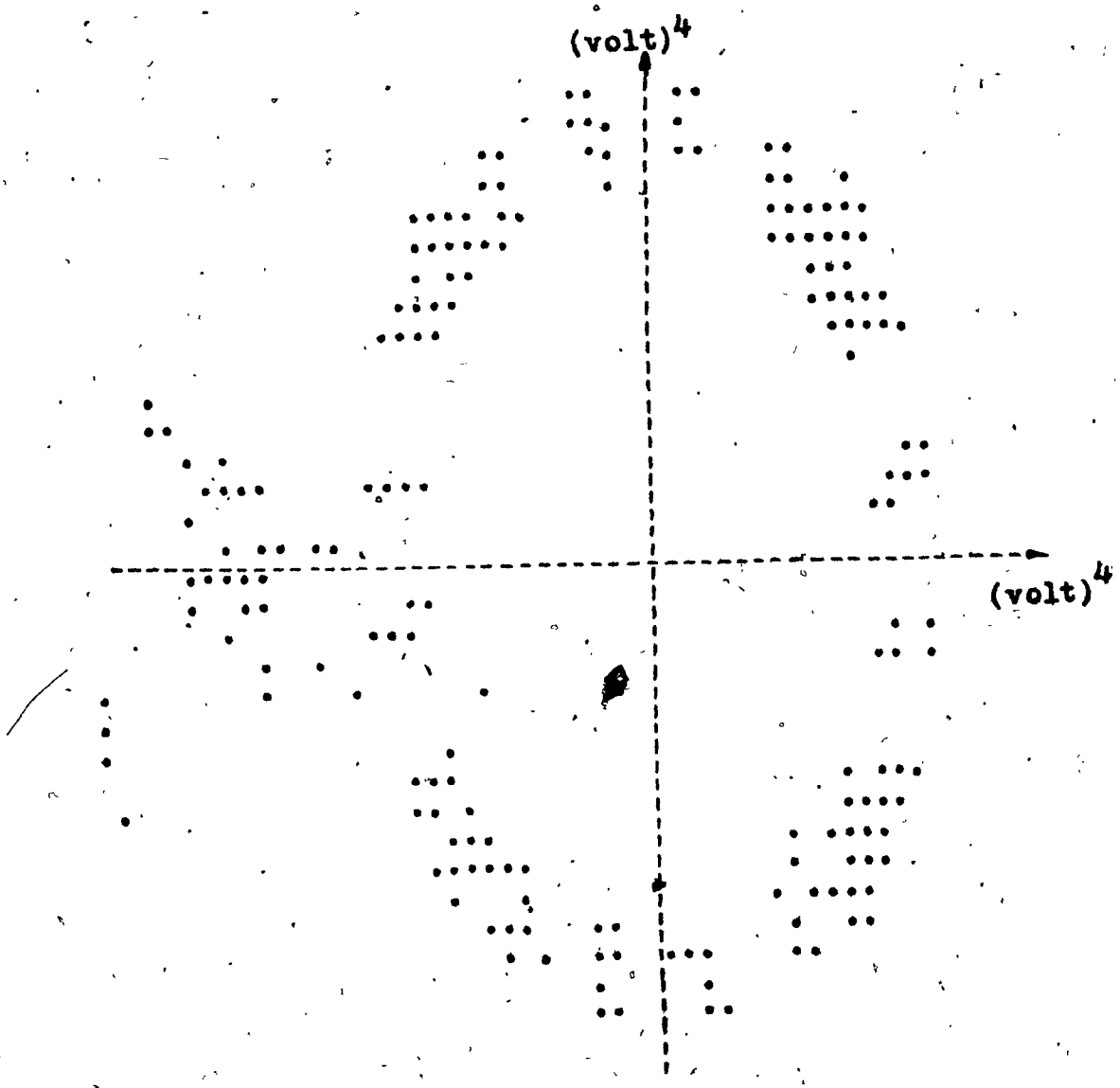

Fig. 4.14.d Fourth-Powered Signal of OKQPSK at the Sampling Instants

$$\ldots\ldots\ 0\,1\,0\,1\,0\,1\ \underbrace{1}_{\text{present bit}}\ 0\,1\,0\,1\,0\,1\,0\ \ldots\ldots\ldots \qquad (4.23)$$

n previous bits; present bit; n future bits

aries. For example, for n = 80, the eye pattern which is obtained using the analysis presented in Chapter 2 has only 17% eye width and the envelope fluctuations are very large (varying along lines AB or CD) for channel at the sampling instants of the other channel (Fig. 4. 15).

If n is assumed infinite, then this variation can become the infinite lines (the dotted portion) shown in Fig. 4. 14. When fourth powered, it can scatter to infinity as shown by the dotted line of Fig. 4. 14.d.

Hence, even in the absence of noise and intersymbol interference, the OKQPSK (or MSK) signal can have inherently very large amplitude fluctuations at the sampling instants. In Ref. [Murakami et al, 4. 2], the relative amount of phase jitter of the recovered carrier for these three types of signals was obtained using computer simulation. These results show that the phase jitter of the recovered carrier in QPSK is indeed much smaller than that of OKQPSK (and MSK) in a narrowband channel .

(Lines AB and CD as shown in Fig. 4.14.c)

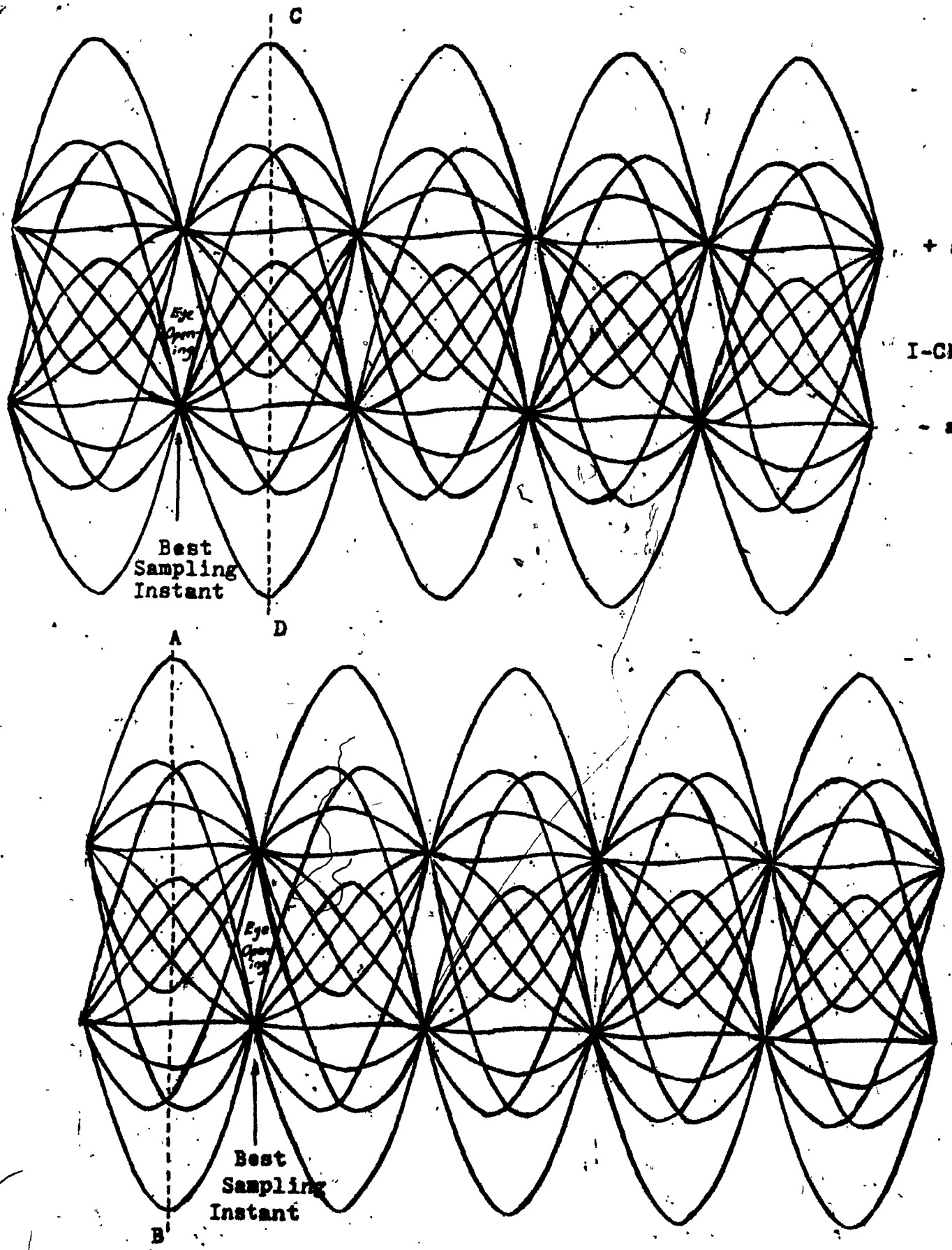

Fig. 4.15 I- and Q-Channel Eye Diagrams when (sin x/x) Pulses are Used as Signaling Elements in OKQPSK

4.5 Spectrum Spreading

In Chapter 2, two types of baseband signals were considered. The first one contains certain amount of data pattern jitter while the second one is jitter free. In this section, we will study spectrum spreading which occurs when these two types of signals are modulated separately by a carrier as in Binary PSK (BPSK) and then hardlimited. Although spectrum spreading is not the major concern in this thesis [El-Torky, 4.15], this section is included as a complete entity of our study on pulse shaping technique covered in Chapter 2.

Type 1: Spectrum Restoration

Fig. 4.16 shows a filtered random data being modulated by a carrier as in the Binary PSK. At the keying instants, phase transitions of 180° occur for both the unfiltered and filtered BPSK signal (Figs. 4.16.a and 4.16.b) [Andren, 4.16]. At these 180° phase transitions, the filtered BPSK signal has zero amplitude as the signal vector is shifted through the origin.

When the signal shown in Fig. 4.16.b is passed through an ideal limiter, the limited signal (Fig. 4.16.a) is exactly identical to that of the unfiltered signal. The filtered jitter free and limited signal therefore, has the same infinite bandwidth spectrum as that of the original

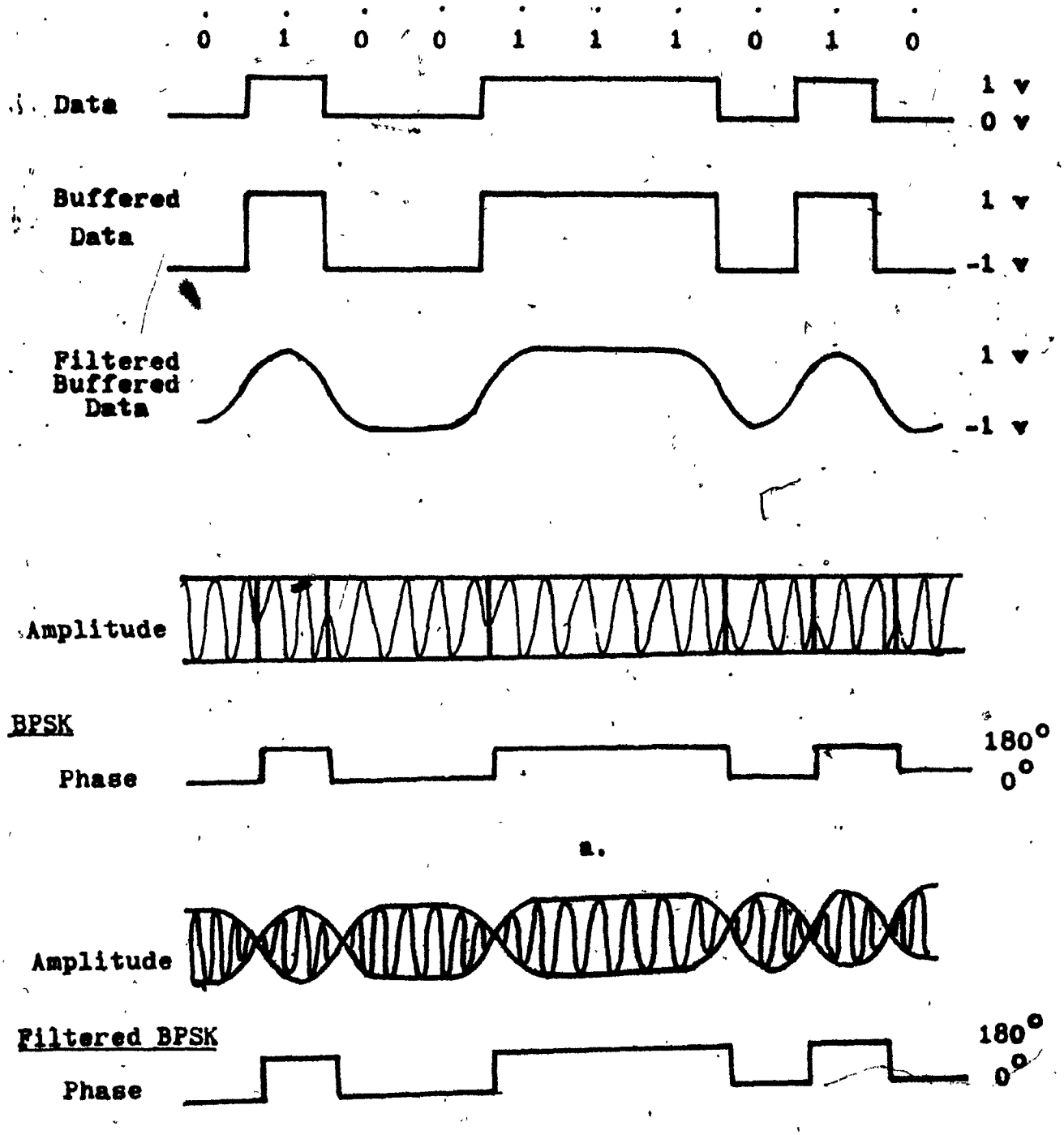

Fig. 4.16 Filtered and Limited Waveforms of BPSK

unfiltered signal. In other words, the spectrum is completely restored.

To demonstrate that this is indeed the case, the following experiment was carried out.

The random data stream, that was generated by the nonlinear switching method described in Chapter 2, was modulated by a carrier.

The IF eye diagram,as shown in the upper trace of Fig. 4. 17. a, has neither ISI nor jitter as in the baseband system. The lower trace in the same photo shows the limited signal after it passed through a hardlimiter. The limited signal appears to be identical to that illustrated in Fig. 4. 16. e.

Figs. 4. 17. b and 4. 17. c show the corresponding spectra of the jitter free IF signal and the limited signal. Complete spectrum restoration is evident from the (sin x/x) spectrum shown in Fig. 4. 17. c. Based on this, we conclude that complete spectrum restoration is caused by hardlimiting of the signal.

Type 2: Spectrum Regrowth and Modification

If a random data stream which has almost zero ISI but with a certain amount of jitter, such as shown in either Figs. 2. 5. a or 2. 5. b was also modulated by a carrier and then hardlimited, the spectrum of the limited signal in this case, shows that in addition to the restoration of sidelobes, the nulls disappear from the modified spread spectrum.

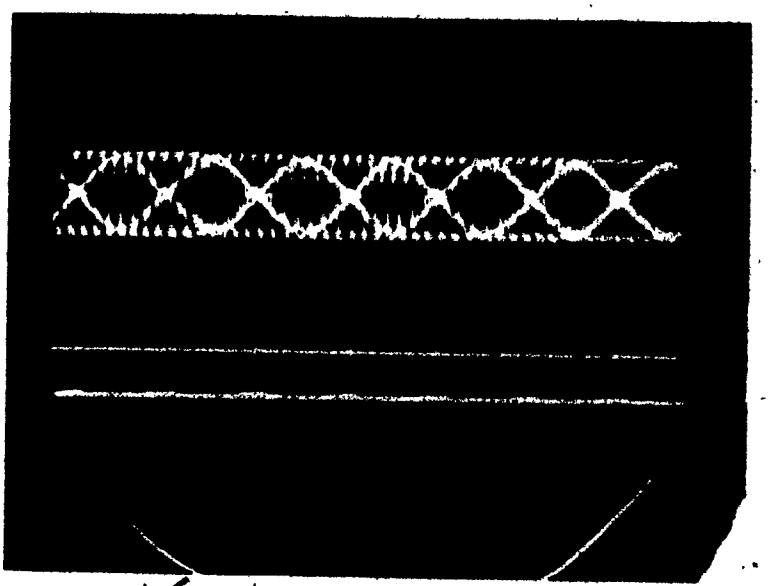

a.

Upper trace:

BPSK-modulated Signal of a jitt free data stream

Lower trace:

Above Signal Limited

bit rate: 32 kb/s

f_c : 500 kHz

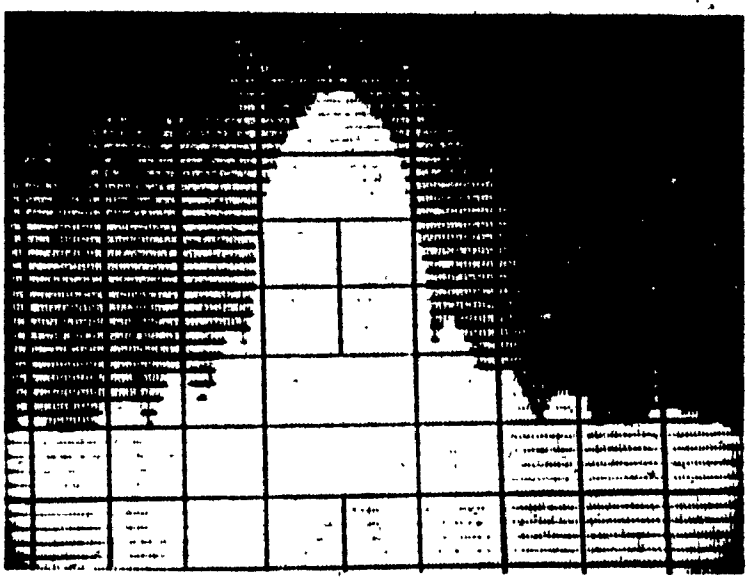

b.

Spectrum of the Signal Shown in the Upper Trace of Fig. 4.17.a

V. 10 dB/div.

H. 25 kHz/div.

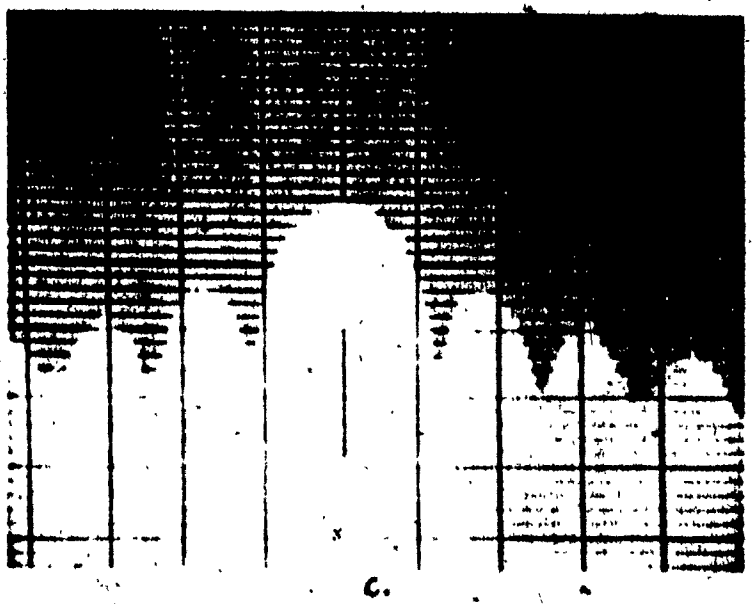

c.

Spectrum of the Signal Shown in the Lower Trace of Fig. 4.17.a

Fig. 4.17 BPSK Hard-Limiting and Spec-rum Spreading

Spectrum modification can thus be partly attributed to the timing jitter of the signal, although a large part of spectrum spreading is still caused by hardlimiting.

Since QPSK is a quadrature combination of two BPSK signals, the same reasoning also applies. This means that filtered QPSK signal, after passing through a nonlinear device, will also induce spectrum spreading. Spectrum spreading of filtered QPSK signal as well as that of filtered OKQPSK and MSK signals have been considered in great details in Ref. [Palmer et al, 4.13][Rhodes, 4.17] [Marsan et al, 4.18] [El-Torky et al, 4.19].

In the following, we will demonstrate experimentally spectrum spreading of QPSK and OKQPSK which occurs when they are hardlimited. Figs. 4.18.a and 4.18.b show the filtered QPSK and OKQPSK signals before and after hardlimiting. Amplitude fluctuations of zero crossings in the filtered QPSK signal can clearly be seen. The filtered OKQPSK signal shows more smooth amplitude variations.

The spectra of filtered QPSK and OKQPSK signal before hardlimiting, are identical as shown in Fig. 4.18.c. After hardlimiting, the spectrum of QPSK is almost completely restored while that of OKQPSK is only partially restored.

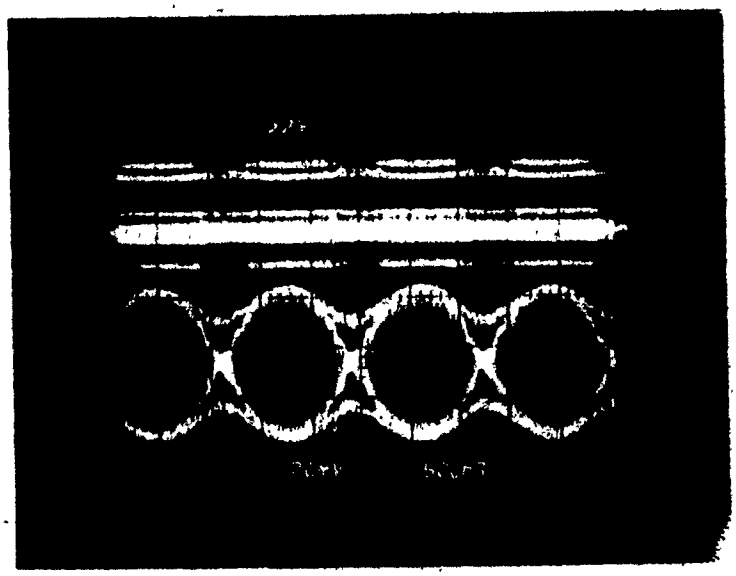

Fig. 4.18.a Filtered QPSK Signal Before and After Hardlimiting

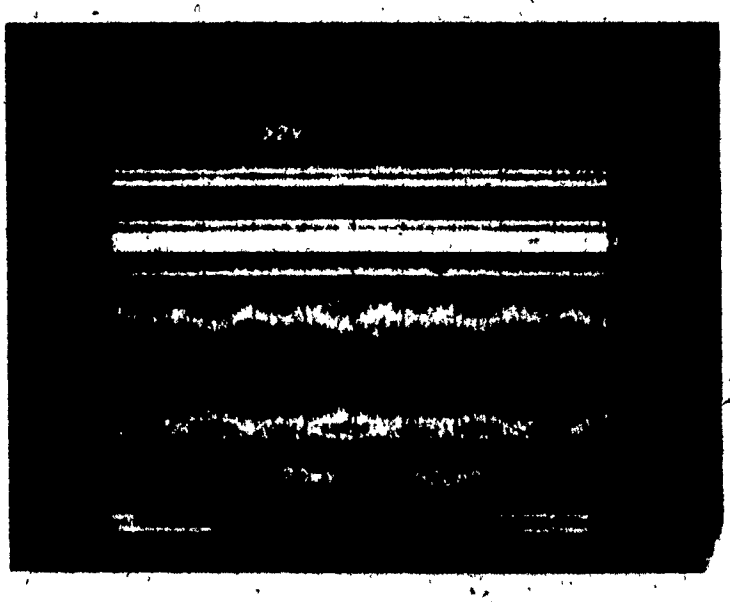

Fig. 4.18.b Filtered OKQPSK Signal Before and After Hardlimiting

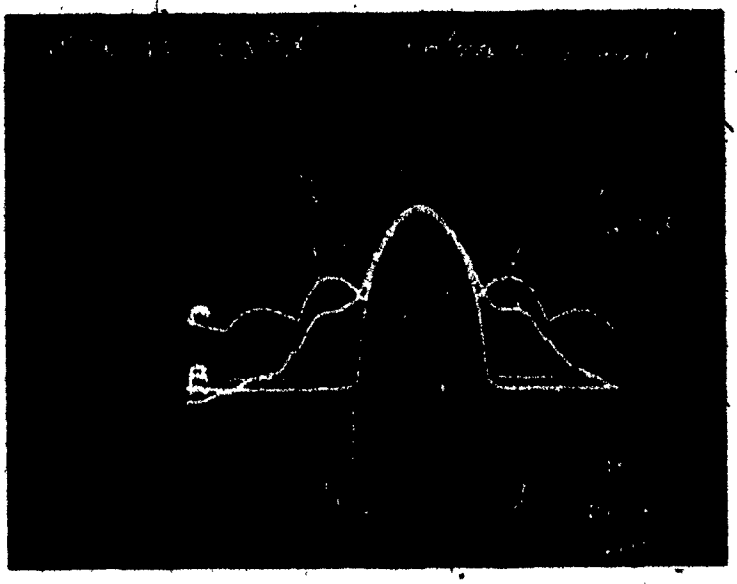

Fig. 4.18.c Spectra of Filtered and Limited QPSK, and OKQPSK Signals

4.6 Performance Study of Bandlimited QPSK, OKQPSK and MSK Signals Through Cascaded Nonlinearities

As discussed earlier, QPSK, OKQPSK and MSK are the three modulation schemes most frequently considered for a nonlinear satellite communication channel. The main advantages of using these three modulation techniques are that they are bandwidth efficient (theoretically, 2 b/s/Hz, practically about 1.8 b/s/Hz) and that they have low interchannel interference susceptibility [Feher, 4.4]. Also the hardware design of QPSK is relatively simple while that of OKQPSK and MSK, even though slightly more involved, is not very complex.

Since their inventions in the 1960's [Chang, 4.27] [Kwan, 4.28] [Doelz et al, 4.29], both OKQPSK and MSK have been proposed, as an alternative to QPSK, for use in bandlimited satellite channels. The main reason cited is that either OKQPSK or MSK, when bandlimited and then passed through a hardlimiter, has less spectrum regeneration than QPSK [Palmer et al, 4.13] [Moreno, 4.14] [Rhodes, 4.17] [Constellano, 4.20].

MSK, as illustrated earlier in section 4.2, can be considered one form of OKQPSK with half cosine pulse shaping. Due to its inherent wider main spectral lobe, it is generally agreed that in narrowband channel environment, the performance of MSK degrades more than that of OKQPSK. For example, in Ref. [4.3], Gronemeyer and Mcbride showed that for $BT < 1.1$, OKQPSK has an advantage over MSK while for $BT > 1.1$, the performance of MSK is superior to that of OKQPSK. (B is the noise bandwidth of the two cascaded filters used in their simulation). In Ref. [4.20], Constellano

concluded that the best way to utilize the spectral characteristics of MSK is to use wideband filters. A similar conclusion was also presented by [Murabami et al, 4.2] and [Lundquist, 4.21].

The comparative performance of QPSK and OKQPSK, on the other hand, has not yet reached a consensus. As mentioned earlier, it is generally agreed that a filtered OKQPSK signal induces less spectrum spreading than a filtered QPSK signal after each passing through a saturated nonlinear power amplifier. Yet, for overall system performance comparison, other factors, beside spectrum regeneration, must also be considered.

Constellano [4.20] in his simulation study showed that, based on the trade off between in-band degradation and adjacent channel interference, OKQPSK requires less transmitter power than QPSK for the satellite uplink subsystem. His study concluded that OKQPSK is more resistant to carrier phase offset and group delay distortions than QPSK, but less resistant to linear amplitude distortions. In Ref. [4.22], Gilton and Ho also demonstrated that OKQPSK has an improved phase jitter immunity than QPSK.

On the other hand, [Murakami et al, 4.2] showed that the error rate performance of QPSK is superior to OKQPSK. They also demonstrated that phase jitter of the recovered carrier in QPSK is smaller than that of OKQPSK. In the study of the European Communication Satellite (ECS) 120 Mb/s system, Harris [4.24] presented the rationale in choosing QPSK over OKQPSK. In the narrowband channel environment of ECS, OKQPSK appears to degrade more from nonlinear distortion than QPSK. Lundquist

[4.21], in his study for the Intelsat V's 60 Mb/s satellite system through a 36 MHz bandwidth channel, also concluded that QPSK outperforms OKQPSK in a nonlinear channel. A similar conclusion was also reached by Chakraborty et al [4.25].

The reason that OKQPSK suffers more phase jitter in the recovered carrier is its large amplitude fluctuations at the sampling instants. This was explained earlier in section 4.4.

QPSK, on the other hand, has less phase jitter in its recovered carrier. Even though QPSK induces more spectrum spreading than OKQPSK when passing through a saturated nonlinear power amplifier, its overall performance is still better than that of OKQPSK. By properly designing the QPSK modem in the linear mode and by operating the HPA and TWT input power a few dB below saturation, a compromising performance for QPSK can be achieved. In Ref. [Chakraborty et al, 4.25], it was concluded that the optimum HPA and TWT operating points for QPSK are at about 6 and 4 dB input backoff, respectively.

4.6.1 Computer Simulation Model

In the following, the computer simulation used in our study will be described. Afterwards, results obtained from this simulation study will be presented. As few details were discussed in the available literature, comments and comparison with other computer simulation methods are somewhat difficult. The conflicting results obtained by Constellano [4.20], versus those given by Harris [4.24] and Lundquist [4.21], all sponsored

by the European Space Agency, typify the complexity involved in the simulation study of a nonlinear satellite channel. Nevertheless, an attempt will be made to clarify the method used in our study.

In the linear channel, it is easier to study the system performance by using a computer analysis program, in which the system is excited by applying a single pulse of duration T in the in-phase baseband channel. As the data stream in the quadrature channel is statistically independent of that in the in-phase channel, there is no need to use both quadrature channels in this method.

By the use of the Fast Fourier Transform (FFT), the single-pulsed signal is modified by the frequency responses of the various filters in the systems. Since the system components are all linear, superposition may be used to compute the peak and rms eye closure for a random data sequence. This is because the power spectrum of the single isolated pulse has the same shape as that of a random data stream.

However, this computer analysis program cannot be adopted in a nonlinear satellite channel since the principle of superposition is no longer valid. Hence, a simulation program in which a pseudo-random data sequence is generated must be used. In a similar way, this random data sequence, by means of the FFT algorithm, is alternated between its time-domain and frequency-domain representation. In the frequency domain, it is modified by the complex transfer function of the simulating filters. In the time-domain, it is modified by the nonlinearities of the two cascaded power amplifiers.

Based on the simulation model of Fig. 4. 1, Fig. 4. 19 shows the flow chart of the signal processing in our simulation study. The signaling format for QPSK, OKQPSK and MSK was obtained in the equivalent complex baseband form (Fig. 4. 2) from a pseudo-random data source. After Fourier transformation, it was modified by the frequency response of filter F_1. It was then inverse transformed back in the time domain and modified by the polynomial coefficients of the quadrature model of the HPA [Eric, 4. 26]. Description of the quadrature model for a nonlinear power amplifier such as HPA and TWT are given in Appendix C2.

The distorted signal after the HPA was again Fourier transformed and modified by the frequency response of filter F_2. Inverse Fourier transformed back into the time domain, this signal was again modified by the polynomial coefficients of the quadrature model of the TWT. The signal, after modification by the frequency responses of filters F_3 and F_4, was then decoded at the receiver and compared with the original transmitted data sequence.

White Gaussian noise was added to the signal at the receive filter input (F_4 in Fig. 4. 19). The total noise power at the output of F_4 was then computed. The up-link noise was not included in our simulation as it was quite involved if noise was to be simulated [Chan et al, 4. 11].

Different filtering strategy has been used in the various simulation studies quoted earlier. In the linear channel, the overall system response is usually assumed to be raise cosine. Optimum performance is attained when the raise cosine filtering is partitioned equally between the transmitter

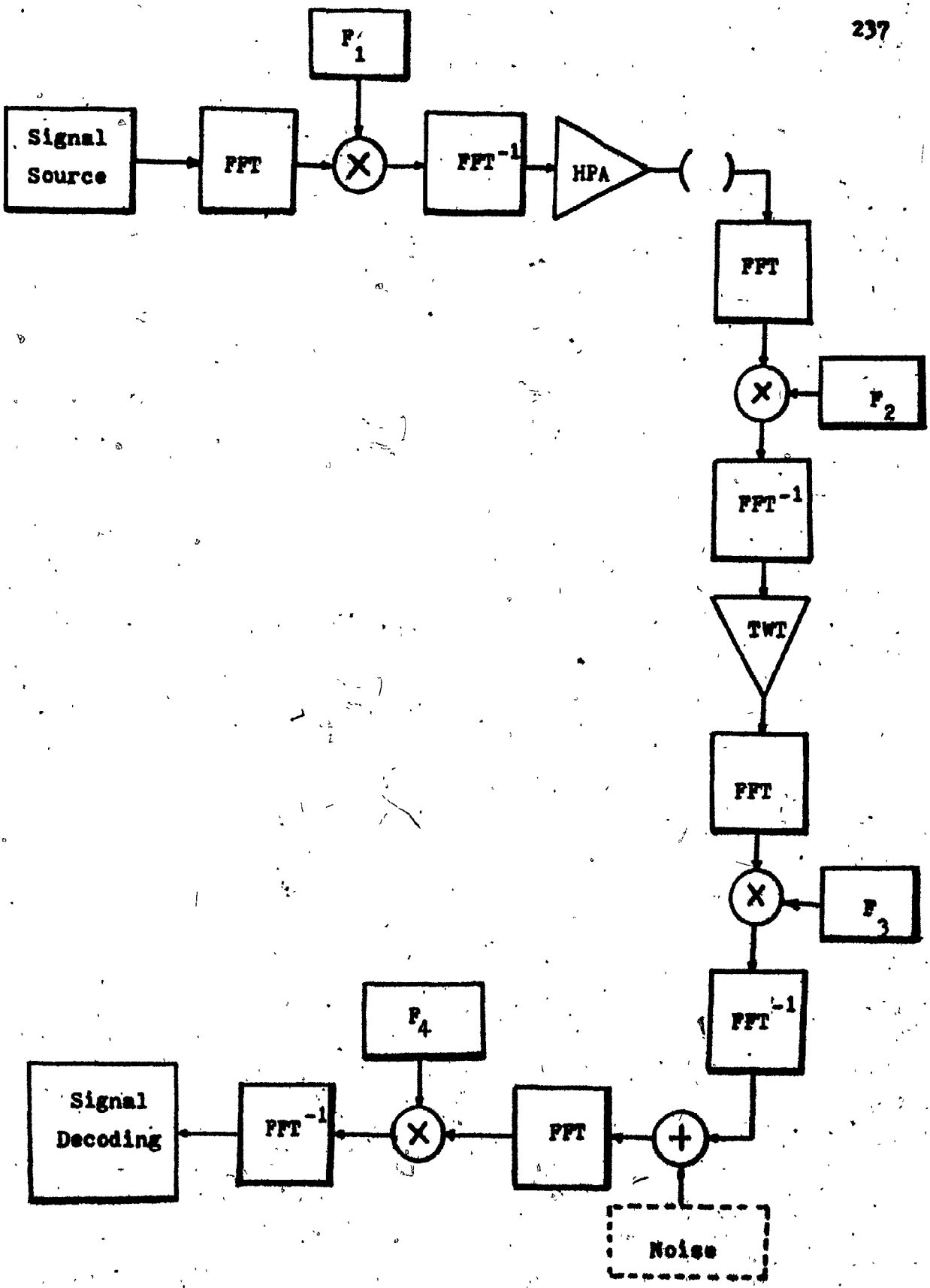

Fig. 4.19 Signal Processin of Computer Simulation

and the receiver. The situation became more complicated in a nonlinear channel. This is because in the actual satellite communication systems, the earth transmitting station and receiving station sometimes might belong to two different countries, with equipment supplied by different manufacturers. In Ref. [Murakami et al, 4.2], the specifications for the transmit and receive filter are simply divided with a sharp cut-off filter at the transmitter and a Nyquist shaping filter with an operature equalizer at the receive side. In Ref. [Lundquist, 4.21], a rolloff factor between 40% and 50% with close to half of Nyquist shaping at the transmitter was employed, while in Ref. [Chakraborty et al, 4.25], a Nyquist shaping filter at the transmitter and an elliptic filter at the receiver were assumed.

The computer programs developed in this study, in their present format, only have the capability to evaluate the single-channel performance of QPSK, OKQPSK and MSK signals through a nonlinear satellite channel. A simulation program capable of evaluating performance of these three signals in a multi-channel environment may become quite involved. Not only the carrier information for the multi-channel information must be included in the simulation, but also an optimization routine having iterative capability must be used to find the optimum filtering parameters.

In our study, a simple approach using a typical filter, namely a 4 pole Chebychev with 0.5 dB passband ripple, was adopted. This filter with different 3 dB bandwidth was assumed for F_1, F_2, F_3 and F_4 in our simulation model shown in Fig. 4.1. In Ref. [4.11], Chan et al also adopted this simplified filtering approach by assuming the transmit and receive

filters to be of Chebychev type. Similarly in Ref. [4.23], Devieux in his QPSK satellite link simulation assumed all the four filters to be of the Butterworth type.

4.6.2 Computer Simulation Results

To check the accuracy of the simulation programs, the wideband performance of these three modulation schemes was obtained and compared as shown in Fig. 4.20. In this wideband model, the BT product of F_1 and F_4 (where B is the double sided 3 dB bandwidth of the Chebchev filters and T is the symbol interval) is equal to 2, while the BT product of F_2 and F_3 is about 2.5. In this case, the OKQPSK performs slightly better than the QPSK and MSK signal. By further increasing the BT product of each of these four filters, all these three types of signals require a SNR of approximately 8.8 dB for a BER of 10^{-4}. In comparison, the theoretical SNR requirement with the noise in the bit rate bandwidth for 10^{-4} is 8.4 dB for these three types of signals.

The narrowband performance of these three signals was then evaluated by reducing the BT product of F_1 and F_4 first to 1.3, and then to 1, while the BT product of F_2 and F_3 was kept about 2.5. This corresponds to the narrowband model used by Devieux [4.23] in his study for the performance of QPSK through two cascaded nonlinearities. In our simulation study, QPSK performs approximately the same as in Devieux's work. Results in Fig. 4.20 also show that the performance of OKQPSK becomes worse than that of QPSK when the BT product of F_1 and F_4 was reduced from 1.3

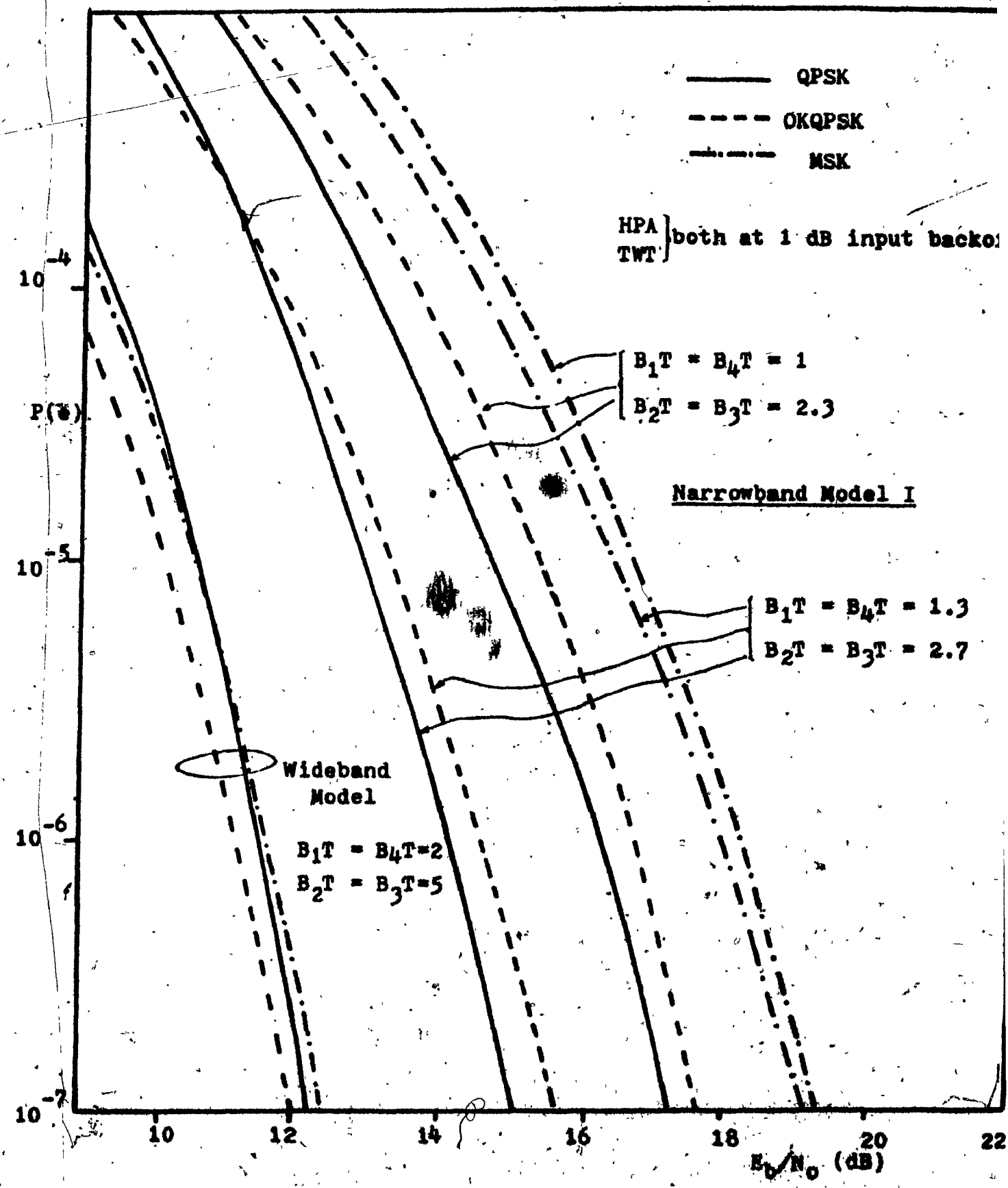

Fig. 4.20 Performance of QPSK, OKQPSK and MSK Signals in the Wideband and Narrowband Model I

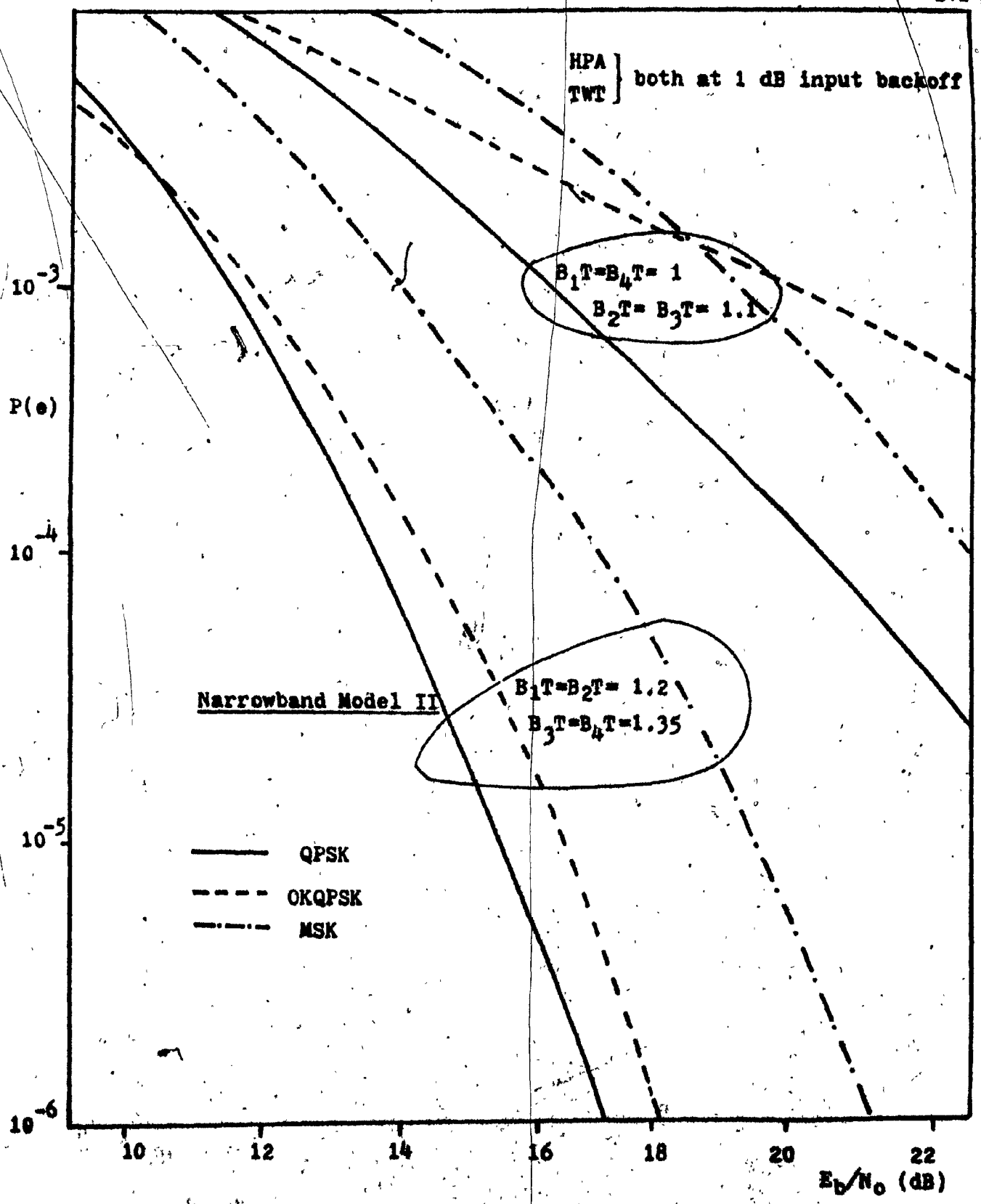

Fig. 4.21 Performance of QPSK, OKQPSK and MSK Signals in Narrowband Model II

to 1. In either situation, the performance of MSK is worse than that of either OKQPSK or QPSK.

In the above model, the bandwidths F_2 and F_3 were made sufficiently wide so that the cascaded nonlinear characteristics of HPA and TWT can be considered as one single nonlinearity. In some satellite channels, the bandwidths of these two filters are also narrowband so as to bandlimit the up-link thermal noise and to reduce the adjacent channel interference.

For this second narrowband model, the BT products of F_1 and F_4 was again kept at either 1.3 or 1, while the BT products of F_2 and F_3 was reduced from 2.5 to 1.1. Results in Fig. 4.2 again show that QPSK performs better than either OKQPSK or MSK in this narrowband model.

Results shown in Fig. 4.20 and Fig. 4.21 are for the HPA and TWTA both operating at 1 dB input backoff. When they both were operated at 12dB input backoff, results in Fig. 4.22 again show that QPSK outperforms OKQPSK in the narrowband model 11. In the narrowband model 1, results plotted in Fig. 4.22 show that in one situation ($B_1T = B_4T = 1.3$, where B_1 and B_4 denote the f_{3dB} bandwidth of filters F_1 and F_4), OKQPSK performs slightly better than QPSK. In the second situation, ($B_1T = B_4T = 1$), QPSK performs better than OKQPSK. In the wideband model, OKQPSK performs slightly better than QPSK.

In our earlier study, it was shown that OKQPSK and MSK have much larger amplitude variations at the sampling instants than QPSK. After passing through the nonlinear amplifiers, in QPSK, the sampled signal amplitude is still concentrated about a fixed point. This results in a smaller

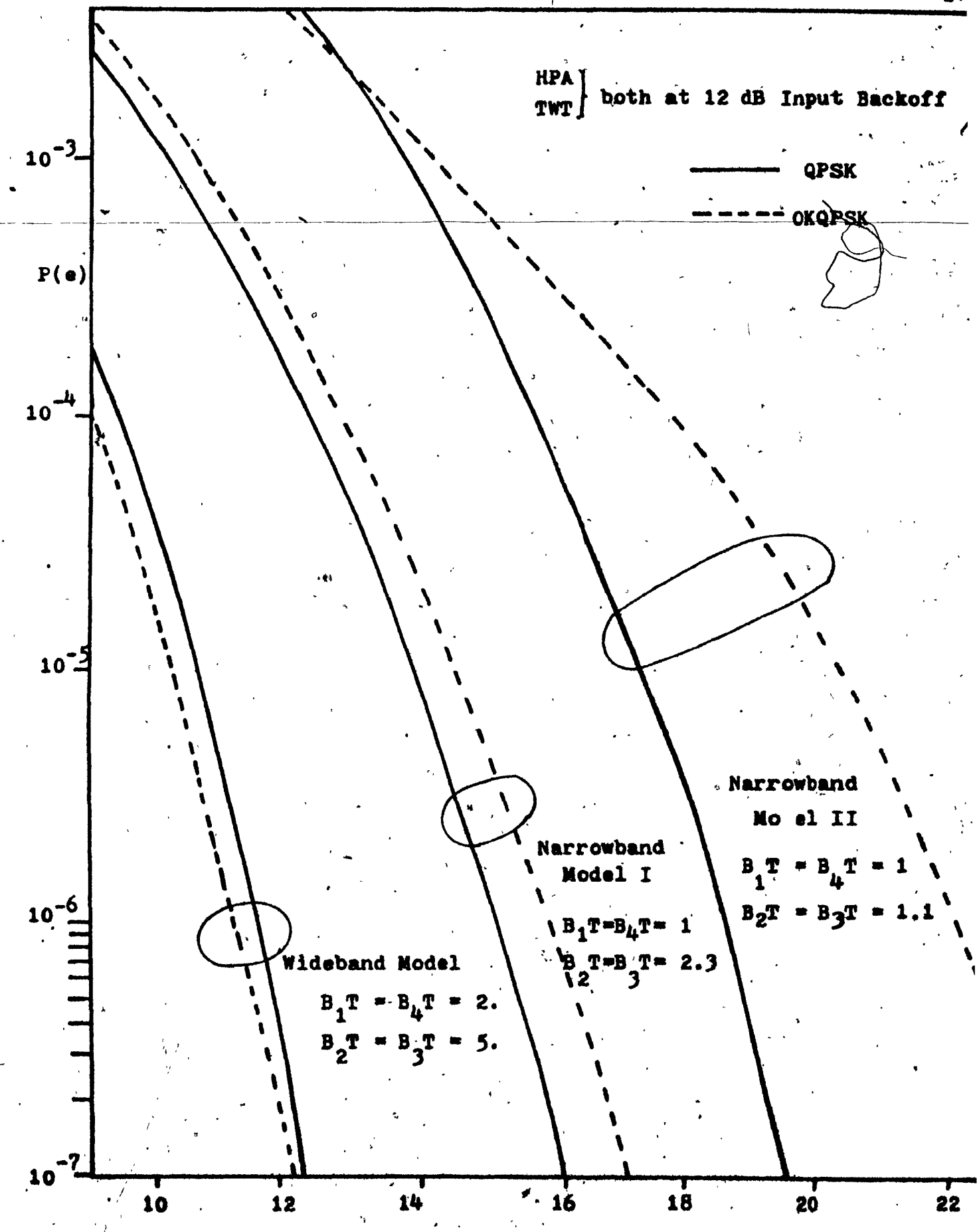

Fig. 4.22 Performance of QPSK, OKQPSK and MSK in Three Models

degree of phase jitter. The coincidence of the sampling points between the in-phase and quadrature channels also induce less cross-modulation interference. On the other hand, the much larger amplitude variation of these two signals at the sampling instants and the misalignment of the sampling instants between the two quadrature channels cause larger degree of signal scattering at the sampling instants. Thus, in a severely band-limited channel, OKQPSK or MSK has a much larger phase jitter than QPSK, resulting in larger overall system performance degradation.

As there are many constraints and parameters involved in the simulation model of a nonlinear satellite channel, the argument in favor of or against the use of OKQPSK versus QPSK still needs further study. Only through practical field testing and measurement, can this problem be solved. Nevertheless, the simulation method and results obtained in this study, after further extension, will help lead to a more favorable answer in the near future.

4.7 Summary of Chapter 4

An analysis to study the amplitude fluctuations, both the overall average and at the sampling instants, of bandlimited QPSK, OKQPSK and MSK signals, was undertaken. Although a filtered OKQPSK (or MSK) signal has less overall amplitude fluctuations than QPSK, it has much larger amplitude fluctuations at the sampling instants. Thus the overall performance of a filtered OKQPSK signal degrades more from nonlinearities than that of QPSK. Both the signal space and scatter diagrams of QPSK, OKQPSK and MSK were verified by computer simulation.

Two types of spectrum spreading that occur when a filtered PSK signal with or without jitter passes through a hardlimited were experimentally demonstrated. The first type of spectrum restoration occurred when a jitter free signal was hardlimited. As there is no timing jitter in the PSK signal, complete spectrum restoration can thus be reasoned as caused entirely by hardlimiting alone. The second type of spectrum restoration and modification arose when a jittery signal was hardlimited. Spectrum modification can thus be partly attributed to the timing jitter that exists in the filtered signal.

By the use of computer simulation, the performance of QPSK, OKQPSK and MSK through cascaded nonlinearities and bandlimiting elements as in a typical satellite channel in a wide-band model and two narrowband models was evaluated. Results from the wide-band model show that OKQPSK performs slightly better than conventional QPSK and MSK. On the contrary, results from the two narrowband models show that conventional QPSK outperforms OKQPSK and MSK.

CHAPTER 5

Chapter 5

Conclusion and Suggested Research Topics

5.1 Conclusion

In this thesis, original research on baseband pulse shaping and partial response spectral shaping techniques as well as investigation of the performance of various modulation methods both in linear and non-linear channels for line-of-sight microwave and satellite communication systems is described. The study leads to a number of important conclusions which are summarized below:

The analytical method presented in Chapter 2 enables the calculation of the peak-to-peak jitter of a raised cosine filter. Such calculated results were shown to be in excellent agreement with those obtained by laboratory measurements and computer simulations. This method can thus be used as a tool for a system engineer to evaluate the design tolerance due to the amplitude and phase distortions of filters.

Time-limited pulses with different shapes and their spectral characteristics were studied for the generation of an ISI and jitter free band-limited Nyquist signal. The criteria obtained by this study are used as a guideline in the search for double-intervaled pulses having low spectral sidelobes but with a main spectral lobe width confined with that of the single-intervaled rectangular pulse. It was noted that the $k=0.8$ modified raised pulse has faster spectral rolloff than that of the raised-cosine

pulse. This pulse might find applications in bandwidth-restricted channels where only a moderate signal to noise ratio (SNR) is available. The time-domain and frequency domain characteristics of the well-known raised cosine pulses were further analyzed for system applications.

Two methods for the generation of a bandwidth efficient Nyquist signal without ISI and jitter by the use of the raised cosine pulses as signaling elements were then presented. The first method used the concept of pulse overlapping while the second utilized Feher's concept of nonlinear switching. These two methods were shown to be equivalent as they both produced the same signals at their outputs. The results obtained from a practical filter designed with this nonlinear switching concept showed an excellent agreement with theoretical predictions. Its simple design and low production cost will promote its application in near future low bit rate satellite communication systems.

The concept of pulse overlapping was further applied to the generation of multi-level-partial response (PR) signals. Pulse overlapping was shown to be equivalent to introducing correlation between the neighboring bits of a random data stream. The transfer function of a PR filter was thus obtained from the Fourier transform of the overlapping pulse in cascade with that of a brick-wall Nyquist filter. The power spectra of different types of multi-level PR signals were also derived using this concept. This approach therefore provides more insight into the physical interpretation of the PR signaling technique.

The study and extension of Lender's PR system model confirmed the already known result that Qureshi's model has a higher SNR requirement than Kretzmer's model. Due to the unequal filtering between the transmitter and the receiver, Lender's model was also shown to have a higher SNR requirement than Kretzmer's model.

The results from the computer simulation of the performance of QPRS digital radio systems both in linear and nonlinear channels provide a number of design rules in system applications. It is recommended that for a system to have a performance degradation less than 2 dB from theory the filter passband ripples should be less than .01 dB and the phase of the filters equalized. In order to reduce the AM/PM conversion effect on the system performance, the power amplifiers used in QPRS radio systems should be placed before the [illegible] and equalizers for group-delay [illegible].

The amplitude fluctuations of filtered QPSK, OKQPSK and MSK signals were studied. Although QPSK has larger overall amplitude fluctuations, its amplitude fluctuations at the sampling instants were shown to be much smaller than those of OKQPSK and MSK. The phase jitter in its recovered carrier is thus smaller than that of OKQPSK and MSK. Computer simulated signal space diagrams and fourth powered signal diagrams were shown to agree with this theoretical analysis.

Two types of spectrum spreadings were experimentally shown to occur when a filtered PSK signal, with or without jitter, passes through a hardlimiter. The first type of spectrum restoration occurred when a jitter free signal was hardlimited. As there is no jitter in the PSK signal, complete spectrum restoration is thus entirely caused by hardlimiting. The second type of spectrum restoration and modification arose when a jitter signal was hardlimited. Spectrum modification can thus be partly attributed to the data transition jitter that exists in the filtered signal.

Computer simulation programs were developed to study the performance of bandlimited QPSK, OKQPSK and MSK signals through cascaded nonlinearities. Results obtained for these three types of signals showed that in the wideband model, OKQPSK performs slightly better than QPSK or MSK. These results agree to the earlier theoretical analysis and computer simulation prediction on the signal amplitude fluctuations at the sampling instants. Similar results were also obtained by Ishizuki et al, Harris, Lundquist and Chakravarty et al. However, the explanation is in

disagreement with those obtained by Constellano who assumed only one nonlinearity in his simulation model.

5.2 Suggested Research Topics

Research work related to this thesis which can be extended using the methods or results presented in this study is briefly described in this final section.

In the analysis of data pattern dependent jitter described in Chapter 2, the phase of the filter was assumed to be linear and phase distortion was thus excluded. Results were also limited to peak-to-peak jitter. In practical applications, the effect of phase distortion cannot be ignored. A study could also be made to understand the dependence of probability density of the jitter on pattern variations.

The symbol timing clock jitter problem presents another related subject. In order to properly regenerate the transmitted data sequence from the received signal, precise clock timing information is required. Most of the literature that deals with clock jitter problems assumes that the incoming pulse train has no data pattern dependent jitter. Further research is recommended to study the effect of a jittery signal on the performance of symbol timing recovery circuitry used in synchronous systems.

In the computer simulation study on the performance of QPRS radio systems and QPSK, OKQPSK or MSK satellite systems, the effect of adjacent channel interference was not considered. The effect of digital radio systems

are operated in a multi-channel interference environment, extensions of the presented programs to include two neighboring adjacent channels would be of great interest.

In Section 2.5, we mentioned briefly that the error rate performance of a digital baseband transmission system in a coloured gaussian noise environment is identical to that in a white gaussian noise environment if the SNR at the regenerator input is the same. This result has also been verified to be valid in a microwave FM system. As the noise at the demodulator output in most of the modulation systems is frequently non-white, it will be of interest to check if this conclusion is also valid in different modulation systems.

APPENDIX

APPENDIX A

(1)

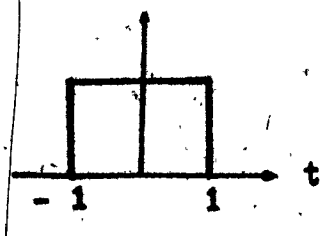

The Fourier transform of a rectangular pulse can be easily obtained and is given as follows:

$$S(f) = 2\,\frac{\text{Sin } 2\pi f}{2\pi f} \qquad (A1)$$

$$= 2\,A(f)$$

where $A(f) = \dfrac{\text{Sin } 2\pi f}{2\pi f}$

(2)

$$s(t) = \begin{cases} \text{Cos } (a\,t) & \text{for } |t| \leq 1 \\ 0 & \text{elsewhere} \end{cases}$$

The Fourier transform of a cosine pulse is given by:

$$S(f) = A\left(\frac{a}{2\pi} - f\right) + A\left(\frac{a}{2\pi} + f\right) \qquad (A3)$$

Using Eqs. (A1) and R(A2), we will derive the Fourier transforms of the Raisz Amoroso's and Kaiet's pulses.

(3).

$$s(t) = \begin{cases} \frac{1}{2}\left[1 + \cos\left(\pi t - U \sin 2\pi t\right)\right] & \text{for } |t| \le 1 \\ 0 & \text{elsewhere} \end{cases}$$

$$\cos(\pi t - U \sin 2\pi t)$$
$$= \cos\pi t \cos(U \sin 2\pi t) + \sin\pi t \sin(U \sin 2\pi t)$$

Using Bessel expansion:

$$\cos(U \sin 2\pi t) = J_0(U) + 2 \sum_n J_{2n}(U) \cos(4n\pi t)$$

$$\sin(U \sin 2\pi t) = 2 \sum_n J_{2n-1}(U) \sin(2n-1)\, 2\pi t$$

By means of Eqs.((A1) and (A3), we find

$$S(f) = A(f) + J_0(U)\, A_0(f)$$
$$+ \sum_n J_{2n}(U) \left[A(2n+\tfrac{1}{2}-f) + A(2n+\tfrac{1}{2}+f) + A(2n-\tfrac{1}{2}-f) + A(2n-\tfrac{1}{2}+f) \right]$$
$$+ \sum_n J_{2n-1}(U) \left[A(2n-\tfrac{3}{2}-f) + A(2n-\tfrac{3}{2}+f) + A(2n+\tfrac{3}{2}-f) + A(2n+\tfrac{3}{2}+f) \right]$$
$$= A(f) + J_0(U)\, A_0(f) + 2 \sum_n J_{2n}(U)\, B_{2n}(f) + 2 \sum_n J_{2n-1}(U)\, B_{2n-1}(f) \qquad (A4)$$

(4).

$$s(t) = \begin{cases} \frac{1}{2}\left[1 + \sin\left(\frac{\pi}{2}\cos \pi t\right)\right] & \text{for } |t| \leq 1 \\ 0 & \text{elsewhere} \end{cases}$$

Using Bessel expansion:

$$\sin\left(\frac{\pi}{2}\cos \pi t\right) = 2 \sum_{K} (-1)^{k-1} J_{2k-1}\left(\frac{\pi}{2}\right)\left[\cos (2k-1)\, t\right]$$

By meansns of (A1) and (A3), we have:

$$S(f) = A(f) + \sum_{K} (-1)^{k-1} J_{2k-1}\left(\frac{\pi}{2}\right) \cdot \left[A\left(\frac{(2k-1)}{2} - f\right) + A\left(\frac{(2k-1)}{2} + f\right)\right] \quad (A5)$$

where $= A(f) + 2 \sum_{K} (-1)^{k-1} J_{2k-1}\left(\frac{\pi}{2}\right) C_{2n}(f)$

(5).

$$s(t) = \begin{cases} \frac{1}{2}\left[1 + \sin\left[\cos\frac{\pi t}{T} - (1 - \frac{\pi}{2})\cos^3\frac{\pi t}{T}\right]\right] & \text{for } |t| \leq \\ 0 & \text{elsewhere} \end{cases}$$

The second on the right-handed side can be expanded as follows:

$$\sin\left[\cos\frac{\pi t}{T} - (1 - \frac{\pi}{2})\cos^3\frac{\pi t}{T}\right]$$

$$= \sin\left[\cos\frac{\pi t}{T} - \tfrac{1}{4}(1 - \frac{\pi}{2})\left(\cos\frac{3\pi t}{T} + 3\cos\frac{\pi t}{T}\right)\right]$$

$$= \sin\left[\tfrac{1}{4}(1 + \frac{3\pi}{2})\cos\frac{\pi t}{T} - \tfrac{1}{4}(1 - \frac{\pi}{2})\cos\frac{3\pi t}{T}\right]$$

$$= \sin\left[\tfrac{1}{4}(1 + \frac{3\pi}{2})\cos\frac{\pi t}{T}\right]\cos\left[\tfrac{1}{4}(1 - \frac{\pi}{2})\cos\frac{3\pi t}{T}\right]$$

$$- \left[\tfrac{1}{4}(1 + \frac{3\pi}{2})\cos\frac{\pi t}{T}\right]\left[\tfrac{1}{4}(1 - \frac{\pi}{2})\cos\frac{3\pi t}{T}\right]$$

Using the Bessel expansion and Eqs. (A1) and (A3), the Fourier transform S(f) can be obtained after lengthy manipulation.

(6).

$$s(t) = \begin{cases} 0.5 + 0.75 \cos \pi t - 0.25 \cos^3 \pi t & \text{for } |t| \leq 1 \\ 0 & \text{elsewhere} \end{cases}$$

$$\cos^3 \pi t = \tfrac{1}{4} (\cos 3\pi t + 3 \cos \pi t)$$

Hence, s(t) can be re-written as:

$$s(t) = \begin{cases} 0.5 + \frac{2.25}{4} \cos \pi t - \frac{0.25}{4} \cos 3\pi t & \text{for } |t| \leq 1 \\ 0 & \text{elsewhere} \end{cases}$$

By means of Eqs. (A1) and (A3),

$$S(f) = \frac{\sin 2\pi f}{2\pi f} + \frac{2.25 f \sin 2\pi f}{\pi(1-2f)(1+2f)} - \frac{0.25 f \sin (\frac{2\pi f}{3})}{\pi(3-2f)(3+2f)}$$

(7).

$$s(t) = \begin{cases} 0.5 + 0.9375 \cos \pi t - 0.625 \cos^3 \pi t + 0.1875 \cos^5 \pi t & \text{for } |t| \leq 1 \\ 0 & \text{elsewhere} \end{cases}$$

$$\cos^5 \pi t = \frac{1}{8} (5 \cos \pi t + \frac{5}{2} \cos 3\pi t + \tfrac{1}{8} \cos 5\pi t)$$

Hence, s(t) can be re-written as :

$$s(t) = \begin{cases} 0.5 + .5859375 \cos \pi t - .097656 \cos 3\pi t \\ \qquad + .01171875 \cos 5\pi t & \text{for } |t| \leq 1 \\ 0 & \text{elsewhere} \end{cases}$$

Using Eqs. (A1) and (A3), we have:

$$S(f) = \frac{\sin 2\pi f}{2\pi f} + \frac{2.34375\, f \sin 2\pi f}{\pi(1-2f)(1+2f)} - \frac{0.390624\, f \sin \frac{2\pi f}{3}}{\pi(3-2f)(3+2f)} + \frac{0.0468748\, f \sin \frac{2\pi f}{5}}{\pi(5-2f)(5+2f)}$$

(8).
$$s(t) = \begin{cases} 0.5 + 1.09375 \cos \pi t - 1.09375 \cos^3 \pi t \\ \qquad + 0.65625 \cos^5 \pi t - 0.15625 \cos^7 \pi t & \text{for } |t| \leq 1 \\ 0 & \text{elsewhere} \end{cases}$$

$$\cos^7 \pi t = \frac{35}{64} \cos \pi t + \frac{21}{64} \cos 3\pi t + \frac{7}{64} \cos 5\pi t + \frac{1}{64} \cos 7\pi t$$

Hence, s(t) can be re-written as:

$$s(t) = \begin{cases} 0.5 + 0.5981445 \cos \pi t - 0.1196288 \cos 3\pi t \\ \qquad + 0.023925 \cos 5\pi t - 0.0024414 \cos 7\pi t & \text{for } |t| \leq 1 \\ 0 & \text{elsewhere} \end{cases}$$

In a similar way, S(f) can be

(A)

APPENDIX B

```
      PROGRAM QPRS(INPUT,OUTPUT)
*********************************************************************
*
*     JOHN C. HUANG, AUGUST 1978, CONCORDIA UNIVERSITY
*
*     THIS SIMULATION PROGRAM STUDIES THE EFFECTS OF FILTERING AND
*          NONLINEARITY ON THE PERFORMANCE OF A QPRS SIGNAL
*
*     FOR INSTRUCTION ON HOW TO RUN THIS PROGRAM, READ THE MANUAL
*        ENTITLED-- PERFORMANCE OF QPSK, OKQPSK AND MSK SIGNALS
*        THROUGH CASCADED NONLINEARITIES AND BANDLIMITING--
*
*
*********************************************************************
      DIMENSION NX(11),NY(11),NRX(11),NRY(11),DATA(512),DATA1(512)
      DIMENSION TATA1(512)
      DIMENSION C(15)
      DIMENSION TF(512),TFTX(512),TFR(512),PE(25),PEI(25),SNRDB(25)
      LDIM=512
      NN=LDIM/2
      DATA NTOTAL,NERROR,LOOP,II,IK/0,0,0,0,0/
      DATA NY(1),NY(2),NY(3),NY(4),NY(5),NY(6),NY(7)/-1,-1,1,1,1,1,-1/
      DATA JLAST,JTAP,LLTNOM,FBANDW/7,1,50,85./
C
      PRINT 1
    1 FORMAT(1H1,29H SIMULATION OF COHERENT 4-PRS)
      PRINT 2
    2 FORMAT(49H REQUEST(BIRATE,AVAMP,TWTIN,TWTOUT,PSHIFT,LSAMPL)/,
     ,51H FORMAT(F6.2,1X,F9.6,1X,F6.3,1X,F6.3,1X,F8.6,1X,I2)/)
      READ *,BIRATE,TWTIN,TWTOUT,PSHIFT,LSAMPL
      READ *,FBW1,FBW2,KNK,KO
      READ *,(C(IK),IK=1,KO)
      DO 306 IK=1,KO
      PRINT 305,C(IK)
  305 FORMAT(5X,F10.4)
  306 CONTINUE
      AVAMP=SQRT(2.)
      FNORMI=TWTIN/AVAMP
      FNORMO=TWTOUT/AVAMP
C
      DFBW=5.
      DBRATE=10.
       II=0
       IK=0
      DO 107 KM=1,KNK
      PRINT 20,BIRATE,AVAMP,TWTIN,TWTOUT,PSHIFT,LSAMPL
   20 FORMAT(1X,F6.2,9X,F9.6,6X,F6.3,9X,F6.3,9X,F8.6,7X,I2,/)
C
      DO 4 I=1,JLAST
      NX(I)=-1
      NRY(I)=NY(I)
    4 NRX(I)=-1
C
C
      [illegible]
      [illegible]
```

```
      DO 5 I=1,NSNR
      PE(I)=0.
      PEI(I)=0.
      SNRDB(I)=4.+DSNRDB
      DSNRDB=DSNRDB+DSNR
    5 CONTINUE
C
      CALL CALCON(LSAMPL,LLTNOM,KKK,LLT,NSYMB,JLAST,LOOPM,LDIM,BIRATE,
     +SBANDW)
      CALL CF4P5(SBANDW,FBW1,TFTX,LDIM,K0,C)
      CALL CF4P5(SBANDW,FBW2,TFR,LDIM,K0,C)
      CALL HHGG(TFR,PNOISE,LSAMPL,LDIM)
      CALL BISINC(DATA,TFTX,TFR,LSAMPL,NSTART,LSTART,LDIM)
      CALL LOADPR(DATA,KKK,LSAMPL,NX,NY,II,JLAST,JTAP,LDIM)
      CALL PR(DATA,LDIM)
      CALL FILTER(DATA,TFTX,NN,LDIM)
      CALL LOADPR(DATA1,KKK,LSAMPL,NX,NY,II,JLAST,JTAP,LDIM)
      CALL PR(DATA1,LDIM)
      CALL FILTER(DATA1,TFTX,NN,LDIM)
      CALL ADTAIL(DATA,DATA1,LLT,LDIM)
      CALL TWT1(DATA,LSAMPL,NSTART,KKK,FNORMI,FNORMO,LDIM)
      CALL FILTER(DATA,TFR,NN,LDIM)
C
   50 CONTINUE
C
      DO 12 I=1,LDIM
      DATA1(I)=DATA(I)
   12 DATA(I)=DATA1(I)
C
      CALL LOADPR(DATA1,KKK,LSAMPL,NX,NY,II,JLAST,JTAP,LDIM)
      CALL PR(DATA1,LDIM)
      CALL FILTER(DATA1,TFTX,NN,LDIM)
      CALL ADTAIL(DATA,DATA1,LLT,LDIM)
      CALL TWT1(DATA,LSAMPL,NSTART,KKK,FNORMI,FNORMO,LDIM)
      CALL FILTER(DATA,TFR,NN,LDIM)
      CALL ADTAIL(DATA1,DATA,LLT,LDIM)
      CALL DECDPR(DATA1,NRX,NRY,PE,PEI,KKK,LSAMPL,LSTART,NSNR,NERROR,
     +SNRDB,IK,NTOTAL,PNOISE,LOOP,JLAST,JTAP,NSYMB,PSHIFT)
      IF (LOOP.GT.LOOPM) GO TO 100
      GO TO 50
  100 CONTINUE
      BIRATE=BIRATE+DBRATE
      NTOTAL=0
      NERROR=0
      LOOP=0
    1 II=0
      IK=0
  107 CONTINUE
      STOP
      END
```

```
      SUBROUTINE LOADPR(DATA,KKK,LSAMPL,NX,NY,I,JLAST,JTAP,LDIM)
*****************************************************************
*
*     THIS SUBROUTINE GENERATES AN EQUIVALENT BASEBAND QPRS SIGNAL
*
*****************************************************************
      DIMENSION DATA(512),DADA(512),NX(11),NY(11)
      JA=2*LSAMPL
C
C     GENERATING ONE SYMBOL AND PRECODING
C
      IF(I.EQ.JLAST) I=0
      I=I+1
      J=I-JTAP
      IF(I.LE.JTAP) J=J+JLAST
      IX=NX(J)*VK(I)
      IY=NY(J)*VK(I)
      NX(I)=IX
      NY(I)=IY
C
      DO 5 MN=1,31,2
      DADA(MN)=-1.
      DATA(MN)=DADA(MN)
      IF(IX.EQ.1) DATA(MN)=-DADA(MN)
      DADA(MN+1)=1.
      DATA(MN+1)=DADA(MN+1)
      IF(IY.EQ.1) DATA(MN+1)=-DADA(MN+1)
    5 CONTINUE
C
      DO 1 K=1,11
      IF(I.EQ.JLAST) I=0
      I=I+1
      J=I-JTAP
      IF(I.LE.JTAP) J=J+JLAST
      IX=NX(J)*VK(I)
      IY=NY(J)*VK(I)
      NX(I)=IX
      NY(I)=IY
C
      J1=K*JA+1
      J2=(K+1)*JA-1
      DO 2 J3=J1,J2,2
      J4=J3-JA
      DATA(J3)=DATA(J4)
      IF(IX.EQ.1) DATA(J3)=-DATA(J4)
      DATA(J3+1)=DATA(J4+1)
      IF(IY.EQ.1) DATA(J3+1)=-DATA(J4+1)
    2 CONTINUE
    1 CONTINUE
C
C     THE REMAINING DATA ARE SET TO ZERO FOR[illegible] PURPOSE
C
      J3=J2+2
      DO 200 JJ=J3,LDIM
  200 DATA(JJ)=0.
      RETURN
      END
```

```
      SUBROUTINE DECDPR(DATA,NRX,NRY,PE,PEI,KKK,LSAMPL,LSTART,NSNR,
     *NERROR,SNRDB,I,NTOTAL,PNOISE,LOOP,JLAST,JTAP,NSYMB,PSHIFT)
C*****************************************************************
C*
C*    THIS SUBROUTINE FIRST RECTIFIES THE 3-LEVEL PR SIGNAL
C*       AND THEN USES THE PRECODING DETECTING SCHEME
C*       FOR COMPARING WITH THE TRANSMITTED DATA.
C*
C*****************************************************************
      DIMENSION DATA(512),NRX(11),NRY(11),PE(25),PEI(25),SNRDB(25)
      COSPS=COS(PSHIFT)
      SINPS=SIN(PSHIFT)
      RT2=1.

      DO 1 K=1,KKK

CCCCC REGENERATING THE TRANSMITTED SYMBOLS

      IF(I.EQ.JLAST) I=0
      I=I+1
      J=I-JTAP
      IF(I.LE.JTAP) J=J+JLAST
      IX=NRX(J)*NRX(I)
      IY=NRY(J)*NRY(I)
      NRX(I)=IX
      NRY(I)=IY

CCCCC FIRST LOOP SYMBOLS ARE NOT PROCESSED

      IF(LOOP.EQ.0) GO TO 1

CCCCC DECODING

      J1=LSTART+2*LSAMPL*(K-1)
      J2=LSTART+2*(LSAMPL*K-1)
      AMPLIX=0.
      AMPLIY=0.

CCCCC AVERAGED SYMBOL AMPLITUDE

      DO 2 J3=J1,J2,2
      AMPLIX=AMPLIX+DATA(J3)
    2 AMPLIY=AMPLIY+DATA(J3+1)
      AMPLIX=AMPLIX/FLOAT(LSAMPL)
      AMPLIY=AMPLIY/FLOAT(LSAMPL)
      AXBAR=AMPLIX*COSPS+AMPLIY*SINPS
      AYBAR=AMPLIY*COSPS-AMPLIX*SINPS

CCCCC RECTIFYING

      AMPLIX=ABS(AMPLIX)
      AMPLIY=ABS(AMPLIY)

      AX=RT2-AMPLIX
      AY=RT2-AMPLIY
      AXBAR=AX*COSPS+AY*SINPS
      AYBAR=AY*COSPS-AX*SINPS
```

```
C
      INDEXX=0
      IF(SIGN(1.,AXBAR).NE.IX) INDEXX=1
      INDEXY=0
      IF(SIGN(1.,AYBAR).NE.IY) INDEXY=1
      IF((INDEXX.EQ.1).OR.(INDEXY.EQ.1)) NERROR=NERROR+1
C
CCC   COMPUTE PROBABILITY OF ERROR FOR THIS SYMBOL
C
      CALL PERR4(AXBAR,AYBAR,INDEXX,INDEXY,SNRDB,PEI,PNOISE,NSNR)
C
      DO 5 KK=1,NSNR
    5 PE(KK)=PE(KK)+PEI(KK)
C
      NTOTAL=NTOTAL+1
      IF(NTOTAL.NE.NSYMB) GO TO 1
      PRINT 150
  150 FORMAT(/4H SNR,10X,14HPROB. OF ERROR/)
      DO 500 II=1,NSNR
  500 PEI(II)=PE(II)/FLOAT(NSYMB)
      PRINT 151,(SNRDB(II),PEI(II),II=1,NSNR)
  151 FORMAT(F5.1,10X,E13.6)
      PRINT 102,NERROR
  102 FORMAT(/2X,7HERRORS=,I5)
      GO TO 132
    1 CONTINUE
  132 LOOP=LOOP+1
      RETURN
      END
```

```
      SUBROUTINE PR(DATA,LDIM)
      DIMENSION DATA(512),DADA(512)
      JA=32
C
CCC   PARTIAL RESPONSE CODING
C
      DO 111 M=1,LDIM
  111 DADA(M)=DATA(M)
      DO 112 NA=1,31,2
      DATA(NA)=DATA(NA)-1.
  112 DATA(NA+1)=DATA(NA+1)+1.
      DO 119 K=1,11
      J5=K*JA+1
      J6=(K+1)*JA-1
      DO 110 J7=J5,J6,2
      J8=J7-JA
      DATA(J7)=DATA(J7)+DADA(J8)
  110 DATA(J7+1)=DATA(J7+1)+DADA(J8+1)
  119 CONTINUE
      RETURN
      END
```

Other Subroutines Needed:

BITREV	NONCOM	CONJUG	TTERFC
PERR4	BISINC	CF4P5	TWT
CALCON	HHGG	ADTAIL	FILTER

APPENDIX C1

In Section 4.2.2, it was noted that QPSK and OKQPSK have the same spectrum. As power spectrum is a linear averaging process, the timing offset of the two data streams in OKQPSK will not affect the spectrum shape in the linear system, i.e. it is still identical to that of QPSK when both pass through identical filters. In this section, this fact will be mathematically demonstrated.

The filtered OKQPSK signal as shown in Eq. (4.15) has its power spectrum given by:

$$P(\omega) = E_s\left[\frac{1}{T_s}\left(\int_{-\infty}^{\infty} e^{-j\omega\xi}\left[y(\xi) - j\, z(\xi)\right] d\xi \left[y(\eta) + j\, z(\eta)\right] e^{j\omega\eta} V_o(\eta)\, d\eta\right)\right] \quad (1)$$

where E_s denotes the expected value taken on the set 'S' of random variables (a_k , b_k) of the binary sequence (Eq. (4.10)), and,

$$V_o(t) = \begin{cases} 1 & |t| \leq \frac{T_s}{2} \\ 0 & \text{otherwise} \end{cases} \quad (2)$$

Since,

$$E_s\left\{\left[y(\xi) - j\, z(\xi)\right]\left[y(\eta) + j\, z(\eta)\right]\right\} = \sum_{-\infty}^{\infty}\left[R(\eta-kT_s)R(\xi-kT_s) + I(\eta-\frac{T_s}{2}-kT_s)\, I(\xi-\frac{T_s}{2}-kT_s)\right] + j\sum_{-\infty}^{\infty}\left[R(\xi-kT_s)I(\eta-kT_s) - R(\eta-\frac{T_s}{2}-kT_s)I(\xi-\frac{T_s}{2}-kT_s)\right] \quad (3)$$

Substituting Eq. (3) into Eq. (1), we obtain four terms in the expansion of Eq. (1):

The first term of the new Eq. (1) can be re-written as:

$$\frac{1}{T_s}\int_{-\infty}^{\infty} V_o(\eta)\left[\sum_{-\infty}^{\infty} R(\eta - kT_s)\, e^{j\omega(\eta - kT_s)}\, d\eta \int_{-\infty}^{\infty} R(\xi)\, e^{-j\omega\xi}\, d\xi \right. \tag{4}$$

From Poisson's formula [2.12],

$$\sum_{-\infty}^{\infty} R(\eta - kT_s)\, e^{j\omega(\eta - kT_s)} = \frac{1}{T_s}\sum_{-\infty}^{\infty} Q\left(\frac{k}{T_s}\right) e^{j\left(\frac{2\pi}{T_s}\right)k\eta}$$

where,

$$Q(x) = \int_{-\infty}^{\infty} R(\eta)\, e^{j\omega\eta}\, e^{-j\eta x}\, d\eta \tag{5}$$

Thus,

$$\begin{aligned} &\int_{-\infty}^{\infty} V_o(\eta)\left[\frac{1}{T_s}\sum_{-\infty}^{\infty} Q\left(\frac{k}{T_s}\right) e^{j\left(\frac{2\pi}{T_s}\right)k\eta}\right] d\eta \\ &= \frac{1}{T_s}\int_{-\frac{T_s}{2}}^{\frac{T_s}{2}} Q(0)\, d\eta \\ &= Q(0) \\ &= \int_{-\infty}^{\infty} R(\eta)\, e^{j\omega\eta}\, d\eta \end{aligned} \tag{6}$$

and the first term in the new Eq. (1) becomes:

$$\begin{aligned} &\frac{1}{T_s}\int_{-\infty}^{\infty} R(\eta)\, e^{j\omega\eta}\, d\eta \int_{-\infty}^{\infty} R(\xi)\, e^{-j\omega\xi}\, d\xi \\ &= \frac{1}{T_s}\left|\int_{-\infty}^{\infty} R(t)\, e^{j\omega t}\, dt\right|^2 \end{aligned} \tag{7}$$

Similarly, the second term of new Eq. (1) can be re-written as:

$$\begin{aligned} &\frac{1}{T_s}\left|\int I(t - \frac{T_s}{2})\, e^{j\omega t}\, dt\right|^2 \\ &= \frac{1}{T_s}\left|e^{j\omega\frac{T_s}{2}}\int I(t')\, e^{j\omega t'}\, dt'\right|^2 \\ &= \frac{1}{T_s}\left|\int I(t')\, e^{j\omega t'}\, dt'\right|^2 \end{aligned} \tag{8}$$

From Eq. (8), it is noted that the offset effect is removed in the averaging process.

The remaining two other terms in the new Eq. (1) are found to be zero.

Comparing Eq. (7) and Eq. (8) with those in Ref. [1.24], the spectrum of filtered OKQPSK signal is found to be identical to that of filtered QPSK signal.

Appendix C2

Instruction Manual

&

Program Listings

for

Computer Simulation of the Performance of Bandlimited QPSK, OKQPSK

and

MSK Signals Through Cascaded Nonlinearities

This appendix contains the instruction manual and listing of the simulation programs used in the study of the comparative performance of bandlimited QPSK, OKQPSK and MSK signals through cascaded nonlinearities as in a typical satellite channel. This manual is written for a practicing engineer who will be able, without too much effort, to adopt these programs to his particular needs. For this purpose, this manual is self-contained with certain background information duplicated from that of Chapter 4. This manual can also be used for the QPRS computer simulation program listed in Appendix B.

Acknowledgments

I would like to express my deep thankfulness to Dr. H.C. Chan, Communication Research Laboratory, McMaster University, for his helpful assistance and suggestions in the development of the computer simulation programs.

Table of Contents of Appendix C2

1. Background Information

In satellite communication systems, the high power amplifier (HPA) at the earth transmitting station and the travelling wave tube amplifier (TWT) at the satellite transponder are usually operated near saturation and therefore exhibit the nonlinear characterisitcs of AM/AM and AM/PM conversion. The AM/AM conversion will cause spectral spreading of the filtered signal which will then interfere with signals in the neighboring channels. In the case of M-ary PSK modulated signals, substantial AM/PM conversion will deteriorate the system performance.

Three modulation techniques have frequently been considered in such a nonlinear satellite channel: conventional QPSK, OKQPSK and MSK. MSK is also known as FFSK. These two names will be used interchangeably in this manual.

These three modulation techniques are basically of quaternary phase shift keying and are a kind of quadrature amplitude modulation. The circuit block diagrams and the signal space diagrams of these three modulation schemes are illustrated in Fig. 1.

In conventional QPSK, the in-phase and the quadrature phase data streams are aligned coincidently. An instantaneous phase shift of 180° occurs when both channel data change phase simultaneously. The envelope of a filtered QPSK signal goes through zero during these 180° phase transitions. This inherent envelope fluctuation of a QPSK signal causes distortion and spectrum spreading when it passes through a nonlinear amplifier.

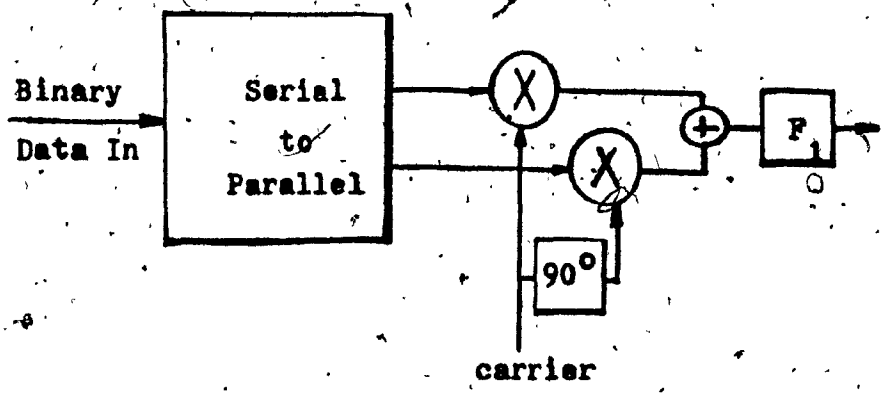

a. Conventional QPSK

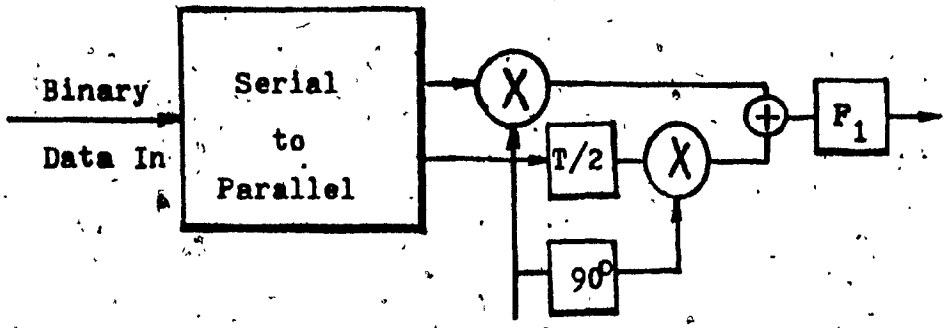

b. Offset QPSK

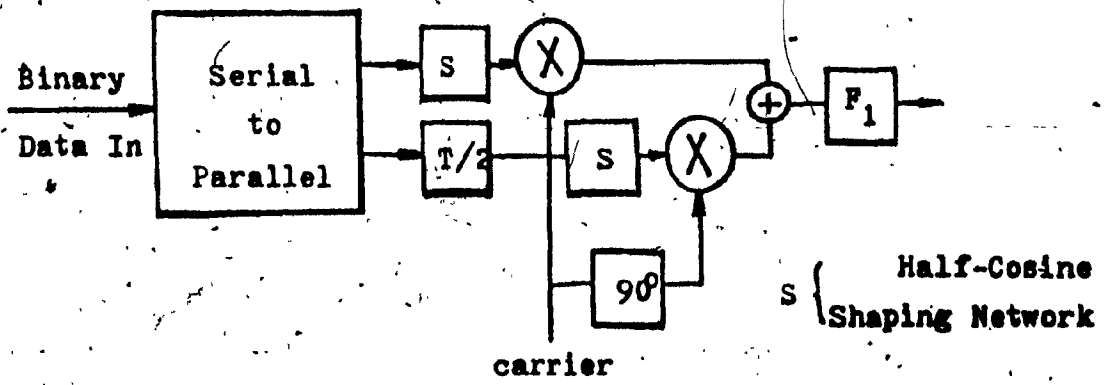

c. MSK

Fig. 1 Block Diagrams of QPSK, OKQPSK and MSK.

In OKQPSK and MSK, one data stream is delayed by one half of a symbol interval T in comparison with the other data stream. The instantaneous phase shift of 180° does not occur and filtered OKQPSK and MSK signals do not go through zero. The envelope fluctuation of these two signals is smaller when compared with that of the QPSK signal and therefore, less spectrum spreading will occur when they pass through a nonlinear device. Based on this, it has been predicted that either OKQPSK or MSK is more suitable than QPSK in a satellite channel.

The difference between OKQPSK and MSK lies in the extra pulse shaping networks which shape the rectangular pulses of OKQPSK into the half cosine pulses of MSK as shown in Fig. 1. Although an MSK signal has a smoother phase transition than that of an OKQPSK signal, the main spectral lobe of an MSK signal is 50% wider than that of a conventional QPSK or an OKQPSK signal.

This manual contains the description of the programs that simulate these three types of signal passing through a typical satellite channel and evaluates their performance degradation due to filter bandlimiting and nonlinear distortions of HPA and TWT. These three programs are modified from the McMaster University Internal Report CRL-18. For a basic understanding of the simulation methods, this report should be used in conjunction with this manual.

The computer simulation model used herewith is shown in Fig. 2. The satellite link considered, consists of the earth transmitting station, the

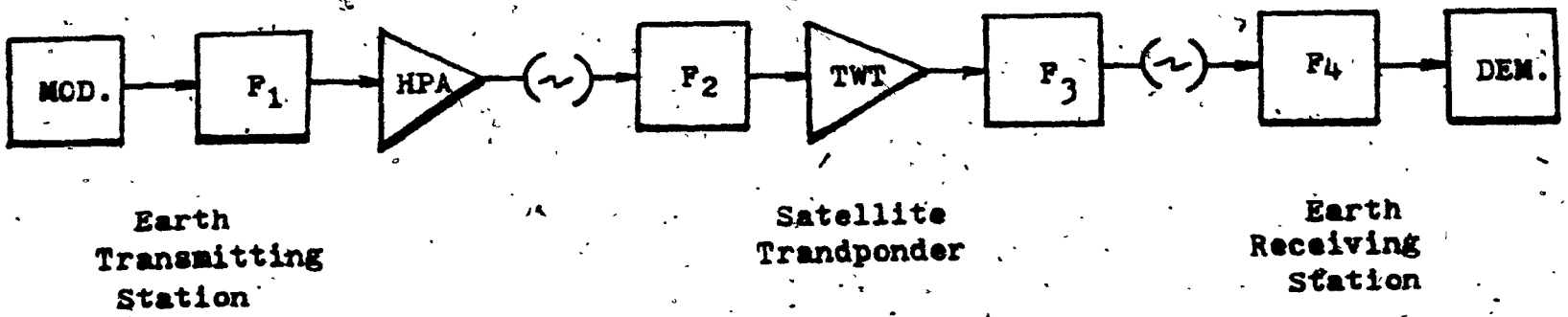

Fig. 2 Block Diagram of Computer Simulation

satellite transponder and the earth receiving station. At the earth transmitting station, the transmit bandpass filter (F_1 in Fig. 2) which is used to bandlimit the spectrum causes intersymbol interference (ISI); the HPA, operated hear saturation, causes both AM/AM and AM/PM conversion of the signal and degrades the system performance. The two filters (F_2 and F_3 in Fig. 2) in the satellite transponder, which are used to bandlimit the thermal noise and minimize adjacent channel interference, also cause ISI degradation. The TWT at the satellite transponder further degrades the signal performance because of its AM/AM and AM/PM conversions. At the earth receiving station, the receive filter (F_4 in Fig. 2) is used to bandlimit the thermal noise and reduce adjacent channel interference to the receiver.

Based on this simulation model, the simulation block diagram is shown in Fig. 3. The signal source generates a pseudo random data sequence which is then loaded into two arrays representing the complex signal as QPSK, OKQPSK or MSK. By use of the Fast Fourier Transform (FFT) algorithm, this signal is alternated between its time and frequency domain representation. In the frequency domain, it is modified by the filter transfer functions. In the time domain, it is modified by the nonlinear devices HPA and TWT. The passage of the signal through a satellite channel is thus simulated by successive modifications of the signals.

The simulation is performed based on the equivalent baseband concept. All signals are processed in complex baseband form. Bandpass filters are also represented by equivalent baseband filters. Due to the large

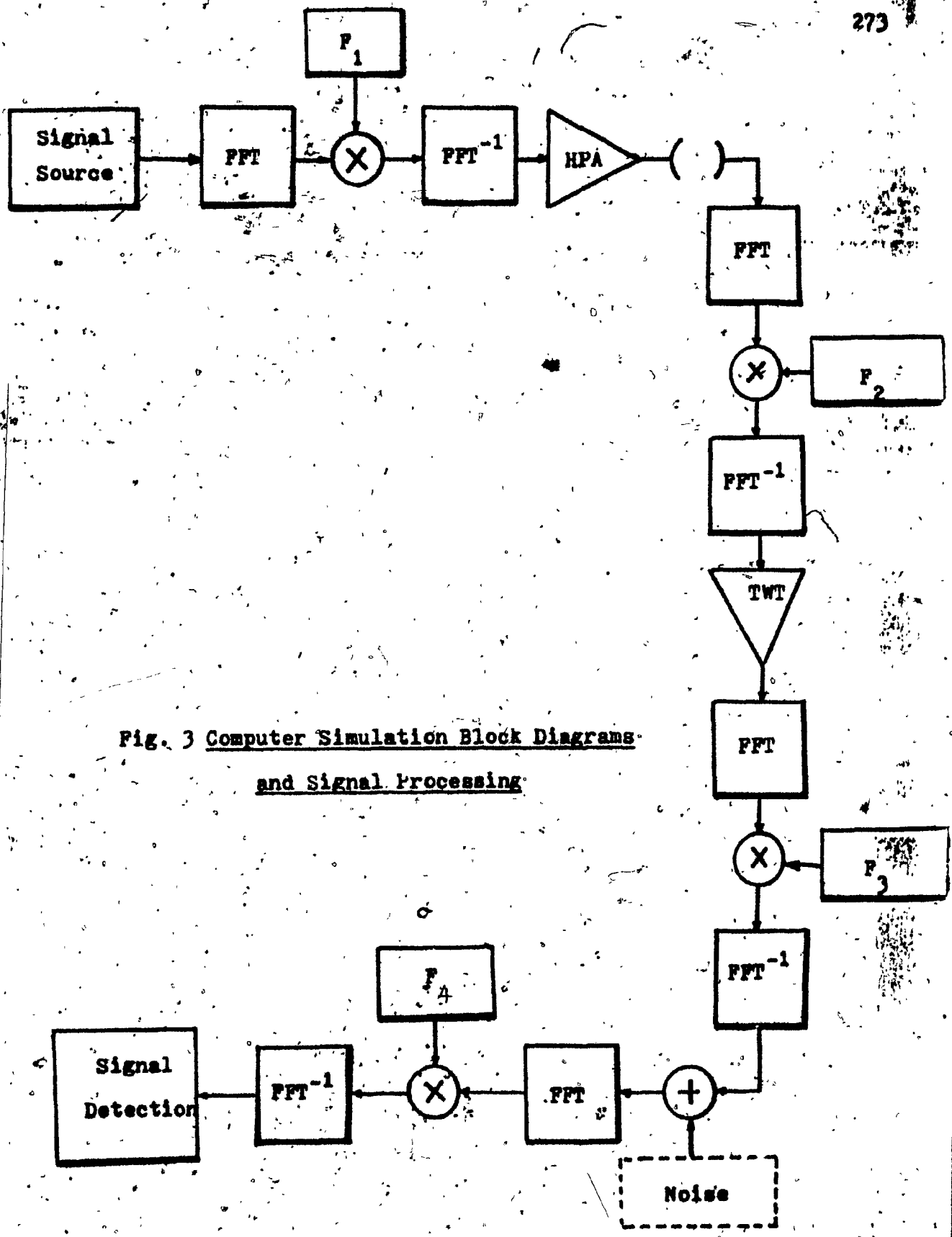

Fig. 3 Computer Simulation Block Diagrams and Signal Processing

amount of computer time required in the simulation of noise, the noise power at the output of the receive filter is computed according to theory. The signal is simulated in the absence of noise.

At the receiver, the probability of error P(e) for each signal symbol is computed from the received symbol energy and the computed noise power. The overall probability of error is obtained by averaging the probability of error in all symbols. The longer the signal sequence is, the better the approximation to the actual error rate will be. Due to the limitation of computer memory size and execution time, the length of the pseudo random sequence used in the simulation is chosen to be 127. This makes little difference in performance evaluation of QPSK, OKQPSK and MSK, as there are two relatively shifted sequences which are used to simulate the in-phase and quadrature channel. A relatively uniform distribution of symbol sequence patterns thus exists in the simulation.

2. Summary and Functions of Fortran Programs & Subroutines

Program Names:
1. QPSK
2. OKQPSK
3. MSK (FFSK)

Running Times:

Compilation Time - 8 CPU seconds/each program

Execution Time - 20 CPU seconds/each program

(Based on CDC 6600, Concordia Computer Center)

Fortran Programs and Subroutines:

QPSK	OKQPSK	FFSK
LOAD4	LOSPSK	LOFFSK
DECOD4	DOSPSK	DOFFSK
PERR4	PERR2	PERR2

HPA
TWT
CF4P5
MEASUR
FILTER
NONCOM
CONJUG
BITREV
CALCON
HHGG
ADTAIL
TTERFC
DELAY
BISINC

used with the IMSLIB subroutine "FFT2RV"

TABLE 1

SUMMARY of the FUNCTIONS of FORTRAN PROGRAMS & SUBROUTINES

QPSK	OKQPSK	FFSK	Main Program
LOAD4	LOSPSK	LOFFSK	Transmit Data Generation
DECOD4	DOSPSK	DOFFSK	Receive Data Decoding & P(e) Calculation
PERR4	PERR2	PERR2	P(e) Calculation of each decoded symbol
	HPA TWT		Quadrature models of HPA and TWT also delay compensation of data due to preceding filtering effect
	CF4P5		Computation of complex transfer function of a standard filter (i.e., a 6 pole Chebychev with $\frac{1}{2}$ db pass-band ripples)
	MEASUR		Computation of complex transfer function of a filter whose measured amplitude and phase characteristics are known)
	FILTER		Filtering distortion processing
	NONCOM CONJUG BITREV		Used with IMSLIB subroutine FFT2RV for performing FFT and FFT^{-1}
	CALCON		Calculation of some required constants
	HHGG		Calculation of effective noise at receive filter output
	ADTAIL		Adding the tail part of a sectioned data to the front part of the data in the previous section
	TTERFC		Complementary error function
	DELAY		Delay compensation of data due to preceding filtering effect
	BISINC		Bit synchronization of the TX data and RX data

3. Description of Main Program

The QPSK program will be used as an example to outline the general description of the Fortran programs used in the simulation. In the section of the manual of the OKQPSK and FFSK programs, only the difference will be pointed out. For easier reference, the names of the variables (either Integer or Real) used in the program will be adopted in this description.

3.1 Data Generation and Decoding

Two shift registers whose initializing numbers II and IK (both equal to zero) and initial registers (NX(I) and NY(I) at the transmitter and NRX(I) and NRY(I) at the receiver) are used to load (subroutine LOAD4) and to decode (subroutine DECOD4) the data sequences (DATA(I), DATA1(I), DATA2(I) and DATA3(I)).

The number of shift registers (JLAST) is currently 7 (can be changed to 11 or larger) and the tap location (JTAP) is 1.

The received data sequences (tracked by IK at the main program subroutine DECOD4) and the transmitted data sequence (tracked by II at the main program and subroutine LOAD4) are synchronized through the subroutine BISINC. The subroutine BISINC will compute the delays of the signal by each filter. These delays are then compensated either internally at subroutines HPA, TWT and DECOD4 or, at the subroutine DELAY, so that the received data can be compared with the transmitted data at the

subroutine DECOD4. The energy of each received symbol is computed. The P(e) of this symbol at the pre-chosen SNR is then calculated. The final P(e) is computed at the subroutine DECOD4 by averaging the P(e) of all the processed symbols (127 symbols currently for the 7 shift registers used).

3.2 Sectioning of the Data Sequence

Since the number of shift registers (JLAST) used is 7, therefore the total number of symbols generated in the real channel (x-channel) and imaginary channel (y-channel) is 127 ($2^7 - 1$), respectively. Because of the computer memory size limitation, these 127 symbols (NSYMB) are sectioned into 11 loops (LOOPM = 11, obtained in the subroutine CALCON) as shown in Fig. 4. Each loop contains 12 symbols in both the x-channel and y-channel (KKK = 12, also obtained in CALCON and used at LOAD4 and DECOD4)

Each symbol is then sampled 16 times (LSAMPI = 16). This makes up 192 samples in the x- and y-channel. The DATA array are interleaved with the odd-numbered data array for x-channel and the even-numbered data array for y-channel. To take care of the spillover effect due to filtering, 64 arrays with zero value are added to each channel, making up 256 samples in each channel or 512 samples in one section of data (LDIM = 512).

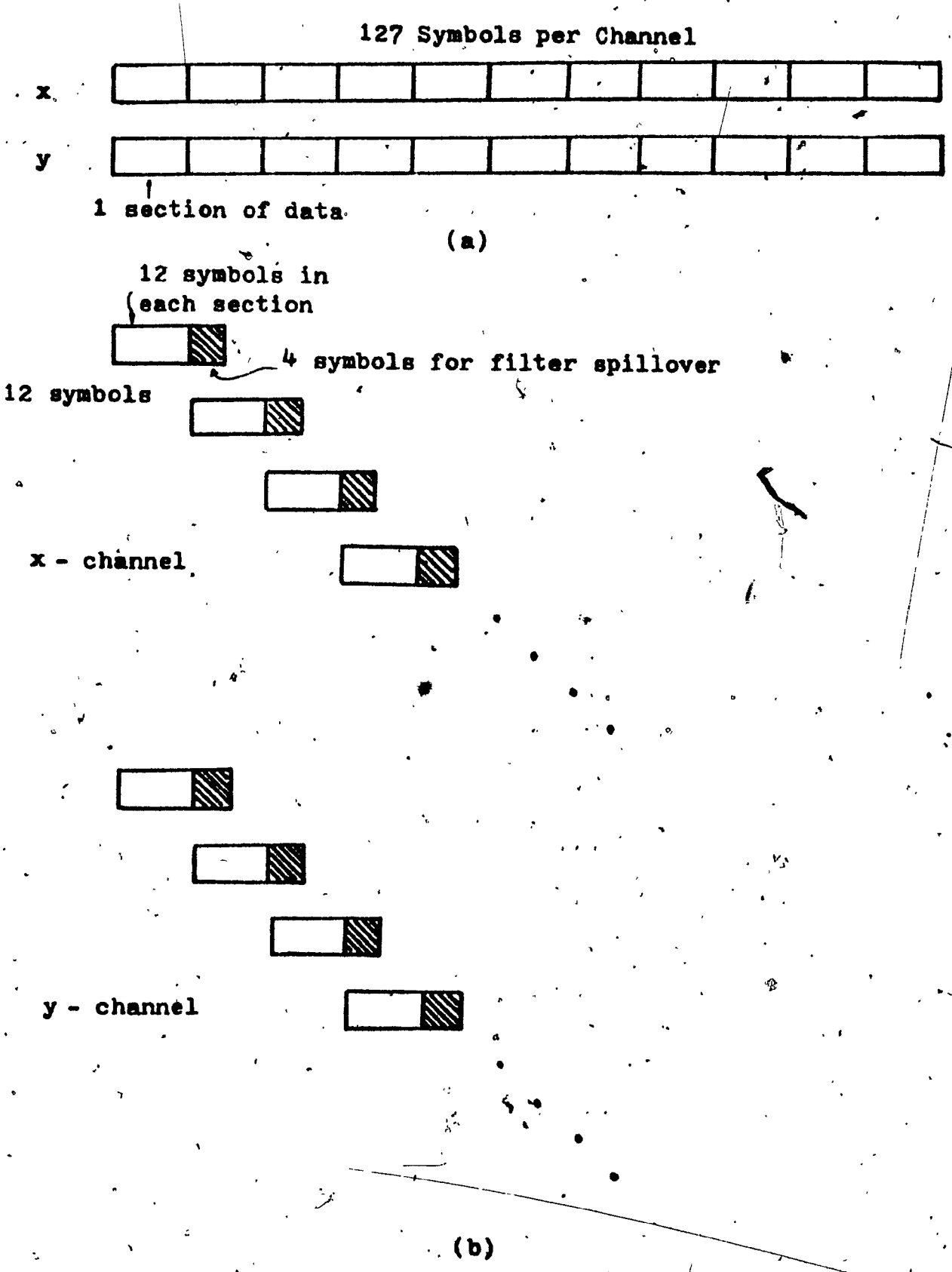

Fig. 4 Sectioning of the Data Sequence

In each section of data array, the signal therefore looks as shown in Fig. 5.

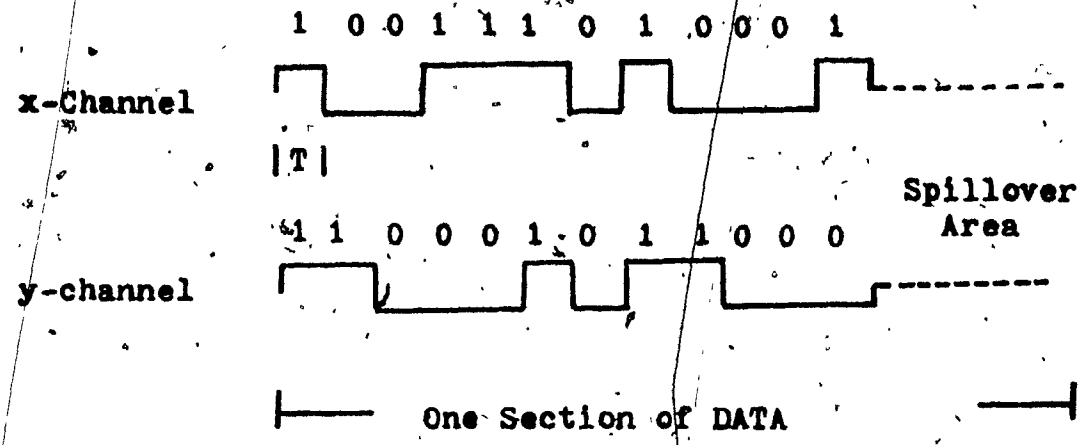

Fig. 5 One Section of Data Array

When sharp filters are used, the spillover area may have to be lengthened. In this situation, the complete data sequence without any sectioning may have to be used.

3.3 Signal Processing

Each sectioned DATA array will then be processed according to the system model shown in Fig. 2. Detailed operation of this processing is shown in Fig. 6. Four DATA arrays (DATA, DATA1, DATA2 and DATA3) are created. Another additional array, TATA1, is also created for storing the DATA array once it has been completly processed. TATA1 is then ready for final decoding at the DECOD4.

As shown in Fig. 6, each sectioned DATA array after passing through a filter must go through the subroutine ADTAIL where the filter spillover effect is taken care of. Besides processing the nonlinear distortion of HPA and TWT on the signal, the subroutines HPA and TWT also perform the compensation of the delay introduced by the preceding filter on the signal. The delay introduced by filter F_3 is being compensated at the subroutine DELAY, while delay introduced by filter F_4 is compensated at the subroutine DECOD4.

After the DATA array in LOOP 0 (first loop) is stored in the reserve array TATA1, then DATA1, DATA2 and DATA3 are shifted into the data arrays DATA, DATA1, and DATA2 respectively. In this way, the data array DATA3 is now empty and ready for another new section of data array (LOOP 1). A DO-LOOP is processed up to LOOP = LOOPM, which is the maximum number of loops of data to be processed. The first section of the data array (LOOP = 0) is not to be decoded at DECOD4 because its front portion is not processed for filter spillover effect.

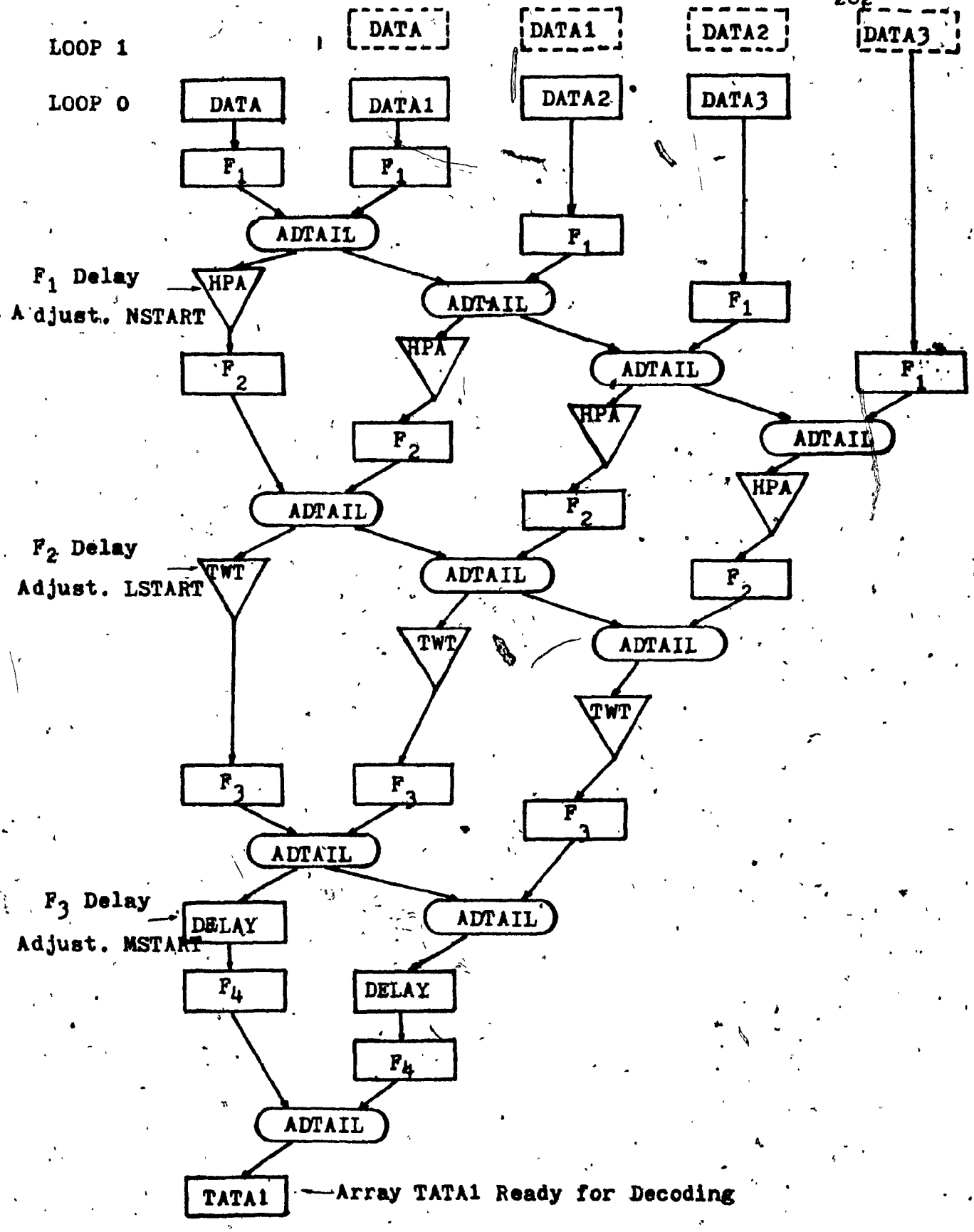

Fig. 6 Signal Processing of the Main Program

The remaining processed data arrays are then decoded symbol by symbol. The P(e) of each processed symbol is computed at the subroutine PERR4. The final P(e) is obtained by averaging all the P(e) of all the symbols.

```
      PROGRAM QPSK(INPUT,OUTPUT)
C*****************************************************************
C
C     JOHN C. HUANG, SEPTEMBER, 1978 CONCORDIA UNIVERSITY
C
C     THIS PROGRAM SIMULATES A QPSK SIGNAL PASSING THROUGH A NONLINEAR
C     SATELLITE CHANNEL. AT THE EARTH TRANSMITTING STATION,THE SIMULATED
C     QPSK SIGNAL PASSES THROUGH FILTER TF1,HIGH POWER AMPLIFIER HPA.
C     AT THE SATELLITE TRANSPONDER, THE SIGNAL PASSES THROUGH FILTER TF2,
C     THE SATELLITE TRAVELLING WAVE TUBE AMPLIFIER TWT AND FILTER TF3.
C     FINALLY, AT THE RECEIVING EARTH STATION, THE RECEIVED SIGNAL PASSES
C     THROUGH FILTER TF4 BEFORE IT IS DECODED FOR P(E) CALCULATION.
C
C        INPUT DATA REQUIRED.....
C     BIRATE= BIT RATE OF INTEREST
C     LSAMPL= NUMBER OF SAMPLES IN A SYMBOL. USUALLY = 16.
C     KNK= NUMBER OF LOOPS THAT THE BIT RATE IS INCREMENTED.
C     DBRATE= INCREMENT OF BIT RATE
C     TWT1IN,TWT1OU,PSH1---OPERATING POINTS OF HPA
C     TWT2IN,TWT2OU,PSH2---OPERATING POINTS OF TWT
C       .....TO OBTAIN THE COEFFICIENTS THAT CHARACTERIZE THE IN-PHASE A
C             QUADRATURE MODEL OF HPA AND TWT, SEE THE MANUAL
C     FBW1,FBW2,FBW3,FBW4  3 DB FREQUENCIES OF TF1,TF2,TF3,TF4.
C
C     INSTRUCTION FOR INPUT DATA THAT CHARACTERIZE FILTERS OF
C     INTEREST IS GIVEN WHERE APPLICABLE.
C
C*****************************************************************
      DIMENSION DATA(512),DATA1(512),DATA2(512),DATA3(512),TATA1(512)
      DIMENSION NX(11),NY(11),NRX(11),NRY(11),PE(25),PEI(25),SNRDB(25)
      DIMENSION TF(512),TF1(512),TF2(512),TF3(512),TF4(512)
      DIMENSION C(15),C1(15),C2(15),C3(15),C4(15)
      DIMENSION CA1(14),CA2(14),CA3(14),CA4(14)
      DIMENSION CP1(14),CP2(14),CP3(14),CP4(14)
      DATA NTOTAL,NERROR,LOOP,II,IK/0,0,0,0,0/
      DATA JLAST,JTAP,LLTNOM/7,1,50/
      DATA NY(1),NY(2),NY(3),NY(4),NY(5),NY(6),NY(7)/-1,-1,1,1,1,1,-1/
C
      LDIM=512
      NN=LDIM/2
      PRINT 1
    1 FORMAT(29H SIMULATION OF COHERENT 4-PSK)
C
      READ *,BIRATE,LSAMPL,KNK,DBRATE
C
C     CHANGE BIT RATE INTO BAUD RATE
C
      BAUD=BIRATE/2.
C
C     THE OPERATING POINTS OF HPA AND TWT ARE REQUERED
C
      READ *,TWT1IN,TWT1OU,PSH1
      READ *,TWT2IN,TWT2OU,PSH2
      PRINT *,TWT1IN,TWT1OU,PSH1
      PRINT *,TWT2IN,TWT2OU,PSH2
C
C     IF ALL THE FILTERS USED ARE IDENTICAL WITH SAME NUMBER OF POLES
```

```
C     AND OF STANDARD TYPE (WITH DIFFERENT F -3DB BW),ENTER IDENT=1
C     IF NOT IDENTICAL,BUT STILL OF STANDARD TYPES,ENTER IDENT=2
C     IF OBTAINED FROM MEASURED AMPLITUDES AND GROUP DELAY,ENTER
C     IDENT=3 (SEE MANUAL FOR INSTRUCTION)
C
      READ *,IDENT
      IF(IDENT.EQ.2) GO TO 52
      IF(IDENT.EQ.3) GO TO 53
C
C     THESE FOUR FILTERS ARE IDENTICAL AND OF STANDARD TYPES.
C
      READ *,FBW1,FBW2,FBW3,FBW4
      PRINT *,FBW1,FBW2,FBW3,FBW4
      READ *,IC
      PRINT 601
  601 FORMAT(/5X,*IDENTICAL AND STANDARD TYPES OF FILTERS*/)
      PRINT *,IC
      READ *,(C(N),N=1,IC)
      PRINT *,(C(N),N=1,IC)
      DO 301 N=1,IC
      IC1=IC
      IC2=IC
      IC3=IC
      IC4=IC
      C1(N)=C(N)
      C2(N)=C(N)
      C3(N)=C(N)
      C4(N)=C(N)
  301 CONTINUE
C
      GO TO 54
C
C     THESE FOUR FILTERS ARE NOT IDENTICAL, BUT STILL OF STANDARD TYPES
C
   52 PRINT 602
  602 FORMAT(/5X,*UNIDENTICAL BUT STANDARD TYPES OF FILTERS*/)
      READ *,FBW1,IC1
      READ *,(C1(N),N=1,IC1)
      READ *,FBW2,IC2
      READ *,(C2(N),N=1,IC2)
      READ *,FBW3,IC3
      READ *,(C3(N),N=1,IC3)
      READ *,FBW4,IC4
      READ *,(C4(N),N=1,IC4)
C
      PRINT *,FBW1,IC1
      PRINT *,(C1(N),N=1,IC1)
      PRINT *,FBW2,IC2
      PRINT *,(C2(N),N=1,IC2)
      PRINT *,FBW3,IC3
      PRINT *,(C3(N),N=1,IC3)
      PRINT *,FBW4,C4
      PRINT *,(C4(N),N=1,IC4)
C
      GO TO 54
C
   53 CONTINUE
```

```
C
C     MEASURED AMPLITUDE AND PHASE DISTORTION CHARACTERISTICS OF THE
C     FOUR FILTERS WILL BE USED IN THE SIMULATION.
C
C     IF ALL THESE FILTERS ARE IDENTICAL, ENTER IDENTO= 1
C     OTHERWISE ENTER IDENTO= 2.
C
      READ *,IDENTO
C
      IF(IDENTO.EQ.2) GO TO 541
C
      READ *,(CA1(J),J=1,14)
      READ *,(CP1(J),J=1,14)
C
      PRINT 603
  603 FORMAT(/5X,*MEASURED FILTER CHARACTERISTICS,IDENTICAL FILTERS*/)
      PRINT *,(CA1(J),J=1,14)
      PRINT *,(CP1(J),J=1,14)
C
      DO 302 J=1,14
      CA2(J)=CA1(J)
      CP2(J)=CP1(J)
      CA3(J)=CA1(J)
      CP3(J)=CP1(J)
      CA4(J)=CA1(J)
      CP4(J)=CP1(J)
  302 CONTINUE
      GO TO 54
C
  541 CONTINUE
      READ *,(CA1(J),J=1,14)
      READ *,(CA2(J),J=1,14)
      READ *,(CA3(J),J=1,14)
      READ *,(CA4(J),J=1,14)
       DO 901 I=1,14
       CP1(I)=0.
       CP2(I)=0.
       CP3(I)=0.
       CP4(I)=0.
  901  CONTINUE
C
      PRINT 604
  604 FORMAT(/5X,*MEASURED FILTER CHARACTERISTC,UNIDENTICAL FILTERS*/)
      PRINT *,(CA1(J),J=1,14)
      PRINT *,(CP1(J),J=1,14)
      PRINT *,(CA2(J),J=1,14)
      PRINT *,(CP2(J),J=1,14)
      PRINT *,(CA3(J),J=1,14)
      PRINT *,(CP3(J),J=1,14)
      PRINT *,(CA4(J),J=1,14)
      PRINT *,(CP4(J),J=1,14)
C
C
   54 CONTINUE
      AVAMP=SQRT(2.)
      FNORM=1.0/AVAMP
```

```
      FNORO1=TWT1OU/AVAMP
      FNORI2=TWT2IN/AVAMP
      FNORO2=TWT2OU/AVAMP
      PSHIFT=PSH1+PSH2
      DO 507 KK=1,KNK
      PRINT *,BIRATE,PSHIFT,LSAMPL
      DO 4 I=1,JLAST
      NX(I)=-1
      NRY(I)=NY(I)
    4 NRX(I)=-1
      NSNR=25
      DSNR=1.
      DSNRDB=0.
      DO 5 I=1,NSNR
      PE(I)=0.
      SNRDB(I)=4.+DSNRDB
      DSNRDB=DSNRDB+DSNR
    5 CONTINUE
C
      CALL CALCON(LSAMPL,LLTNOM,KKK,LLT,NSYMB,JLAST,LOOPM,LDIM,BAUD,
     +SBANDW)
C
      IF(IDENT.EQ.3) GO TO 34
C
      CALL CF4P5(SBANDW,FBW4,DATA1,LDIM,C4,IC4)
      CALL HHGG(DATA1,PNOISE,LSAMPL,LDIM)
C
CCC   STANDARD TYPES OF FILTERS USED IN THE SIMULATION
C
      CALL CF4P5(SBANDW,FBW1,TF1,LDIM,C1,IC1)
      CALL CF4P5(SBANDW,FBW2,TF2,LDIM,C2,IC2)
      CALL CF4P5(SBANDW,FBW3,TF3,LDIM,C3,IC3)
      CALL CF4P5(SBANDW,FBW4,TF4,LDIM,C4,IC4)
C
      GO TO 35
C
CCCC  MEASUED AMPLITUDE AND PHASE CHARACTERISTICS OF THE FILTERS USED
      IN THE SIMULATIONS
C
   34 CONTINUE
      CALL MEASUR(SBANDW,FBW4,DATA1,LDIM,CA4,CP4)
      CALL HHGG(DATA1,PNOISE,LSAMPL,LDIM)
C
      CALL MEASUR(SBANDW,FBW1,TF1,LDIM,CA1,CP1)
      CALL MEASUR(SBANDW,FBW2,TF2,LDIM,CA2,CP2)
      CALL MEASUR(SBANDW,FBW3,TF3,LDIM,CA3,CP3)
      CALL MEASUR(SBANDW,FBW4,TF4,LDIM,CA4,CP4)
C
   35 CONTINUE
C
      CALL BISINC(DATA,TF1,TF2,TF3,TF4,LSAMPL,NSTART,LSTART,MSTART,
     +JSTART,LDIM)
C
      CALL LOAD4(DATA,KKK,LSAMPL,NX,NY,II,JLAST,JTAP,LDIM)
      CALL FILTER(DATA,TF1,NN,LDIM)
      CALL LOAD4(DATA1,KKK,LSAMPL,NX,NY,II,JLAST,JTAP,LDIM)
      CALL FILTER(DATA1,TF1,NN,LDIM)
```

```
      CALL ADTAIL(DATA,DATA1,LLT,LDIM)
C
      CALL LOAD4(DATA2,KKK,LSAMPL,NX,NY,II,JLAST,JTAP,LDIM)
      CALL FILTER(DATA2,TF1,NN,LDIM)
      CALL ADTAIL(DATA1,DATA2,LLT,LDIM)
      CALL LOAD4(DATA3,KKK,LSAMPL,NX,NY,II,JLAST,JTAP,LDIM)
      CALL FILTER(DATA3,TF1,NN,LDIM)
      CALL ADTAIL(DATA2,DATA3,LLT,LDIM)
C
      CALL HPA(DATA,LSAMPL,NSTART,KKK,FNORI1,FNORD1,LDIM)
      CALL FILTER(DATA,TF2,NN,LDIM)
C
      CALL HPA(DATA1,LSAMPL,NSTART,KKK,FNORI1,FNORD1,LDIM)
      CALL FILTER(DATA1,TF2,NN,LDIM)
      CALL ADTAIL(DATA,DATA1,LLT,LDIM)
      CALL HPA(DATA2,LSAMPL,NSTART,KKK,FNORI1,FNORD1,LDIM)
      CALL FILTER(DATA2,TF2,NN,LDIM)
      CALL ADTAIL(DATA1,DATA2,LLT,LDIM)
C
      CALL TWT(DATA,LSAMPL,LSTART,KKK,FNORI2,FNORD2,LDIM)
      CALL FILTER(DATA,TF3,NN,LDIM)
C
      CALL TWT(DATA1,LSAMPL,LSTART,KKK,FNORI2,FNORD2,LDIM)
      CALL FILTER(DATA1,TF3,NN,LDIM)
      CALL ADTAIL(DATA,DATA1,LLT,LDIM)
C
      CALL DELAY(DATA,LSAMPL,NSTART,KKK,LDIM)
      CALL FILTER(DATA,TF4,NN,LDIM)
C
   50 CONTINUE
      DO 12 I=1,LDIM
      TATA1(I)=DATA(I)
      DATA(I)=DATA1(I)
      DATA1(I)=DATA2(I)
      DATA2(I)=DATA3(I)
   12 CONTINUE
C
      CALL LOAD4(DATA3,KKK,LSAMPL,NX,NY,II,JLAST,JTAP,LDIM)
      CALL FILTER(DATA3,TF1,NN,LDIM)
      CALL ADTAIL(DATA2,DATA3,LLT,LDIM)
C
      CALL HPA(DATA2,LSAMPL,NSTART,KKK,FNORI1,FNORD1,LDIM)
      CALL FILTER(DATA2,TF2,NN,LDIM)
      CALL ADTAIL(DATA1,DATA2,LLT,LDIM)
C
      CALL TWT(DATA1,LSAMPL,LSTART,KKK,FNORI2,FNORD2,LDIM)
      CALL FILTER(DATA1,TF3,NN,LDIM)
      CALL ADTAIL(DATA,DATA1,LLT,LDIM)
C
      CALL DELAY(DATA,LSAMPL,NSTART,KKK,LDIM)
      CALL FILTER(DATA,TF4,NN,LDIM)
      CALL ADTAIL(TATA1,DATA,LLT,LDIM)
      CALL DECOD4(TATA1,NRX,NRY,PE,PEI,KKK,LSAMPL,JSTART,NSNR,NERROR,
     *SNRDB,IK,NTOTAL,PNOISE,LOOP,JLAST,JTAP,NSYMB,PSHIFT)
C
      IF(LOOP.GT.LOOPM) GO TO 100
      GO TO 50
```

```
  100  CONTINUE
       BIRATE=BIRATE+DBRATE
       NTOTAL=0
       NERROR=0
       LOOP=0
       II=0
       IK=0
  507  CONTINUE
       STOP
       END
```

4.1 Subroutine LOAD4

From the tracking integers II and shift register contents NX(I) and NY(I), this subroutine generates a random sequence for both the x-channel and y-channel (12 symbols sampled at 16 times in each channel) and loads them into the DATA array (odd-numbered array for x-channel and even array for y-channel). This makes up 284 samples of DATA. The rest of the DATA array (from 385 to 512) are filled with zero for spillover effect of filters).

```
      SUBROUTINE LOAD4(DATA,KKK,LSAMPL,NX,NY,I,JLAST,JTAP,LDTM)
C**********************************************************************
C*
C*
C*    THIS SUBROUTINE GENERATES AN EQUIVALENT BASEBAND QPSK SIGNAL
C*
C*
C**********************************************************************
      DIMENSION DATA(512),NX(11),NY(11)
      DO 1 K=1,KKK
C
C     GENERATING ONE SYMBOL
C
      IF(I.EQ.JLAST) I=0
      I=I+1
      J=I-JTAP
      IF(I.LE.JTAP) J=J+JLAST
      IX=NX(J)*NX(I)
      IY=NY(J)*NY(I)
      NX(I)=IX
      NY(I)=IY
C
C     LOAD INTO THE ARRAY DATA TO BE FOURIER TRANSFORMED
C
      JA=2*LSAMPLI
      JB=K*JA
      J1=JB-JA+1
      J2=JB-1
      DO 2 J3=J1,J2,2
      DATA(J3)=IX
    2 DATA(J3+1)=IY
    1 CONTINUE
C
C     FILL THE REST OF THE ARRAY DATA WITH ZEROS FOR SPILL OVER EFFECT
C     OF FILTERS
C
      J4=J2+2
      DO 3 J3=J4,LDTM
    3 DATA(J3)=0.
      RETURN
      END
```

4.2 Subroutine DECOD4

From the tracking integer IK and shift register contents NRX(I) and NRY(I), this subroutine generates the same transmitted data for comparison with the received data. An integrate and dump filter is used to integrate the signal over one symbol interval and the average symbol energy is then calculated for probability of error P(e) computation. If the sign of this received symbol is different from that of the transmitted symbol, an error is registered. This means that the intersymbol interference caused by filtering effect is severe enough to cause an error in the absence of noise. After all the symbols are processed (NTOTAL = NSYMB), the P(e) of each symbol is summed up and then averaged over all symbols (NSYMB = 127).

N.B. For the systems considered in this study, an integrate and dump filter is not an optimum detector. However, the performance degradation due to mismatching is small. It is thus used to simplify the receiver decoding scheme. If a sampler is to be used, the noise has to be simulated. Simulation of noise requires long computer time, while the noise power at the output of the integrate and dump filter can be easily computed See Subroutine HHGG

```
      SUBROUTINE DECOD4(DATA,NRX,NRY,PE,PEI,KKK,LSAMPL,LSTART,NSNR,
     +NERROR,SNRDB,I,NTOTAL,PNOISE,LOOP,JLAST,JTAP,NSYMB,PSHIFT)
C*****************************************************************
C*
C*
C*    THIS SUBROUTINE DECODES THE RECEIVED DATA AFTER IT PASSES
C*    THE I AND D DETECTOR AND THEN COMPARES IT WITH THE TRANSMITTED DATA
C*    FOR ERROR DETECTION. EACH RECEIVED SYMBOL HAS A SCALED
C*    AMPLITUDE CHANGE BECAUSE OF DISTORTION BY THE FILTERS AND
C*    THE TWO CASCADED NONLINEARITIES. BASED ON THIS, TOGETHER
C*    WITH THE EFFECTIVE NOISE COMPUTED AFTER IT PASSES THROUGH
C*    THE RECEIVE FILTER TF4 (PERFORMED AT THE SUBROUTINE HHGG),
C*    THE AVERAGED P(E) OVER ALL SYMBOLS IS THEN OBTAINED.
C*
C*
C*
C*****************************************************************
      DIMENSION DATA(512),NRX(11),NRY(11),PE(25),PEI(25),SNRDB(25)
      COSPS=COS(PSHIFT)
      SINPS=SIN(PSHIFT)
      DO 1 K=1,KKK
C
C     REGENERATING THE TRANSMITTED SYMBOLS
C
      IF(I.EQ.JLAST) I=0
      I=I+1
      J=I-JTAP
      IF(I.LE.JTAP) J=J+JLAST
      IX=NRX(J)*NRX(I)
      IY=NRY(J)*NRY(I)
      NRX(I)=IX
      NRY(I)=IY
C
C     FIRST LOOP SYMBOLS ARE NOT PROCESSED
C
      IF(LOOP.EQ.0) GO TO 1
C
C     DECODING
C
      J1=LSTART+2*LSAMPL*(K-1)
      J2=LSTART+2*(LSAMPL*K-1)
      AMPLIX=0.
      AMPLIY=0.
      DO 2 J3=J1,J2,2
C
C     AVERAGED SYMBOL AMPLITUDE
C
      AMPLIX=AMPLIX+DATA(J3)
    2 AMPLIY=AMPLIY+DATA(J3+1)
      AMPLIX=AMPLIX/LSAMPL
      AMPLIY=AMPLIY/LSAMPL
      AXBAR=AMPLIX*COSPS+AMPLIY*SINPS
      AYBAR=AMPLIY*COSPS-AMPLIX*SINPS
      INDEXX=0
      IF(SIGN(1.,AXBAR).NE.IX) INDEXX=1
      INDEXY=0
```

```
      IF(SIGN(1.,AYBAR).NE.IY) INDEXY=1
      IF((INDEXX.EQ.1).OR.(INDEXY.EQ.1)) NERROR=NERROR+1
C
C     COMPUTE PROBABILITY OF ERROR FOR THIS SYMBOL
C
      CALL PERR4(AXBAR,AYBAR,INDEXX,INDEXY,SNRDB,PEI,PNOISE,NSNR)
      DO 5 KK=1,NSNR
    5 PE(KK)=PE(KK)+PEI(KK)
      NTOTAL=NTOTAL+1
      IF(NTOTAL.NE.NSYMB) GO TO 1
      PRINT 150
  150 FORMAT(/4H SNR,10X,14HPROB. OF ERROR/)
      DO 500 II=1,NSNR
  500 PEI(II)=PE(II)/NSYMB
C
C     THE FOLLOWING STEP IS NEEDED TO CONVERT THE COMPUTED
C     ES/NO TO EB/NO (BOTH IN DB) WHERE ES IS THE SYMBOL
C     ENERGY AND EB IS THE BIT ENERGY. THE DIFFERENCE
C     BETWEEN THEM IS 3 DB FOR QPSK.
C
      DO 152 II=1,NSNR
      SNRDB(II)=SNRDB(II)-3.
  152 CONTINUE
C
      PRINT 151,(SNRDB(II),PEI(II),II=1,NSNR)
  151 FORMAT(F5.1,10X,E13.6)
      PRINT 102,NERROR
  102 FORMAT(/2X,7HERRORS=,I5)
      GO TO 132
    1 CONTINUE
  132 LOOP=LOOP+1
      RETURN
      END
```

4.3 Subroutine BISINC

To synchronize the transmitted data with the received data and compare them on a symbol-by-symbol basis for proper decoding, this subroutine computes the delays of the signal caused by a series of filters.

A single pulse of 16 samples is generated and passed through the first filter. Depending on the transfer function of this filter, the distorted pulse in comparison with the transmitted pulse is shown in Fig. 7 below:

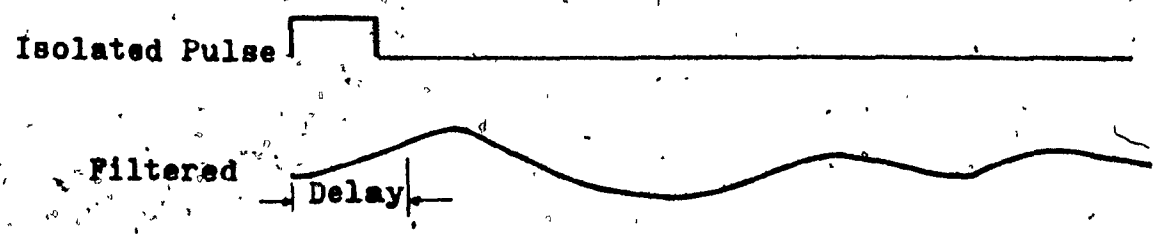

Fig. 7 Pulse Response of Filter

The distorted sampled signal is then summed 16 times to find the largest enclosed area (sum). The starting location of the largest enclosed area is then the delay of the signal caused by this filter (call NSTART).

Afterwards, this distorted signal is passed through the next filter used in the simulation. The same procedure is used to find the delays caused by each filter as shown in Fig. 8. The flow chart for this subroutine is illustrated in Fig. 9.

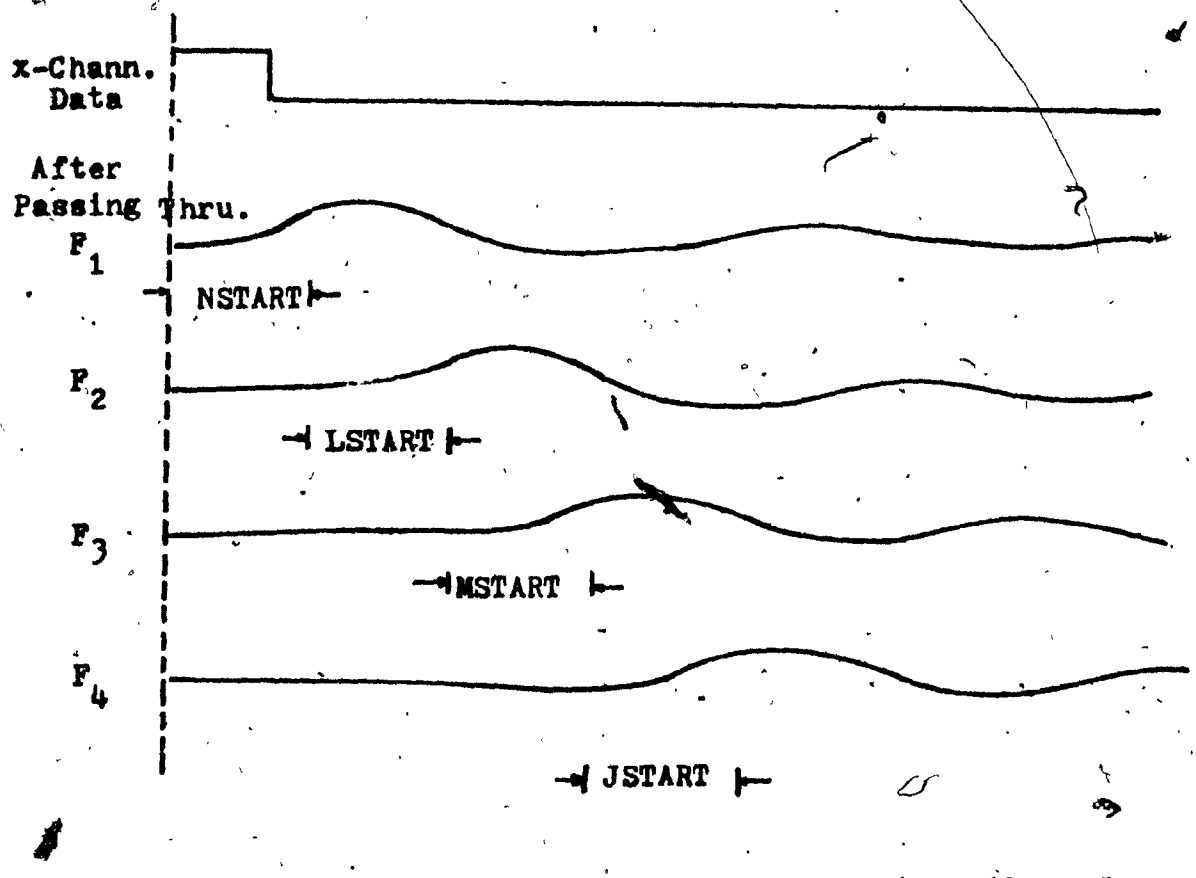

Fig. 8 Signal Waveforms before and after Being Filtered and the Associated Delays

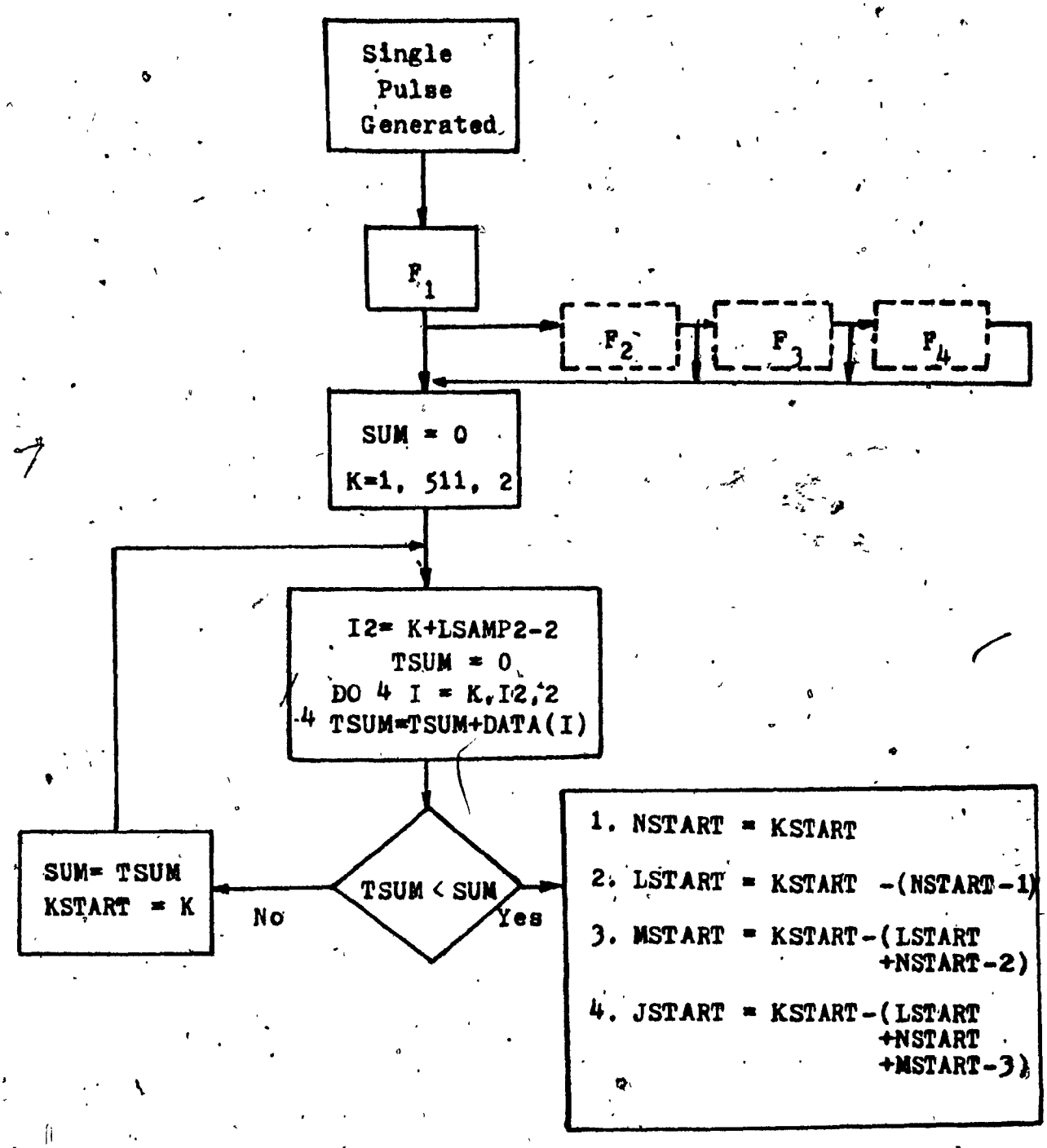

Fig. 9 Flow Chart for the Subroutine BISINC

```
      SUBROUTINE BISINC(DATA,TF1,TF2,TF3,TF4,LSAMPL,NSTART,LSTART,
     +MSTART,JSTART,LDIM)
C*****************************************************************
C
C     TO SYNCHRONIZE THE TRANSMITTED DATA WITH THE RECEIVED DATA
C        FOR PROPER DECODING AT SUBROUTINE DECOD4, THIS SUBROUTINE
C        WILL COMPUTE THE DELAY INTRODUCED BY THE FOUR FILTERS.
C        THESE DELAYS ARE NAMED  NSTART, LSTART, MSTART AND JSTART.
C        (FOR EXPLANATION SEE MANUAL UNDER THE SECTION BIT SYNCHRO-
C         NATION).
C
C
C*****************************************************************
      DIMENSION DATA(512),TF1(512),TF2(512),TF3(512),TF4(512)
      INDEX=0
      DO 1 I=1,LDIM
    1 DATA(I)=0.
      LSAMP2=2*LSAMPL
      I1=LSAMP2-1
      DO 2 I=1,I1,2
    2 DATA(I)=1.
      CALL FILTER(DATA,TF1,256,LDIM)
    5 SUM=0.
      DO 3 K=1,511,2
      I2=K+LSAMP2-2
      TSUM=0.
      DO 4 I=K,I2,2
    4 TSUM=TSUM+DATA(I)
      IF(TSUM.LT.SUM)GO TO 3
      SUM=TSUM
      KSTART=K
    3 CONTINUE
      INDEX=INDEX+1
      IF(INDEX.GT.1)GO TO 6
      NSTART=KSTART
      CALL FILTER(DATA,TF2,256,LDIM)
      GO TO 5
    6 LSTART=KSTART-(NSTART-1)
      INDEX=0
      CALL FILTER(DATA,TF3,256,LDIM)
    7 SUM=0.
      DO 13 K=1,511,2
      I2=K+LSAMP2-2
      TSUM=0.
      DO 14 I=K,I2,2
   14 TSUM=TSUM+DATA(I)
      IF(TSUM.LT.SUM) GO TO 13
      SUM=TSUM
      KSTART=K
   13 CONTINUE
      INDEX=INDEX+1
      IF(INDEX.GT.1) GO TO 16
      MSTART=KSTART-(LSTART+NSTART-2)
      CALL FILTER(DATA,TF4,256,LDIM)
      GO TO 7
   16 JSTART=KSTART-(LSTART+MSTART+NSTART-3)
      PRINT 36,NSTART,LSTART,MSTART,JSTART
   36 FORMAT(/5X,'NSTART=',I3,'  LSTART=',I3,'  MSTART=',I3,'  JSTART=',
     +I3/)
      RETURN
      END
```

4.4 Subroutine CF4P5

This subroutine generates the complex transfer function of a Chebychev (or Butterworth) filter from the polynomial coefficients.

For example, the polynomial of a 4 pole Chebychev filter can be written as:

$$H(s) = C_1 + C_2 s + C_3 s^2 + C_4 s^3 + s^4$$

where $s = \sigma + j\omega$ is the complex variable.

The transfer function is arranged as shown in Fig. 10

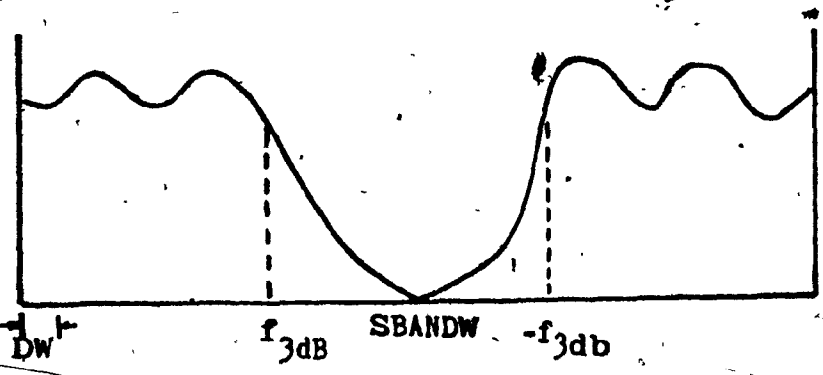

$$DW = \frac{SBANDW}{FBANDW * 128}$$

$$s = j\omega = j\,(N)\,DW$$

Fig. 10 Amplitude Transfer Function of a Filter

Real part of the transfer function = $C_1 + C_3\ W^2 + W^4$

Imaginary part of the transfer function = $C_2 W + C_4 W^3$

The coefficient of W^4 is 1, so $C_5 = 1$. In CF4P5, IC is the number of poles. When a Chebychev or Butterworth type of filter is used, it is always assumed that the coefficient C(IC+1) = 1.

```
      SUBROUTINE CF4P5(SBANDW,FBANDW,TF,LDIM,C,IC)
*****************************************************************************
*
*     THIS SUBROUTINE COMPUTES THE COMPLEX TRANSFER FUNCTION OF A
*     STANDARD FILTER SUCH AS A CHEBYCHEV FILTER WHOSE COMPLEX
*     POLYNOMIAL COEFFICIENTS C(I) AND WHOSE NUMBER OF POLES ARE
*     KNOWN. IF THE POLES ARE KNOWN, REPLACE THIS SUBROUTINE WITH
*     CF4PA FROM THE MANUAL. FOR BUTTERWORTH FILTERS, SLIGHT
*     MODIFICATIONS ARE NEEDED.
*
*****************************************************************************
      DIMENSION C(15),WW(20),TF(512)
      JK=IC+1
      C(JK)=1.
      JJ=JK
      NH=LDIM/2
      NO=LDIM/4
      DW=SBANDW/FLOAT(NH)/FBANDW*2.
      DO 1 I=2,NO
      W=DW*FLOAT(I-1)
      WS=-W*W
      SW=1.
      DO 2 J=1,JJ,2
      J1=J+1
      WW(J)=SW
      WW(J1)=SW*W
    2 SW=SW*WS
      SX=0.
      DO 3 J=1,JJ,2
    3 SX=SX+C(J)*WW(J)
      SY=0.
      DO 4 J=2,JJ,2
    4 SY=SY+C(J)*WW(J)
      SS=SX*SX+SY*SY
      SS=SS/C(1)
      X=SX/SS
      Y=SY/SS
      I2=I*2
      I1=I2-1
      TF(I1)=X
      TF(I2)=-Y
      I2=2*(NH-I+2)
      I1=I2-1
      TF(I1)=X
      TF(I2)=Y
    1 CONTINUE
      TF(1)=1.
      TF(2)=0.
      TF(NH+1)=0.
      TF(NH+2)=0.
      RETURN
      END
```

4.5 Subroutine MEASUR

From the measured amplitude and phase characteristics of a filter, the program RAWFIT, or any curve fitting subroutine, can be used to obtain the coefficients of the polynomials that fit these two measured curves (or measured data). This subroutine will then compute the complex transfer function of this filter from these coefficients (CA(I) and GP(I) respectively).

```
      SUBROUTINE MEASUR(SBANDW,FBANDW,TF,LDIM,CA,CP)
C*****************************************************************
C
C     MEASURED AMPLITUDE AND PHASE CHARACTERISTICS OF THE FILTER
C     ARE TRANSFORMED INTO COMPLEX TRANSFER FUNCTION
C
C*****************************************************************
      DIMENSION TF(512),CA(14),CP(14)
      NH=LDIM/2
      NO=LDIM/4
      DW=SBANDW/FLOAT(NH)/FBANDW*2.
C
      DO 31 I=1,LDIM
   31 TF(I)=0.
C
      DO 4 I=2,NO
      W=DW*FLOAT(I-1)
      W=W*FBANDW/2.
      F1=W
      F2=F1*F1
      F3=F2*F1
      F4=F2*F2
      F5=F4*F1
      F6=F3*F3
      F7=F6*F1
      F8=F4*F4
      F9=F8*F1
      F10=F5*F5
      F11=F10*F1
      F12=F6*F6
      F13=F12*F1
      X=CA(14)+CA(1)*F1+CA(2)*F2+CA(3)*F3+CA(4)*F4+CA(5)*F5
     *      +CA(6)*F6+CA(7)*F7+CA(8)*F8+CA(9)*F9+CA(10)*F10
     *       +CA(11)*F11+CA(12)*F12+CA(13)*F13
      Y=CP(1)*F1+CP(2)*F2+CP(3)*F3+CP(4)*F4+CP(5)*F5
     *      +CP(6)*F6+CP(7)*F7+CP(8)*F8+CP(9)*F9
     *       +CP(10)*F10+CP(11)*F11+CP(12)*F12+CP(13)*F13
```

```
C
      IF(X.LT.0.) GO TO 5
      Y=Y/57.2957795
      XX=X*COS(Y)
      YY=X*SIN(Y)
      SS=CA(14)
      XX=XX/SS
      YY=YY/SS
C
      I2=I+2
      I1=I2-1
      TF(I1)=XX
      TF(I2)=-YY
      I2=2*(NH-I+2)
      I1=I2-1
      TF(I1)=XX
      TF(I2)=YY
    4 CONTINUE
    5 CONTINUE
      TF(1)=1.
      TF(2)=0.
      TF(NH+1)=0.
      TF(NH+2)=0.
      RETURN
      END
```

4.6 Subroutines HPA and TWT

These two subroutines are basically identical. The only difference lies in the polynomial coefficients that represent the nonlinear characteristics of these two power devices. The model used in the simulation is based on Eric's quadrature model (C2) such as shown in Fig. 11.

If the input signal to a nonlinear power amplifier is given by:

$$V_i(t) = r(t) \cos\left[w_c t + \theta(t)\right]$$
$$= \mathrm{Re}\left\{\left[x(t) + j\,y(t)\right] \cdot e^{jw_c t}\right\} \qquad (C1)$$

where, r(t) and $\theta(t)$ are the envelope and phase functions respectively, and x(t) and y(t) are the real and imaginary parts of the complex baseband signal. (w_c is the carrier frequency in radian.)

Then, the output complex baseband signal of the nonlinear power amplifier is given by:

$$V_o(t) = Z(t) \cos\left[w_c t + \theta(t) + \phi(t)\right] \qquad (C2)$$

where,

$Z(t) = Z(r(t))$ is the amplitude distortion and,

$\phi(t) = \phi(r(t))$ is the phase distortion introduced by the nonlinear power amplifier.

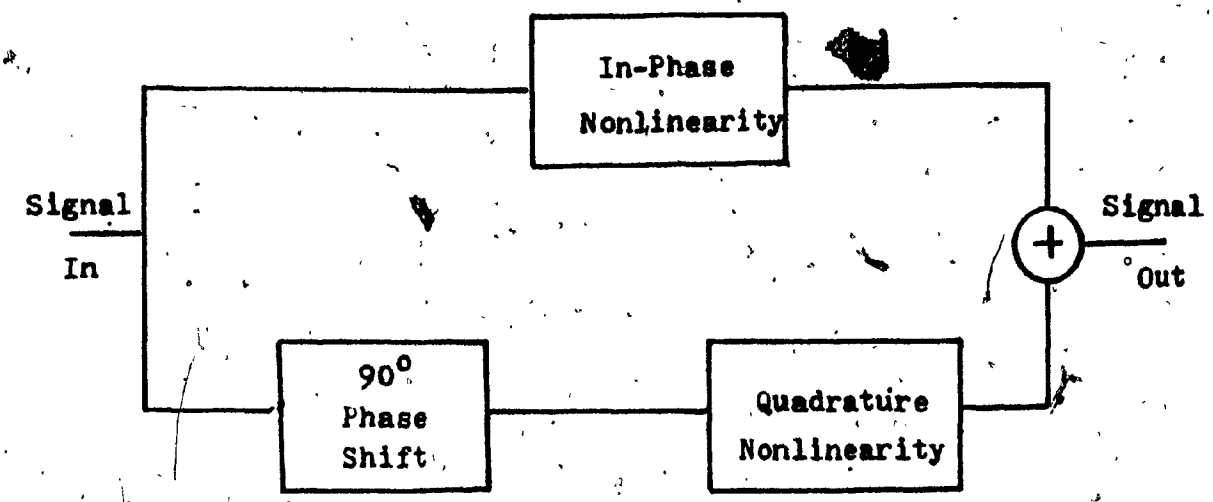

Fig. 11 Quadrature Model of a Nonlinear Power Amplifier

The quadrature model of the nonlinear devices gives:

$$V_o(t) = Z_p(r) \cos\left[w_c t + \theta(t)\right] - Z_q(r) \sin\left[w_c t + \theta(t)\right] \qquad (C3)$$

where

$$Z_p(r) = Z(r) \cos \phi(r) \qquad (C4)$$

and

$$Z_q(r) = Z(r) \sin \phi(r)$$

The polynomial representation of $Z_p(V)$ and $Z_q(r)$ contain only the odd-power (C1) and are given by:

$$Z_p(r) = \sum_{i=0}^{N} a_{2i+1} \; r^{2i+1}$$

and (C5)

$$Z_q(r) = \sum_{i=0}^{N} b_{2i+1} \; r^{2i+1}$$

Procedures in Computing the Coefficients a_{2i+1} and b_{2i+1}

From the experimentally measured curves of output power and phase shift versus input power, such as shown in Fig. 12, Fig. 13 is obtained using the following power and voltage relationships:

a) Input peak voltage x mV

$$P_{in}(\text{input power}) = \frac{1}{2}\frac{(x.\,10^{-3})^2}{1\,\Omega} = \frac{1}{2}\,(x^2 .\,10^{-3})\ \text{mW} \tag{C6}$$

Expressed in dBm,

$$P_{in} = 10\log_{10}\tfrac{1}{2}(x^2 .\,10^{-3}) = \left[20\log_{10} x - 33\right]\ \text{dBm} \tag{C7}$$

b) Output peak voltage y V,

$$P_{out}(\text{output power}) = \frac{1}{2}\ \frac{y^2}{1\Omega}\ \text{W} \tag{C8}$$

Expressed in dBW,

$$P_{out} = 10\log_{10}\tfrac{1}{2}\,y^2 = \left[20\log_{10} y - 3\right]\ \text{dBW} \tag{C9}$$

From Fig. 13, Fig. 14 is obtained (point by point for those data points of interest) using Eqs. (C4) and (C5).

As explained previously, $Z_p(x)$ and $Z_q(x)$ of the quadrature model are odd functions of x (Eq. (C5)). To obtain the polynomials that will fit these two curves using program RAWFIT or any other curve fitting subroutine, third quadrant data points must be used. For example, if n data

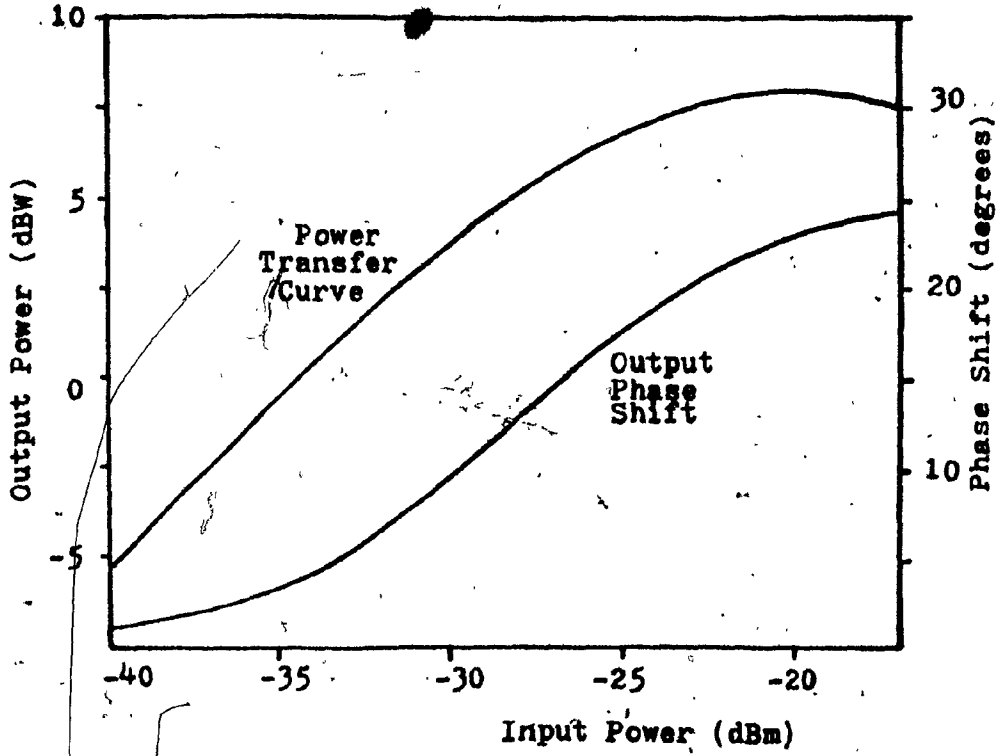

Fig. 12 The Single-Carrier Characteristics of Hughes 261-H TWT

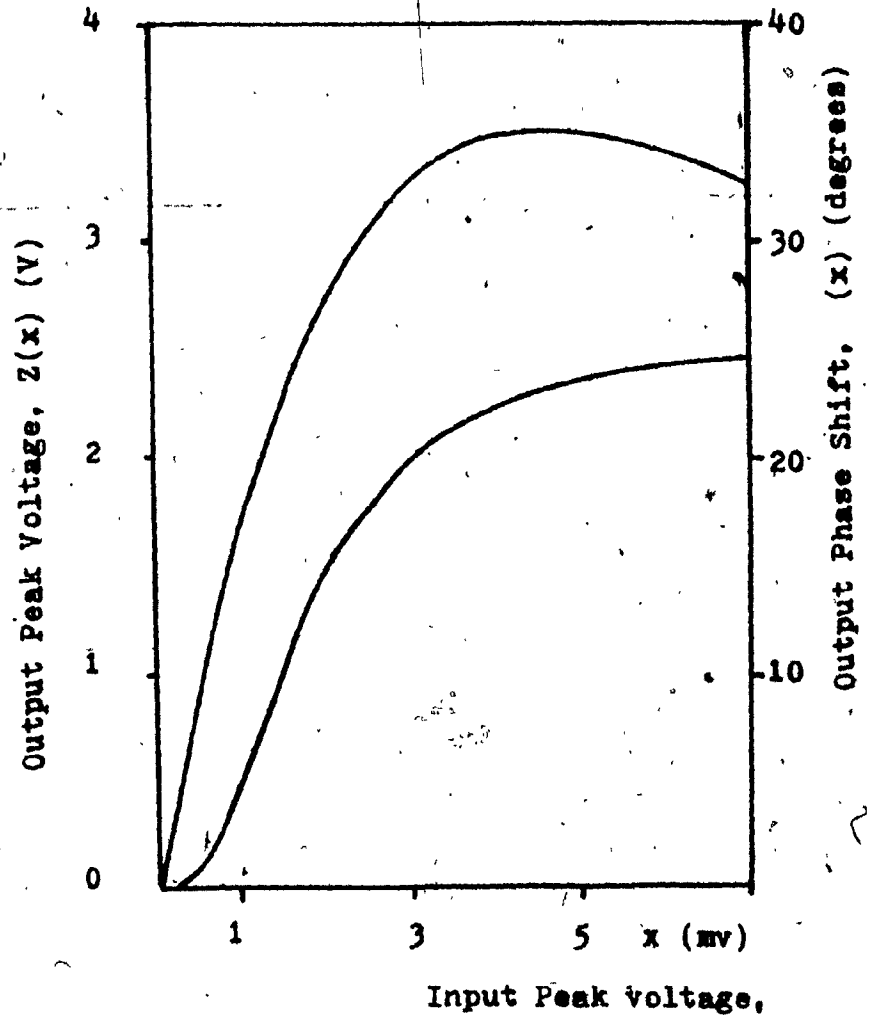

Fig. 13 Curves Z(x) and (x), Derived from Measured Curves of Fig. 12

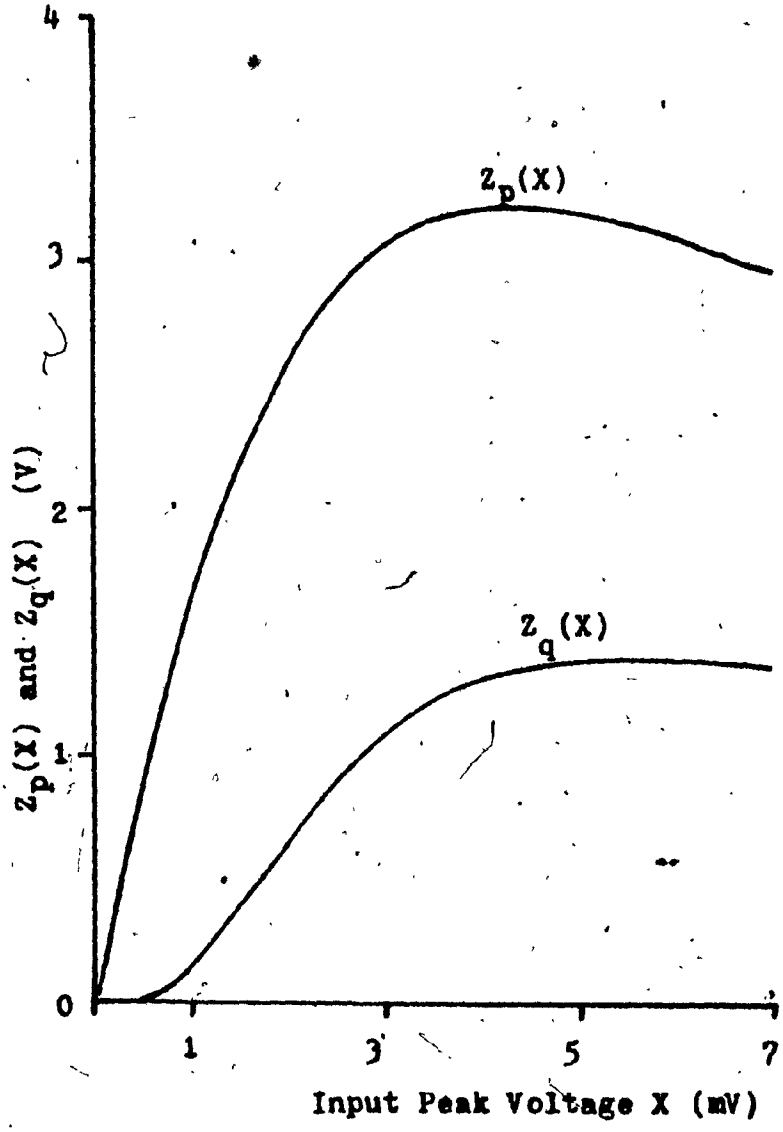

Fig. 14 The Polynomial Fits to $Z_p(X)$ and $Z_q(X)$

points of $Z_p(x)$ are used, then n mirror image points of $Z_p(x)$, plus the origin, (together making up 2n+1 data points) are also needed. In this way, only coefficients of the odd powered polynomial will come out of the curve fitting subroutine.

Fig. 15 serves as an example.

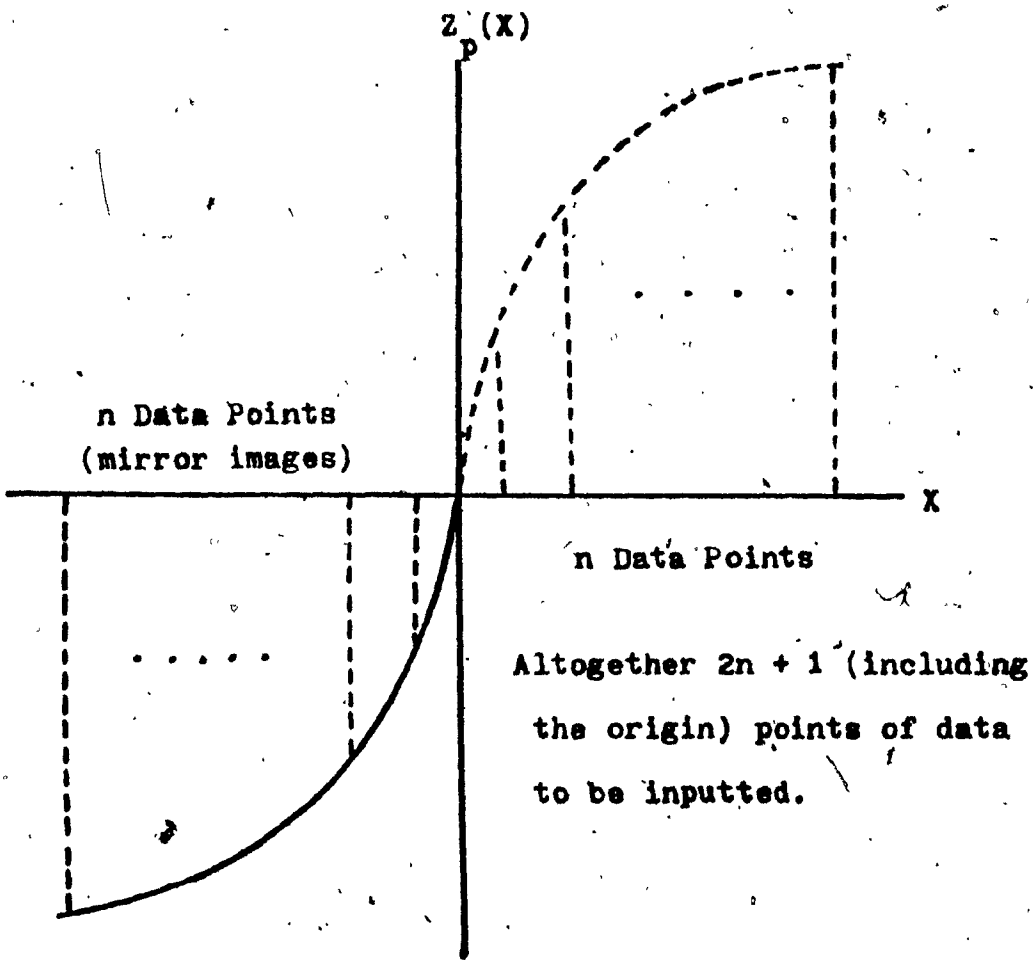

Fig. 15 Curve-fitting Data Points for Odd-Powered Polynomial Fitting

```
      SUBROUTINE HPA(DATA,LSAMPL,NSTART,KKK,FNORMI,FNORMO,LDIM)
C*****************************************************************
C
C     TO OBTAIN THE FOLLOWING POLYNOMIAL COEFFICIENTS OF THE
C     QUADRATURE MODEL OF HPA, SEE INSTRUCTION MANUAL.
C
C     THIS SUBROUTINE FOLLOWS THE DESCRIPTION IN THE MCMASTER
C          REPORT.....
C
C     IF HPA IS TO BE BYPASSED, SET SW1 = TRUE.
C
C     THIS SUBROUTINE ALSO PERFORMS THE DELAY COMPENSATION
C     INTRODUCED BY THE FILTER BEFORE THE HPA.
C
C*****************************************************************
      DIMENSION DATA(512),ZP(9),ZQ(9)
      LOGICAL SW1
      DATA ZP(1),ZP(2),ZP(3),ZP(4),ZP(5),ZP(6),ZP(7),ZP(8),ZP(9)
     1/1.76245,-1.59871E-1,1.35508E-2,-9.07704E-4,4.2041E-5,
     2-1.28062E-6,2.41983E-8,-2.5508E-10,1.1074E-12/
      DATA ZQ(1),ZQ(2),ZQ(3),ZQ(4),ZQ(5),ZQ(6),ZQ(7),ZQ(8),ZQ(9)
     1/-1.99286E-3,1.81398E-1,-3.43698E-2,3.37647E-3,-1.93769E-4,
     26.67438E-6,-1.35523E-7,1.49262E-9,-6.86914E-12/
      DATA ZPMAX,ZQMAX,VMAX/3.09,1.31,6./
      J2=9
      I1=2*KKK*LSAMPL
      SW1=F
      IF(SW1) GO TO 5
    6 CONTINUE
      DO 120 II=1,I1,2
      I2=II+NSTART-1
      X=DATA(I2)*FNORMI
      Y=DATA(I2+1)*FNORMI
      RR=X*X+Y*Y
      R=SQRT(RR)
      IF(R.GT.VMAX)GO TO 1
      P=ZP(1)
      Q=ZQ(1)
      DO 121 JJ=2,J2
      Q=Q+ZQ(JJ)*RR**(JJ-1)
      P=P+ZP(JJ)*RR**(JJ-1)
  121 CONTINUE
      DATA(II)=(P*X-Q*Y)/FNORMO
      DATA(II+1)=(Q*X+P*Y)/FNORMO
      GO TO 120
    1 DATA(II)=(ZPMAX*X-ZQMAX*Y)/FNORMO/R
      DATA(II+1)=(ZQMAX*X+ZPMAX*Y)/FNORMO/R
  120 CONTINUE
      GO TO 23
    5 CONTINUE
      DO 22 II=1,I1,2
      I2=II+NSTART-1
      DATA(II)=DATA(I2)
      DATA(II+1)=DATA(I2+1)
   22 CONTINUE
   23 I3=I1+1
      DO 122 II=I3,LDIM
```

```
      DATA(II)=0.
  122 CONTINUE
      RETURN
      END
```

```
      SUBROUTINE TWT(DATA,LSAMPL,NSTART,KKK,FNORMI,FNORMO,LDIM)
*****************************************************************
*
*     TO OBTAIN THE FLLOWING POLYNOMIAL COEFFICIENTS OF THE
*     QUADRATURE MODEL OF TWT, SEE INSTRUCTION MANUAL.
*
*     THIS SUBROUTINE FOLLOWS THE DESCRIPTION IN THE MCMASTER
*          REPORT.......
*
*     IF TWT IS TO BE BYPASSED, SET SW2 = TRUE.
*
*     THIS SUBROUTINE ALSO PERFORMS THE DELAY COMPENSATION
*     INTRODUCED BY THE FILTER BEFORE THE TWT.
*
*****************************************************************
      DIMENSION DATA(512),ZP(9),ZQ(9)
      LOGICAL SW2
      DATA ZP(1),ZP(2),ZP(3),ZP(4),ZP(5),ZP(6),ZP(7),ZP(8),ZP(9)
     1/1.76245,-1.53871E-1,1.35508E-2,-9.07704E-4,4.2041E-5,
     2-1.28062E-6,2.41983E-8,-2.5508E-10,1.1074E-12/
      DATA ZQ(1),ZQ(2),ZQ(3),ZQ(4),ZQ(5),ZQ(6),ZQ(7),ZQ(8),ZQ(9)
     1/-1.99286E-3,1.81398E-1,-3.43698E-2,3.37647E-3,-1.93769E-4,
     26.67438E-6,-1.35523E-7,1.49262E-9,-6.86914E-12/
      DATA ZPMAX,ZQMAX,VMAX/3.09,1.31,6./
      J2=9
      I1=2*KKK*LSAMPL
      SW2=F
      IF(SW2) GO TO 5
    6 CONTINUE
      DO 120 II=1,I1,2
      I2=II+NSTART-1
      X=DATA(I2)*FNORMI
      Y=DATA(I2+1)*FNORMI
      RR=X*X+Y*Y
      R=SQRT(RR)
      IF(R.GT.VMAX) GO TO 1
      P=ZP(1)
      Q=ZQ(1)
      DO 121 JJ=2,J2
```

```
      Q=Q+ZQ(JJ)*(RR**(JJ-1))
      P=P+ZP(JJ)*(RR**(JJ-1))
  121 CONTINUE
      DATA(II)=(P*X-Q*Y)/FNORMO
      DATA(II+1)=(Q*X+P*Y)/FNORMO
      GO TO 120
    1 DATA(II)=(ZPMAX*X-ZQMAX*Y)/FNORMO/R
      DATA(II+1)=(ZQMAX*X+ZPMAX*Y)/FNORMO/R
  120 CONTINUE
      GO TO 23
    5 CONTINUE
      DO 22 II=1,I1,2
      I2=II+NSTART-1
      DATA(II)=DATA(I2)
      DATA(II+1)=DATA(I2+1)
   22 CONTINUE
   23 I3=I1+1
      DO 122 II=I3,LDIM
      DATA(II)=0.
  122 CONTINUE
      RETURN
      END
```

```
      SUBROUTINE DELAY(DATA,LSAMPL,NSTART,KKK,LDIM)
*****************************************************************
*
*     THIS SUBROUTINES TAKES CARE OF THE DELAY INTRODUCED BY THE
*          FILTER.
*     THIS OPERATION ALSO OCCURS AT THE HPA AND TWT
*          (SEE SUBROUTINES HPA AND TWT)
*
*****************************************************************
      DIMENSION DATA(512)
      I1=2*KKK*LSAMPL
      DO 120 II=1,I1,2
      I2=II+NSTART-1
      DATA(II)=DATA(I2)
      DATA(II+1)=DATA(I2+1)
  120 CONTINUE
      I3=I1+1
      DO 122 II=I3,LDIM
      DATA(II)=0.
  122 CONTINUE
      RETURN
      END
```

4.8

```
      SUBROUTINE PERR(AMPLIX,AMPLIY,INDEXX,INDEXY,SNRDB,PEI,
     +PNOISE,NSNR)
*****************************************************************
*
*     THIS SUBROUTINE COMPUTES P(E) OF EACH DETECTED SYMBOL
*
*****************************************************************
      DIMENSION PEI(25),SNRDB(25)
      DO 1 M=1,NSNR
      SNR=EXP(SNRDB(M)*.23026)
      SCALE=SQRT(SNR/PNOISE/2.)
      XX=AMPLIX*SCALE
      ABSX=ABS(XX)
      CALL TTERFC(ABSX,EX)
      EX=EX/2.
      IF(INDEXX.EQ.1) EX=1.-EX
      YY=AMPLIY*SCALE
      ABSY=ABS(YY)
      CALL TTERFC(ABSY,EY)
      EY=EY/2.
      IF(INDEXY.EQ.1) EY=1.-EY
    1 PEI(M)=EX+EY-EX*EY
      RETURN
      END
```

4.9

```
      SUBROUTINE ADTAIL(ARRAYA,ARRAYB,LLT,LDIM)
*****************************************************************
*                                                               *
*     THIS SUBROUTINE PERFORMS THE ADD-THE-TAIL OPERATION       *
*     TO COMPENSATE OF THE SPILLOVER EFFECT OF FILTERING        *
*                                                               *
*****************************************************************
      DIMENSION ARRAYA(512),ARRAYB(512)
      I2=2*LLT
      DO 1 II=1,I2
      IJ=LDIM-I2+II
      ARRAYB(II)=ARRAYB(II)+ARRAYA(IJ)
    1 ARRAYA(IJ)=ARRAYB(II)
      RETURN
      END
```

4.10

```
      SUBROUTINE CALCON(LSAMPL,LLTNOM,KKK,LLT,NSYMB,JLAST,
     1LOOPM,LDIM,BIRATE,SBANDW)
*****************************************************************
*                                                               *
*     THIS SUBROUTINE COMPUTES FROM THE INPUT DATA CONSTANTS    *
*          NEEDED IN THE SIMULATION                             *
*                                                               *
*****************************************************************
      SBANDW=BIRATE*LSAMPL
      LL=LDIM/2
      AKK=(LL-LLTNOM)/LSAMPL
      KKK=IFIX(AKK)
      LLT=LL-(KKK*LSAMPL)
      NSYMB=2**JLAST-1
      SYMB=NSYMB
      SKK=KKK
      POOL=SYMB/SKK
      LOOPM=IFIX(POOL)
      X=LOOPM
      IF(X.LT.POOL)LOOPM=LOOPM+1
      RETURN
      END
```

4.11

```
      SUBROUTINE HHGG(TF,PNOISE,LSAMPL,LDIM)
*****************************************************************
*
*     THIS SUBROUTINE COMPUTES THE EFFECTIVE NOISE (PNOISE)
*     AT THE OUTPUT OF THE RECEIVE FILTER TF4 AND THE I AND D
*     DETECTOR
*
*****************************************************************
      DIMENSION TF(512)
      LL=LDIM/2
      SAMPLE=LSAMPL
      SUM=SAMPLE**2
      ANG=3.141593/LL
      DO 1 L=2,LL
      LX=2*L-1
      LY=2*L
      HH=TF(LX)**2+TF(LY)**2
      ANGLE=ANG*FLOAT(L-1)
      ANGLES=ANGLE*SAMPLE
      GG=(SIN(ANGLES)/SIN(ANGLE))**2
      SUM=SUM+HH*GG
    1 CONTINUE
      SHHGG=SUM/SAMPLE**2
      PNOISE=SHHGG*SAMPLE/LL
      RETURN
      END
```

```
      SUBROUTINE FILTER(SIGNAL,TF,N,LDIM)
*************************************************************************
*
*     THIS SUBROUTINE PERFORMS THE OPERATION OF FOURIER TRANSFORM,
*     THE SIGNAL ARRAY INTO FREQUENCY DOMAIN AND MULTIPLYING IT
*     WITH THE FILTER TRANSFER FUNCTION TF. THE RESULT IS STORED
*     IN THE ARRAY SIGNAL.
*
*     THE SUBROUTINE FFT2RV IS ATTACHED FROM IMSLIB. ALSO THE
*     FOLLOWING THREE SUBROUTINES ARE NEEDED  NONCOM,CONJUG, BITREV
*
*************************************************************************
      DIMENSION SIGNAL(1024),TF(1024)
      DIMENSION IWK(9)
      COMPLEX A(512)
C
      CALL CONJUG(A,SIGNAL,N,1.)
C
      CALL BITREV(A,N)
C
      CALL FFT2RV(A,B,IWK)
C
      CALL NONCOM(A,SIGNAL,N)
      CALL CONJUG(A,SIGNAL,N,-1.)
      CALL NONCOM(A,SIGNAL,N)
C
      DO 1 II=1,LDIM,2
           X=SIGNAL(II)
           Y=SIGNAL(II+1)
           SIGNAL(II)=TF(II)*X - TF(II+1)*Y
           SIGNAL(II+1)=TF(II+1)*X + TF(II)*Y
    1 CONTINUE
C
      CALL CONJUG(A,SIGNAL,N,1.)
C
      CALL BITREV(A,N)
C
      CALL FFT2RV(A,B,IWK)
C
      CALL NONCOM(A,SIGNAL,N)
C
      CALL CONJUG(A,SIGNAL,N,-1.)
      CALL NONCOM(A,SIGNAL,N)
C
      DO 11 I=1,LDIM
           SIGNAL(I)=SIGNAL(I)/FLOAT(N)
   11 CONTINUE
C
      RETURN
      END
```

4.13

```
      SUBROUTINE BITREV(SIGNAL,LDIM)
*************************************************************************
*                                                                       *
*     THIS SUBROUTINE PERFORMS THE BIT REVERSING ORDER REQIURED         *
*          CALLED FOR AFTER FFT.                                        *
*                                                                       *
*************************************************************************
      DIMENSION SIGNAL(512),INDEX(512),Y(512)
      COMPLEX SIGNAL,Y
      INDEX(1)=1
      INDEX(2)=1+LDIM/2
      J=2
      IDIV=1
 20   CONTINUE
      IDIV=IDIV*2
      INCR=LDIM/IDIV
      IF(INCR .EQ. 1) GO TO 50
      K=1
      DO 10 I=1,LDIM,INCR
            J=J+1
            INDEX(J)=INDEX(K)+INCR/2
            K=K+1
 10   CONTINUE
      GO TO 20
 50   CONTINUE
      DO 100 I=1,LDIM
            Y(I)=SIGNAL(I)
 100  CONTINUE
      DO 1000 I=1,LDIM
            K=INDEX(I)
            SIGNAL(I)=Y(K)
 1000 CONTINUE
      RETURN
      END
```

4.14

```
      SUBROUTINE NONCOM(A,SIGNAL,N)
*****************************************************************
*                                                               *
*     THIS SUBROUTINE CHANGES A COMPLEX NUMBER INTO REAL AND IMAGINARY PARTS
*                                                               *
*****************************************************************
C
      DIMENSION A(512),SIGNAL(1024)
      COMPLEX A
      DO 11 I=1,N
            II=I*2
            IR=II-1
            SIGNAL(IR)=REAL(A(I))
            SIGNAL(II)=AIMAG(A(I))
11    CONTINUE
      RETURN
      END
```

4.15

```
      SUBROUTINE CONJUG(A,SIGNAL,N,R)
C
C     THIS SUBROUTINE OBTAINS A COMPLEX NUMBER FROM ITS REAL AND
C          IMAGINARY PARTS
C
      DIMENSION SIGNAL(1024),XR(512),XI(512)
      COMPLEX A(512)
      DO 11 I=1,N
            II=I*2
            IR=II-1
            XR(I)=SIGNAL(IR)
            XI(I)=SIGNAL(II)*R
            A(I)=CMPLX(XR(I),XI(I))
11    CONTINUE
      RETURN
      END
```

```
      SUBROUTINE ITERFC(Y,Z)
*********************************************************************
*
*     THIS SUBROUTINE COMPUTES THE COMPLEMENTARY ERROR FUNCTION
*          THE ACCURACY IS ONLY GOOD TO ABOUT E-10.
*
*********************************************************************
      DIMENSION A(10),P(8),Q(9)
      DATA C/1.1283792/
      DATA A(1),A(2),A(3),A(4),A(5),A(6),A(7),A(8),A(9),A(10)
     1/1.,-0.33333333,0.1,-0.023809238,0.46296296E-2,
     2-0.75757576E-3,1.0683761E-4,-1.3227513E-5,1.4589169E-6,
     3-1.4503855E-7/
      DATA P(1),P(2),P(3),P(4),P(5),P(6),P(7),P(8)
     1/883.47894,1549.6793,1347.1941,723.04,255.50049,
     259.24001,8.3765311,.56418956/
      DATA Q(1),Q(2),Q(3),Q(4),Q(5),Q(6),Q(7),Q(8),Q(9)
     1/883.47894,2546.5785,3337.2214,2606.712,1333.57,
     2460.28512,105.50025,14.847012,1./
      KRET=1
    5 X=Y
      MD=0
   10 ISW=2
      IF(X.GE.0.)GO TO 15
      ISW=1
      X=-X
   15 IF(KRET.NE.2)GO TO 60
      IF(X.LE.5.5)GO TO 20
      Z=1.
      IF(ISW.EQ.1)Z=-1.
      GO TO 100
   20 IF(X.LE..47)GO TO 45
      KRET=1
   25 SN=P(8)
      SD=Q(9)
      DO 30 J=1,7,1
      I=8-J
      SN=SN*X+P(I)
   30 CONTINUE
      DO 35 J=1,8
      I=9-J
      SD=SD*X+Q(I)
   35 CONTINUE
      Z=SN/SD*EXP(-X*X)
      IF(KRET.NE.1)GO TO 40
      Z=1.-Z
      IF(ISW.NE.2)Z=-Z
      GO TO 100
   40 IF(ISW.NE.2)Z=2.-Z
      IF(MD.NE.0)Z=.5*Z
      GO TO 100
   45 XX=X*X
      Z=A(10)
      DO 50 J=1,9
      I=10-J
      Z=Z*XX+A(I)
   50 CONTINUE
```

```
      Z=C*Z*X
      IF (KRET.NE.2) GO TO 55
      IF (ISW.NE.2) Z=-Z
      GO TO 100
   55 Z=1.-Z
      GO TO 40
   60 IF(X.LE.9.)GO TO 65
      Z=0.
      GO TO 40
   65 IF(X.LE..47)GO TO 70
      KRET=2
      GO TO 25
   70 IF(X.GT.1.E-15)GO TO 45
      Z=1.
      GO TO 40
  100 RETURN
      END
```

5. How to Input the Necessary Data of Interest and Run the Program

The following are the step by step procedures for inputting the required data (such as bit rate, the nonlinear characteristics of HPA and TWT, and the filter characteristics). It also includes some examples of how to run the time-sharing TELEX at Concordia University where CDC 6600 is currently available.

5.1 READ*, BIRATE, ISAMPLE, KNK, DBRATE

BIRATE: bit rate of interest, i.e., 90 Mb/s, then input 90.

LSAMPL: normally input 16

KNK: the number of incremental increase of BIRATE. For example, for BIRATE = 90., KNK = 3 will run the programs three times at 90., 95. and 100. Mb/s if the incremental increase DBRATE is set at 5 Mb/s.

DBRATE: the incremental change of BIRATE

5.2 READ*, TWT1IN, TWT1OU, PSH1

READ*, TWT2IN, TWT2OU, PSH2

TWT1IN and TWT1OU stand for the input operating voltage in mV and corresponding output voltage in V, respectively. PSH1 stands for the phase shift at

the operating point of HPA.

For example, if the Hughes 261-H TWT (Fig.) is operated at 12 dB input backoff, then TWT1IN = 1.123, TWT1OU = 1.795, and PSH1 = .11187 (in radian).

The same principle applies to TWT2IN, TWT2OU, PSH2.

5.3 READ*, IDENT

Three situations will arise.

a) If all the four filters used are identical with the same number of poles except different FBANDW (f_{3dB}) bandwidth, then enter 1 for IDENT.

Afterwards, READ*, FBW1, FBW2, FBW3, FBW4

The f_{3dB} bandwidth of the four filters to be entered, for example, 54. 60. 60. 54. (MHz)

READ*, IC

The number of poles of these four filters.

READ*, (C(N), N=1, IC)

The polynomial coefficients of these four filters.

For example, a 4 pole $\frac{1}{2}$ dB ripple Chebychev

IC: 4

C(N): 0.37905
1.02546
1.71687
1.19739

Example A

```
78/09/01. 11.16.07.
Concordia University  -  CYBER 172/2.   NOS 1.2-446
USER NUMBER:
            TERMINAL:    16, TTY

RECOVER?

READY.
bat
$RFL, 0.

/GET,QPSK
FTN, i=QPSK, L=LIST.
S
S
       8.15 COMPILATION SECONDS

/NEW, XYZ/ND
TEXT
ENTER TEXT MODE
90. 16 2. 10.
1.123 1.795 .11187
1.123 1.795 .11187
1
54. 125. 125. 54.
4
0.37905
1.02546
1.71687
1.19739          ..... Polynomial Coefficients of 4 Pole
                        2 dB Chebychev Filter

EXIT TEXT MODE
PACK
PACK COMPLETE

/CALL, PROC
      39.25 EXECUTION SECONDS

/PRINT,ABC, RS.
  IDENTIFICATION?
```

PRINTOUT for Example A.

```
1.123 1.795 .11187
1.123 1.795 .11187
54. 125. 125. 54.
.37905 1.02546 1.71687 1.19739 1.
45. .22374 16

    NSTART= 29  LSTART= 11  MSTART= 13  JSTART= 27


SNR          PROB. OF ERROR

 4.0             .150011E+00
 5.0             .112978E+00
 6.0             .812110E-01
 7.0             .554198E-01
 8.0             .356929E-01
 9.0             .215447E-01
10.0             .120844E-01
11.0             .623292E-02
12.0             .292001E-02
13.0             .122505E-02
14.0             .452744E-03
15.0             .144420E-03
16.0             .386901E-04
17.0             .837423E-05
18.0             .138531E-05
19.0             .162096E-06
20.0             .121041E-07
21.0             .506399E-09
22.0             .101113E-10
23.0             .790723E-13

 ERRORS=  0
```

b) If these four filters are not identical with different numbers of poles:

Enter 2 for IDENT

Afterwards, READ*, FBW1, IC1

READ*, (C1(N), N=1, IC1)

FBW1: f_{3dB} bandwidth of F_1

IC1: Number of poles of F_1

C1(N): Polynomial coefficients of F_1

READ*, FBW2, IC2

READ*, (C2(N), N=1, IC2)

READ*, FBW3, IC3

READ*, (C3(N), N=1, IC3)

READ*, FBW4, IC4

READ*, (C4(N), N=1, IC4)

The characteristics of the other three filters to be inputted in a similar way.

c) If the measured amplitude and phase response of the filters are to be used.

Enter 3 for IDENT

Again, two possible situations arise:

1. All four filters are identical
2. All four filters are different

A. For the first case:

Enter 1 for IDENTO

READ*, (CA1(J), J = 1, 14)

the polynomial coefficients of the amplitude response, normally up to 13th degree or 14 coefficients to be inputted.

READ*, (CP1(J), J = 1, 14)

the polynomial coefficients of the phase response, normally up to 13th degree or 14 coefficients (the dc term, though, is usually set at 0).

PRINTOUT for Example B

```
SIMULATION OF COHERENT 4-PSK

1.123 1.795 .11187
1.123 1.795 .11187
54. 125. 125. 54.

.04615313 -.0433213 .01513692 -.002524709 .0002289047
-.00001168216 3.299346E-6 -4.732201e-9 2.628698E-11          CA(J)
0. 0. 0. 0. 0.99928

0. 0. 0. 0. 0. 0. 0. 0. 0. 0. 0. 0. 0. 0. 0.                 CP(J)

90. .22374 16

     NSTART= 1  LSTART= 1  MSTART= 1  JSTART= 1

SNR          PROB. OF ERROR

 1.0           .135005E+00
 2.0           .104877E+00
 3.0           .795212E-01
 4.0           .592661E-01
 5.0           .434635E-01
 6.0           .315071E-01
 7.0           .229659E-01
 8.0           .169013E-01
 9.0           .124526E-01
10.0           .938444E-02
11.0           .713386E-02
12.0           .559152E-02
13.0           .437619E-02
14.0           .341467E-02
15.0           .262648E-02
16.0           .196904E-02
17.0           .142313E-02
18.0           .980742E-03
19.0           .635903E-03
20.0           .384765E-03
21.0           .213108E-03
22.0           .105311E-03
23.0           .465495E-04
24.0           .174244E-04
25.0           .529726E-05

 ERRORS=    0
```

B. For the second case:

Since the four filters are different, the f_{3dB} amplitude and phase polynomial coefficients (CA(J) and CP(J), J = 1, 14) of the four filters have to be inputted separately:

```
READ*, (CA1(J), J = 1, 14)
READ*, (CP1(J), J = 1, 14)
READ*, (CA2(J), J = 1, 14)
READ*, (CP2(J), J = 1, 14)
READ*, (CA3(J), J = 1, 14)
READ*, (CP3(J), J = 1, 14)
READ*, (CA4(J), J = 1, 14)
READ*, (CP4(J), J = 1, 14)
```

In the two examples given above, there is a /call, proceeding after all the required data are stored in the input file called "XYZ". This is the procedure file which first GRAB (or ATTACH) the IMSLIB from the computer library and load the input file for executing the program and store the output result in the file "ABC".

Procedure file: PROC

```
/ATTACH, IMSLIB/UN=LIBRARY.
/LDSET (LIB=IMSLIB)
/LGO, XYZ, ABC.
```

Finally, to print out the output data file,

```
/PRINT, ABC. RS.
IDENTIFICATION
GOOD LUCK
```

Go to the terminal, and pick up the printout.

Or, you can print it out at the TELEX,

```
/+ntxed, ABC
READY
? L* (* stands for listing all results).
```

```
      PROGRAM OKQPSK(INPUT,OUTPUT)
C*****************************************************************
C*                                                               *
C*     JOHN C. HUANG, SEPTEMBER 1978 CONCORDIA UNIVERSITY        *
C*                                                               *
C*     THIS PROGRAM SIMULATES AN OKQPSK SIGNAL PASSING THROUGH A NONLINEAR
C*     SATELLITE CHANNEL. AT THE EARTH TRANSMITTING STATION, THE SIMULATED
C*     OKQPSK SIGNAL PASSES THROUGH FILTER TF1, HIGH POWER AMPLIFIER HPA.
C*     AT THE SATELLITE TRANSPONDER, THE SIGNAL PASSES THROUGH FILTER TF2,
C*     THE SATELLITE TRAVELLING WAVE TUBE AMPLIFIER TWT AND FILTER TF3.
C*     FINALLY, AT THE RECEIVING EARTH STATION, THE RECEIVED SIGNAL PASSES
C*     THROUGH FILTER TF4 BEFORE IT IS DECODED FOR P(E) CALCULATION.
C*                                                               *
C*     INPUT DATA REQUIRED                                       *
C*                                                               *
C*     BIRATE= BIT RATE OF INTEREST                              *
C*     LSAMPL= NUMBER OF SAMPLES IN A SYMBOL, USUALLY = 16.      *
C*     KNK= NUMBER OF LOOPS THAT THE BIT RATE IS INCREMENTED.    *
C*     DBRATE= INCREMENT OF BIT RATE                             *
C*     TWT1IN, TWT1OU, PSHI....OPERATING POINTS OF HPA           *
C*     TWT2IN, TWT2OU, PSH2....OPERATING POINTS OF TWT           *
C*     IC.....NUMBER OF POLES OF FILTER                          *
C*     FBWI, I=1, 2, 3, 4, THE 3DB BANDWIDTH OF THE FOUR FILERS USED
C*     C(I),I=1,2,.....,  THE POLYNOMIAL COEFFECIENTS OF CHEBYCHEV/BUTTER-
C*                   WORTH FILTERS                               *
C*     CA(I),CP(I),I=1,2.....,  AMPLITUDE AND PHASE POLYNOMIAL COEFFICIENTS
C*           OF MEASURED FILTER CHARACTERISTICS                   *
C*     TO OBTAIN THESE COEFFICIENTS, SEE THE INSTRUCTION MANUAL  *
C*                                                               *
C*****************************************************************
      DIMENSION WX(11),NRX(11),DATA(512),DATA1(512),DATA2(512),DATA3(512)
      DIMENSION PE(25),PEI(25),SNRDB(25),TATA1(512)
      DIMENSION TF1(512),TF2(512),TF3(512),TF4(512),TF(512)
      DIMENSION C(15),C1(15),C2(15),C3(15),C4(15)
      DIMENSION CA1(14),CA2(14),CA3(14),CA4(14)
      DIMENSION CP1(14),CP2(14),CP3(14),CP4(14)
      DATA NTOTAL,NERROR,LOOP,TI,IK/0,0,0,0,0/
      DATA INDEXL,INDEXR,XL,YL/-1,-1,1.,1./
      DATA JLAST,JTAP,LLINON/7,1,50/
      PRINT 1
    1 FORMAT(26H SIMULATION OF OFFSET QPSK)
      LDIM=512
      NN=LDIM/2
      READ *,BIRATE,LSAMPL,KNK,DBRATE
C
C     CHANGE THE BIT RATE INTO BAUD RATE
C
      BAUD=BIRATE/2.
C
C     THE OPERATING POINTS OF HPA AND TWT ARE REQUIRED
C
      READ *,TWT1IN,TWT1OU,PSH1
      READ *,TWT2IN,TWT2OU,PSH2
      PRINT *,TWT1IN,TWT1OU,PSH1
      PRINT *,TWT2IN,TWT2OU,PSH2
      AVAMP=SQRT(2.)
      FNORM1=TWT1IN/AVAMP
```

```
      FNORO1=TWT1OU/AVAMP
      FNORI2=TWT2IN/AVAMP
      FNORO2=TWT2OU/AVAMP
      PSHIFT=PSH1+PBH2
C
C     IF ALL THE FILTERS USED ARE IDENTICAL WITH SAME NUMBER OF POLES
C     AND OF STANDARD TYPES (WITH DIFFERENT 3DB BW), ENTER IDENT=1
C     IF NOT IDENTICAL, BUT STILL OF STANDARD TYPES, ENTER IDENT=2
C     IF OBTAINED FROM MEASURED AMPLITUDES AND GROUP DELAY, ENTER
C     IDENT=3 (SEE MANUAL FOR INSTRUCTION)
C
      READ *,IDENT
      IF(IDENT.EQ.2) GO TO 52
      IF(IDENT.EQ.3) GO TO 53
C
C     THESE FOUR FILTERS ARE IDENTICAL AND OF STANDARD TYPES
C
      READ *,FBW1,FBW2,FBW3,FBW4
      PRINT *,FBW1,FBW2,FBW3,FBW4
      READ *,IC
      PRINT 601
  601 FORMAT(/5X,*IDENTICAL AND STANDARD TYPES OF FILTERS*/)
      PRINT *,IC
      READ *,(C(N),N=1,IC)
      PRINT *,(C(N),N=1,IC)
      DO 301 N=1,IC
      IC1=IC
      IC2=IC
      IC3=IC
      IC4=IC
      C1(N)=C(N)
      C2(N)=C(N)
      C3(N)=C(N)
      C4(N)=C(N)
  301 CONTINUE
C
      GO TO 54
C
C     THESE FOUR FILTERS ARE NOT IDENTICAL, BUT STILL OF STANDARD TYPES
C
   52 PRINT 602
  602 FORMAT(/5X,*UNIDENTICAL BUT STANDARD TYPES OF FILTERS*/)
      READ *,FBW1,IC1
      READ *,(C1(N),N=1,IC1)
      READ *,FBW2,IC2
      READ *,(C2(N),N=1,IC2)
      READ *,FBW3,IC3
      READ *,(C3(N),N=1,IC3)
      READ *,FBW4,IC4
      READ *,(C4(N),N=1,IC4)
C
      PRINT *,FBW1,IC1
      PRINT *,(C1(N),N=1,IC1)
      PRINT *,FBW2,IC2
      PRINT *,(C2(N),N=1,IC2)
      PRINT *,FBW3,IC3
      PRINT *,(C3(N),N=1,IC3)
```

```
      PRINT *,FBW4,IC4
      PRINT *,(C4(N),N=1,IC4)
C
      GO TO 54
C
   53 CONTINUE
CCCCCCCC
      MEASURED AMPLITUDE AND PHASE DISTORTION CHARACTERISTICS OF THE
      FOUR FILTERS WILL BE USED IN THE SIMULATION

      IF ALL THESE FILTERS ARE IDENTICAL, ENTER IDENTO= 1
      OTHERWISE ENTER IDENTO= 2.
C
      READ *,IDENTO
C
      IF(IDENTO.EQ.2) GO TO 541
C
      READ *,(CA1(J),J=1,14)
      READ *,(CP1(JJ),J=1,14)
C
      PRINT 603
  603 FORMAT(/5X,'MEASURED FILTER CHARACTERISTICS,IDENTICAL FILTERS'/)
      PRINT *,(CA1(J),J=1,14)
      PRINT *,(CP1(J),J=1,14)
C
      DO 302 J=1,14
      CA2(J)=CA1(J)
      CP2(J)=CP1(J)
      CA3(J)=CA1(J)
      CP3(J)=CP1(J)
      CA4(J)=CA1(J)
      CP4(J)=CP1(J)
  302 CONTINUE
C
      GO TO 54
C
  541 READ *,(CA1(J),J=1,14)
      READ *,(CP1(J),J=1,14)
      READ *,(CA2(J),J=1,14)
      READ *,(CP2(J),J=1,14)
      READ *,(CA3(J),J=1,14)
      READ *,(CP3(J),J=1,14)
      READ *,(CA4(J),J=1,14)
      READ *,(CP4(J),J=1,14)
C
      PRINT 604
  604 FORMAT(/5X,'MEASURED FILTER CHARACTERISTICS,UNIDENTICAL FILTERS'/)
      PRINT *,(CA1(J),J=1,14)
      PRINT *,(CP1(J),J=1,14)
      PRINT *,(CA2(J),J=1,14)
      PRINT *,(CP2(J),J=1,14)
      PRINT *,(CA3(J),J=1,14)
      PRINT *,(CP3(J),J=1,14)
      PRINT *,(CA4(J),J=1,14)
      PRINT *,(CP4(J),J=1,14)
C
```

```
   54  CONTINUE
C
       DO 507 KM=1,KNK
       PRINT *,BIRATE,PSHIFT,LSAMPL
       DO 4 I=1,JLAST
       NX(I)=-1
    4  NRX(I)=-1
       DSNR=1.
       NSNR=25
       DSNRDB=0.
       DO 5 I=1,NSNR
       PE(I)=0.
       PEI(I)=0.
       SNRDB(I)=4.+DSNRDB
       DSNRDB=DSNRDB+DSNR
    5  CONTINUE
       CALL CALCON(LSAMPL,LLTNOM,KKK,LLT,NSYMB,JLAST,LOOPM,LDIM,
      1BAUD,SBANDW)
C
       IF(IDENT.EQ.3) GO TO 34
C
C
C      STANDARD TYPES OF FILTERS USED IN THE SIMULATION
C
C      DATA1 IS JUST USED AS DUMMY HERE
       CALL CF4P5(SBANDW,FBW4,DATA1,LDIM,C4,IC4)
       CALL HHGG(DATA1,PNOISE,LSAMPL,LDIM)
C
C
       CALL CF4P5(SBANDW,FBW1,TF1,LDIM,C1,IC1)
       CALL CF4P5(SBANDW,FBW2,TF2,LDIM,C2,IC2)
       CALL CF4P5(SBANDW,FBW3,TF3,LDIM,C3,IC3)
       CALL CF4P5(SBANDW,FBW4,TF4,LDIM,C4,IC4)
C
       GO TO 35
C
C      MEASURED AMPLITUDE AND PHASE CHARACTERISTICS OF THE FILTERS USED
C      IN THE SIMULATION
C
   34  CONTINUE
C
       CALL MEASUR(SBANDW,FBW4,DATA1,LDIM,CA4,CP4)
       CALL HHGG(DATA1,PNOISE,LSAMPL,LDIM)
C
       CALL MEASUR(SBANDW,FBW1,TF1,LDIM,CA1,CP1)
       CALL MEASUR(SBANDW,FBW2,TF2,LDIM,CA2,CP2)
       CALL MEASUR(SBANDW,FBW3,TF3,LDIM,CA3,CP3)
       CALL MEASUR(SBANDW,FBW4,TF4,LDIM,CA4,CP4)
C
   35  CONTINUE
C
       CALL BISINC(DATA,TF1,TF2,TF3,TF4,LSAMPL,NSTART,LSTART,NSTART,
      +JSTART,LDIM)
C
       CALL LOSPSK(DATA,KKK,LSAMPL,NX,II,JLAST,JTAP,INDEXL,XL,YL,LDIM)
       CALL FILTER(DATA,TF1,NN,LDIM)
       CALL LOSPSK(DATA1,KKK,LSAMPL,NX,II,JLAST,JTAP,INDEXL,XL,YL,LDIM)
```

```
      CALL FILTER(DATA1,TF1,NN,LDIM)
      CALL ADTAIL(DATA,DATA1,LLT,LDIM)
C
      CALL LOSPSK(DATA2,KKK,LSAMPL,NX,II,JLAST,JTAP,INDEXL,XL,YL,LDIM)
      CALL FILTER(DATA2,TF1,NN,LDIM)
      CALL ADTAIL(DATA1,DATA2,LLT,LDIM)
C
      CALL LOSPSK(DATA3,KKK,LSAMPL,NX,II,JLAST,JTAP,INDEXL,XL,YL,LDIM)
      CALL FILTER(DATA3,TF1,NN,LDIM)
      CALL ADTAIL(DATA2,DATA3,LLT,LDIM)
C
      CALL HPA(DATA,LSAMPL,NSTART,KKK,FNORI1,FNORO1,LDIM)
      CALL FILTER(DATA,TF2,NN,LDIM)
C
      CALL HPA(DATA1,LSAMPL,NSTART,KKK,FNORI1,FNORO1,LDIM)
      CALL FILTER(DATA1,TF2,NN,LDIM)
      CALL ADTAIL(DATA,DATA1,LLT,LDIM)
C
      CALL HPA(DATA2,LSAMPL,NSTART,KKK,FNORI1,FNORO1,LDIM)
      CALL FILTER(DATA2,TF2,NN,LDIM)
      CALL ADTAIL(DATA1,DATA2,LLT,LDIM)
C
      CALL TWT(DATA,LSAMPL,LSTART,KKK,FNORI2,FNORO2,LDIM)
      CALL FILTER(DATA,TF3,NN,LDIM)
C
      CALL TWT(DATA1,LSAMPL,LSTART,KKK,FNORI2,FNORO2,LDIM)
      CALL FILTER(DATA1,TF3,NN,LDIM)
      CALL ADTAIL(DATA,DATA1,LLT,LDIM)
C
      CALL DELAY(DATA,LSAMPL,MSTART,KKK,LDIM)
      CALL FILTER(DATA,TF4,NN,LDIM)
C
   50 CONTINUE
      DO 12 I=1,LDIM
      DATA1(I)=DATA(I)
      DATA(I)=DATA1(I)
      DATA1(I)=DATA2(I)
      DATA2(I)=DATA3(I)
   12 CONTINUE
C
      CALL LOSPSK(DATA3,KKK,LSAMPL,NX,II,JLAST,JTAP,INDEXL,XL,YL,LDIM)
      CALL FILTER(DATA3,TF1,NN,LDIM)
      CALL ADTAIL(DATA2,DATA3,LLT,LDIM)
C
      CALL HPA(DATA2,LSAMPL,NSTART,KKK,FNORI1,FNORO1,LDIM)
      CALL FILTER(DATA2,TF2,NN,LDIM)
      CALL ADTAIL(DATA1,DATA2,LLT,LDIM)
C
      CALL TWT(DATA1,LSAMPL,LSTART,KKK,FNORI2,FNORO2,LDIM)
      CALL FILTER(DATA1,TF3,NN,LDIM)
      CALL ADTAIL(DATA,DATA1,LLT,LDIM)
C
      CALL DELAY(DATA,LSAMPL,MSTART,KKK,LDIM)
      CALL FILTER(DATA,TF4,NN,LDIM)
      CALL ADTAIL(DATA1,DATA,LLT,LDIM)
      CALL DOSPSK(DATA1,NRX,PE,PEI,KKK,LSAMPL,JSTART,NBNR,NERROR,
     1SNRDB,IK,NTOTAL,PNOISE,LDOP,JLAST,JTAP,NSYNB,PSHIFT,INDEXR)
```

```
C
      IF(LOOP.GT.LOOPM) GO TO 100
      GO TO 50
  100 CONTINUE
      BIRATE=BIRATE+DBRATE
      NTOTAL=0
      NERROR=0
      LOOP=0
      II=0
      IK=0
  507 CONTINUE
      STOP
      END


      SUBROUTINE LOSPSK(DATA,KKK,LSAMPL,NX,I,JLAST,JTAP,INDEXL
     +,X,Y,LDIM)
C*****************************************************************
C*                                                               *
C*     THIS SUBROUTINE GENERATES AN EQUIVALENT BASEBAND OKQPSK SIGNAL
C*                                                               *
C*                                                               *
C*****************************************************************
      DIMENSION DATA(512),NX(11)
      KNO=KKK
      DO 1 K=1,KNO
C
C     GENERATING ONE SYMBOL
C
      IF(I.EQ.JLAST) I=0
      I=I+1
      J=I-JTAP
      IF(I.LE.JTAP) J=J+JLAST
      IX=NX(J)*NX(I)
      NX(I)=IX
      IF(INDEXL.GT.0) GO TO 2
      X=IX
      GO TO 3
    2 Y=IX
C
C     LOAD INTO THE ARRAY DATA TO BE FOURIER TRANSFORMED
C
    3 JA=LSAMPL*2
      JB=K*JA
      J1=JB-JA+1
      J2=JB-1
      DO 4 J3=J1,J2,2
      DATA(J3)=X
    4 DATA(J3+1)=Y
      INDEXL=-INDEXL
    1 CONTINUE
C
C     FILL THE REST OF THE ARRAY DATA WITH ZEROS FOR SPILLOVER EFFECTS
C     OF THE FILTERS
C
      J4=J2+2
      DO 5 J3=J4,LDIM
    5 DATA(J3)=0.
      RETURN
      END
```

```
      SUBROUTINE DOSPSK(DATA,NRX,PE,PEI,KKK,LSAMPL,LSTART,NSYR,
     1NERROR,SNRDB,I,NTOTAL,PNOISE,LOOP,JLAST,JTAP,NSYMB,PSHIFT,
     2INDEXR)
C*****************************************************************
C*
C*
C*    THIS SUBROUTINE DECODES THE RECEIVED DATA AFTER IT PASSES
C*    THE I AND D DETECTOR AND THEN COMPARES IT WITH THE TRANSMITTED DATA
C*    FOR ERROR DETECTION. EACH RECEIVED SYMBOL HAS A SCALED
C*    AMPLITUDE CHANGE BECAUSE OF DISTORTION BY THE FILTERS AND
C*    THE TWO CASCADED NONLINEARITIES. BASED ON THIS TOGETHER WITH
C*    THE EFFECTIVE NOISE COMPUTED AFTER IT PASSES THROUGH THE
C*    RECEIVE FILTER TF4 (PERFORMED AT THE SUBROUTINE HHGG), THE
C*    AVERAGED P(E) OVER ALL SYMBOLS IS THEN OBTAINED
C*
C*    IF A SAMPLE DETECTOR IS TO BE USED. SEE THE MODIFIED PORTION
C*       OF THIS SUBROUTINE IN THE MANUAL
C*
C*
C*****************************************************************
      DIMENSION DATA(512),NRX(11),PE(25),PEI(25),SNRDB(25)
      COSPS=COS(PSHIFT)
      SINPS=SIN(PSHIFT)
      DLSAMP=LSAMPL*SQRT(2.)
      KMO=KKK
      DO 1 K=1,KMO
C
C     REGENERATING TRANSMITTED SYMBOLS
C
      IF(I.EQ.JLAST)I=0
      I=I+1
      J=I-JTAP
      IF(I.LE.JTAP) J=J+JLAST
      IX=NRX(J)*NRX(I)
      NRX(I)=IX
C
C     FIRST LOOP SYMBOLS ARE NOT PROCESSED.
C
      IF(LOOP.EQ.0) GO TO 130
C
C     AVERAGE SYMBOL AMPLITUDE
C
      J1=LSTART+LSAMPL*(K-1)*2
      J2=J1+4*LSAMPL-2
      AMPLIX=0.
      AMPLIY=0.
      IF(INDEXR.GT.0) GO TO 2
      DO 4 JJ=J1,J2,2
    4 AMPLIX=AMPLIX+DATA(JJ)*COSPS+DATA(JJ+1)*SINPS
      AMP=AMPLIX/DLSAMP
      GO TO 3
    2 DO 6 JJ=J1,J2,2
    6 AMPLIY=AMPLIY+DATA(JJ+1)*COSPS-DATA(JJ)*SINPS
      AMP=AMPLIY/DLSAMP
    3 ID=SIGN(1.,AMP)
      INDEX=0
      IF(ID.NE.IX) INDEX=1
```

```
SUBROUTINE DOSPSK      73/172  OPT=1

C
C  INDEX=0 INDICATES A CORRECTLY RECEIVED SYMBOL,
C  OTHERWISE AN INCORRECT DECISION WAS MADE.
C
      IF(INDEX.EQ.1) NERROR=NERROR+1
C
C  COMPUTE PROBABILITY OF ERROR FOR THIS SYMBOL.
C
      CALL PERR2(AMP,INDEX,SNRDB,PEI,PNOISE,NSNR)
      DO 5 KK=1,NSNR
    5 PE(KK)=PE(KK)+PEI(KK)
      NTOTAL=NTOTAL+1
      IF(NTOTAL.NE.NSYMB) GO TO 130
      PRINT 150
  150 FORMAT(/3HSNR,10X,14HPROB. OF ERROR/)
      DO 500 II=1,NSNR
  500 PEI(II)=PE(II)/NSYMB
      PRINT 151,(SNRDB(II),PEI(II),II=1,NSNR)
  151 FORMAT(F5.1,10X,E13.6)
      PRINT 102,NERROR
  102 FORMAT(/2X,7HERRORS=,I5/)
      GO TO 155
  130 INDEXR=-INDEXR
    1 CONTINUE
  155 LOOP=LOOP+1
      RETURN
      END


      SUBROUTINE PERR2(AMPLIX,INDEX,SNRDB,PEI,PNOISE,NSNR)
C*****************************************************************
C*
C*    THIS SUBROUTINE COMPUTES P(E) OF EACH DETECTED SYMBOL (OKQPSK AND
C*                        MSK)
C*
C*****************************************************************
      DIMENSION SNRDB(25),PEI(25)
      DO 1 M=1,NSNR
      SNR=EXP(SNRDB(M)*.23026)
      SCALE=SQRT(SNR/PNOISE/2.)
      XX=AMPLIX*SCALE
      ABSX=ABS(XX)
      CALL TTERFC(ABSX,EX)
      EX=EX/2.
      IF(INDEX.NE.1) GO TO 1
      EX=1.-EX
    1 PEI(M)=EX
      RETURN
      END
```

```
      PROGRAM MSK(INPUT,OUTPUT)
C*****************************************************************
C
C     JOHN C. HUANG, SEPTEMBER, 1978 CONCORDIA UNIVERSITY
C
C     THIS PROGRAM SIMULATES AN MSK SIGNAL PASSING THROUGH A NONLINEAR
C     SATELLITE CHANNEL. AT THE EARTH TRANSMITTING STATION, THE SIMULATED
C     QPSK SIGNAL PASSES THROUGH FILTER TF1, HIGH POWER AMPLIFIER HPA.
C     AT THE SATELLITE TRANSPONDER, THE SIGNAL PASSES THROUGH FILTER TF2,
C     THE SATELLITE TRAVELLING WAVE TUBE AMPLIFIER TWT AND FILTER TF3.
C     FINALLY, AT THE RECEIVING EARTH STATION, THE RECEIVED SIGNAL PASSES
C     THROUGH FILTER TF4 BEFORE IT IS DECODED FOR P(E) CALCULATION.
C
C        INPUT DATA REQUIRED ...................
C     BIRATE= BIT RATE OF INTEREST
C     LSAMPL= NUMBER OF SAMPLES IN A SYMBOL. USUALLY = 16.
C     KNK= NUMBER OF LOOPS THAT THE BIT RATE IS INCREMENTED.
C     DBRATE= INCREMENT OF BIT RATE
C     TWT1IN,TWT1OU,PSH1---OPERATING POINTS OF HPA.
C     TWT2IN,TWT2OU,PSH2---OPERATING POINTS OF TWT
C     .......TO OBTAIN THE COEFFICIENTS THAT CHARACTERIZE THE IN-PHASE AND
C             QUADRATURE MODEL OF HPA AND TWT, SEE APPENDIX 1
C     FBW1,FBW2,FBW3,FBW4  3 DB FREQUENCIES OF TF1,TF2,TF3,TF4.
C
C     INSTRUCTION FOR INPUT DATA THAT CHARACTERIZE FILTERS OF
C     INTEREST IS GIVEN WHERE APPLICABLE.
C
C*****************************************************************
      DIMENSION DATA(512),DATA1(512),DATA2(512),DATA3(512),TATA1(512)
      DIMENSION NX(11),NY(11),NRX(11),NRY(11),PE(25),PEI(25),SNRDB(25)
      DIMENSION TF(512),TF1(512),TF2(512),TF3(512),TF4(512)
      DIMENSION C(15),C1(15),C2(15),C3(15),C4(15)
      DIMENSION CA1(14),CA2(14),CA3(14),CA4(14)
      DIMENSION CP1(14),CP2(14),CP3(14),CP4(14)
      DATA NTOTAL,NERROR,LOOP,II,IK/0,0,0,0,0/
      DATA JLAST,JTAP,LLTNOM/7,1,50/
      DATA NY(1),NY(2),NY(3),NY(4),NY(5),NY(6),NY(7)/-1,-1,1,1,1,1,-1/
C
      LDIM=512
      NN=LDIM/2
      PRINT 1
    1 FORMAT(27H SIMULATION OF COHERENT MSK)
C
      READ *,BIRATE,LSAMPL,KNK,DBRATE
C
C     CHANGE BIT RATE INTO BAUD RATE
C
      BAUD=BIRATE/2.
C
C     THE OPERATING POINTS OF HPA AND TWT ARE REQUIRED
C
      READ *,TWT1IN,TWT1OU,PSH1
      READ *,TWT2IN,TWT2OU,PSH2
      PRINT *,TWT1IN,TWT1OU,PSH1
      PRINT *,TWT2IN,TWT2OU,PSH2
C
C     IF ALL THE FILTERS USED ARE IDENTICAL WITH SAME NUMBER OF POLES
```

```
C     AND OF STANDARD TYPE (WITH DIFFERENT F.3DB BW),ENTER IDENT=1
C     IF NOT IDENTICAL,BUT STILL OF STANDARD TYPES,ENTER IDENT=2
C     IF OBTAINED FROM MEASURED AMPLITUDES AND GROUP DELAY,ENTER
C     IDENT=3 (SEE MANUAL FOR INSTRUCTION)
C
      READ *,IDENT
      IF(IDENT.EQ.2) GO TO 52
      IF(IDENT.EQ.3) GO TO 53
C
C     THESE FOUR FILTERS ARE IDENTICAL AND OF STANDARD TYPES.
C
      READ *,FBW1,FBW2,FBW3,FBW4
      PRINT *,FBW1,FBW2,FBW3,FBW4
      READ *,IC
      PRINT 601
  601 FORMAT(/5X,*IDENTICAL AND STANDARD TYPES OF FILTERS*/)
      PRINT *,IC
      READ *,(C(N),N=1,IC)
      PRINT *,(C(N),N=1,IC)
      DO 301 N=1,IC
      IC1=IC
      IC2=IC
      IC3=IC
      IC4=IC
      C1(N)=C(N)
      C2(N)=C(N)
      C3(N)=C(N)
      C4(N)=C(N)
  301 CONTINUE
      GO TO 54
C
C     THESE FOUR FILTERS ARE NOT IDENTICAL, BUT STILL OF STANDARD TYPES
C
   52 PRINT 602
  602 FORMAT(/5X,*UNIDENTICAL BUT STANDARD TYPES OF FILTERS*/)
   52 READ *,FBW1,IC1
      READ *,(C1(N),N=1,IC1)
      READ *,FBW2,IC2
      READ *,(C2(N),N=1,IC2)
      READ *,FBW3,IC3
      READ *,(C3(N),N=1,IC3)
      READ *,FBW4,IC4
      READ *,(C4(N),N=1,IC4)
C
      PRINT *,FBW1,IC1
      PRINT *,(C1(N),N=1,IC1)
      PRINT *,FBW2,IC2
      PRINT *,(C2(N),N=1,IC2)
      PRINT *,FBW3,IC3
      PRINT *,(C3(N),N=1,IC3)
      PRINT *,FBW4,C4
      PRINT *,(C4(N),N=1,IC4)
C
      GO TO 54
C
   53 CONTINUE
```

```
C
C     MEASURED AMPLITUDE AND PHASE DISTORTION CHARACTERISTICS OF THE
C     FOUR FILTERS WILL BE USED IN THE SIMULATION.
C
C     IF ALL THESE FILTERS ARE IDENTICAL, ENTER IDENTO= 1
C     OTHERWISE ENTER IDENTO= 2.
C
      READ *,IDENTO
C
      IF(IDENTO.EQ.2) GO TO 541
C
      READ *,(CA1(J),J=1,14)
      READ *,(CP1(J),J=1,14)
C
      PRINT 603
  603 FORMAT(/5X,*MEASURED FILTER CHARACTERISTICS,IDENTICAL FILTERS*/)
      PRINT *,(CA1(J),J=1,14)
      PRINT *,(CP1(J),J=1,14)
C
      DO 302 J=1,14
      CA2(J)=CA1(J)
      CP2(J)=CP1(J)
      CA3(J)=CA1(J)
      CP3(J)=CP1(J)
      CA4(J)=CA1(J)
      CP4(J)=CP1(J)
  302 CONTINUE
C
      GO TO 54
C
  541 CONTINUE
      READ *,(CA1(J),J=1,14)
      READ *,(CA2(J),J=1,14)
      READ *,(CA3(J),J=1,14)
      READ *,(CA4(J),J=1,14)
      READ *,(CP1(J),J=1,14)
      READ *,(CP2(J),J=1,14)
      READ *,(CP3(J),J=1,14)
      READ *,(CP4(J),J=1,14)
C
      PRINT 604
  604 FORMAT(/5X,*MEASURED FILTER CHARACTERISTICS,UNIDENTICAL FILTERS*/)
      PRINT *,(CA1(J),J=1,14)
      PRINT *,(CP1(J),J=1,14)
      PRINT *,(CA2(J),J=1,14)
      PRINT *,(CP2(J),J=1,14)
      PRINT *,(CA3(J),J=1,14)
      PRINT *,(CP3(J),J=1,14)
      PRINT *,(CA4(J),J=1,14)
      PRINT *,(CP4(J),J=1,14)
C
C
C
   54 CONTINUE
      AVAMP=SQRT(2.)
      FNORI1=TWTIIN/AVAMP
      FNORQ1=TWTIQU/AVAMP
```

```
      FNORI2=TWT2IN/AVAMP
      FNORO2=TWT2OU/AVAMP
      PSHIFT=PSH1+PSH2
      DO 507 KM=1,KNK
      PRINT *,BIRATE,PSHIFT,LSAMPL
      DO 4 I=1,JLAST
      NX(I)=-1
      NRY(I)=NY(I)
    4 NRX(I)=-1
      NSNR=25
      DSNR=1.
      DSNRDB=0.
      DO 5 I=1,NSNR
      PE(I)=0.
      SNRDB(I)=4.+DSNRDB
      DSNRDB=DSNRDB+DSNR
    5 CONTINUE
C
      CALL CALCON(LSAMPL,LLTNOM,KKK,LLT,NSYMB,JLAST,LOOPM,LDIM,BAUD,
     +SBANDW)
C
      IF(IDENT.EQ.3) GO TO 34
C
      CALL CF4P5(SBANDW,FBW4,DATA1,LDIM,C4,IC4)
      CALL HHGG(DATA1,PNOISE,LSAMPL,LDIM)
C
C     STANDARD TYPES OF FILTERS USED IN THE SIMULATION
C
C     DATA1 USED AS A DUMMY ARRAY
C
      CALL CF4P5(SBANDW,FBW4,DATA1,LDIM,C4,IC4)
      CALL HHGG(DATA1,PNOISE,LSAMPL,LDIM)
C
      CALL CF4P5(SBANDW,FBW1,TF1,LDIM,C1,IC1)
      CALL CF4P5(SBANDW,FBW2,TF2,LDIM,C2,IC2)
      CALL CF4P5(SBANDW,FBW3,TF3,LDIM,C3,IC3)
      CALL CF4P5(SBANDW,FBW4,TF4,LDIM,C4,IC4)
C
      GO TO 35
C
C     MEASURED AMPLITUDE AND PHASE CHARACTERISTICS OF THE FILTERS USED
C     IN THE SIMULATION
C
   34 CONTINUE
      CALL MEASUR(SBANDW,FBW4,DATA1,LDIM,CA4,CP4)
      CALL HHGG(DATA1,PNOISE,LSAMPL,LDIM)
C
      CALL MEASUR(SBANDW,TF1,LDIM,CA1,CP1)
      CALL MEASUR(SBANDW,TF2,LDIM,CA2,CP2)
      CALL MEASUR(SBANDW,TF3,LDIM,CA3,CP3)
      CALL MEASUR(SBANDW,TF4,LDIM,CA4,CP4)
C
   35 CONTINUE
C
      CALL BISINC(DATA,TF1,TF2,TF3,TF4,LSAMPL,NSTART,LSTART,MSTART,
     * JSTART,LDIM)
      CALL LOFFSK(DATA,KKK,LSAMPL,NX,II,JLAST,JTAP,MN,XS,YS,LDIM)
```

```
      CALL FILTER(DATA,TF1,NN,LDIM)
      CALL LOFFSK(DATA1,KKK,LSAMPL,NX,II,JLAST,JTAP,MN,XS,YS,LDIM)
      CALL FILTER(DATA1,TF1,NN,LDIM)
      CALL ADTAIL(DATA,DATA1,LLT,LDIM)
C
      CALL LOFFSK(DATA2,KKK,LSAMPL,NX,II,JLAST,JTAP,MN,XS,YS,LDIM)
      CALL FILTER(DATA2,TF1,NN,LDIM)
      CALL ADTAIL(DATA1,DATA2,LLT,LDIM)
      CALL LOFFSK(DATA3,KKK,LSAMPL,NX,II,JLAST,JTAP,MN,XS,YS,LDIM)
      CALL FILTER(DATA3,TF1,NN,LDIM)
      CALL ADTAIL(DATA2,DATA3,LLT,LDIM)
C
      CALL HPA(DATA,LSAMPL,NSTART,KKK,FNORI1,FNORO1,LDIM)
      CALL FILTER(DATA,TF2,NN,LDIM)
C
      CALL HPA(DATA1,LSAMPL,NSTART,KKK,FNORI1,FNORO1,LDIM)
      CALL FILTER(DATA1,TF2,NN,LDIM)
      CALL ADTAIL(DATA,DATA1,LLT,LDIM)
      CALL HPA(DATA2,LSAMPL,NSTART,KKK,FNORI1,FNORO1,LDIM)
      CALL FILTER(DATA2,TF2,NN,LDIM)
      CALL ADTAIL(DATA1,DATA2,LLT,LDIM)
C
      CALL TWT(DATA,LSAMPL,LSTART,KKK,FNORI2,FNORO2,LDIM)
      CALL FILTER(DATA,TF3,NN,LDIM)
C
      CALL TWT(DATA1,LSAMPL,LSTART,KKK,FNORI2,FNORO2,LDIM)
      CALL FILTER(DATA1,TF3,NN,LDIM)
      CALL ADTAIL(DATA,DATA1,LLT,LDIM)
C
      CALL DELAY(DATA,LSAMPL,MSTART,KKK,LDIM)
      CALL FILTER(DATA,TF4,NN,LDIM)
C
   50 CONTINUE
      DO 12 I=1,LDIM
      TATA1(I)=DATA(I)
      DATA(I)=DATA1(I)
      DATA1(I)=DATA2(I)
      DATA2(I)=DATA3(I)
   12 CONTINUE
C
      CALL LOFFSK(DATA3,KKK,LSAMPL,NX,II,JLAST,JTAP,MN,XS,YS,LDIM)
      CALL FILTER(DATA3,TF1,NN,LDIM)
      CALL ADTAIL(DATA2,DATA3,LLT,LDIM)
C
      CALL HPA(DATA2,LSAMPL,NSTART,KKK,FNORI1,FNORO1,LDIM)
      CALL FILTER(DATA2,TF2,NN,LDIM)
      CALL ADTAIL(DATA1,DATA2,LLT,LDIM)
C
      CALL TWT(DATA1,LSAMPL,LSTART,KKK,FNORI2,FNORO2,LDIM)
      CALL FILTER(DATA1,TF3,NN,LDIM)
      CALL ADTAIL(DATA,DATA1,LLT,LDIM)
C
      CALL DELAY(DATA,LSAMPL,MSTART,KKK,LDIM)
      CALL FILTER(DATA,TF4,NN,LDIM)
      CALL ADTAIL(TATA1,DATA,LLT,LDIM)
      CALL DCFFSK(TATA1,NRX,PE,PEI,KKK,LSAMPL,JSTART,VSNR,NERROR,
     *SNRDB,IK,NTOTAL,PNOISE,LOOP,JLAST,JTAP,VSYNB,PSHIFT,INDEXR,
```

```
     *INDEXD)
      IF(LOOP.GT.LOOPMI GO TO 100
      GO TO 50
  100 CONTINUE
      BIRATE=BIRATE*DBRATE
      NTOTAL=0
      NERROR=0
      LOOP=0
      II=0
      IK=0
  507 CONTINUE
      STOP
      END
```

```
      SUBROUTINE LOFFSK(DATA,KKK,LSAMPL,NX,I,JLAST,JTAP,MN,XS,
     *YS,LDIM)
C*****************************************************************
C*                                                               *
C*     THIS SUBROUTINE GENERATES AN EQUIVALENT BASEBAND MSK SIGNAL*
C*                                                               *
C*                                                               *
C*****************************************************************
      DIMENSION DATA(512),NX(11),COSL(30),SINL(30)
      DIMENSION DADA(512)
      KNO=2**KKK
      RT2=SQRT(2.)
      LSAMP2=LSAMPL
      L2=8-1
      IF(MN.GT.0) GO TO 2
      DELTA=3.141593/LSAMPL
C
C     GENERATING SINE AND COSINE TABLE
C
      DO 1 L=1,L2
      COSL(L)=COS(L*DELTA)
      SINL(L)=SIN(L*DELTA)
    1 CONTINUE
      MN=1
    2 DO 3 K=1,KNO
C
C     GENERATING ONE BIT
C
      IF(I.EQ.JLAST) I=0
      I=I+1
      J=I-JTAP
      IF(I.LE.JTAP) J=J+JLAST
      IX=NX(J)*NX(I)
      NX(I)=IX
      SX=IX
C
C     DETERMINE COMPLEX BASEBAND SIGNAL AND LOAD INTO ARRAY
C
      J1=(K-1)*LSAMP2+1
      J2=K*LSAMP2-1
      DATA(J1)=XS*RT2
      DATA(J1+1)=YS*RT2
      J1=J1+2
      DO 4 J3=1,L2
      JJ=J1+2*(J3-1)
      DATA(JJ)=RT2*(COSL(J3)*XS-SX*SINL(J3)*YS)
    4 DATA(JJ+1)=RT2*(SX*SINL(J3)*XS+COSL(J3)*YS)
      XS1=-SX*YS
      YS1=SX*XS
      XS=XS1
      YS=YS1
    3 CONTINUE
C
C     FILL THE REST OF THE ARRAY WITH ZEROS FOR OVERLAP
C
      [redacted]
```

```
      SUBROUTINE DCFFSK(DATA,NRX,PE,PEI,KKK,LSAMPL,LSTART,NSNR,
     +NERROR,SNRDB,I,NTOTAL,PNOISE,LOOP,JLAST,JTAP,NSYMB,PSHIFT,
     +INDEXR,INDEXD)
C*****************************************************************
C*                                                               *
C*                                                               *
C*     THIS SUBROUTINE DECODES THE RECEIVED DATA AFTER IT PASSES *
C*     THE I AND D DETECTOR AND THEN COMPARES THE TRANSMITTED DATA*
C*     FOR ERROR DETECTION. EACH RECEIVED SYMBOL HAS A SCALED    *
C*     AMPLITUDE CHANGE BECAUSE OF DISTORTION BY THE FILTERS AND *
C*     THE TWO CASCADED NONLINEARITIES. BASED ON THIS, TOGETHER WITH*
C*     THE EFFECTIVE NOISE, WHICH IS COMPUTED AT THE SUBROUTINE MMSE,*
C*     THE AVERAGED P(E) OVER ALL SYMBOLS IS THEN OBTAINED.      *
C*                                                               *
C*     IF A SAMPLE DETECTOR IS TO BE USED, SEE THE MODIFIED PORTION*
C*          OF THIS SUBROUTINE IN THE MANUAL.                    *
C*                                                               *
C*****************************************************************
      DIMENSION DATA(512),NRX(11),PE(25),PEI(25),SNRDB(25)
      COSPS=COS(PSHIFT)
      SINPS=SIN(PSHIFT)
      RT2=SQRT(2.)
CCCC
CCCC  THE BIT ENERGY IS ESTIMATED FROM THE AVERAGE SIGNAL
CCCC  AMPLITUDE IN A BIT INTERVAL.
CCCC
      DLSAMP=LSAMPL
      KM0=2*KKK
      DO 1 K=1,KM0
CCCC
CCCC  REGENERATING TRANSMITTED SYMBOLS
CCCC
      IF(I.EQ.JLAST) I=0
      I=I+1
      J=I-JTAP
      IF(I.LE.JTAP) J=J+JLAST
      IX=NRX(J)*NRX(I)
      NRX(I)=IX
CCCC
CCCC  BIT ENERGY CALCULATION
CCCC
      J1=LSTART+LSAMPL*(K-1)
      J2=J1+2*LSAMPL-2
      AMPLIX=0.
      AMPLIY=0.
      IF(INDEXR.GT.0) GO TO 2
      DO 4 JJ=J1,J2,2
    4 AMPLIX=AMPLIX+DATA(JJ)*COSPS+DATA(JJ+1)*SINPS
      IO=ISIGN(1.,AMPLIX)
      AMP=RT2*AMPLIX/DLSAMP
      GO TO 3
    2 DO 5 JJ=J1,J2,2
    5 AMPLIY=AMPLIY+DATA(JJ+1)*COSPS-DATA(JJ)*SINPS
      IO=ISIGN(1.,AMPLIY)
      AMP=RT2*AMPLIY/DLSAMP
    3 [illegible]
```

[illegible]

```
C       FIRST LOOP SYMBOLS ARE NOT COMPUTED FOR P.E.
        IF(LOOP.EQ.0) GO TO 130
        INDEX=0
        IF(IDP.NE.IX) INDEX=1
C
C       INDEX=0 INDICATES A CORRECTLY RECEIVED SYMBOL,
C       OTHERWISE AN INCORRECT DECISION WAS MADE
C
        IF(INDEX.EQ.1) NERROR=NERROR+1
C
C       COMPUTE PROBABILITY OF ERROR FOR THIS SYMBOL
C
        CALL PERR2(AMP,INDEX,SNRDB,PEI,PNOISE,NSNR)
        DO 5 KK=1,NSNR
    5   PE(KK)=PE(KK)+PEI(KK)
        NTOTAL=NTOTAL+1
        IF(NTOTAL.NE.NSYMB) GO TO 130
        PRINT 150
  150   FORMAT(/4H SNR,10X,14HPROB. OF ERROR/)
        DO 500 II=1,NSNR
  500   PEI(II)=PE(II)/NSYMB
        PRINT 151,(SNRDB(II),PEI(II),II=1,NSNR)
  151   FORMAT(F5.1,10X,E13.6)
        PRINT 102,NERROR
  102   FORMAT(/2X,8H ERRORS=,I5/)
        GO TO 155
  130   INDEXR=-INDEXR
        INDEXD=ID
    1   CONTINUE
  155   LOOP=LOOP+1
        RETURN
        END
```

REFERENCES ACCORDING TO THE CHAPTERS

Chapter 1

1.1 Feher, K.

"Digital Modulation Techniques in an Interference Environment", Don White Consultants, Inc., 1977.

1.2 El-Torky, M. and Feher, K.

"Analysis and Design of Bandlimiting Filters to Meet FCC Restrictions for Digital QPSK Radio Systems in an Interference Environment", International Conference on Communication, Toronto, Canada, June 1978, pp. 15.3-1--15.3-5.

1.3 Gendron, M. and Feher, K.

"Une nouvelle famille de filtre non-linéaire", Canadian Communication & Power Conference, Montreal, Canada, October 1978, pp. 5-8.

1.4 Bennett, W.R, and Davey, J.R.

"Data Transmission", McGraw-Hill, 1965.

1.5 Greenstein, L.J.

"Spectra of PSK Signaling with Overlapping Baseband Pulses", IEEE Transactions on Communication, May 1977, pp. 523-530.

1.6 Aulin, T. and Sundberg, C.

"M-ary CPFSK Type of Signaling with Input Data Symbol Pulse Shaping - Minimum Distance and Spectrum", Report LUTEDX/(TETT-7111)/1-94/(1978), Univ. of Lund, Lund, Sweden.

1.7 Feher, K.

"Digital/Analog Microwave Transmission Study", Ph. D. Thesis, Univ. de Sherbrooke, Sherbrooke, Quebec, Canada, 1974.

1.8 Lender, A.

"The Duobinary Technique for High-Speed Data Transmission", IEEE Transactions on Communication Technology, Vol. COM-14, February 1966, pp. 47-56.

1.9 Kretzmer, E.R.

"Generalisation of a Technique for Binary Data Communications", IEEE Transactions on Communication Technology, Vol. COM-14, February 1966, pp. 67-68.

1.10 Kabal, P. and Pasupathy, S.

"Partial-Response Signaling", IEEE Transactions on Communication, Vol. COM-23, September 1975, pp. 921-934.

1.11 Qureshi, S.U.H. and Newhall, E.E.

"An Adaptive Receiver for Data Transmission Over Time-Dispersive Channels", IEEE Transactions on Information Theory, Vol. IT-19, July 1973, pp. 448-457.

1.12 Chang, R.W.

"High Speed Multi-channel Data Transmission with Bandlimited Orthogonal Signlas", Bell System Technical Journal, Vol. 45, 1966, pp. 1775-1796.

1.13 Saltzberg, B.R.

"Perfromance of an Efficient Parallel Data Transmission System", IEEE Transactions on Communication Technology, Vol. COM-15, December 1967, pp. 805-811.

1.14 Kwan, R.K.

"The Effect of Filtering and Limiting a Double-Binary PSK Signals", IEEE Transactions on Aerospace and Electronics System, Vol. AES-5, July 1969, pp. 589-594.

1.15 Rhodes, S.A.

"Effects of Hardlimiting on Bandlimited Transmission with Conventional and Offset QPSK",Modulation", National Telecommunication Conference, Houston, U.S.A., December 1972, pp. 20f/1-7.

1.16 Deels, M.L. and Heald, E.H.

"Minimum Shift Data Communication System", U.S. Patent No. 2,977,417, March 28, 1961 (Assigned to Collins Radio Company).

1.17 de Buda, R.

"Fast PSK Signals and Their Demodulation", Canadian Electrical Engineering Journal, Vol. 1, No. 1, 1976, pp. 28-34.

1.18 Murakami, S., Furuya, Y. Matsuo, Y. and Sugiyama, M.

"Modulation Schemes Comparative Study for Non-linear Satellite Channel", International Conference on Communication, Toronto, Canada, June 1978, pp. 19.2.1-19.2.5.

1.19 Huang, J.C.Y. and Feher, K.

"Performance of QPSK, OKQPSK and MSK Signals Through a Satellite Link", Canadian Communication & Power Conference, Montreal, Canada, October 1978, pp. 86-89.

1.20 Harris, R.A.

"Transmission Analysis and Design for the ECS System", Fourth International Conference on Digital Satellite Communication, Montreal, Canada, October 1978, pp. 81-93.

1.21 Lundquist, L.

"Modulation Techniques for Band and Power Limited Satellite Channels", Fourth International Conference on Satellite Communication, Montreal, Canada, October, 1978, pp. 94-100.

1.22 Chakraborty, D., Noguchi, T., Campanella, S.J., and Wolejsza, C.J.

"Digital Modem Design for Nonlinear Satellite Channels", Fourth International Conference on Satellite Communication, Montreal, Canada, October 1978; pp. 123-130.

1.23 Constellano, E.

"Relative Performance of Conventional QPSK and Staggered QPSK Modulations in a Nonlinear Channel", European Space Agency Journal, Vol. 2, 1978, pp. 37-47.

1.24 Robinson, G., Shimbo, O. and Fang, R.

"PSK Power Spectrum Spreading Produced by Nonlinear Distortion", COMSAT Technical Review, Vol. 3, No. 2, Fall 1973, pp. 227-[illegible].

1.25 Moreno, L.

"Sensitivity of PSK Modulation Techniques to Nonlinear Distortion", To be Published in in the IEEE Transactions on Communication.

Chapter 2

2.1 Bennett, W.R. and Davey, J.R.

See Ref. 1.4

2.2 Lucky, R.W., Salz, J. and Weldon, Jr., E.J.

"Principles of Data Transmission", McGraw-Hill, 1968.

2.3 Bennett, W.R.

"Introduction to Signal Transmission", McGraw-Hill, 1970.

2.4 El-Torky, M. and Feher, K.

See Ref. 1.2

2.5 Spaulding, D.A.

"Synthesis of Pulse-Shaping Networks in the Time Domain", Bell System Technical Journal, Vol. 48, September 1969, pp. 2425-2444.

2.6 de Cristofaro, R.

"Transversal Filter Design and Applications in Satellite Communications", M. Eng. Thesis, Concordia University, Montreal, Canada, 1976.

2.7 Gendron, M. and Feher, K.

See Ref. 1.3

2.8 Simon, M.

"A Generalization of Minimum-Shift-Keying Type Signaling Based on Input Data Symbol Pulse Shaping", IEEE Transactions on Communication, Vol. COM-24, No. 8, August 1976, pp. 845-855.

2.9 Kalet, I.

"A Look at Crosstalk in Quadrature-Carrier Modulation Systems", IEEE Transactions on Communications, Vol. COM-25, No. 9, September 1977, pp. 884-892.

2.10 Aulin, T. and Sundberg, C.

See Ref. 1.6

2.11 Amoroso, F.

"Pulse and Spectrum Manipulation in the Minimum (Frequency) Shift Keying (MSK) Format", IEEE Transactions on Communications, March 1976, pp. 381-384.

2.12 Abramowitz, M. and Stegun, L.A.

"Handbook of Mathematical Functions", National Bureau of Standards, Department of Commerce, Washington, D.C., Applied Mathematics Series-55, June 1964, p.361.

2.13 de Jagar, F. and Dekker, C.B.

"Tamed Frequency Modulation, a Novel Method to Achieve Spectrum Economy in Digital Transmission", IEEE Transactions on Communications, Vol. COM-26, May 1978, pp. 534-542.

2.14 Manley, J.M.

"The Generation and Accumulation of Timing Noise in PCM Systems - An Experimental and Technical Study", Bell System Technical Journal, Vol. 48, March 1969, pp. 541-641.

2.15 Van Trees, H.L.

"Detection Estimation and Modulation Theory", Part 1, John Wiley, 1968.

2.16 Feher, K.

"See Ref. 1.7

2.17 Feher, K. and Huang, J.C.Y.

"PAM- Microwave Transmission in Coloured Gaussian Noise Environment", Institute of Electronic and Radio Engineers Journal (London), April 1977, pp. 167-171.

2.18 Taub, H. and Schilling, D.L.

"Principles of Communication Systems", McGraw-Hill, 1971.

2.19 Milstein, L. B. and Austin, M. C.

"Performance of Noncoherent FSK and AM-PSK Systems with Postdetecting Filtering", IEEE Transactions on Communications, November 1975, pp. 1300-1306.

Chapter 3

3.1 Lucky, R.W., Salz, J. and Weldon, Jr., E.J.

See Ref. 2.2

3.2 Lender, A.

See Ref. 1.8

3.3 Lender, A.

"Correlative Digital Communication"Techniques", IEEE Transactions on Communication Technology, December 1964, pp. 128-135.

3.4 Pasupathy, S.

"Correlative Coding", IEEE Communication Society Magazine, July 1977, pp. 4-11.

3.5 Kretzmer, E.R.

"Binary Data Communication by Partial Response Transmission", IEEE Communication Conference Record, 1965, pp. 451-455.

3.6 GTE Practices

"Digital Transmission over 2 GHz Radio System", Engineering - Plant Series, GTE Lenkurt, Section 813-786-075.

3.7 Lender, A.

"Seven Level Correlative Digital Transmission over Radio", International Conference on Communications, Philadephia, U.S.A., June 1976, pp. 18-22 - 18-26.

3.8 Jurling, D.W. and Pachynski, A.L.

"Duobinary PCM System - Double Capacity of T1 Facilities", International Conference on Communications, Chicago, U.S.A., June 1977, pp. 32.2-297 - 32.2-301.

3.9 Barber, S.C. and Anderson, C.W.

"Modulation Consideration for the DRS-8 91 Mb/s Digital Radio", International Conference on Communications, Chicago, U.S.A., June 1977, pp. 5.6-111 - 5.6-115.

3.10 Kurematsu, H., Ogawa, K. and Katoh, T.

"The QAM2G-10R Digital Radio Equipment Using a Partial Response System", Fujitsu Scientific & Technical Journal, June 1977, pp. 27-48.

3.11 Avantek

Data Sheet, ADS-1141 11-76.

3.12 Kabal, P. and Pasupathy, S.

See Ref. 1.10

3.13 Feher, K.

See Ref. 1.7

3.14 Wachira, M.

"Partial Response Transmission Systems", M.A. Sc. Thesis, University of Ottawa, 1979.

3.15 Feher, K.

See Ref. 1.1

3.16 Howson, R.D.

"An Analysis of the Capabilities of Polybinary Data Transmission", IERE Transactions on Communication Technology, Vol. 13, No. 3, September 1965, pp. 312-319.

3.17 Fish, R.H. and Walker, A.C.

"Digital Transmission from DC to Light", International Cpnference on Communications, Minneapolis, U.S.A., June 1974, pp. 42B-1 - 42.c-4.

3.18 Qureshi, S.U.H. and Newhall, E.E.

See Ref. 1.11

3.19 Gill, W.

"Digital Microwave for T-carrier Transmission", Telephony, May 8, 1972

3.20 Morais, D. and Feher, K.

"A Survey of North American 2 GHz Digital Radio Systems", Horizon House, Intelcom - 77, Atlanta, U.S.A., October 1977

3.21 Bell Blue Book

"Transmission System for Communications", Bell Telephon Laboratories, 1971

Chapter 4

4.1 Wolejsza, C.

"State of the Art of PSK Modulation Techniques", Second International Conference on Digital Satellite Communications, Paris 1972

4.2 Murakami, S., Furuya, Y., Matsuo, Y. and Sagiyamo, M.

See Ref. 1.18

4.3 Gronemeyer, S. and McBride, A.

"MSK and Offset QPSK Modulation", IEEE Transactions on Communications, Vol. COM-24, No. 8, August 1976, pp. 809-819.

4.4 Feher, K.

See Ref. 1.1

4.5 Bell Blue Book

See Ref. 3.21

4.6 de Buda, R.

See Ref. 1.17

4.7 Kalet, I.

See Ref. 2.9

4.8 Simon, M.

See Ref. 2.8

4.9 Bennett, W.R. and Davey, J.R.

See Ref. 1.4

4.10 Robinson, G. Shimbo, O. and Fang, R.

See Ref. 1.24

4.11 Chan, H.C., Taylor, D.R. and Haykin, S.S.

"Comparative Evaluation of Digital Modulation Techniques: Simulation Study", Communication Research Laboratory, McMaster University, Hamilton, Canada, Internal Report CRL-18.

4.12 Lucky, R.W., Salz. J., and Weldon, Jr., E.J.

"See Ref. 2.2

4.13 Palmer, L.C. and Labowitz, S.

"Computer Simulation of Solid State Amplifiers", COMSAT Technical Review, Vol. 8, No. 2, Fall 1978, pp. 372-403.

4.14 Moreno, L.

See Ref. 1.25

4.15 El-Topky, M. and Feher, K.

"The Effect of Transmitter Power Amplifier Non-linearity on QPSK and Offset QPSK Radio Transmission over Severely Bandlimited Channels", Canadian Communication & Power Conference, Montreal, Canada, October 1978, pp. 153-156.

4.16 Andren, C.

"PSK Sidebands Reduced by Premodulation Filtering", Microwave Journal, January 1978, pp. 69-72.

4.17 Rhodes, A.

See Ref. 1.15

4.18 Marsan, M.A. and Biglieri, E.

"Power Spectra of Complex PSK for Satellite Communications", Alta Frequensa, Vol. XLVI, No. 6, Giugno 1977, pp. 263-270.

4.19 El-Torky, M.

"Performance of Digital Radio Systems in an Interference Environment", Ph. D. Thesis, Concordia University, to be Submitted

4.20 Constellano, E.

See Ref. 1.23

4.21 Lundquist, L.

See Ref. 1.21

4.22 Gilten, R.D. and Ho. E.Y.

"The Performance of Staggered Quadrature Amplitude Modulation in the Presence of Phase Jitter", IEEE Transactions on Communications, Vol COM-23, No. 3, March 1975, pp.348-352.

4.23 Devieux, Jr., C.

"QPSK Bit Error Rate Performance as Affected by Cascaded Linear and Nonlinear Elements", COMSAT Technical Review, Vol. 8, Spring 1978, pp. 205-218.

4.24 Harris, R.A.

See Ref. 1.20

4.25 Chakraborty, D., Noguchi, T., Campanella, S.J. and Wolejsza, C.

See Ref. 1.[illegible]

4.26 Eric, M.J.

"Intermodulation Analysis oaf Nonlinear Devices for Multi-carrier Inputs", Communication Research Center Report No. 1234, Ottawa, Canada, 1972

4.27 Chang, R.W.

See Ref. 1.12

4.28 Kwan, R.K.

See Ref. 1.14

4.29 Doels, M.L. and Heald, E.H.

See Ref. 1.16